THE SECRET LIVES OF CEPHEIDS

A MULTI-WAVELENGTH STUDY OF THE ATMOSPHERES AND REAL-TIME EVOLUTION OF CLASSICAL CEPHEIDS

Thesis submitted in March, 2014,
revised thesis submitted in October, 2014, by

Scott Gerard ENGLE BSc (Astronomy & Astrophysics)
Villanova University, PA USA

for the degree of Doctor of Philosophy,
School of Engineering and Physical Sciences'
Centre for Astronomy
James Cook University, Australia

STATEMENT OF CONTRIBUTIONS TO THE THESIS

Leonid Berdnikov – Astronomer at Sternberg Astronomical Institute, Moscow University
- Provided, in digital form, the O-C data he had gathered/published for β Dor

Neil Butterworth – AAVSO observer
- Gathered dSLR photometry of β Dor

Kenneth Carpenter – HST Operations Project Scientist at NASA / Goddard Space Flight Center
- Discussion about the stability, performance and analysis of COS UV spectra

Kyle Conroy – Graduate Student, Vanderbilt University
- Wrote the Fourier Series fitting routine used in determining Cepheid times of maximum light and light amplitudes

Nancy Evans – Astrophysicist at Harvard-Smithsonian Center for Astrophysics (retired)
- PI of the Chandra X-ray proposal for Polaris in 2006 (NASA grant Chandra-GO6-7011A)
- Numerous helpful discussions on various aspects of Cepheids

Ed Guinan – Primary Advisor / Professor of Astrophysics & Planetary Science, Villanova University
- Served as PI on all grants used in the thesis
- Many discussions on the direction and methodologies of the study

Petr Harmanec – Astronomer, Astronomical Institute of the Academy of Sciences of the Czech Republic
- Discussions on photometric calibrations
- Provided a list of suitable, photoelectric standards

Graham Harper – Assistant Professor, Director of Teaching and Learning Undergrad Physics at Trinity College, Dublin
- A fount of astrophysical knowledge, especially UV emission lines and stellar atmospheres

David Turner – Professor Emeritus at St. Mary's University, Canada
- Discussion on Cepheid period changes and evolution.
- Provided, in digital form, his updated period change data and also his newest equation used to calculate instability strip crossings and period change rates.

Rick Wasatonic – Adjunct Faculty / Research Associate at Villanova University
- Carried out (and continues to carry out) *BV* photometry of Polaris

Ian Whittingham – co-Advisor / Professor Emeritus at James Cook University
- Discussions on thesis formatting, organization and presentation

Grants Associated with the Thesis:
NSF grant AST05-07542
NASA grants: HST-GO11726X, HST-GO12302X, HST-GO13019X, XMM-GO050314X, XMM-GO055241X, XMM-GO060374X, XMM-GO06547X, XMM-GO072354X, SST-GO40968X

ACKNOWLEDGEMENTS

This thesis is dedicated to:

My best buddy Julie, who has been incredibly loving during this rather long road. Her support, through a great many delays, has meant the world to me, and I'll always be lucky to have her.

Mom and Rusty, whose pride has always been felt.

Ms. S and Karen, who always make it feel like I'm part of the family.

Nan, who cut out every (even loosely) Astronomy-related newspaper article, "just in case I was interested…"

Troy, who always had to know where the Moon was.

Ed Guinan, my primary advisor and mentor, who took a chance by allowing me to "wrap up my Polaris study" and then encouraged its expansion into this thesis, which was only possible because of him.

Lena and Ava, who'll grow up to be the best and the smartest of us all.

ABSTRACT

Classical Cepheids are variable, yellow supergiants that undergo radial pulsations primarily arising from opacity variations in their stellar interiors. Over a century ago, the discovery of a reliable relationship between the period of a Cepheid's pulsations and its luminosity made them "standard candles" and, as such, interest in studying Cepheids boomed. The generally held belief that their pulsations are essentially static over human timescales has sadly led to a narrowing in the field of Cepheid studies. This is in addition to the widespread adoption of high-sensitivity CCD instruments that can quickly saturate when observing nearby Cepheids. The result is that many of the brightest Cepheids, with the longest observational histories, have recently stopped being systematically observed. The primary overall goal of this study is to observe how complex the behaviors of Cepheids can be, and to show how the continued monitoring of Cepheids at multiple wavelengths can begin to reveal their "secret lives."

We aim to achieve this goal through optical photometry, UV spectroscopy and X-ray imaging. Through Villanova University's guaranteed access to ground-based photometric telescopes, we have endeavored to secure well-covered light curves of a 10 Cepheid selection as regularly as possible. Amplitudes and times of maximum brightness were obtained from these lightcurves, and compared to previous literature results. At UV wavelengths, we have been very fortunate to secure numerous high-resolution spectra of two nearby Cepheids – δ Cep and β Dor – with the Cosmic Origins Spectrograph (COS) onboard the Hubble Space Telescope (HST) and additional future spectra have recently been approved. Finally, at X-ray wavelengths, we have (again, very fortunately) thus far obtained images and X-ray (0.3 – 5 keV) fluxes and luminosities of five Cepheids with XMM-Newton and the Chandra X-ray Observatory, and further observations with both satellites have been proposed for (XMM) and approved (Chandra).

Our analysis of optical photometry has shown that 8 of the 10 observed Cepheids have amplitude variability, or hints thereof, and all 10 Cepheids show evidence of period variability (recent, long-term or even possibly periodic). The UV spectra reveal a wealth of emission lines from heated atmospheric plasmas of 10^4 – 10^5 K that vary in phase with the Cepheid pulsation periods. The X-ray images have detected the three nearest Cepheids observed (Polaris, δ Cep and β Dor), while the distances of the farther two Cepheids place their fluxes likely at or below detector background levels. The X-ray fluxes for δ Cep show possible phased variability, but possibly anti-correlated with the UV emission line fluxes (i.e. high X-ray flux at phases of low UV flux, and vice versa).

In conclusion, the optical studies have shown that Cepheids may likely undergo period and amplitude variations akin to the Blazhko Effect observed in RR Lyr stars, but on longer

timescales. The heating mechanism(s) of their atmospheres appears to be a combination of magnetic/acoustic activity, common in many cool stars, along with pulsation-related effects (shock propagation and possibly convective strength variability). Further data are required to ultimately confirm Blazhko-like cycles in Cepheids, X-ray variability with phase and the particulars of the high-energy variability such as phase-lags between atmospheric plasma emissions of different temperature and the exact contributions of the possible heating mechanisms.

TABLE OF CONTENTS

LIST OF TABLES

LIST OF FIGURES

CHAPTER 1 – A CEPHEID OVERVIEW

1.1 Introduction – The Importance of Cepheids

Type I, or Classical, Cepheids (also known as δ Cep variables and, in this paper, shall hereafter be referred to simply as Cepheids) are a fundamentally important class of pulsating variable stars. Cepheids are among the first classes of variable star discovered, and have played a crucial role in Astronomy and Astrophysics for over two centuries. The study of Cepheids is not only valuable to understand a complex stage of stellar evolution, but to also measure the Universe itself. In Astrophysics and especially Cosmology, the most important aspect of Cepheids is likely their use as extragalactic "standard candles." This is done by way of the Period-Luminosity Law (P-L Law or Leavitt Law hereafter) for Cepheids – first discovered by Henrietta Leavitt in 1912 (Leavitt 1912). The usefulness of the law is bolstered by the fact that the (pulsational) period of a Cepheid can be easily measured through either near-UV – near-IR photometric or spectrophotometric observations, or through radial velocity measurements. A properly calibrated Leavitt Law can then use that period to calculate the Cepheid's luminosity which can, in turn, then be used to calculate the distance to the Cepheid. With the large number of extragalactic Cepheids known, they are at the forefront of studies into the dimensions of our Universe. However, there are some difficulties in calibrating the Leavitt Law. The elimination of these flaws and precise calibration of the Leavitt Law is the aim of several research groups and studies, notably the Hubble Key Project (Freedman et al. 2011).

Cepheids play as important a role in stellar evolution as they do Cosmology. Cepheids exist in an important phase of stellar evolution, as post Hydrogen core-burning stars that have evolved off the main sequence. In the H-R Diagram, Cepheids are aligned into what is called the Classical Cepheid Instability Strip – a sub-section of the general *instability strip* of the H-R Diagram, sometimes called the *classical instability strip*, and marked by the dashed oval shape in Fig. 1. It is within this strip that all Cepheids are found (although non-variable supergiants also exist in this region) and, as with the Leavitt Law, the exact dimensions and extent of the strip are constantly being refined. As they evolve, Cepheids will cross the strip. The "first crossing" of the Instability Strip is from the blue edge of the strip to the red edge – i.e. from higher stellar surface temperatures to lower. Cepheids of sufficient mass will make multiple crossings of the strip as they burn different fuels in different stellar layers. The minimum mass required for a Cepheid to cross the strip more than once is up for debate, and depends on exactly what parameters are used for computing the evolutionary tracks. Aside from the precision of the Instability Strip and the Leavitt Law (and how massive the star must be to carry out multiple crossings), there is no

argument that a very specific area of the H-R diagram marks the location of Cepheid variables, that this location is defined by the physical properties (interior structure, chemical composition, density…) necessary to sustain Cepheid pulsations, and that their periods and luminosities are related.

1.2 The General Picture of Cepheids

Cepheids are young (50 – 300 Myr), intermediate-mass (typically 4–10 $M_\odot$), luminous (~10^3–10^5 $L_\odot$), white-yellow (spectral types of approximately F6–K2) Population I supergiants (luminosity classes of Ia, Ib and II) whose radial pulsations produce periodic variations in radius, temperature and, consequently, brightness. The pulsation periods of Cepheids range from around 1.5-days to as long as ~45-days (for SV Vul, but as long as ~60-days or even longer depending on the classification of S Vul and other possible long period Cepheids). The prototype of Cepheids is δ Cep. Although recognized as the prototype of its class, δ Cep was actually the second Cepheid to be discovered, with η Aql owning the distinction of being the first. Both stars were discovered to be variable in 1784. Edward Pigott discovered the variability of η Aql in September of 1784, and John Goodricke (whom Pigott had mentored in Astronomical observing) discovered the variability of δ Cep just a month or so later (Pigott 1785; Goodricke 1786). There are currently more than 800 known Classical Cepheids in the Milky Way and thousands of extragalactic Cepheids (Szabados 2003; 2010). In the visual and photoelectric eras of observational astronomy, Cepheids were often targeted, with numerous studies published per Cepheid. With the widespread adoption of CCD instruments in modern observatories, recent observations of the brightest Cepheids are becoming rarer, as they pose saturation problems for these high-sensitivity instruments. However, the

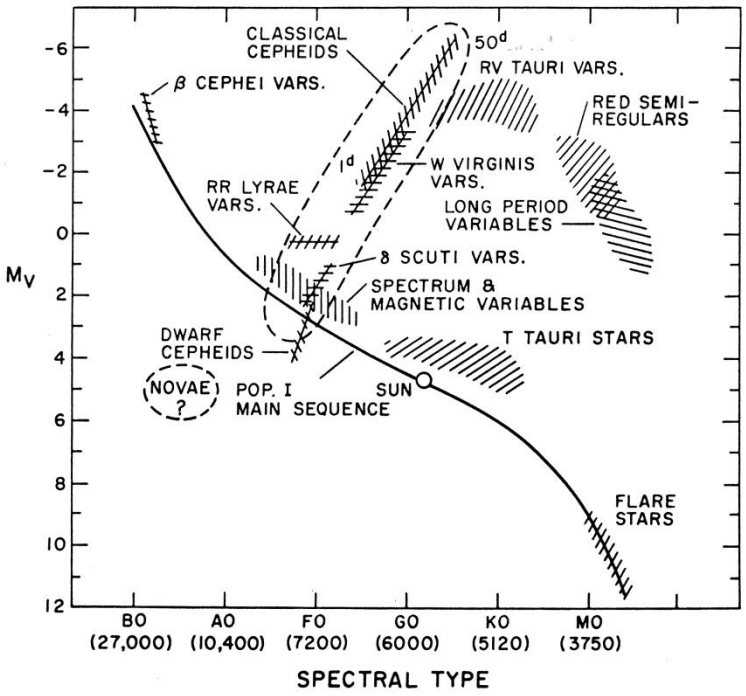

Figure 1 – Hertzsprung-Russell diagram showing the locations of various types of intrinsic variables, including Classical Cepheids at the top-center of the diagram (From Cox 1974).

proximity of these bright Cepheids to the Earth makes them attractive targets for time-precious instruments, such as those onboard satellites. Also, the brightest Cepheids usually have the longest observational timelines, crucial for providing insights into long-term behaviors and possibly even evolutionary changes taking place along human timescales.

1.3 The Cepheid Pulsation Mechanism

The source of Cepheid light and radial velocity variations posed a long-standing problem for astrophysicists, with a great amount of work devoted to understanding it. Several theories were proposed and studied, with the two most prominent being the pulsations of a single star, or the variability of a binary system. German physicist August Ritter (1879) was the first to propose a simple radial pulsation model to explain variable stars, and even showed that the pulsation period would be proportional to the inverse square-root of the stellar density (this is now known as the *period-density relationship*).

$$P \propto \sqrt{1/\bar{\rho}}$$

where P is the pulsation period and $\bar{\rho}$ is the average density. However, this theory was decades away from acceptance and so Ritter's work unfortunately seemed to gather no interest from astronomers of the time. Aristarkh Apollonovich Belopolsky first showed that Cepheids underwent changes in radial velocity (RV) when he observed and plotted the periodic RV variations in δ Cep (Belopolsky, 1894, 1895). Schwarzschild (1900) then discovered that the color of η Aql varied over its pulsation period, and that the brightness variability had a larger amplitude in photographic (blue) light than in visual (green) light. This showed the brightness changes to be accompanied by temperature changes. Although it was with great difficulty, astronomers labored to include the new data into binary theory, giving rise to more complicated orbital solutions, sometimes involving multiple bodies. In 1913, Brunt (1913) wrote "The problem of the Cepheid Variables" where he gave a rather comprehensive description of the problems associated with the binary theory, yet he never questioned it, instead saying, early in the article,

> *The discovery of the binary nature of δ Cephei was made by Belopolsky in 1894… Since then most of the short-period variables have been shown to be binary stars (Brunt 1913).*

In the same year, Plummer (1913) pointed out the serious problems in interpreting the radial velocity variations of the Cepheid ζ Gem. One year later, Plummer (1914) qualitatively suggested that a radial pulsation mechanism in single stars would avoid the numerous and serious problems

in explaining "certain classes" of variable stars. The theory of binarity was dealt its strongest blow by the seminal paper of Shapley (1914), in which he also highlighted its various shortcomings. Shapley made note of the errors associated with fitting binary orbits to Cepheid RV curves. He then combined numerous radial velocity studies of Cepheids with the new stellar classification scheme of Hertzsprung (1909) and Russell (1913), which firmly placed Cepheids in the Supergiant class, and showed that if Cepheids were in fact spectroscopic binaries, the orbital separation of the two stars would place the secondary within the surface of the visible Cepheid. This was the most convincing argument against the binary theory. Despite Shapley's work, some Astronomers continued to research and defend the binary theory into the 1920s and 30s, however the rate of publications was steadily decreasing. One such study was that of the renowned astronomer Jeans (1925) who hypothesized that Cepheids, and long-period variables, were binary stars in the process of fission. One of the latest studies was that of Hoyle & Lyttleton (1943) who revisited Jeans' theory and proposed that Cepheids could be contact systems surrounded by a common envelope that remains independent of the motion of its contained binary system. Despite these later studies, the focus primarily shifted to the dynamics of single stars being responsible for the observed variations. Eddington (1917, 1918) published two papers in which he offered an astrophysical explanation of the stellar pulsations he believed were at work in Cepheids. Eddington proposed that Cepheids act as "heat engines" and, although in his 1917 paper he did not yet understand the *exact* mechanism allowing them to do this, he proposed that:

> *"Possibly during the pulsation, variations of the transparency, which governs the flow of heat, might cause the engine to be fed in the required manner" (Eddington, 1917).*

Though the physics of the process would take some time to develop, the general theory would turn out to be correct. Just over a decade later, Baade (1926) devised a rather important test of the pulsation theory. If the Cepheids were radially pulsating, this would be accompanied by periodic changes in the stellar surface area. The observed luminosity and temperature changes were evidence of this; however, the two variations could be separated to achieve a plot of radius vs. phase. Additionally, the RV data showed the change in radius over time, and could serve as an independent check of the radius variability. His method was improved upon by other astronomers, most notably by Wesselink (1946), and it is now known as the Baade-Wesselink method and is a rather important method of physically calibrating classical pulsators.

Even while the exact cause of their light and velocity variations was still unclear, Cepheids nonetheless rose to a prominent position in astronomy, thanks to the work of a "female computer" – Henrietta Leavitt. Leavitt was hired in 1893 by Edward Pickering, director of the observatory,

as one of his "computers" – women whom he hired to measure and catalog the vast amount of photographic plates the observatory possessed and continued to gather. The general view was that women were well-suited to the job, since they earned less than men (so more could be hired for the same overall cost) and were also not allowed to observe on the telescopes, so their time could be focused on plate analysis. Fifteen years after beginning at the observatory, Leavitt remarked in one sentence a behavior that would form one of the most important laws in astronomy: *"It is worthy of notice that in Table VI the brighter variables have the longer periods*" (Leavitt, 1908). At the time the implications were most likely not understood, but this simple sentence announced that ground-breaking research was afoot. Four years later, Leavitt would release a more detailed study confirming the results:

> *"A remarkable relation between the brightness of these variables and the length of their periods will be noticed. In H.A. 60, No. 4, [the 1908 paper] attention was called to the fact that the brighter variables have the longer periods, but at that time it was felt that the number was too small to warrant the drawing of general conclusions. The periods of 8 additional variables which have been determined since that time, however, conform to the same law" (Leavitt & Pickering, 1912).*

In addition to confirming the earlier suspicions of an apparent relationship between period and brightness, Leavitt further noted:

> *"They resemble the variables found in globular clusters, diminishing slowly in brightness, remaining near minimum for the greater part of the time, and increasing very rapidly to a brief maximum. Since the variables are probably at nearly the same distance from the Earth, their periods are apparently associated with their actual emission of light, as determined by their mass, density, and surface brightness" (Leavitt & Pickering, 1912).*

Thus was the "official confirmation" of what would become known as the Cepheid Period-Luminosity Law (P-L Law), also recently redubbed the Leavitt Law. Leavitt did not know it at the time, but she was comparing Population I Cepheids (Classical Cepheids – "they" in the quoted text) and Population II Cepheids (previously called W Virginis Stars before separate sub-classes were created – "the variables found in globular clusters"). The two stellar classes exhibit similar light and velocity changes, but are completely different stars brought to a similar location in the H-R Diagram by ways of unrelated evolutionary tracks. The inclusion of both Cepheid types led to larger uncertainties in the Law, since Type II Cepheids are ~1.5-mag fainter than

Type I Cepheids of the same period. This continued until Walter Baade (1944) first discovered two distinct stellar populations of stars in his detailed study of M31, M32 and NGC 205. Later, specifically in regard to problems encountered calibrating the P-L Law, he wrote:

> *"Miss Leavitt's cepheids in the Magellanic Clouds and the classical cepheids in our galaxy are clearly members of population I, while the cluster-type variables and the long-period cepheids of the globular clusters are members of population II. Since the color-magnitude diagrams of the two populations leave no doubt that … we are dealing with stars in different physical states, there was no a priori reason to expect that two cepheids of the same period, the one a member of population I, the other a member of population II, should have the same luminosity (Baade 1956)."*

The Leavitt Law has played a crucial role in astrophysics since its discovery. The Shapley-Curtis "Great Debate" highlighted the importance of scale in our modern understanding of the Universe. Great astronomers such as Hertzsprung, Shapley and Hubble all used the Law to determine accurate distances to some of the nearest and most prominent extragalactic objects, such as the Magellanic Clouds, globular clusters and the Andromeda Galaxy. The Leavitt Law helped astronomers understand that the Universe was, in fact, *much* larger than originally thought. The tight, linear arrangement of Cepheids in the HR Diagram is illustrative of the Law they have become associated with, but what is responsible for such an arrangement is the pulsation mechanism at work and the internal structure/dynamics of Cepheids.

As mentioned, much work has been devoted to understanding the pulsation mechanisms of Cepheids. The foundation of a modern theory of Cepheid pulsations was laid down in an important paper by Eddington (1941), in which the "valve" mechanism controlling the pulsations was incorrectly ascribed to hydrogen as the crucial element. Further, Eddington considered core nuclear reactions to be the direct driver of the pulsations. Two decades later, Baker & Kippenhahn (1962), Cox (1963) and Zhevakin (1963) would detail a Cepheid pulsation mechanism via the non-adiabatic opacity modulations of ionizing gas regions existing in the internal stellar envelope, specifically partially ionized He II zones in the upper layers of Cepheids. This ionization mechanism causes the layer to absorb heat during compression and then release it during expansion. For Cepheid pulsations to be successfully driven, two basic criteria must be satisfied: a sufficient amount of ionizing material (He II in the case of Cepheids) must exist at the transition within the star from adiabacity to non-adiabacity (Cox 1985). More specifically, a star must contain a concentration of at least 10-15% helium (number fraction), half of which is

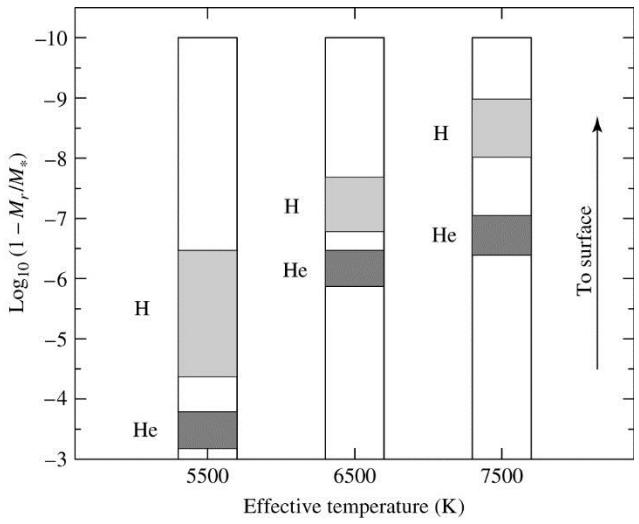

Figure 2 – Hydrogen and Helium ionization zones in stars of different temperatures. For each point in the star, the vertical axis displays the logarithm of the fraction of the star's mass that lies *above* that point. (From Carroll & Ostlie 2006).

ionized (Kukarkin 1975). Also, the helium ionization zone can only exist within the temperature range 35000-55000 K (Bohm-Vitense 1958). The stellar depth at which these temperatures exist progresses from nearer to the surface in hotter (earlier-type) stars down to depths nearer the core in cooler (later-type) stars, as shown in Fig. 2. Because of the stringent requirements on ionization zone depth, combined with the dampening effect of strong convection in cooler stars (see Gastine & Dintrans 2011 and references therein), Cepheid pulsations can only be maintained in a specific range of effective temperature. This range is defined as the nearly vertical "classical instability strip" where Type I Cepheids are found on the HR diagram (Fig. 1).

Though the He II ionization zone is regarded as the primary driving force behind Cepheid pulsations, it is one of three mechanisms at work. Under adiabatic conditions, the compression of a gas would increase its temperature. In partial ionization zones, however, compression energy (that would normally be converted to thermal energy) is used to further ionize the gas. This prevents the temperature from rising, although the density of the region *is* allowed to rise, and therefore opacity also rises, in accord with *Kramer's opacity law*

$$\bar{\kappa} \propto {}^{\rho}/_{T^{3.5}}$$

where opacity (or mass absorption coefficient) is indicated with the Greek letter kappa (κ), ρ is the density and T is the temperature. In this scenario, opacity increases upon compression, and energy is trapped (due to the increased opacity) within the ionization zone during compression. Also, the increased opacity of the region causes pressure to build beneath it, driving stellar expansion. This expansion reduces the opacity, allowing pressure and energy to be released. The consequence is that the energy released upon expansion is larger than it would be in a purely adiabatic case since, upon expansion and cooling of the gas, the ionization energy is radiated back into the region during recombination, and converted into thermal energy. After the release of the stored pressure and energy, gravitational contraction begins the cycle anew. This is referred to as the "kappa mechanism" (Baker & Kippenhahn 1962) and is responsible for "pumping" the

pulsations of a Cepheid. In addition, since the temperature of the ionization region remains low compared to the surrounding stellar interior, heat flows from the surroundings into the partial ionization region, further driving its full ionization and increasing opacity. This is the "gamma mechanism" (Cox et al. 1966) and is a secondary driver of the pulsations. The final, third mechanism at play is perhaps the most simple and straightforward: the "r mechanism" or "radius mechanism," so named because, upon compression, the star has a smaller surface area from which it can emit radiation. Consequently, the star stores more radiation when smaller than it would at a larger size and this stored radiation builds pressure, also feeding into the pulsation cycle, aiding in the expansion of the star.

However, as mentioned previously, the instability of the He II region within the star to variations in temperature and pressure is *primarily* responsible for the radial pulsations of Cepheid variables. The *Eddington Valve*, now understood to rely on the ionization of He instead of H, serves to store and release heat at specific times to successfully drive stellar pulsations. Since this valve relies heavily on a specific temperature, composition and location within a star to operate, only stars within a certain area of the H-R diagram can support stable, radial pulsations. This, of course, is why the Cepheid Instability Strip is a prominent feature of the H-R diagram, and it is also why Cepheids obey the Period-Luminosity law for which they have become so well-known and cosmologically important.

1.4 The Stellar Evolution of Cepheids

In short, Cepheids are B-type stars (at birth, with masses ranging from ~3–18 $M_{\odot}$, Zombeck 2007) that have evolved off the main sequence and are now passing through the Cepheid Instability Strip. As stellar evolutionary tracks show, a star can enter the instability strip more than once during its post-main sequence lifetime (Fig. 3).

Except for the most massive Cepheids, the first crossing of the instability strip occurs after the exhaustion of hydrogen in the stellar core, when the star has entered the hydrogen shell-burning phase. During this, the star expands, rising above the main sequence and proceeding to the right (towards cooler surface temperatures) on the H-R diagram, towards the red giant region. This initial path through the instability strip occurs as the stellar surface is cooling, and is very rapid, occurring along a Kelvin-Helmholtz (thermal) timescale, generally lasting 10^3–10^4 years (Bono et al. 2000b). After this first crossing of the instability strip, the star exits the red edge of the strip and ascends along the red giant branch of the H-R diagram to the "red giant tip" where core He ignition occurs.

With the onset of core He burning, the star contracts and heats up, descending the red giant branch and moving towards the left on the H-R diagram, towards higher temperatures and bluer colors. This can bring the star into the instability strip for the second time. The star is now undergoing what is called a "blue loop." The exact extent of the blue loop (in color/temperature space) can either cause the star to make two distinct crossings of the instability strip, or it can cause the star to enter the instability trip through the red edge, "turn around" while still within the strip, and evolve back out through the red edge again. In either case, the blueward path of the Cepheid through (or into) the instability strip is referred to as the second crossing, and the redward path through (or back out of) the strip is the third crossing. The specifics of blue loops (and even their very existence for stars of lower masses) are constantly being revised, and generally depend on the abundances and structure of the star as a result of the previous stages of stellar evolution, such as the H core-burning and shell-burning phases, and also factors such as convective core treatment. In general, the extent of the blue loop increases for stars of increasing mass. One consequence of this is that, for a star of low enough mass, the blue loop will not extend far enough to penetrate the red edge of the instability strip. As such, lower mass stars will never undergo more than a first crossing of the strip. This, combined with the short lifetime of the first crossing, can contribute to the lower mass limit observed for Cepheids. For good discussions of blue loops, see Bertelli et al. (2009) and Valle et al. (2009).

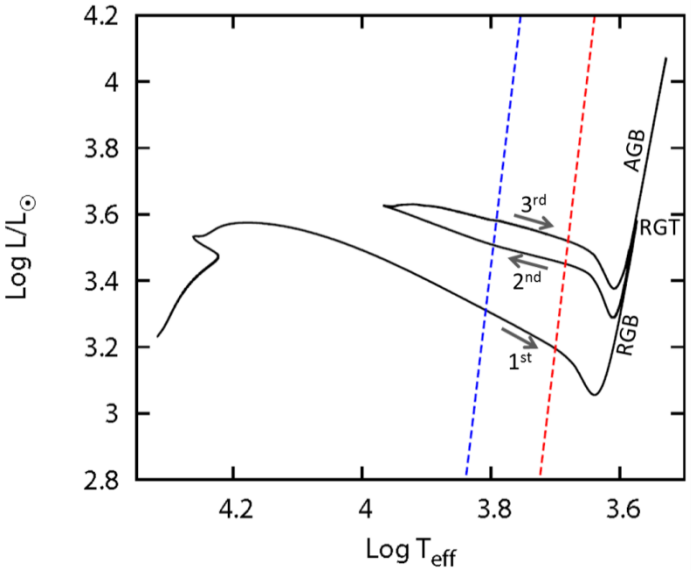

Figure 3 – The evolutionary track of a 7 $M_\odot$ (initial mass) star, computed using the code of Yoon & Langer (2005). The dashed, colored lines show the blue and red edges of the instability strip, based on the study of Bono et al. (2000b). Labels mark the 1st, 2nd and 3rd crossings of the instability strip, as well as the direction of the star along the evolutionary path, as well as the red giant branch (RGB), red giant tip (RGT) and the asymptotic giant branch (AGB).

This second crossing of the instability strip is longer than the first crossing (Bono et al. 2000b), as is (in most cases) the third crossing. This is consistent with the findings of Turner (1998), where most Cepheids are found to be in the second or third crossings of the instability strip. The third crossing of the instability strip occurs with He core exhaustion and contraction, or

can also be the result of He shell-burning. A second blue loop can occur, resulting in fourth and fifth crossings of the instability strip, but this requires specific conditions that are not often met (Becker 1981).

After evolving along the blue loop(s), stellar evolution proceeds as dictated by the star's mass. The intermediate mass Cepheids evolve onto the asymptotic giant branch, eventually losing their stellar envelopes and leaving a degenerate core. The higher mass Cepheids can proceed along further steps of nuclear burning before ending their lives as supernovae.

1.5 Development of the Period–Luminosity Law

As mentioned, Henrietta Leavitt was the first to observe and remark on a relationship between Cepheid periods and luminosities (Leavitt 1908), using Harvard Observatory photographic plates of the Magellanic Clouds. Her 1912 publication was based upon the study of Cepheids in the Small Magellanic Cloud (SMC) alone, which allowed her to comfortably use the apparent magnitudes of the Cepheids in her sample, since they were all assumed to have essentially the same distances (Fig. 4).

This original relationship, having been based on apparent magnitudes, was of limited technical use outside of the SMC. However, it showed that perhaps an absolute law should exist, and the importance of such a law was quickly recognized, motivating further studies. Since Leavitt's original work, many famous Astronomers have contributed to this task: Hubble, Shapley and Baade, to name a few (Hubble 1925; Shapley 1927; Baade 1956). Modern formulations of the Leavitt Law generally take the form:

$$\langle M \rangle = \alpha + \beta \log P$$

where M is the Cepheid's mean absolute magnitude at the particular wavelength of study, α is the zero point of the relationship, β is the slope, and P is the pulsation period (usually in days). Even when using the most accurate data possible, there is a luminosity scatter to the relationship, which is a consequence of the appreciable width to the Cepheid instability strip. After much work investigating the scatter found in the relationship, many authors determined that a color term should also be included (see Tammann et al. 2003). The general form of the Period-Luminosity-Color (PLC) relationship is:

$$\langle M_\lambda \rangle = \alpha + \beta \log P + \gamma(CI)$$

where CI now represents the specific color index being used in the relationship, λ is the coefficient of the color index, and M_λ is the absolute magnitude at a given wavelength bin or photometric band.

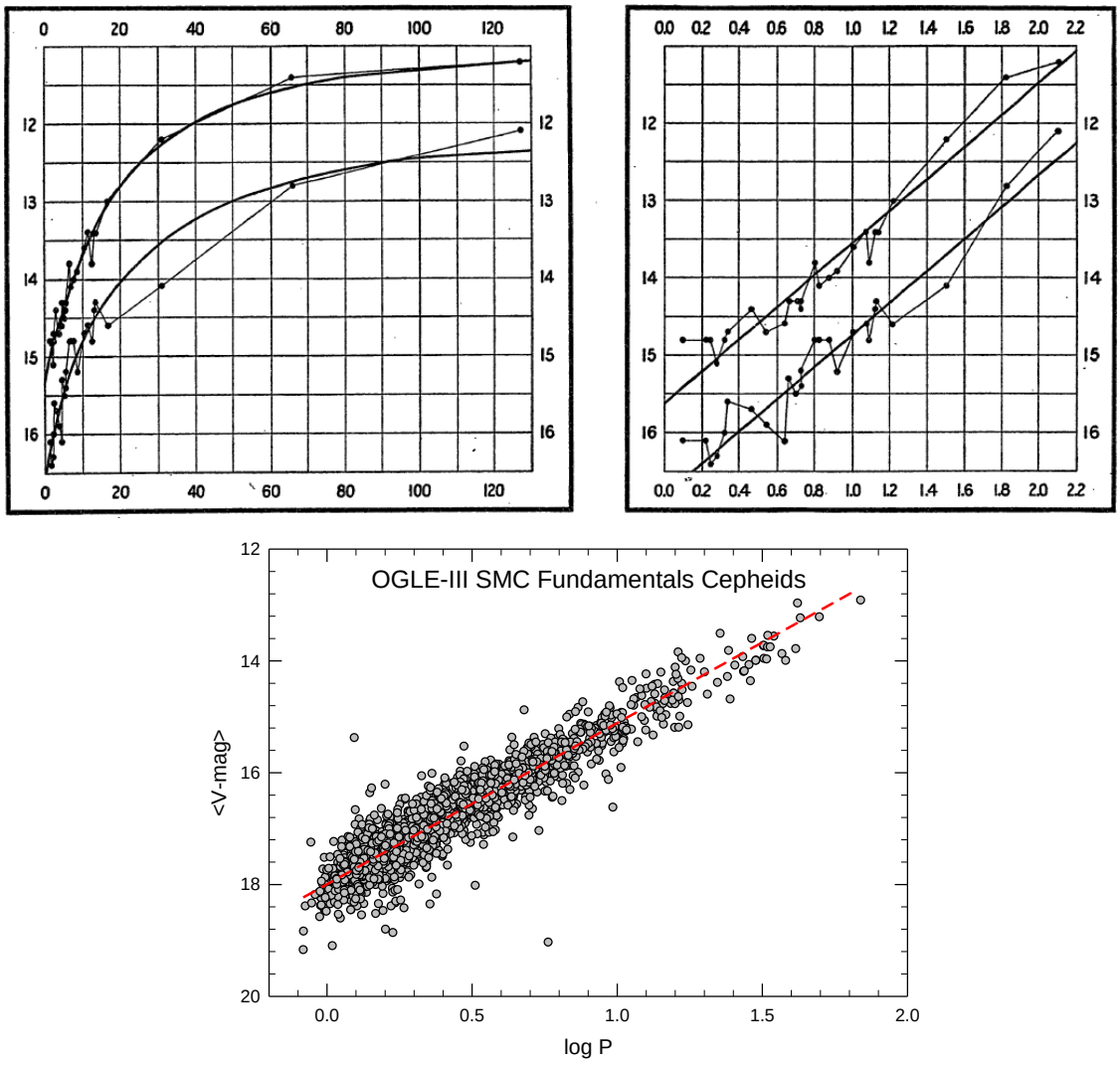

Figure 4 – (Top Plots) The Original "P-L Law" of Leavitt (1912). The y-axes of both graphs gives the apparent magnitudes, and the x-axes give period in days (left) and log period in days (right). (Bottom Plot) The full OGLE-III inventory of SMC fundamental mode Cepheids with available average V-magnitudes and (log) pulsation periods (http://ogledb.astrouw.edu.pl/~ogle/CVS/). The resulting relationship, with 3σ errors, is: $\langle V \rangle = 17.9944(10) - 2.8839(20) \log P$.

In order for the P-L Law to achieve its full potential, there must be a precise zero point. This precision can be most directly obtained through absolute trigonometric parallaxes of Cepheids with a variety of pulsation periods. Benedict et al. (2007) used the very precise Hubble Space Telescope Fine Guidance Sensors (FGS) to determine absolute parallaxes for a sample of 10 galactic Cepheids. In addition, van Leeuwen et al. (2007) analyzed revised *Hipparcos Satellite* parallaxes of a group of Cepheids, combined with the results of Benedict et al. (2007), to return a very accurate PLC relationship of:

$$\langle M_W \rangle = -2.58 - 3.288(\pm 0.151) \log P + 2.45(V - I)$$

where M_W represents the absolute Wesenheit magnitude, an extinction-corrected magnitude, following the prescription of Freedman et al. (2001).

1.6 Period Studies of Cepheids

In addition to being one of a Cepheid's most readily determinable properties, and also one that can be determined with the highest precision, the pulsation period of a Cepheid can also provide astrophysically relevant information on the star (e.g. evolutionary status, luminosity). Bezdenezhnyj (2007) conducted a study of 473 Cepheids with known periods found in the 4th edition of the General Catalog of Variable Stars (GCVS), and Fig. 5 below gives the results of his study.

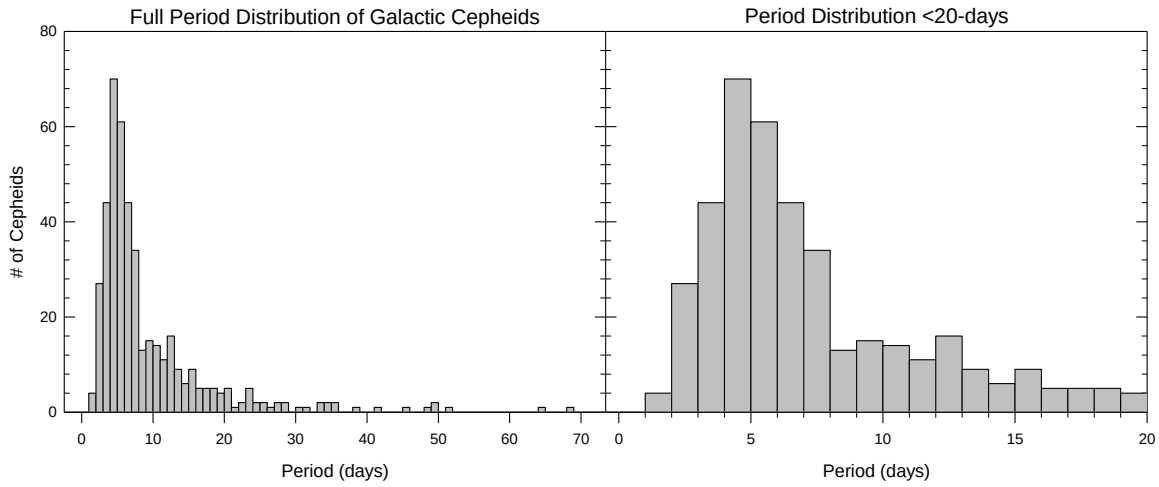

Figure 5 – Results of the galactic Cepheid period distribution study of Bezdenezhnyi (2007). The left-hand plot shows the full distribution, while the right-hand plot shows only the period shorter than 20-days. The strong, primary maximum around periods of 5-days can clearly be seen, along with the possible secondary maximum in periods of around 10-days.

As can be seen, there is a clear maximum in the period distribution for Cepheids with periods around 5-days. There is also a possible secondary maximum at around 10-days. In studying the period distributions of Cepheids in the LMC and SMC, Soszynski et al. (2010) found the most prominent periods to be around 3.2-days in the LMC and 1.6-days in the SMC. This is a metallicity effect, since the LMC has a lower mean metallicity than the Milky Way, and the SMC has an even lower metallicity ($[Fe/H]_{LMC} \approx -0.34$, $[Fe/H]_{SMC} \approx -0.68$ – Storm et al. 2011). Stellar evolutionary tracks show the blue loops to extend out to higher temperatures (and bluer colors) with decreasing metallicity. This extension of the blue loops would allow lower mass stars to undergo second and third crossings of the instability strip. Since stars of lower mass are relatively

more numerous, a region (or galaxy) of lower metallicity would naturally have more Cepheids of lower masses and shorter periods.

In addition to statistical studies of Cepheid pulsation periods, there are characteristic light curve behaviors to Cepheids of different periods. Cepheids with "short" and "long" periods display, for the most part, smooth light curves with a shorter-duration rise to maximum light and a longer-duration fall to minimum light (the 'saw tooth' pattern). Hertzsprung (1926) was the first to notice that Cepheids with periods primarily between ~6–16 days (but possibly even longer), however, display a "bump" on their lightcurves. At P ≈ 6 days, a small "bump" (local increase in brightness) appears at an appreciable distance (in phase-space) from maximum light, on the descending branch of the lightcurve, progressing up the descending branch (nearer maximum light) and becoming more prominent as the period of the Cepheid increases. The bump is very close to the phase of maximum light in Cepheids with ~9–12-day periods, proceeding down the ascending branch of the lightcurve as period increases further. The migration of the bump is called *the Hertzsprung progression*, and Cepheids within this period range, although still Classical Cepheids, are sometimes referred to as *Bump Cepheids* or *Bump Resonance Cepheids*.

Two proposed models to explain the Hertzpsrung progression are the echo model and the resonance model (hence the title of Bump Resonance Cepheids). In the echo model, pressure waves are generated within the Cepheid. The inward-traveling wave reflects (or echoes) off the stellar core, and then causes the bump as it reaches the stellar surface. In the resonance model, the bumps are the results of a resonance between second overtone and fundamental pulsations in the Cepheid. For a thorough discussion of the Hertzsprung progression and the proposed models, see Bono et al. (2000a). Fig. 6 shows the lightcurve of 5 selected Bump Cepheids. The gray line in each plot illustrates the approximate location of the bump and the black arrow indicates the direction of progression along the lightcurve (except in the case of VX Cyg where the bump is, in theory, no longer progressing).

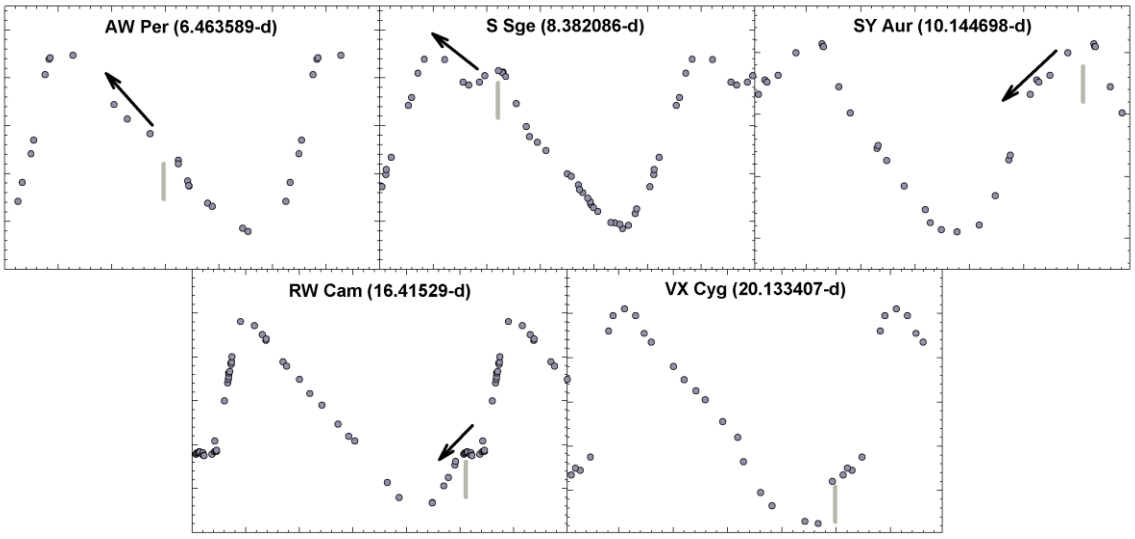

Figure 6 – The lightcurves for five selected Bump Cepheids are shown, (literature data obtained from the **McMaster Cepheid Photometry and Radial Velocity Data Archive** – http://crocus.physics.mcmaster.ca/Cepheid/) covering essentially the full period-span of the Hertzsprung progression. The gray lines under each lightcurve mark the phase of the bump maximum, and the black arrows indicate the direction (in phase-space) in which the bump is progressing.

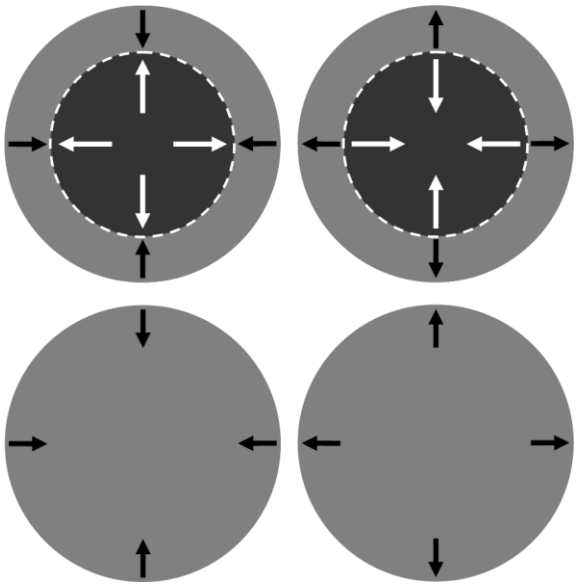

Figure 7 – Illustration of a first overtone pulsator (top row) vs. a fundamental pulsator (bottom row). Arrows indicate direction of pulsation, and the white dashed line shows the pulsation node inside a first overtone pulsator.

Among short-period Classical Cepheids (P < 5-days), there is another subgroup of stars. These Cepheids are generally characterized by smaller amplitudes (< 0.5-mag) and more symmetrical (sinusoidal) light curves (Luck et al. 2008). Their increased symmetry is responsible for their title as *s-Cepheids*. The *Secret Lives of Cepheids* (SLiC) Program (under which this thesis has been carried out – see Section 1.9 for program description) presently contains three s-Cepheids: Polaris (although still debated), SZ Tau and SU Cas. It has been suggested that s-Cepheids pulsate in the first-overtone mode and, where many s-Cepheids have indeed been found to be first-overtone pulsators, there are also some known fundamental mode s-Cepheids (see Luck et al. 2008). When dealing with the Cepheid Period-Luminosity law, s-Cepheids are usually treated as first-overtone pulsators. The 'simplest' pulsations that a Cepheid can undergo are the aptly named fundamental mode pulsations, where the entire star contracts and expands in unison (bottom row of Fig. 7). The first overtone differs from the fundamental mode in that there are two separate "shells" within the Cepheid which are pulsating in the opposite direction of each other – when one shell is expanding, the other is contracting, and vice versa. These shells are separated by what is called a "node" (white dashed line in top row of Fig. 7), with one shell expanding while the other contracts, and then vice versa. It is this opposite behavior between the shells that is responsible for the increased symmetry in first-overtone Cepheid lightcurves, causing them to appear more sinusoidal, and also results in lower luminosity amplitudes.

Although s-Cepheids and other first-overtone Cepheids share many common traits with fundamental mode Cepheids, they do not behave in exactly the same way. It has been discovered that first-overtone Cepheids, while following Period-Luminosity and Period-Radius relationships, do not follow the same relationships as fundamental mode Cepheids. This difference in behavior has played an important role in determining the true status of Polaris, a SLiC program star and argued to be an s-Cepheid pulsating in the first-overtone mode. Nordgren et al. (2000) used the Navy Prototype Optical Interferometer (NPOI) to directly measure the radius of Polaris to be 46 ± 3 $R_{\odot}$, using the original Hipparcos parallax of 7.56 ± 0.48 mas. For Polaris' observed period of ~3.97-d, this radius is too large for it to fit along the fundamental mode Period-Radius relationship. However, when the derived fundamental period of Polaris, 5.59-days, is used (applying a first-overtone/fundamental period ratio of 0.71 – Aerts et al. (2010), p. 12), the Cepheid fits nicely along the period-Radius relationship. The NPOI result would lend credence to the argument that Polaris pulsates in the first-overtone mode.

Cepheids are most often observed pulsating in either the fundamental or first-overtone modes. Higher overtone modes, and even "Beat Cepheids" that simultaneously pulsate in two or more pulsation modes, are also observed but are much rarer.

1.7 Photometric Properties of Cepheids

The strict periodicity of most Cepheids is perhaps the main characteristic that made them such intriguing and popular targets for early observers and is also partly responsible for their astrophysical importance as distance indicators. However, many Cepheids exhibit a change in period over time. The first record of this behavior seems to have been published by Eddington (1919) in his paper on δ Cep. In this paper, Eddington mentions earlier studies of a period change in δ Cep made by Chandler, but no publication could be found. There are now many Cepheids for which very rich datasets have been used to display and delineate period changes – some linear, and others possessing random, sometimes even repeating, period variations. The main analytical method of characterizing period changes in Cepheids is by constructing O–C diagrams. After a sufficient number of (most commonly) times of maximum light have been observed for a Cepheid, the behavior of the pulsation period can be understood by plotting the observed (O) times of maximum light minus those that are calculated (C) based on the assumption of a known, static period and essentially stable light curve shape. If an O-C diagram appears entirely linear, then the period used to generate such a plot is incorrect. If the O-C curve appears "concave up," then the period is increasing; and if the curve appears "concave-down," such as in SV Vul (a program Cepheid, which will be shown later), then the period is decreasing. Some different O-C curve "shapes" and their period variability implications are shown in Fig. 8. One small trend that has been noticed is that, on average, Cepheids with longer periods display greater changes in period per year. SV Vul, for example, with a pulsation period of ~45 days, undergoes a long-term period decrease of $dP/dt \approx -231$ sec/year. Finally, some O-C plots reveal cyclic changes in the period over time. These periodic changes may be the result of as yet unknown internal changes within the Cepheid, or they may also be the result of the Cepheid being in orbit with a companion star. In the latter case, the orbital motion of a Cepheid would produce a "light-time" effect in which the period would be seen to shorten and lengthen as the star moved towards or away from us.

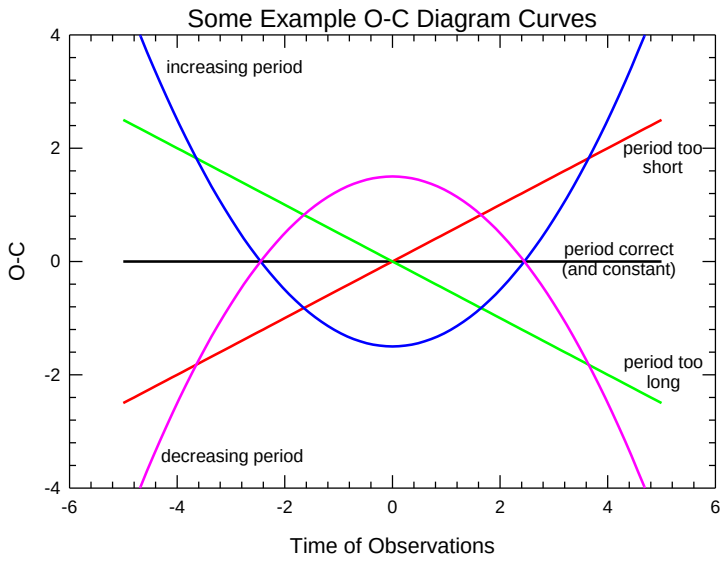

Figure 8 – An illustration of the various shapes that an O-C curve can have, and what basic information the shape can tell us about the period behavior of the variable star.

Cepheid period changes can also give information on the evolutionary state of the Cepheid, as shown in Turner et al. (2006). Specifically, the rate of period change can tell us which crossing of the instability strip the Cepheid is making (see Fig. 9), which is indeed valuable information to have. When looking at Fig. 3, one can see that as Cepheids cross the instability strip they undergo relatively large changes in average temperature as they pass from one edge of the strip to the other. With such temperature changes, one would expect accompanying luminosity changes. As this is not the case, we know that the average radius of a Cepheid also changes while it crosses the instability strip, to compensate for the temperature changes and result in a similar luminosity. When evolving towards the cool edge of the instability strip, the radius of a Cepheid increases, and when evolving towards the hot edge, the radius decreases. The effect of this evolution on pulsation period can be calculated. The basis of this calculation is the well-known period-density relationship for radially pulsating stars, such as Cepheids (Turner et al. 2006):

$$P\rho^{1/2} = \frac{PM^{1/2}}{[(4/3)\pi]^{1/2}R^{3/2}} = Q$$

where P is the pulsation period, ρ is the density, M is the stellar mass, R is the stellar radius and Q is the pulsation constant. The small period dependence $Q \propto P^{1/8}$ (Turner et al. 2006) is taken in to account. Next, the density can be substituted with $\rho = MR^{-3}$ and radius can be substituted using the standard stellar luminosity equation: $L \propto R^2T^4$ where L is the stellar luminosity and T is stellar temperature. It is thus determined that the period should increase as the radius increases

(evolving towards cooler temperatures) and the period should decrease as the radius decreases (towards hotter temperatures). The rate of period change, ΔP, can then be predicted through an equation of the form:

$$\frac{\Delta P}{P} = \frac{5}{8}\frac{\Delta L}{L} - \frac{5}{2}\frac{\Delta T}{T}$$

(the specific coefficients used here result from also including a mass-period relation $M \propto P^{0.4}$: Turner, private communication). Using this equation, in combination with stellar evolutionary tracks, the rates of period change for different crossings of the instability strip, as shown in Fig. 9, were calculated. For a thorough discussion of the evolutionary implications of Cepheid period changes, see Turner et al. (2006) and references therein. It is also very important to mention that, following Turner, the calculated period change rates assume that no mass loss is taking place and have also been calculated for the fourth and fifth instability strip crossings. However, as illustrated in Fig. 3 for a 7 $M_\odot$ star, modern evolutionary tracks do not display strip crossings beyond the third. Recent studies (Neilson et al. 2012b, 2012c) indicate that Cepheids theorized to be in the fourth or fifth instability strip crossing could in fact

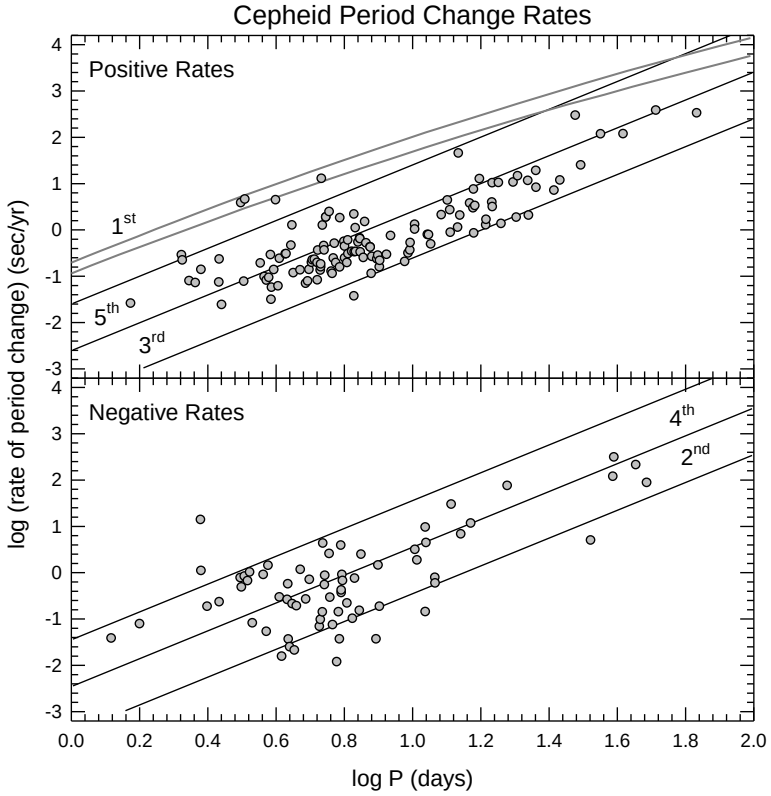

Figure 9 – Galactic Cepheids with known rates of period change, and the possible crossings of the Instability Strip indicated by such rates, as discussed in the text.

be in the second or fourth crossing (respectively), but undergoing enhanced mass loss that would result in larger period change rates. Therefore, period-change studies of Cepheids impact not only our understanding of the targets, but also of stellar evolution and the important topic of mass loss. If confirmed, enhanced rates of mass loss could explain the well-known Cepheid mass discrepancy, where masses calculated from pulsation properties are commonly (and significantly) smaller than those calculated from evolutionary codes (first discussed by Fricke et al. 1972; see Neilson et al. 2011 for a modern discussion). Recent efforts aimed at better understanding (and possibly resolving) this discrepancy concentrate on Cepheids that are members of binary systems, where mass determinations can be made free of either pulsation or evolutionary considerations (e.g. Evans et al. 2008, Pietrzyński et al. 2010).

In addition to period changes in Cepheids, there are also the very rare instances of amplitude changes. In fact, at the time of this publication, the only two Cepheids for which amplitude changes have been published are Polaris and V473 Lyr. Both Cepheids are seen as atypical, however, so trying to characterize their behaviors as applicable to a broad range of Cepheids would be difficult, at best. Polaris is a low amplitude Cepheid, whose true mode(s) of pulsation is still debated (recent results in favor of a fundamental mode are given by Turner et al. 2013). V473 Lyr has the shortest pulsation period of any known galactic Cepheid (~1.49-days), and also has the only *characterized* amplitude cycle (Stothers 2009). Until recently, Polaris had only been observed as undergoing an amplitude decrease, but newer studies have confirmed that Polaris' amplitude is now increasing again (Engle et al. 2004, Engle & Guinan 2012, Spreckley & Stevens 2008, Bruntt et al. 2008). However, given the length of time already covered by Polaris' amplitude changes to date, it appears that covering a full amplitude cycle (if a repeatable cycle exists) will unfortunately take decades of further data.

The closest possible analog for this behavior, from which a theoretical explanation might be extrapolated, would be the much better (yet still not fully) understood Blazhko effect in RR Lyr stars. RR Lyr stars also occupy the classical instability strip of the H-R diagram, but below and to the left (less luminous, but hotter) than the Cepheids (see. Fig. 1). Many RR Lyr stars are known to undergo variations in their pulsation periods and amplitudes. This behavior is termed the Blazhko effect, as it was first observed by Sergey Blazhko in the RR Lyr variable RW Dra (Blazhko 1907). The mechanism responsible for the Blazhko effect is still debated, but three possible sources have risen to prominence: 1) the resonance model, where resonating pulsation modes within the same star are responsible for the effect; 2) the magnetic model, where the geometric structure or alignment of the stellar magnetic field can augment the pulsations, and; 3)

a model where turbulent convection in the ionization zones within variable stars can periodically (or even randomly) vary in strength, and this variation in convective strength would then affect the pulsation amplitude. The third mechanism could also be the work of a stellar magnetic field (Stothers 2006). None of the mechanisms adequately account for every observed aspect of the Blazhko effect. Thus, more than a century after its discovery, the exact cause(s) of the effect is (are) still unknown.

1.8 Super-Photospheric Studies of Cepheids

The term "super-photospheric" is used in this paper to refer to the study of plasmas with temperatures well above that of the stellar photosphere. In terms of the Cepheids (and most other cool stars, for that matter), it specifically references activity originating from excited plasmas in the stellar atmospheres. The nearest example of super-photospheric activity in a cool star is, of course, the Sun. The solar atmosphere is broadly comprised of (in order of increasing distance from the photosphere): the chromosphere and transition region, where plasmas are magnetically heated to temperatures on the order of $10^4 - 10^5$ K, and then the corona, where temperatures extend into the million Kelvin (MK) range. Plasmas in the chromosphere and transition region are the dominant source of emission lines in the UV portion of the solar spectrum, where MK plasmas in the corona are the dominant source of X-ray emission. As such, both regions of the spectrum provide valuable diagnostics into their respective places of origin. Some valuable diagnostic emission lines in the UV region and their approximate formation temperatures (Haisch & Linsky 1976, Doschek et al. 1978 and Doyle et al. 1997) are: the N V λ1240 doublet (~2×10^5 K), C II λ1335 (~$4 - 5 \times 10^4$ K), O I λ1358 (~$1 - 2 \times 10^4$ K), the Si IV λ1400 doublet (~$6 - 8 \times 10^4$ K) and the C IV λ1550 doublet (~1×10^5 K). These emission lines represent a very wide range of temperatures and can offer a detailed look into a stellar atmosphere. In the Sun (and, again, most other cool stars), magnetic activity is the dominant heating mechanism of the outer atmospheres. However, other mechanisms also contribute to the overall heating, such as energetic particles and shocks released from microflare and nanoflare events near the solar photosphere (which are also a result of the magnetic field). The magnetic fields of the Sun and other cool stars are believed to be generated by a solar/stellar magnetic dynamo. The current dynamo model for the Sun is the *shear-interface model* (the α – ω model), where convective motion and differential rotation combine to twist, break and reconnect the once orderly solar magnetic field (caused simply by the large amount of conductive materials in motion throughout the solar interior). However, in certain cases (such as stars lacking strong enough differential rotation, but

possessing robust inward-outward motions) a *turbulent dynamo* (the α^2 model) can also produce similar magnetic fields and activity. For more information about these concepts see Noyes et al. (1984), Canfield (2003), Chabrier & Küker (2006) and Parker (2009). Note that this is simply a small selection of papers, as *numerous* references exist for the dynamo mechanism in cool stars. For variable stars undergoing robust radial pulsations, such as Cepheids, one must also consider the effects of such pulsations, not only on the stellar interiors and the possible dynamo mechanisms at work, but also on the possibility of the pulsations generating shocks which could propagate through the stellar atmospheres and contribute to the heating of plasmas.

The history of Cepheid super-photospheric studies is rather sparse (with most studies being ~30 years old or older) and, as a result, can sometimes go overlooked. The earliest of such studies appears to be that of Kraft (1957), who observed and analyzed the Ca II *H* (3968.5 Å) and *K* (3933.7 Å) emission lines in a large number (20+) of brighter Cepheids. These emission lines originate in plasmas with temperatures in the $8 - 15 \times 10^3$ K range; similar to temperatures found in the lower chromospheres of solar-type stars. Kraft noted that the Ca II *HK* emissions peaked in Cepheids around $\phi \approx 0.8 - 1.0$ (just after the Cepheid has begun to expand from minimum radius). Due to the star's expansion, a shock is expected to pass through the Cepheid photosphere at this phase, which is sometimes referred to as the "piston phase" of Cepheids. From this, Kraft concluded that "the transitory development of Ca II *H&K* emission in Classical Cepheids is associated with the appearance of hot material low in the atmosphere. These hot gases are invariably linked with the onset of a new impulse." Kraft also noted that the Ca II emissions were stronger in Cepheids with longer pulsation periods when compared to those with shorter periods. This important study laid the groundwork for Cepheid atmospheric studies, but the Ca II lines can only probe relatively cool atmospheric plasmas. More than two decades would pass before an investigation into the higher temperature plasmas of Cepheids was conducted.

Schmidt & Parsons (1982, 1984a,b) made the most thorough and revealing study of Cepheid atmospheres using spectra from the International Ultraviolet Explorer (IUE) satellite. The wavelength range of IUE (~1200 – 3200 Å) covers a number of important emission lines with temperatures of $10^4 - 10^5$ K, equivalent to those found in solar-type chromospheres and transition regions. In accord with the results of Kraft (1957), Schmidt & Parsons found these emissions to vary systematically with the pulsation phase, peaking shortly before maximum light (which is also shortly after minimum radius). Again, this is the phase where the stellar photosphere begins to expand. Lines normally associated with hotter, transition region temperatures were also found, but were not as strong as chromospheric emissions and were more easily contaminated by (what appeared to be, as discussed later) the Cepheid photospheric continuum in all but the longest

exposed (and ideally phase-space located) spectra. Still, the detections of such lines served as evidence that Cepheid atmospheres could be more complex (and possibly hotter), and that perhaps a more modern, and higher resolution, instrument could reveal such lines in a more concrete way.

A decade later, Böhm-Vitense & Love (1994) studied IUE archival spectra of the 35-day Cepheid ℓ Car with the purpose of trying to distinguish between line emissions from a solar-like magnetically heated chromosphere and transition region vs. those from an outward-moving shock. Böhm-Vitense and Love measured several emission lines present in the IUE spectra finding that, as with the Schmidt and Parsons studies, the emission line fluxes were variable in phase with the Cepheid pulsations. The line emissions also peaked at or near the phase of minimum radius, as found in other studies. Böhm-Vitense and Love concluded that an outward-moving shock must be at least partially responsible for the UV line fluxes and variability observed, because of the tight phasing of enhanced emissions just before maximum light, along with the excitation of the highly ionized C IV doublet prior to the excitation of the lower ionization C II. This is expected from a shock, as the higher temperatures required for C IV emission would be rapidly achieved. Then, after shock passage, the plasmas would cool down, allowing C II emissions to be observed. Unfortunately, the IUE observations did not cover the 0.8 – 0.9 phase-space, which prevented a detailed measure of the phase of maximum C IV emission, but it was still observed to peak earlier in phase than C II.

Motivated by these results, an analysis of FUSE (~920 – 1190 Å) spectra was carried out, and new observations were successfully proposed for. Sadly, although multiple FUSE observations of additional Cepheids were approved, just one observation (for β Dor) was carried out before the fatal failure of the mission's guidance system. The "FUSE Cepheid database" therefore includes only Polaris and β Dor (and only β Dor has multiple observations, but of somewhat poor phase coverage). However, both the C III 977Å and O VI 1032/1038Å line emissions were not only found in the spectra of both Cepheids, but were found to increase in strength at the piston phase of β Dor ($\phi \approx 0.8$, Engle et al. 2009). This result is in agreement with the phase of peak N V 1240 Å emission (N V forming at comparable, albeit slightly cooler, temperatures to O VI), found from our HST/COS observations (discussed later). The C III emission and variability was somewhat expected, given that it forms at similar temperatures (~ $5 – 10 \times 10^4$ K) to emission lines studied in the archival IUE spectra. However, the discovery of the O VI doublet was "a pleasant surprise," given that it forms in plasmas with temperatures of ~ $3 – 4 \times 10^5$ K (Redfield et al. 2002). The O VI lines were, at that time, the hottest plasma emissions observed from a Cepheid. This study raised the questions: just how hot is a Cepheid's outer atmosphere, and how is it being heated?

Given the phase-timing of the enhanced emissions, again the most plausible explanation is the formation of a shock that excites the atmospheric plasmas surrounding the photosphere. However, a pulsation-driven α^2 equivalent dynamo mechanism (Chabrier & Küker 2006) where the inward-outward convective motions are enhanced, or even replaced, by pulsational motions is also a viable and interesting alternative.

UV line emissions from 10^6 K (MK) plasmas are rare, typically weak, and only appear in the most active of stars (e.g. see Linsky et al. 1995 for a discussion of the coronal *Fe XXI* λ1354 Å emission line for Capella). Thus, to detect and study Cepheids at these high temperatures, X-ray observations are needed. The only pointed X-ray observations of Cepheids, prior to those carried out as part of this study, were those of the *Einstein Observatory* (*High Energy Astrophysical Observatory 2 – HEAO-2*) and the *Röntgen Satellite* (*ROSAT*). *Einstein* observations were approved for δ Cep, β Dor and Polaris, although no successful pointings on Polaris were ever achieved. Fig. 10 shows the Einstein Imaging Proportional Counter (IPC) images (taken in 1980/81) for the δ Cep and β Dor fields, with the Cepheids' approximate locations encircled. As the figures show, the Einstein satellite was unable to detect either Cepheid. However, the Einstein IPC did not have the sensitivity of later missions, and the exposures of δ Cep and β Dor are a mere 3563 and 838 seconds, respectively. Given the short exposures and low sensitivity, it was

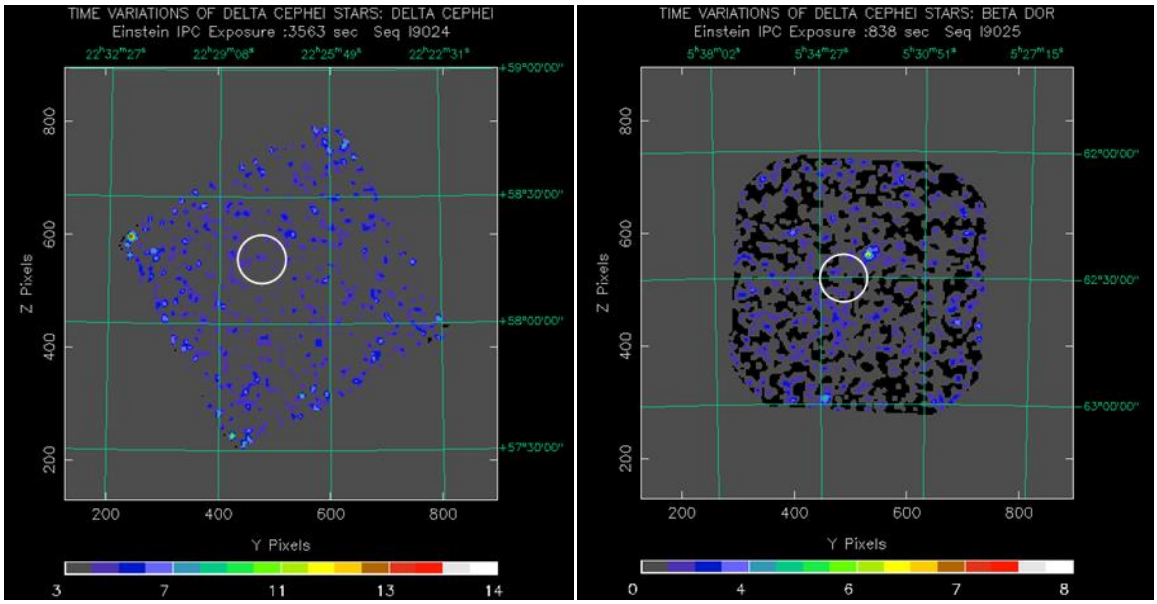

Figure 10 – Einstein IPC observations of δ Cep (left) and β Dor (right) are shown. The white circle in each image marks the location of the respective Cepheids. As can be seen, there are no detections of X-rays from either Cepheid above the noise level of the observations. This is not surprising, however, given the Cepheid distances and the short duration of the exposures.

quite possible that both Cepheids could in fact be weak, soft X-ray sources and yet still go undetected in the observations. The online Einstein catalog quotes upper limits on the log L_X values of δ Cep and β Dor as 29.1 and 29.4, respectively. However, X-ray activity in Cepheids was considered possible in papers such as Bejgman & Stepanov (1981) and Sasselov & Lester (1994). Their suggested mechanism was that shocks forming within the atmospheres of Cepheids and RR Lyrae stars could produce sufficient temperatures to excite and ionize heavy elements present in Cepheid atmospheres, producing soft X-ray activity. Another possible cause for X-ray activity in Cepheids is also linked to their pulsations. As a Cepheid pulsates, the elements within the atmosphere will undergo turbulent mixing and substantial motions. This could generate a "faux dynamo" (as previously mentioned) which would then generate soft X-ray activity. The "faux" quality of the dynamo is that the dynamo is not generated through convective transport, but rather through "pulsational transport." Despite such studies and theories, the failure of early efforts to detect X-rays with pointed observations reinforced the idea that Cepheids are not significant X-ray sources. Even with *log* $L_X \approx 29$ erg/s, the problem with detecting X-rays from Cepheids is that these stars (except for Polaris at ~133 pc – van Leeuwen 2007) are far away (d > 250 pc). Thus, they are expected to have relatively weak X-ray fluxes ($f_X < 10^{-14}$ ergs/s/cm$^{2)}$. Though Polaris was in fact detected on the 3σ level in a ROSAT High Resolution Imager (HRI) archival image (several years after the observation was carried out), a definitive detection of X-rays from Polaris and other "nearby" Cepheids had to wait for the arrival of powerful X-ray observatories like the X-ray Multi-Mirror Mission (XMM-Newton) and the Chandra X-ray Observatory, as discussed later.

1.9 Thesis: The *Secret Lives of Cepheids* (SLiC) program

The overall aim of this thesis is to expand our understanding of Cepheid variability. We look to do this by documenting previously unconfirmed or unknown behaviors in one of Astronomy's oldest and most important classes of variable stars. The thesis can be divided into two main studies: the optical study and the high-energy study.

For the optical study, ground-based photometry has been carried out for a selection of 10 bright Cepheids (δ Cep, η Aql, EU Tau, Polaris, SU Cas, SV Vul, SZ Cas, SZ Tau, VY Cyg and ζ Gem), selected primarily to represent a range of pulsation periods. However, target selection could also be influenced by: a long timeline of observations, which would aid in the study, or perhaps pre-existing evidence for the period/amplitude variability we are looking for. We combine our own photometry with that found in the literature for each Cepheid:

- Providing well-covered, modern, multi-band (either Johnson/Cousins *UBVRI* or Strömgren *uvby*) lightcurves for each Cepheid, from which new ephemerides have been calculated [note: *BV* photometry only has been carried out for Polaris, as discussed later]
- Extending O-C diagrams for each Cepheid and calculating a new rate of period change, if one is found,
- Studying the V-band (or equivalent) amplitudes of each Cepheid over time, to search for possible amplitude changes

In the high-energy (X-ray–UV) study new, high-quality UV spectroscopy has been carried out for Polaris, δ Cep and β Dor with the Cosmic Origins Spectrograph (COS) onboard the Hubble Space Telescope (HST), along with pointed X-ray observations from either the Chandra or XMM-Newton satellites. For this aspect of the study, the stars chosen represent some of the nearest Cepheids, important for efficiently achieving quality data from satellites where observing time is rather precious. In this study:

- The UV data will be analyzed to improve upon the studies of Schmidt and Parsons and Böhm-Vitense and Love and give further insights into the mechanism(s) responsible for the super-photospheric activity
- The X-ray data will be analyzed to confirm X-ray activity in Cepheids other than Polaris, to establish the temperature of the X-ray emitting plasmas and also to search for possible X-ray variability in addition to that of the UV emission lines

To conclude, we will summarize the work done and the results obtained. We will discuss the implications of the work, and possible explanations for the results. We will also outline what future work we have planned, and would like to undertake, in order to achieve the fullest understanding possible of the Secret Lives of Cepheids.

CHAPTER 2 – THE OPTICAL STUDY

2.1 Instrument and Observing Method

All of the Cepheids studied here are bright enough to be well-suited for photoelectric photometry. Many would quickly saturate CCD detectors, making the selection and accurate measure of nearby comparison stars very difficult. Also, every target has been the subject of multiple other photoelectric studies in recent decades. Choosing to continue with photoelectric photometry for this program allows the issue of target brightness to be easily handled, and also allows a more direct comparison to previous studies.

The overwhelming majority of the Cepheid photometry obtained in this program comes from the *Four College Automatic Photoelectric Telescope* (FCAPT) housed at *Fairborn Observatory* (Observatory Director – Lou Boyd). The observatory is located roughly 15-km SSE of Patagonia, AZ (observatory coordinates: 31º23'11.8" N 110º41'40.5" W), and at an elevation of ~1723-m. The FCAPT is a classical Cassegrain design with a 0.75-m (30-inch) f/2 primary mirror and a 0.2-m (8-inch) f/8 secondary. The FCAPT mount is a custom-made horseshoe symmetrical design. The telescope is controlled by a 2.8 GHz Pentium 4 computer running Red Hat Linux 5.2, which uses ATIS software for telescope operation. The photometer head consists of (in order of light path): fused silica entrance window; diaphragm wheel; ND filter wheel; flip mirror; fused silica fabry lens; two 10 position bandpass filter wheels; Hamamatsu R943-02 photomultiplier operating at 1750 volts with a divide by 4 prescaler and a 16-bit counter read every 0.1-seconds. "Geneva" statistics (Hayes et al. 1988) are provided for each integration to help detect APT problems. Total integration time is selected in ATIS. The flip mirror turns 180 degrees to select a 25-mm f/0.95 relay lens and a Panasonic GP-MF602 integrating video camera for acquisition and centering, using an Imagenation CX-100 frame grabber. Integrating time and filter are calculated from V and $B–V$ data for each target.

Table 1 gives the available filters and selectable settings for each of the five wheels. One position from each of the five motors (wheels) must be selected for every observation. These settings are determined by the operating system from information in the ATIS input file. There is a sixth stepper in the photometer head which focuses the CCD camera. The entire interior of the photometer head including the filters, PMT, and CCD camera is cooled using a shared 4º C recirculating water chiller. The photometer head is also flooded with -30º C dew point air from a site air drier to prevent condensation.

The FCAPT requires no on-site observer, making it an excellent facility for the long-term monitoring of variable stars. It automatically observes targets from a list maintained and

prioritized by astronomers at institutions with dedicated access to the telescope. Observations were carried out in a very usual fashion for photoelectric set-ups, with variable star measures being bracketed by comparison, check and sky measures (all 10-second integrations): *sky – comp – check – var – comp – sky – var – comp – sky – var – check – comp – sky* being the general order when a night included 3 measures of the variable star. Between 3 and 5 measures of the variable star would be carried out in a single run, depending on the available telescope time in a given night. Also, anywhere from 1 to 3 separate observing sequences would be carried out per Cepheid, per night, again depending on available telescope time, but also depending on the length of the Cepheid's period. More than one run per night would often be carried out on Cepheids of shorter periods, to more efficiently fill in the lightcurves. The photometric filters used in this program were designed to match, as closely as possible, the Johnson/Cousins *UBVRI* and Strömgren *uvby* systems. Cepheids were observed in either system based on brightness and/or photometric history (i.e. which system featured more prominently in the literature for each Cepheid). In the case of brighter Cepheids, either the Strömgren system was used or, if the Johnson/Cousins system was preferred, attenuating (neutral density) filters were also employed to mitigate saturation effects.

Table 1 – Wheel Settings for the 0.8-m *Four College Automatic Photoelectric Telescope* (FCAPT)

Wheel #1 – Diaphragm		**Wheel #4 – Filter Wheel 1a**	
Position 1	15 arcmin opening	Position 0	Clear
Position 2	90 arcsec opening	Position 1	*U*
Position 3	60 arcsec opening	Position 2	*B*
Position 4	45 arcsec opening	Position 3	*V*
Wheel #2 – Flip Mirror		Position 4	*R*
Position 0	CCD	Position 5	*I*
Position 1	PMT	Position 6	*u*
Wheel #3 Neutral Filter Wheel		Position 7	*v*
Position 1	Clear	Position 8	*b*
Position 2	1.25-mag	Position 9	*y*
Position 3	2.5-mag	**Wheel #4 – Filter Wheel 1b**	
Position 4	3.75-mag	Position 1	Clear
Position 5	5.0-mag	Position 2	*Hβ-wide*
		Position 3	*Hβ-narrow*
		Position 4	*Hα-wide*
		Position 5	*Hα-narrow*
		Position 6	Clear
		Position 7	Opaque
		Position 8	*Wing1 A*
		Position 9	*Wing2 B*
		Position 10	Clear

A photometric reduction program written by George McCook (Villanova U.) has been used on FCAPT data since the mid-1990s. The program automatically converts from local time to Heliocentric Julian Date, and also includes atmospheric extinction corrections (coefficients given in Table 2). *UBVRI* and *uvby* standard stars were also observed with the FCAPT, covering a wide range of colors (spectral types). Using the standard star data, instrumental magnitudes were then transformed into standard magnitudes for each Cepheid. A final transformation was then applied to convert Stromgren *y*-mag into Johnson *V*-mag. The transformation equations used in this study are given in Table 3.

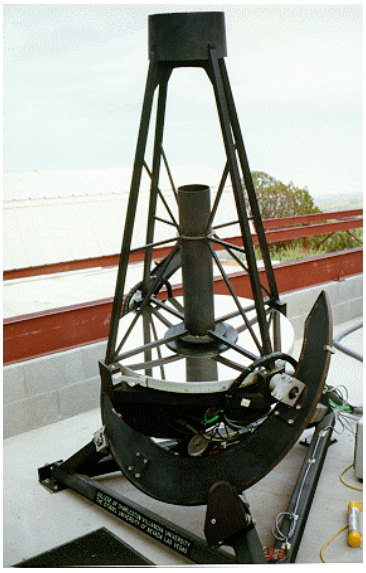

Figure 11 – The FCAPT installed at the Fairborn Observatory.

Table 2 – Average Extinction Coefficients for Filters Used in This Study

	U	*B*	*V*	*R*	*I*
Johnson/Cousins	0.659	0.385	0.237	0.19	0.143
	u	*v*	*b*	*y*	
Strömgren	0.503	0.286	0.176	0.129	

Table 3 – Photometric Transformation Equations for the FCAPT

UBVRI	***uvby***
$U = u + 0.0015 + 0.0491(U–B)$	$u = u' – 0.1538 + 0.1192(u–v)$
$B = b + 0.0125 – 0.0179(B–V)$	$v = v' + 0.0091 + 0.0008(v–b)$
$V = v + 0.0106 – 0.0262(B–V)$	$b = b' – 0.0947 + 0.2148(b–y)$
$R = r + 0.1382 – 0.4611(V–R)$	$y = y' – 0.0233 + 0.0530(b–y)$
$I = i + 0.1537 – 0.5444(R–I)$	
$(U–B) = -0.0111 + 1.1402(u–b)$	$(u–v) = -0.02632 + 1.004(u'–v')$
$(B–V) = 0.0115 + 0.9875(b–v)$	$(v–b) = 0.1131 + 0.8448(v'–b')$
$(V–R) = -0.0473 + 1.3340(v–r)$	$(b–y) = -0.07307 + 1.194(b'–y')$
$(R–I) = -0.0037 + 1.0495(r–i)$	
Strömgren *y* to Johnson *V*	
$V = y – 0.12[(b–y) – 0.55]^2$ (Budding & Demircan 2007, p. 94)	

The FCAPT has a limitation, however, in that the telescope mount does not provide sufficient space for the instrument cluster to allow the telescope to slew above a declination of approximately 76º. Accordingly, Polaris could not be observed with the FCAPT. Originally, Polaris was observed with a photoelectric telescope on the campus of Villanova University, through a filter designed to match the Strömgren *y*-band. Data output from this telescope was also designed so that it could be run through the reduction program of the FCAPT. However, this telescope suffered a hardware crash in 2006, and was retired. In the second half of 2009, AAVSO observer David Williams carried out photoelectric V-band photometry. Finally, collaborator Richard Wasatonic (Villanova U.) kindly agreed to carry out photoelectric *BV* photometry of Polaris beginning in late 2010, and continues to do so.

2.2 Data Analysis for the Optical Study

Each Cepheid in the Optical Study was observed with the goal of obtaining a fully-covered (i.e. to be considered for this study, the phases of minimum and maximum light must be well-detailed) light curve in each observing season. Therefore, high-priority was given to a Cepheid during phases near maximum and minimum light. The minimum criteria were set to allow both products of the light curve to be realized: the time of maximum light and the V-band light amplitude (to facilitate comparison with the oldest, visual observations). Both products were determined by running a Fourier series fit to the standardized, phase-folded photometry. The Fourier series used was of the form:

$$m(\varphi) = A_0 + \sum_{n=1}^{N} A_n \cos[2\pi n(\varphi) + B_n]$$

where $m(\varphi)$ is the calculated magnitude at a given phase, φ. A_0 is the mean magnitude of the light curve, and N is the final order of the fit. Finally, A_n and B_n are the amplitude and phase of the n^{th} order, respectively. For each observed light curve, a synthetic light curve was built from the fitted Fourier coefficients. The synthetic maximum and minimum magnitudes were used to calculate the overall light curve amplitude, and the offset of the nearest observation to the synthetic phase of maximum light was used to calculate the observed time (HJD) of maximum light. Due to the various observational hindrances, primarily stretches of inclement weather or mechanical difficulties during the prime observing season of specific Cepheids, a fully-covered light curve could not be obtained for every target, every year. For almost all Cepheids, multiple fully-covered light curves we obtained.

Literature searches were conducted for all observed Cepheids to obtain these products from archival, fully-covered light curves. Depending on the source quality (e.g. phase-coverage of the

light curve, level of details given in the study [standardizations, observations techniques], etc.), amplitudes and times of maxima were either quoted directly from the source study, or re-determined by Fourier series fit. For each target's O-C diagram, archival data was obtained from the reference given in the stellar properties table (after "Ephemeris for O-C diagram"). For consistency with each source of O-C data, the diagrams presented here either calculate individual errors for the data points, or use a weighting scheme. The plots with error bars indicate studies where individual errors were calculated. For the plots without error bars, a weighting scheme was employed in the following fashion: early visual or photographic measures were weighted 0.5 – 1, and modern photoelectric measures were weighted 2 – 3, with the specific weight depending primarily on the phase-coverage at and around maximum light. For amplitude vs. time plots, errors were determined for recent measures in standard photometric systems (i.e. after the introduction and wide adoption of the Johnson photometric system) and for earlier data sets where individual observations were made accessible. This study aimed to employ a more objective method of error estimation that would account for both the observational scatter and the phase coverage near times of maximum and minimum light. To do this, an appropriate Fourier series order was first determined for each target. Then, Fourier series fits of neighboring orders were run. The standard deviation of these fits was calculated, and assigned as the error for each amplitude value.

2.3 δ Cep

The prototype of all Cepheids, δ Cep is also the 14th variable star ever discovered (http://spider.seds.org/spider/Vars/vars.html), and the 2nd Cepheid for which light variations were observed. It is also currently the 2nd nearest Cepheid (only Polaris is nearer), and the member of a wide binary system with HD 213307 at a projected distance of 40" away from the Cepheid. The companion is an A0-type star (T_{eff} ≈ 10,048 K) according to Prugniel et al. (2007), or a B7 – B8 III – V star with its own F0-type companion, according to the HST parallax study of Benedict et al. (2002). Further, δ Cep is a member of the Cep OB6 star cluster (de Zeeuw et al. 1999), along with the cooler and more luminous K1.5Ib star ζ Cep. Majaess et al. (2012) found the cluster-derived distance of 277 ± 15-pc to agree well with distances derived from other methods, including that from the HST parallax given in Table 4, along with selected other relevant properties of δ Cep (Table adapted from Matthews et al. (2012) and references therein). δ Cep displays the typical "saw tooth" lightcurve, with a quicker rise to maximum brightness, and a much slower fall to minimum brightness, as shown in Fig. 12. The overall form of this variability is mirrored by the color indices.

Table 4 – Relevant Stellar Properties of δ Cep

Spectral Type	F5Ib – G1Ib[1]
T_{eff} (K)	5500 – 6600[1]
Mass (pulsational) ($M_{\odot}$)	4.5 ± 0.3[2]
Mass (evolutionary) ($M_{\odot}$)	5.7 ± 0.5[2]
Mean Luminosity ($L_{\odot}$)	~2000[3]
Mean Radius ($R_{\odot}$)	44.5[3]
Distance (pc)	273 ± 11[4]
Ephemeris (this study) 2455479.905 + 5.366208(14) × E	
Ephemeris for O-C diagram (Berdnikov et al. 2000) 2412028.956 + 5.3663671 × E	

[1]Andrievsky et al. (2005); [2]Caputo et al. (2005); [3]Matthews et al. (2012); [4]Benedict et al. (2007)

Photometry gathered as part of this program started in December, 2007, and provided well-covered light curves at two separate epochs. Fourier analysis of the resulting light curves yielded two times of maximum light, which were added to those found in the literature (Berdnikov et al. 2000), and are presented as the red data points in Fig. 13. As can be seen from the "concave down" parabolic shape of the O-C curve, the period of δ Cep is decreasing over time. From a quadratic fit to the O-C data, the rate of period change is calculated to be −0.100565 ± 0.000172 sec/yr. According to Turner et al. (2007), this rate would mean that δ Cep is currently making its second crossing of the instability strip. The parameters of the quadratic fit to the O-C data are shown in Fig. 13.

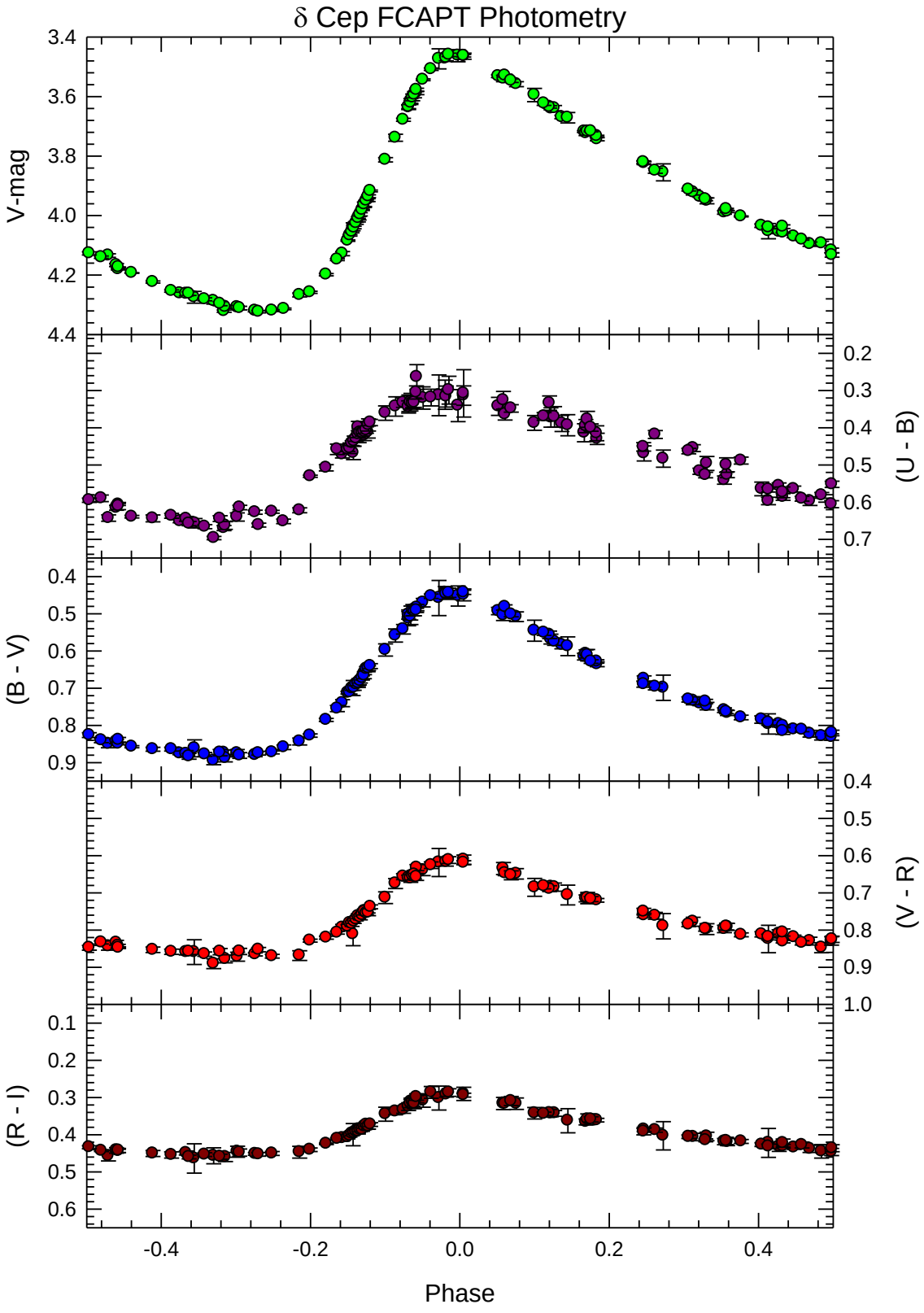

Figure 12 – The *UBVRI* data obtained for δ Cep, phased to the new ephemeris determined in this study (given in Table 4).

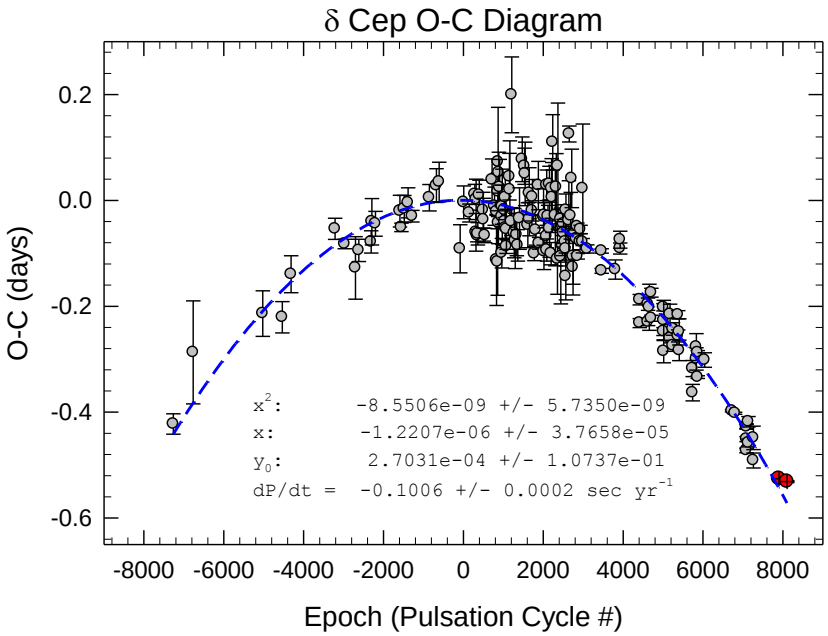

Figure 13 – The O-C diagram for δ Cep, showing the decreasing trend in its pulsation period. Coefficients of the quadratic fit are given in the plot, along with the rate of period change (dP/dt = -0.1006 sec/yr). The O-C points determined from light curves obtained as a part of this program are plotted as the red filled and crossed circles.

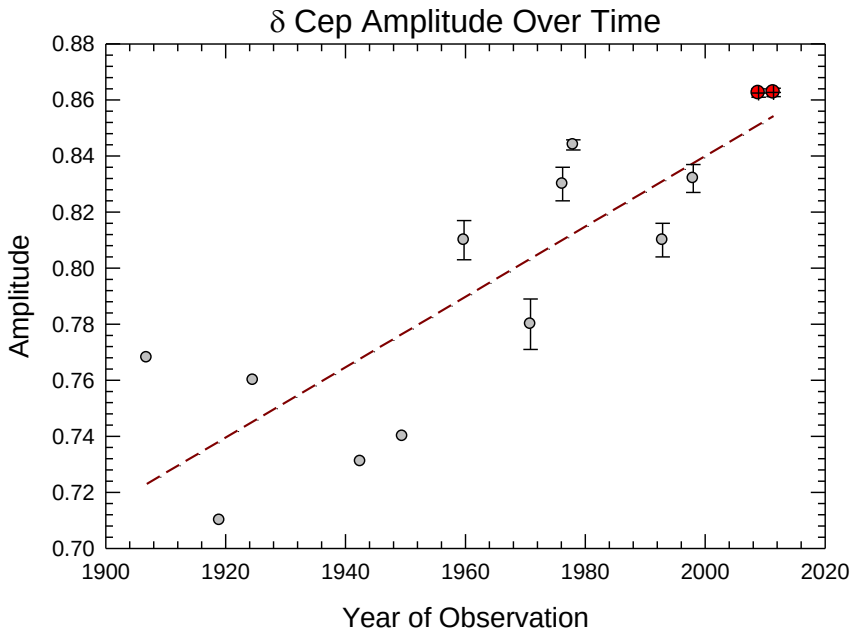

Figure 14 – The observed light amplitudes of δ Cep are plotted vs. the mid-time of the observation set. Points measured as part of this program are indicated by red crosses.

Brightness variability amplitudes were also obtained for the two light curves, and compared to those from archival observations deemed to be of high reliability. The results are shown in Fig. 14, where it can be seen that the light amplitude of δ Cep appears to be increasing over time. If a simple linear trend is assumed, as is plotted in the figure, then the light amplitude of δ Cep appears to be increasing at dA/dt = 1.3-mmag per year. The sparseness of amplitude measures prevents a detailed investigation of possible short-term amplitude variations, although there is a slight hint of amplitude periodicity on a timescale of ~20 – 25 years. It bears repeating, though, that this is only speculation at this point, thanks to the sparse dataset.

2.4 η Aql

η Aql is the 12th variable star discovered, and the 1st Cepheid for which light variations were observed. With a pulsation period of ~7.2-days, η Aql is an excellent example of a "bump Cepheid," displaying a prominent Hertzsprung bump in the middle of the descending phase of its light curve (around $\phi \approx 0.33$), as shown in Fig. 15. As with δ Cep, η Aql is known to have a hot companion of spectral type B9.8 V (Evans 1991), which was recently resolved with HST to lie 0.7" from the Cepheid (Evans 2011).

Table 5 – Relevant Stellar Properties of η Aql

Spectral Type	F7Ib – G2Ib[1]
T_{eff} (K)	5300 – 6400[2]
Mass (pulsational) ($M_\odot$)	4.1 ± 0.4[3]
Mass (evolutionary) ($M_\odot$)	5.7 ± 0.6[3]
Mean Luminosity ($L_\odot$)	~2500
Mean Radius ($R_\odot$)	~49
Distance (pc)	424^{+330}_{-130}
Ephemeris (this study) 2455856.689 + 7.177025(86) × E	
Ephemeris for O-C diagram (Berdnikov et al. 2000) 2411999.693 + 7.1765468 × E	

[1]Kraft (1960); [2]Luck & Andrievsky (2004); [3]Caputo et al. (2005); Neilson et al. (2012a); van Leeuwen (2007)

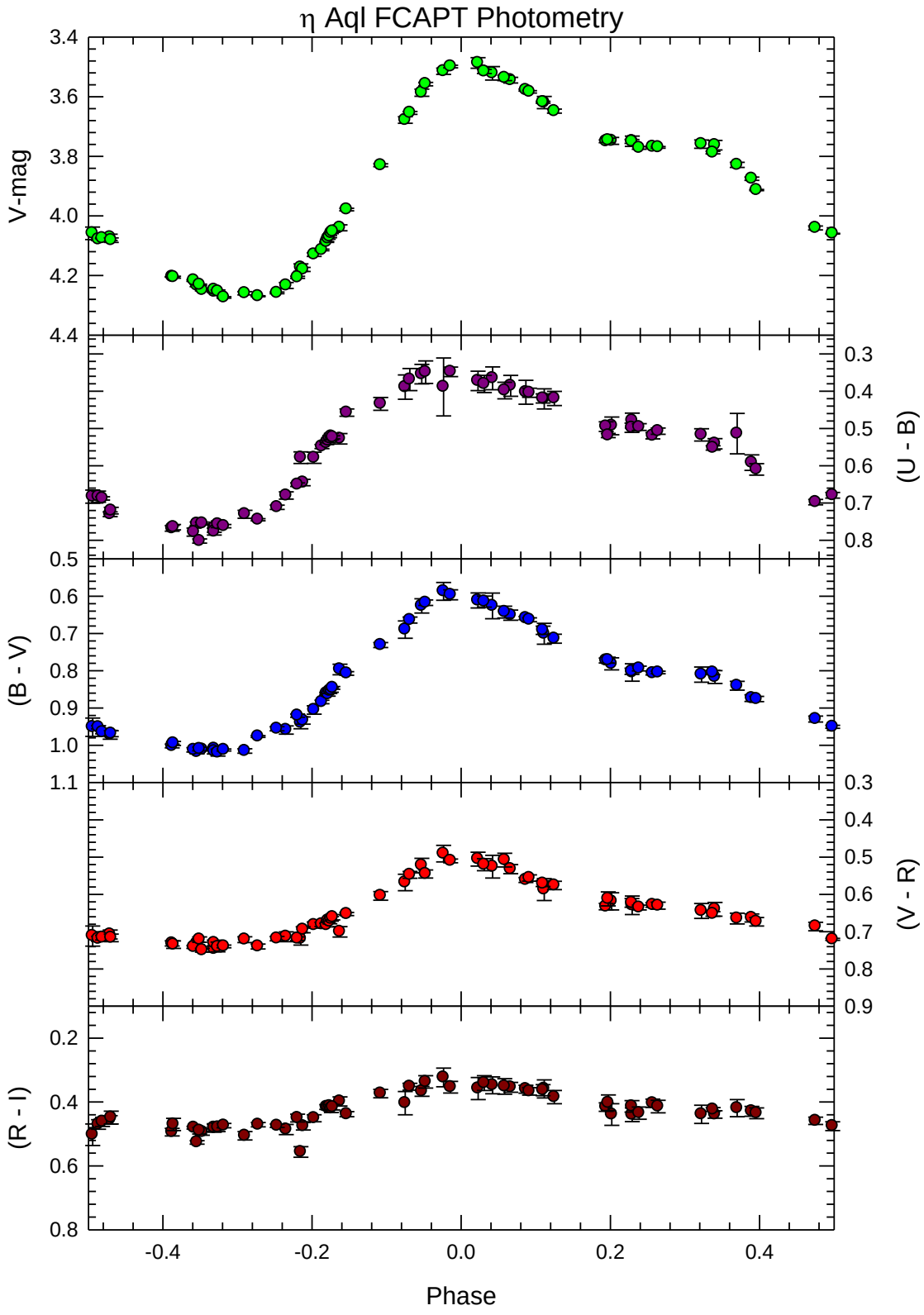

Figure 15 – The *UBVRI* data obtained for η Aql obtained with the FCAPT, phased to the new ephemeris determined in this study (given in Table 5).

A more recent addition to the program, with photometry beginning in June of 2008, one fully-covered light curve of η Aql has been obtained thus far. The Fourier-obtained time of maximum light is plotted in Fig. 16, along with times of maximum light found in the literature (Berdnikov et al. 2000). As shown by the O-C curve, the pulsation period is steadily increasing over time. The rate of period change is calculated to be $dP/dt = 0.255 \pm 0.001$ sec/yr, indicative of a Cepheid undergoing its third crossing of the instability strip (Turner et al. 2007).

The light amplitude of η Aql, when plotted with those found in the literature (Fig. 17), appears to show no coherent variability patterns, either short- or long-term. It's possible that the amplitude of η Aql has remained essentially constant since the time of its discovery.

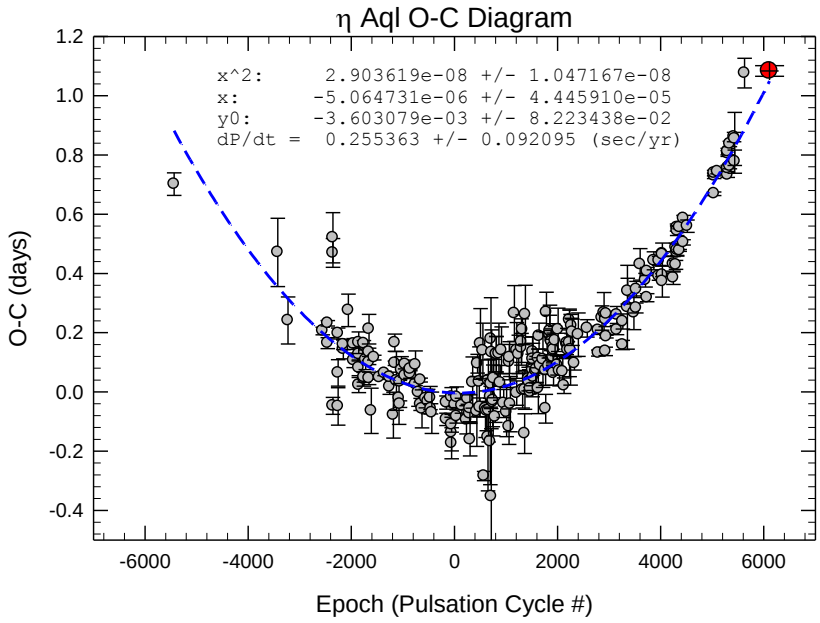

Figure 16 – The O-C diagram for η Aql, showing the increasing trend in its pulsation period. Coefficients of the quadratic fit are given in the plot, along with the rate of period change (dP/dt = 0.255 ± 0.001 sec/yr). The point determined from data obtained as a part of this program is plotted as the red filled and crossed circle.

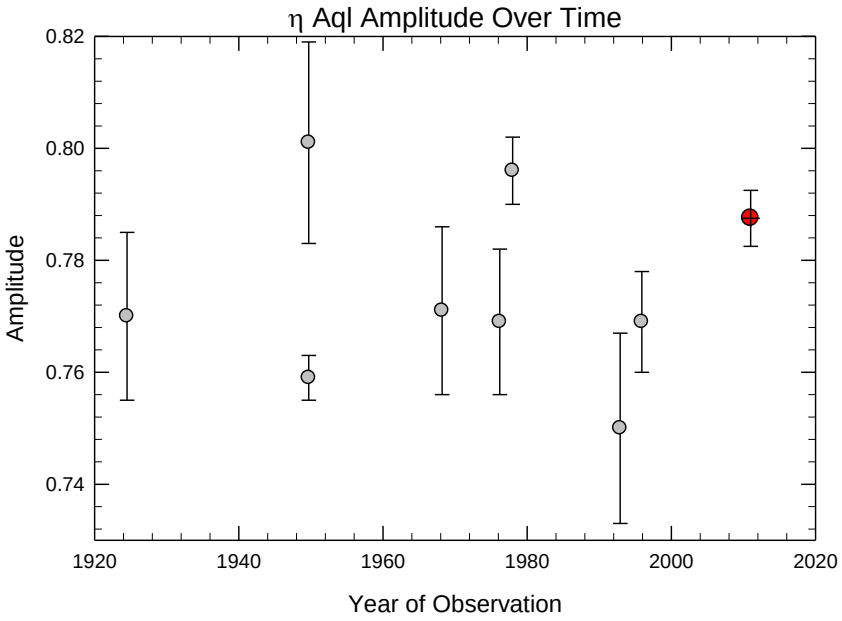

Figure 17 – The observed light amplitudes of η Aql are plotted vs. the mid-time of the observation set. Points measured as part of this program are indicated by red crosses.

2.5 EU Tau

EU Tau is a somewhat "newer" Cepheid, especially in terms of those in this program. This is because earlier studies concluded EU Tau was a W UMa-type variable, until Guinan (1966, 1972) discovered that it was a Cepheid. With its modest V-band amplitude of ~0.32-mag, and more symmetrical light curve (Fig. 18), EU Tau is classified as an s-Cepheid by studies such as Andrievksy et al. (1996), who also suggested that EU Tau could not be in its first crossing of the instability strip, given that it is carbon-deficient. The revised *Hipparcos* parallax for EU Tau is 1.17 ± 1.04 mas. This is an extremely large error, but understood given the distance of the Cepheid. Therefore, the distance calculated by Gieren et al. (1990) is given in Table 6. EU Tau has an unresolved, hot companion of spectral type A1 – A2 V (Kovtyukh et al. 1996).

Table 6 – Relevant Stellar Properties of EU Tau

Spectral Type	F5II – G5II[1]
T_{eff} (K)	~6200 – 6600[2]
Mass (pulsational) ($M_{\odot}$)	4.55 ± 0.54[3]
Mass (evolutionary) ($M_{\odot}$)	4.95 ± 0.2[3]
Mean Luminosity ($L_{\odot}$)	~1040[3]
Mean Radius ($R_{\odot}$)	~30[3]
Distance (calculated – pc)	1191 ± 57[3]
Ephemeris (this study) 2455618.816 + 2.102299(15) × E	
Ephemeris for O-C diagram (Fernie 1987) 2442583.623 + 2.1025112 × E	

[1]Buscombe & Foster (2001); [2]Bersier et al. (1997); [3]Gieren et al. (1990)

One fully-covered light curve was obtained in this program for EU Tau, and the time of maximum light was added to those found in, or determined from, the literature. As shown in Fig. 19, the period of EU Tau is not constant. A quadratic fit has been run through the data, which assumes a steadily decreasing period, but it is important to note that, due to the large data gap before the observations of Peña et al. (2010), this assumption may not hold true. It is entirely

possible that, between the observations of Berdnikov (2008) and Peña et al. (2010), an abrupt change in the period took place. The period could have been constant before the observations of Berndnikov, then shifted, and will now continue for some time at its current, slightly shorter value. If the star does have a steadily decreasing period, the quadratic fit returns a period change rate of $dP/dt = -0.336897 \pm 0.001724$ sec/yr. This value is one possibility due to the sparseness of recent data but, if true, would indicate that EU Tau is undergoing its fourth crossing of the instability strip (albeit with a rather quick period change rate for short-period, fourth crossing Cepheids – Turner et al. 2007). This would agree with the finding of Andrievksy et al. (1996).

A single light amplitude was also determined for EU Tau and plotted against those found in, or determined from, the literature (Fig. 20). A linear trend of dA/dt = -0.2-mmag per year has been run through the data; however, we note that the overall spread in the amplitudes is very small, and within the measurement errors. Thus, it is also likely that EU Tau has undergone no significant change in amplitude.

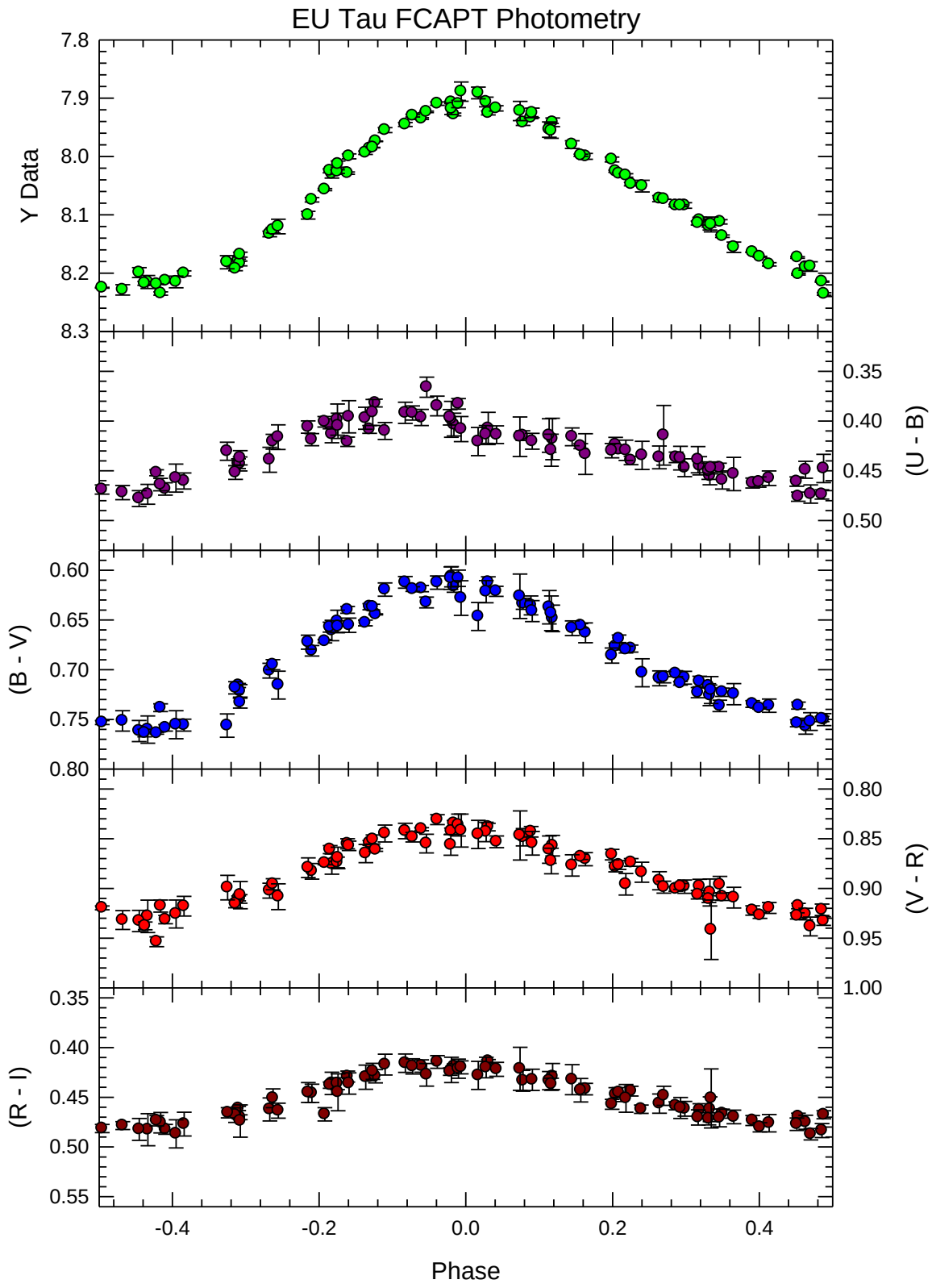

Figure 18 – The *UBVRI* data obtained for EU Tau, phased to the new ephemeris determined in this study (given in Table 6).

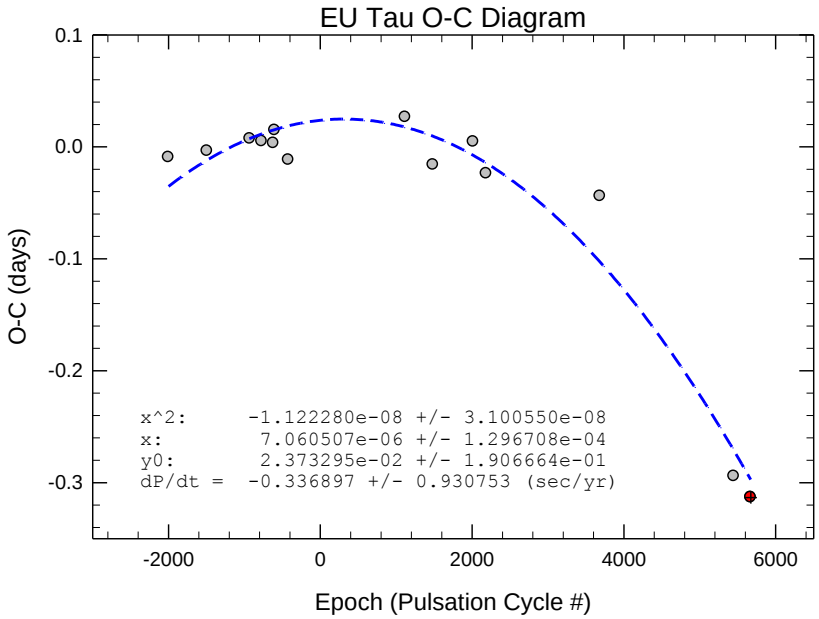

Figure 19 – The O-C diagram for EU Tau. Given the large, recent gap in the data, an unambiguous conclusion cannot be determined. The period of the Cepheid could be smoothly decreasing, as with δ Cep (which is the behavior assumed by the fit), or the Cepheid could have undergone a sudden shift to a shorter period. Coefficients of the quadratic fit are given in the plot, along with the rate of period change (dP/dt). The point determined from data obtained as a part of this program is plotted as the red filled and crossed circle.

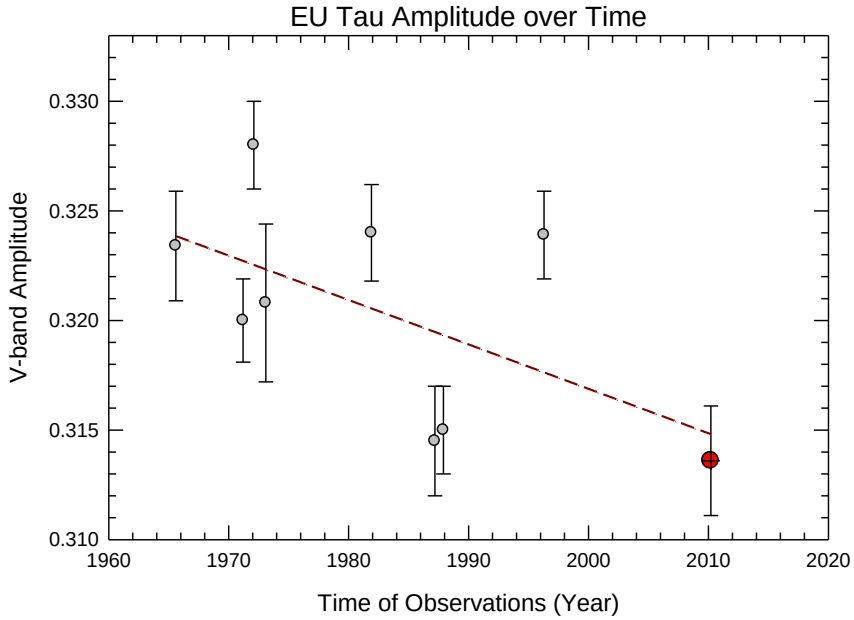

Figure 20 – The observed light amplitudes of EU Tau are plotted vs. the mid-time of the observation set. Points measured as part of this program are indicated by red crosses.

2.6 Polaris

Polaris is best known as the North Star, since it is easily visible to the naked eye and lies within 1° of the north celestial pole. Numerous literary references to Polaris have been made throughout history, with many remarking on its constant, steady nature (referring to its essentially static location) as a quality that can be aspired to in humans. Perhaps the most famous quote is that of Julius Caesar who, in Shakespeare's 1599 play *The Tragedy of Julius Caesar*, boasts:

But I am constant as the northern star,
Of whose true-fix'd and resting quality
There is no fellow in the firmament.
The Tragedy of Julius Caesar (III, i, 60-62)

However, in the latter half of the 19th century the "constant" nature of Polaris was becoming suspect. Hertzpsrung (1911) then confirmed the periodic variability of Polaris, and compared several aspects of it to the Cepheids. Since then, numerous photometric studies have been conducted of Polaris. By far the nearest Cepheid (δ Cep is second nearest, and lies at twice the distance), Polaris is also considered somewhat special among Cepheids because the amplitude of its brightness variation is very low (currently ~0.06-mag – Fig. 21). In fact, the original motivation for the *Secret Lives of Cepheids* program was the study of Arellano Ferro (1983), where the (surprising) declining light amplitude of Polaris was first reported. Since then, numerous studies have confirmed and expanded on this behavior, including a very thorough analysis by Turner et al. (2005). Polaris has what appears to be a very accurate revised *Hipparcos* parallax of $\pi_{Hipp} = 7.54 \pm 0.11$-mas, but doubts still exist as to Polaris' true distance, and whether it is a fundamental mode or an overtone pulsator. One reason for the doubts is the difference between the spectroscopically derived absolute magnitude of $M_V \approx -3.0$ for Polaris (Kovtyuhk et al. (2010), and the value of around $M_V \approx -3.6$ that is calculated using parallax values (thus the spectroscopic magnitude implies that Polaris is closer than the parallax value indicates).

In addition to the changes in Polaris' amplitude, and questions about its precise distance and pulsation mode, the period of Polaris' pulsations is increasing. Fig. 22 shows the O-C data for Polaris, with our own times of maximum light (red filled, and crossed, circles) added to those of Turner et al. 2005 and Spreckley & Stevens (2008). The newly calculated rate of period change is currently $dP/dt = 4.47 \pm 0.08$ sec/yr (Fig. 22), which is quicker than most other Cepheids of similar period, suggesting that Polaris is currently evolving through the short-lived and rarely-observed first crossing of the instability strip.

The declining nature of Polaris' light amplitude prompted further questions. Arellano Ferro (1983) theorized that Polaris might have been evolving out of the instability strip and, therefore,

on its way toward becoming a non-variable supergiant. Subsequent studies, such as that of Fernie et al. (1993), entitled "Goodbye to Polaris the Cepheid", support the theory. However, observations taken as part of this program beginning in the early 2000's indicated that Polaris' light amplitude had not only stopped decreasing, but appeared to begin increasing again (Davis et al. 2002; Engle et al. 2004; Engle & Guinan 2012). Additional studies (Turner et al. 2005 and Spreckley & Stevens 2008) have since supported the original claim. Fig. 23 shows the amplitudes of Polaris going back over a century (from Turner et al. 2005) with the amplitudes observed as part of this program plotted as red filled and crossed circles. The "return" of Polaris' amplitude hints at the possibility of a cycle, as opposed to a simple decline, but more years of observation will be required before a full understanding of Polaris' variable amplitude can be achieved

Table 7 – Relevant Stellar Properties of Polaris

Spectral Type	F7 – F8 Ib–II[1]
T_{eff} (K)	~6000 – 6050[2]
Mass (pulsational) ($M_{\odot}$)	4.5 ± 2.0[3]
Mass (evolutionary) ($M_{\odot}$)	5.8 ± 0.5[3]
Mean Luminosity ($L_{\odot}$)	~2200[4]
Mean Radius ($R_{\odot}$)	~46[3]
Distance (pc)	133 ± 2[5]
Ephemeris (this study) 2455909.910 + 3.972433(520) × E	
Ephemeris for O-C diagram (Turner et al. 2005) 2428260.727 + 3.969251 × E	

[1]Wielen et al. (2000); [2]Turner et al. (2013); [3]Nordgren et al. (2000); [4]Spreckley & Stevens (2008); [5]van Leeuwen (2013),

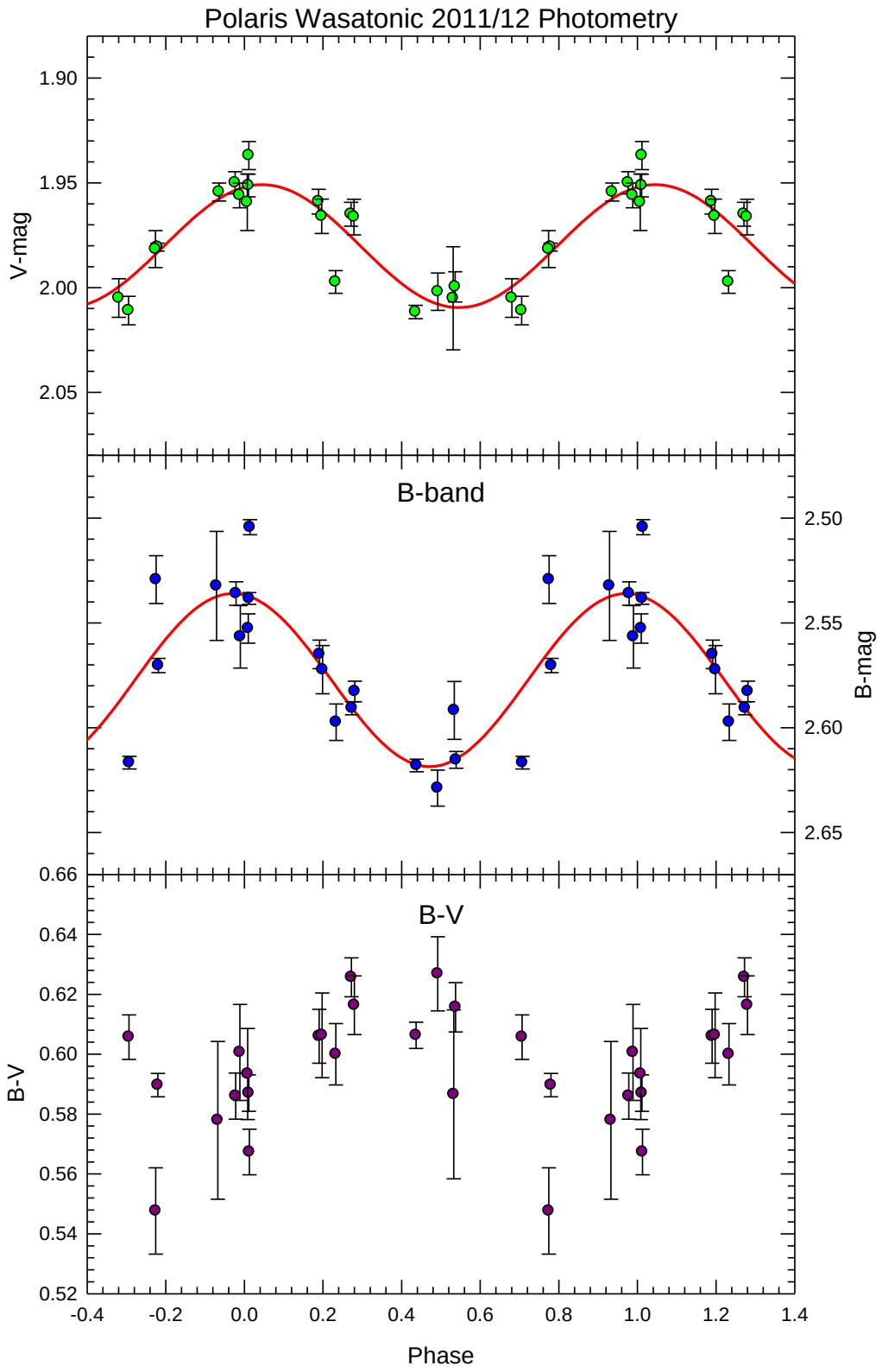

Figure 21 – The most recent *BV* data obtained for Polaris, by observer Rick Wasatonic, phased to the new ephemeris determined in this study (given in Table 7).

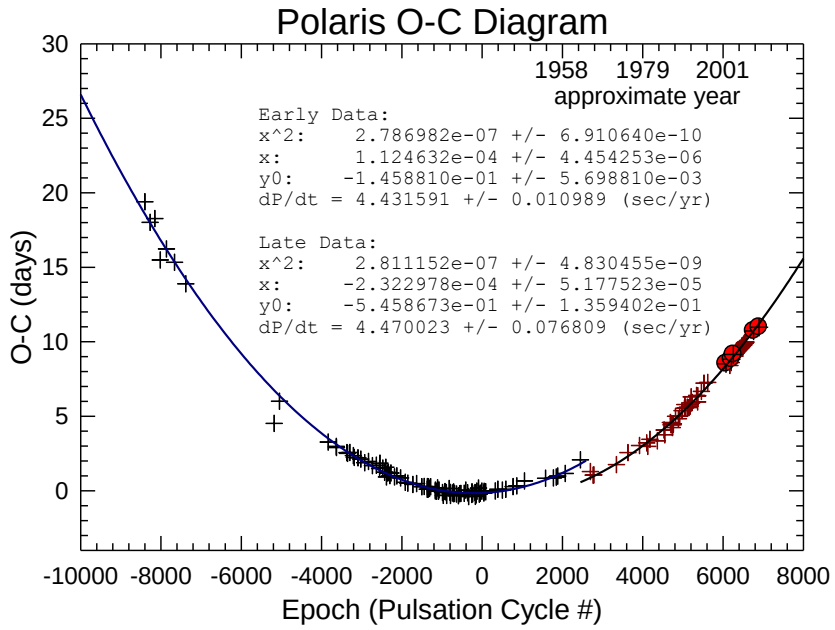

Figure 22 – The O-C diagram for Polaris, which shows the increasing period of Polaris over time. The data has been divided into two epochs: before the "period glitch" in 1963 – 64, and after. Coefficients of the quadratic fit to each epoch are given in the plot, along with the rates of period change (dP/dt = 4.47 ± 0.08 sec/yr). Points determined from this program are plotted as red filled and crossed circles.

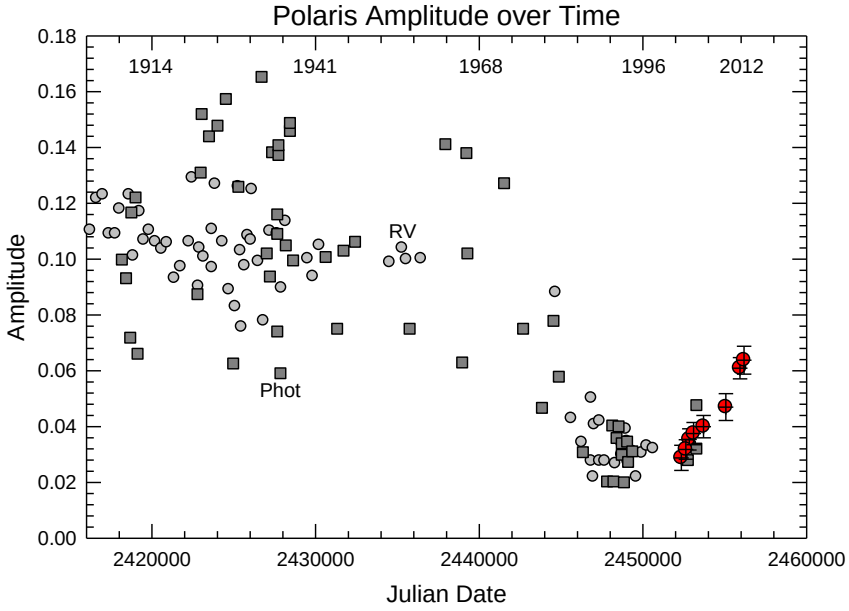

Figure 23 – The observed light amplitudes of Polaris are plotted vs. the mid-time of the observation set (in JD – data obtained from David Turner [private communication]). Points measured as part of this program are indicated by red crosses.

2.7 SU Cas

SU Cas is currently the shortest period Cepheid of the program (~2-days, see Table 8), and a probable member of the open cluster Alessi 95 (Turner et al. 2012). Based on factors such as rate of period change, amplitude of variability (presently ~0.4-mag – see Fig. 24) and luminosity, SU Cas is classified as an s-Cepheid, pulsating in the first overtone, with a fundamental period of ~2.75-days (Milone et al. 1999; Turner et al. 2012). In addition to open cluster membership, IUE observations have revealed SU Cas to have a B9.5 V companion (Evans 1991). SU Cas offers calibrator possibilities, with a reliable trigonometric parallax, along with cluster/binary companions, from which distances and luminosities can be calculated and compared.

Table 8 – Relevant Stellar Properties of SU Cas

Spectral Type	F5 – F7 Ib – II[1,2]
T_{eff} (K)	~6100 – 6600[1]
Mass (pulsational) ($M_{\odot}$)	6.5 ± 0.6[2]
Mass (evolutionary) ($M_{\odot}$)	5.5 ± 0.3[2]
Mean Luminosity ($L_{\odot}$)	~1500[2]
Mean Radius ($R_{\odot}$)	~33[2]
Distance (pc)	395 ± 30[3]
Ephemeris (this study) 2455199.614 + 1.949330(3)	
Ephemeris for O-C diagram (Szabados 1991) 2441645.913 + 1.949325	

[1]Luck et al. (2008); [2]Milone et al. (1999); [3]van Leeuwen (2007)

In this program, three well-covered light curves were obtained for SU Cas, from which times of maximum light and amplitudes were derived. Fig. 25 shows the O-C diagram for SU Cas, with the times of maximum light from this program (red filled and crossed circles) being added to the literature values from Szabados 1991 and Berdnikov et al. 2003. There is a slight gap in recent observational data for SU Cas. One can see that a period increase has taken place, and a quadratic fit has been run through the data, assuming a steady period increase over time. From this fit, a period change rate of dP/dt = 0.0204 ± 0.0002 sec/yr has been calculated. This rate places SU Cas

in the third crossing of the instability strip. It is, of course, very important to note that, just as with EU Tau, SU Cas may not be undergoing a constant period increase, but rather may have undergone an abrupt shift to a slightly longer period. Further data will show us whether the period is constant at its current, slightly longer value, or if it is still increasing.

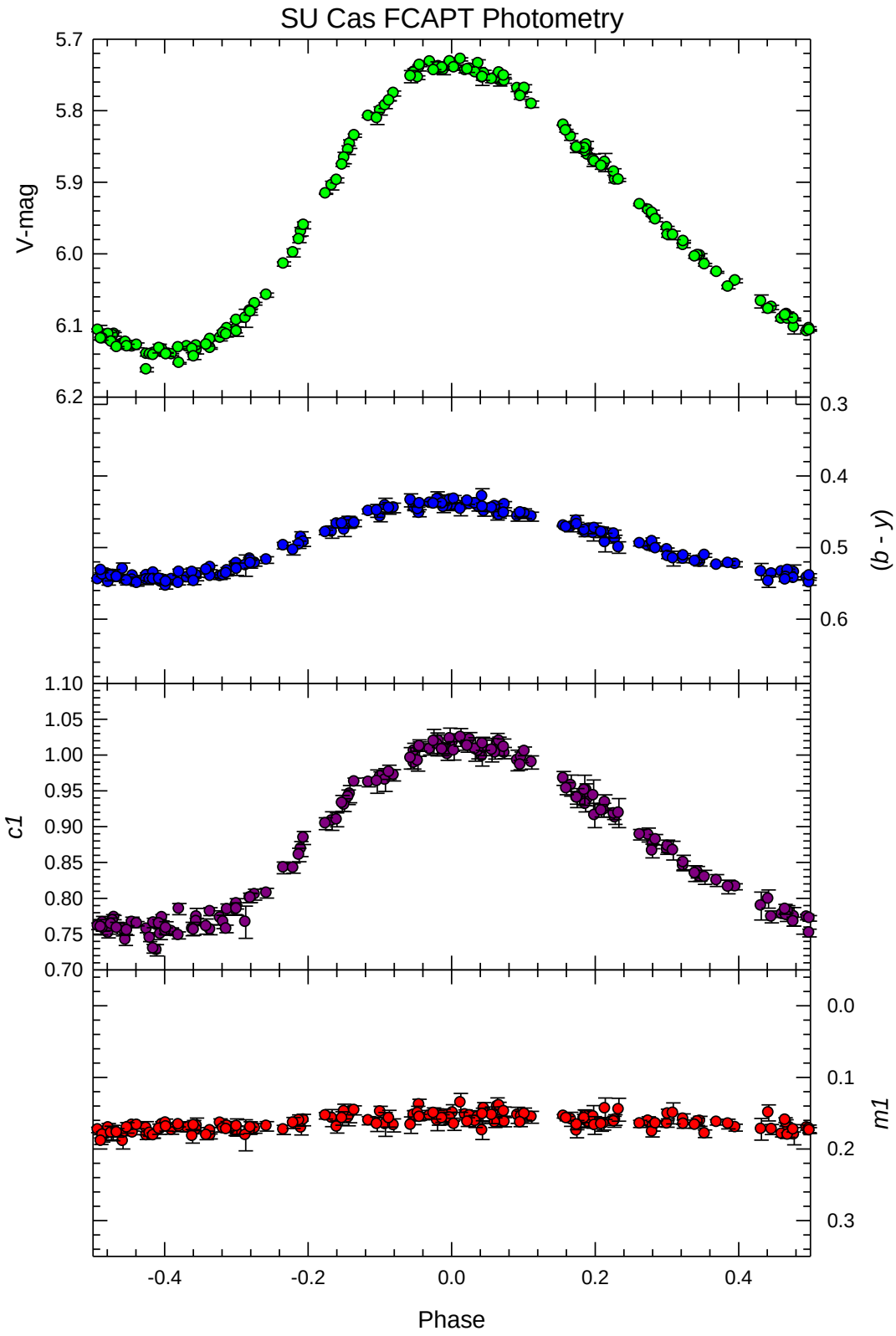

Figure 24 – The *uvby* data obtained for SU Cas. The *y*-band data have been transformed to standard *V*-band magnitudes.

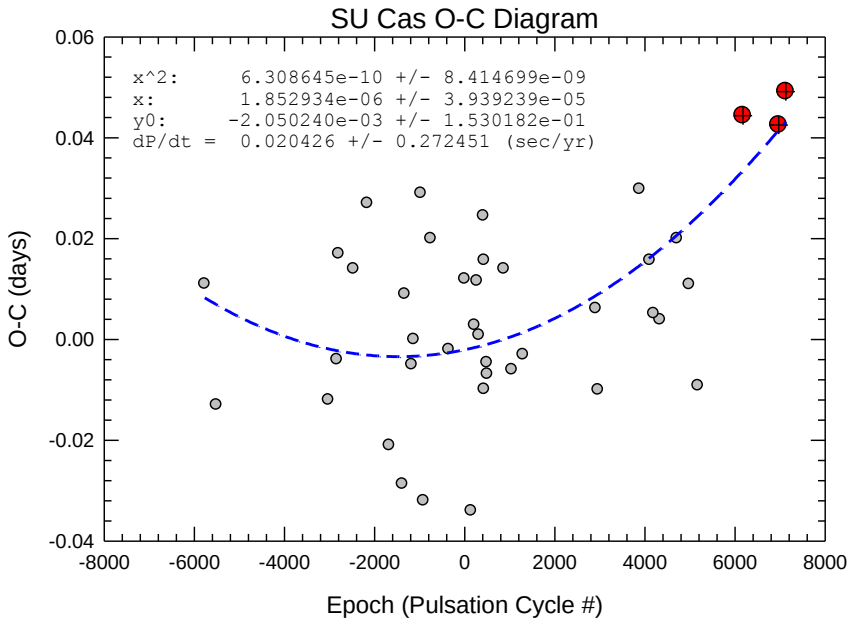

Figure 25 – The O-C diagram for SU Cas. The recent data show an increasing period trend, which before was hinted at but with ambiguity. Coefficients of the quadratic fit are given in the plot, along with the rates of period change (dP/dt = 0.0204 ± 0.0002). Points determined from this program are plotted as red filled and crossed circles.

Fig. 26 below gives the observed amplitudes of SU Cas over time. A linear fit run through the data shows a possible increase of 0.80-mmag over time. However, as can be seen in the graph and the very small rate of increase found, the trend is not concrete and could be covered by the observational errors. As with most Cepheids, the historic data is simply too sparse to *definitively* reveal long- or short-term variations in the amplitude. The variations found between the most modern lightcurves, ours included, as well as between the three amplitudes we have observed as part of this program are enticing but (as always) additional regularly obtained data are necessary to truly understand the amplitude behavior.

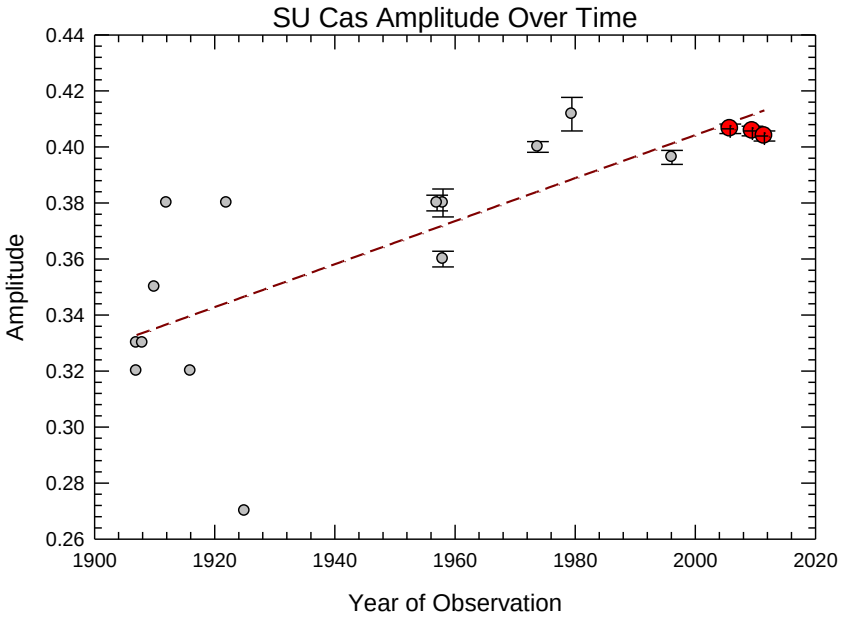

Figure 26 – The observed light amplitudes of SU Cas are plotted vs. the mid-time of the observation set. Points measured as part of this program are indicated by red crosses. A possible linear trend of increasing amplitude over time is hinted at, but relies somewhat on the older, less accurate observations.

2.8 SV Vul

SV Vul is the longest period Cepheid in this study (~45-days, see Table 9), and among the longest period Cepheids known in the galaxy. The lightcurve has a full amplitude (~1-mag, see Fig. 27) and prominently displays the asymmetric, saw-tooth shape. The revised Hipparcos parallax for SV Vul is 0.80 ± 0.81 mas. As with EU Tau, this is an unacceptably large error in distance, from a scientifically relevant standpoint, but understandable given the instrumental limitations at such distances. As such, the distance given for SV Vul in Table 9 is that determined by Turner & Burke (2002) based upon the Cepheid's membership in the NGC 6834/Vul OB1 cluster.

Table 9 – Relevant Stellar Properties of SV Vul

Spectral Type	F7 Iab – K0 Iab[1]
T_{eff} (K)	~4900 – 6100[2]
Mass (pulsational) ($M_{\odot}$)	17.5 ± 3.5[3]
Mass (evolutionary) ($M_{\odot}$)	15.1 ± 0.6[3]
Mean Luminosity ($L_{\odot}$)	~20000[4]
Mean Radius ($R_{\odot}$)	~200[4]
Distance (calculated – pc)	~2200[4]
Ephemeris (this study) 2453564.224 + 44.993007(1705)	
Ephemeris for O-C diagram (Berdnikov 1994) 2448894.50 + 45.02397	

[1]Kraft (1960); [2]Luck et al. (2001); [3]Caputo et al. (2005); [4]Turner & Burke (2002)

As part of this program, five times of maximum light and three light amplitudes were measured for SV Vul; this difference is because, in two observing seasons, the phases around maximum light were well-covered, but the phases around minimum light were not. In looking at the lightcurves presented in Fig. 27, scatter in both amplitude and phase can already be seen. As with other Cepheids in the program, an O-C diagram and amplitude over time plot were constructed to better understand exactly the long-term behavior/stability of this Cepheid's pulsations.

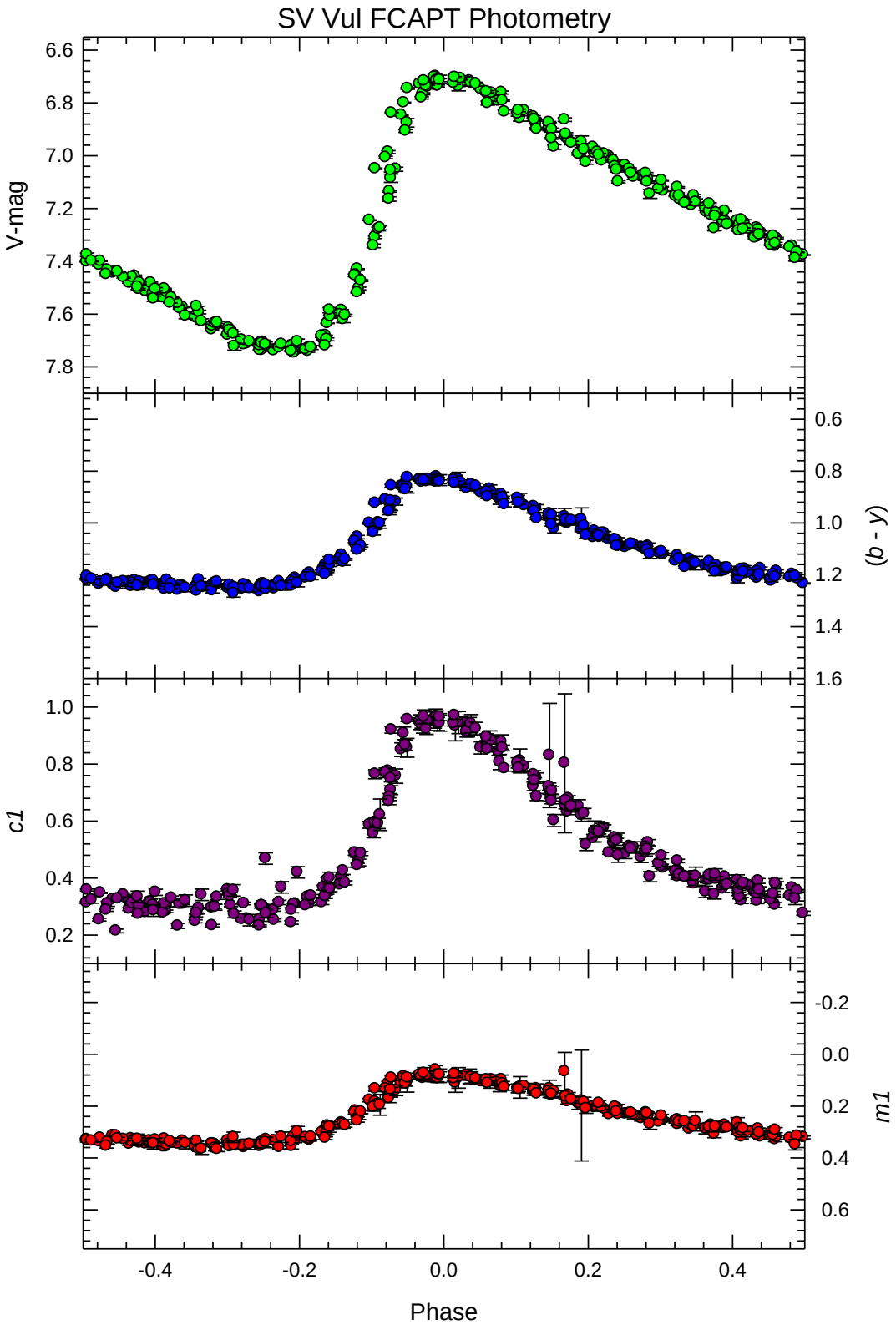

Figure 27 – The *uvby* data obtained for SV Vul. The *y*-band data have been transformed to standard *V*-band magnitudes, and phased to the newly calculated ephemeris given in Table 9.

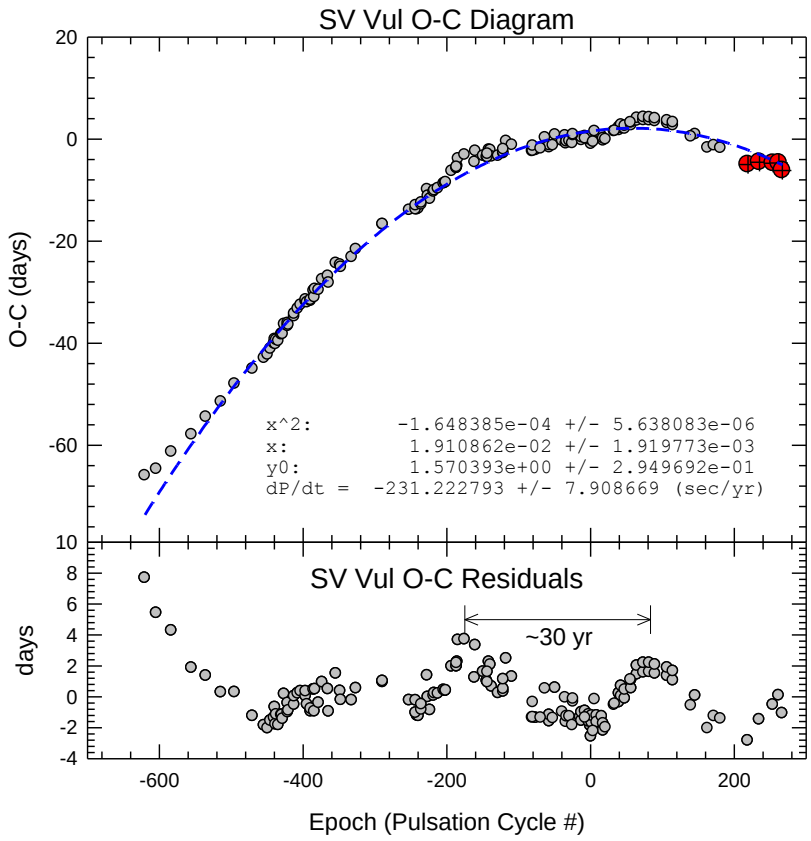

Figure 28 – The O-C diagram for SV Vul, showing the long-term decreasing period trend. Coefficients of the quadratic fit are given in the plot, along with the rates of period change (dP/dt = -231.223 ± 7.909). Points determined from this program are plotted as red filled and crossed circles. On top of the overall trend, there is a very interesting cyclic (~30-yr) behavior, as shown in the residuals plotted in the lower panel. The amplitude of the O-C residuals is too large to be the result of an unseen companion star.

Fig. 28 above shows the O-C diagram for SV Vul. In the top plot, the long-term decreasing behavior of the period is easily visible, and the quadratic fit to the data reveals a period change rate of dP/dt = –231.223 ± 7.909 sec/yr, indicating that SV Vul is currently undergoing its second crossing of the instability strip. However, there is more to the period variability, as shown in the bottom plot where the residuals to the quadratic fit are shown. There seems to be a cyclic variability to the period, with a cycle length of ~30-yr. O-C cycles such as these are not unheard of in a Cepheid, although they are rare. As mentioned earlier, the specific cause of such cyclic variations in period is not yet known.

The light amplitude of SV Vul is also variable, as shown in Fig. 29. For the past 30+ years, SV Vul has been observed more regularly than most Cepheids in the program, and the amplitude over time plot shows that. A linearly increasing trend in the amplitude has been run through the

data, but such a trend is almost entirely dependent on the oldest (visual) datasets, and their large spread in amplitudes. Most striking about the graph, however, is the recent 30+ years of data, where the possibility of an amplitude cycle is seen. The amplitude of SV Vul, in this timespan, is seen to vary from a minimum of just under 1.0-mag, to a maximum of as much as ~1.15-mag. Such a span of amplitudes would lie outside what could be assigned to observational error, and points to a real variability in the light amplitude. It is important to note that Epoch 0 for SV Vul in the O-C diagram (Fig. 28) occurred in 1978–1979, corresponding to the previous minimum in light amplitude in Fig. 29. The amplitude then appears to have roughly followed a ~30-yr cycle, as the period has done. However, within the timespan of this program, the amplitude and period behaviors have not mirrored one another, with the amplitude falling while the period has apparently begun to lengthen again. It is important to note that photometry of all Cepheids continues, and the most recent light curve being gathered for SV Vul (not yet ready for inclusion here) indicates a preliminary amplitude equal to that of the earliest observed by the FCAPT. Therefore, the amplitude may have begun to increase again. What must also be taken into account is that a fully-covered lightcurve of SV Vul almost always consists of more than one ~45-day pulsation, making the possible effects of cycle-to-cycle variations in both period and amplitude (as recently found in *Kepler* satellite photometry of V1154 Cyg – Derekas et al. 2012) difficult to

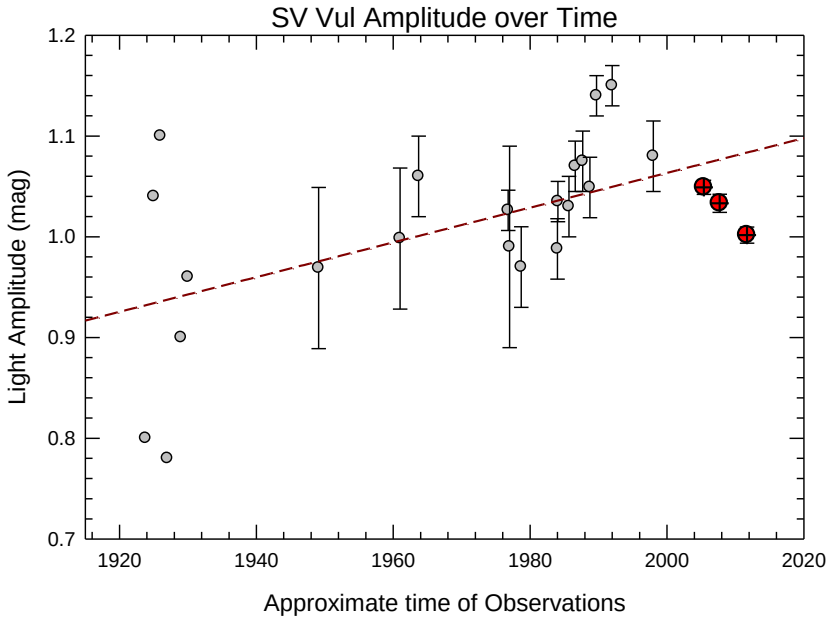

Figure 29 – The observed light amplitudes of SV Vul are plotted vs. the mid-time of the observation set. Points measured as part of this program are indicated by red filled, crossed circles. A possible linear trend of increasing amplitude over time is hinted at, but relies somewhat on the older, less accurate observations.

account for. As such, a point-to-point comparison of the O-C and amplitude data is most likely not as appropriate as a comparison of the overall trends would be. In summary, the amplitude variability of SV Vul is an exciting find that, taken together with the cyclic behavior of the period change, could offer strong evidence for a Blazhko-type behavior from this long-period Cepheid.

2.9 SZ Cas

Few studies have been conducted on the stellar parameters of SZ Cas, which lies near the *h* and χ Per double cluster, and is a possible member of the Per C1 star complex (de la Fuente Marcos & de la Fuente Marcos 2009). SZ Cas pulsates with a low amplitude (~0.38-mag in the V-band – see Fig. 30) for a Cepheid with its period, and the lightcurve has greater symmetry. Both are indicative of first overtone pulsations. Pop & Codreanu (2001) studied amplitude changes in SZ Cas, finding a ~11-year cycle of amplitude variability. Our study differs from theirs in that we combined the photometry of Berdnikov (1986) with Berdnikov (1992), to get a fully covered light curve, and we also believed it best to disregard the later Berdnikov (1995) dataset on the basis that a large data gap exists around maximum light, making an amplitude estimate unreliable at best.

Table 10 – Relevant Stellar Properties of SZ Cas

Spectral Type	F6 – G4 Ib[1]
T_{eff} (K)	~5800 – 6400[1]
Mass (pulsational) ($M_{\odot}$)	~6.5[2]
Mass (evolutionary) ($M_{\odot}$)	~9[2]
Mean Luminosity ($L_{\odot}$)	~8500[2]
Mean Radius ($R_{\odot}$)	~70[3]
Distance (calculated – pc)	~2100[1]
Ephemeris (this study) 2454142.258 + 13.637772(257)	
Ephemeris for O-C diagram (from Szabados 1981) 2443818.142 + 13.637747	

[1]Luck et al. (2006); Cox (1979); [3]Ivanov (1984)

As part of this program, two fully covered lightcurves of SZ Cas have been obtained, from which times of maximum light and amplitudes were calculated. Fig. 31 gives the O-C diagram for SZ Cas, which shows the historic steady increase in period, and the residuals to the quadratic fit. As with many Cepheids, however, observations have become sparse in recent decades. The given quadratic function yields a good fit for the data, showing a steady period increase of $dP/dt = 39.187 \pm 0.685$ sec/yr, indicating a possible 5^{th} crossing of the instability strip (or perhaps a 3^{rd} crossing with larger period change, possibly due to enhanced mass loss) but there are two additional and interesting behaviors at work. The first is what could be a period change cycle, as seen in the residuals, similar to SV Vul but of a much longer period (almost the full length of the dataset gathered to date). The second is that the most recent data hint that the period has perhaps stopped increasing. Both behaviors will require further observations to confirm.

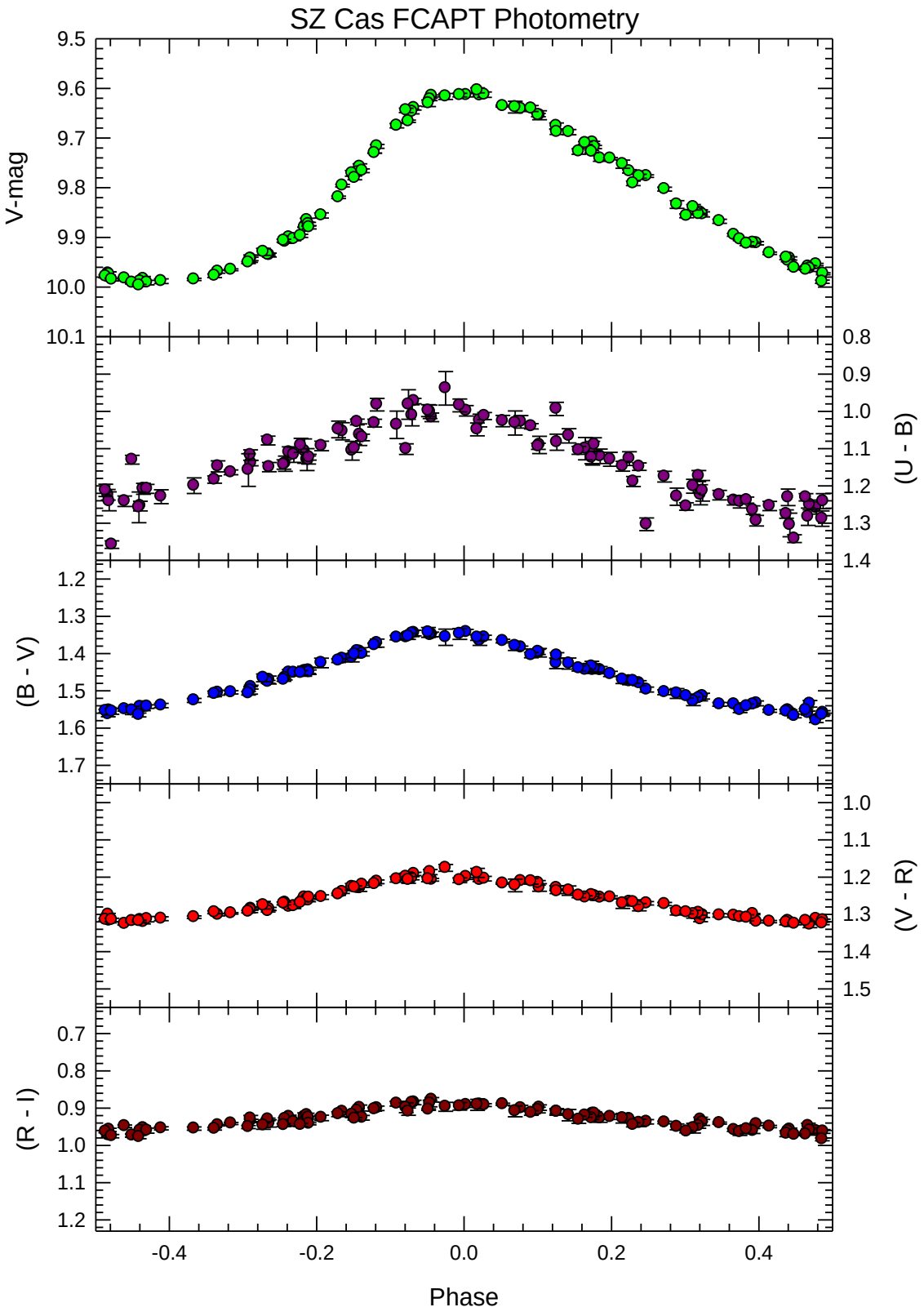

Figure 30 – The UBVRI data obtained for SZ Cas, phased to the new ephemeris calculated (given in Table 10).

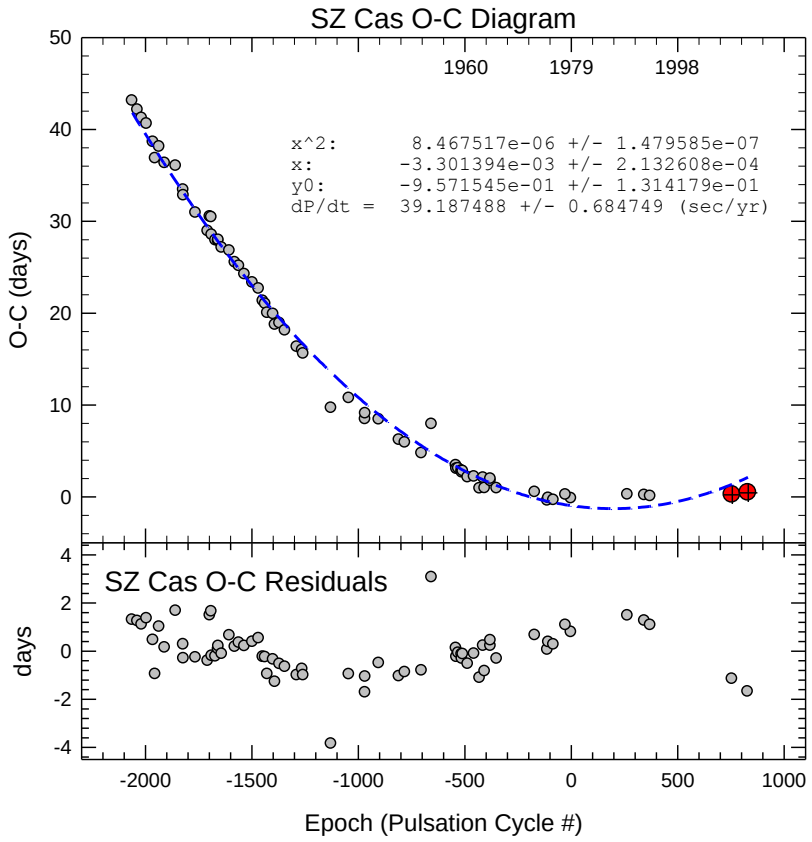

Figure 31 – The O-C diagram for SZ Cas, showing the long-term increasing period trend. Coefficients of the quadratic fit are given in the plot, along with the rate of period change (dP/dt). Points determined from this program are plotted as red filled and crossed circles. On top of the overall trend, there is evidence for a long-term possibly cyclic behavior, as shown in the residuals plotted in the lower panel, but the recent data of this program seem to break the cycle. It is also possible that the long-increasing period of SZ Cas has recently stabilized, but only further data will tell for sure.

Fig. 32 shows the amplitude values for SZ Cas over time. The amplitude appears to have undergone a noticeable decline over the past few decades. The amplitude variability does not seem to correlate to that of the period, as may be the case with SV Vul. However, the sparseness of the amplitude measures must yet again be taken into account. It does seem that amplitude changes have occurred in the past and hopefully future datasets will begin to provide a much clearer picture of the amplitude behavior of SZ Cas. If amplitudes going back to ~1960 are taken into account, a linear fit returns an amplitude change of –0.96 mmag/yr (data from ~1980 to present gives –1.4 mmag/yr), but the true amplitude behavior appears much more complex than a simple linear decrease.

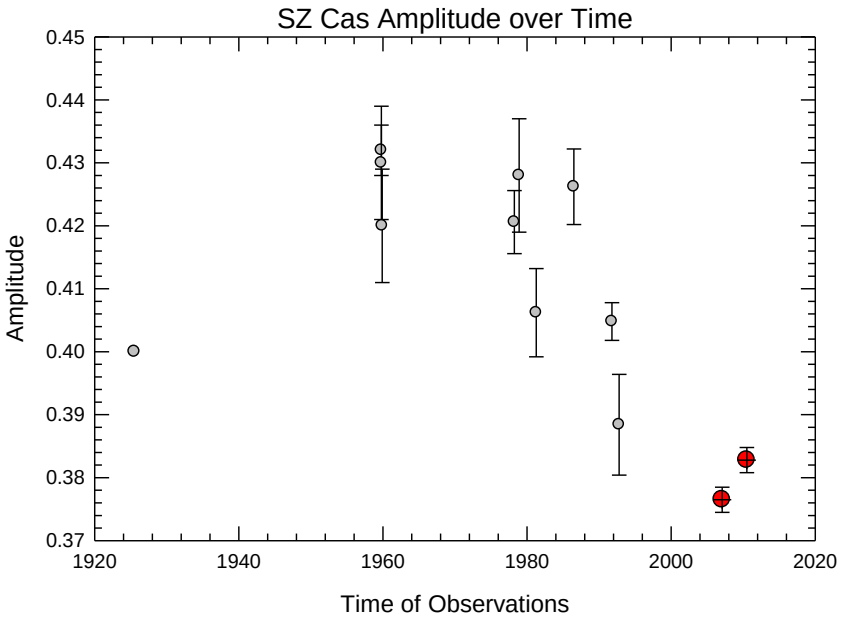

Figure 32 – The observed light amplitudes of SZ Cas are plotted vs. the mid-time of the observation set. Points measured as part of this program are indicated by red filled, crossed circles. There seems to be a very real variability, characterized mainly by a sharp decrease in amplitude in the 1980s and 90s, with a possible resurgence of the amplitude in the 2000s.

2.10 SZ Tau

The ~3.15-day Cepheid SZ Tau is suggested as a possible member member of the young open cluster NGC 1647 (Turner 1992; Rastorguev & Dambis 2011). However, it has also been ruled out as a possible member by Gieren et al. (1997) due to the difference between the cluster distance and the distance indicated for the Cepheid from the Leavitt Law. The lightcurve of SZ Tau displays a high symmetry, a lower V-amplitude of ~0.36 – 0.37-mag (see Fig. 33), and as such it is theorized to be a first overtone s-Cepheid (Postma 2008). Some relevant properties of SZ Tau are given in Table 11.

As part of this program, three fully covered lightcurves were obtained for SZ Tau, from which times of maximum light and amplitudes were calculated. The period variability of SZ Tau has been reported in several other studies, such as that of Berdnikov & Pastukhova (1995) whose data the O-C diagram shown in Fig. 34 is based on. Clearly the period of SZ Tau displays a rich and complex variability beyond what a simple quadratic fit could capture. However, it appears there is indeed a steady period change of dP/dt = –0.353 ± 0.156 sec/yr at work, indicating a possible 4th crossing of the instability strip, but the overtone nature of this Cepheid lends some ambiguity to its exact crossing. The residuals plotted at the bottom of Fig. 34 reveal the complex additional variability present in the period. The residuals do not seem to show an obvious cycle to

them, but a hand-drawn curve has been overplotted to show a possible cycle of ~59-yrs. It is unknown exactly why the period of SZ Tau exhibits such complex variability.

The amplitude behavior of SZ Tau over time seems to be a much simpler case, as seen in Fig. 35. A linear fit to the data reveals that SZ Tau's amplitude is currently increasing at a rate of ~0.8-mmag per year (0.08-mag per decade). There is a hint of cyclic variability in addition to the linear increase, but it is not concrete. It is interesting to note that the amplitude of SZ Tau has been increasing for essentially the entire ~100-yrs that have elapsed since its discovery as a Cepheid (Schwarzschild 1910). In fact, the light amplitude of SZ Tau is now almost 25% stronger than it was in the early 1900s.

Table 11 – Relevant Stellar Properties of SZ Tau

Spectral Type	F6 – F9 Ib[1]
T_{eff} (K)	~5750 – 6300[1]
Mass (pulsational) ($M_{\odot}$)	~4.9[2]
Mass (evolutionary) ($M_{\odot}$)	~5.3[2]
Mean Luminosity ($L_{\odot}$)	~2140[1]
Mean Radius ($R_{\odot}$)	~42.5[1]
Distance (pc)	417^{+185}_{-95}[3]
Ephemeris (this study) 2454409.139 + 3.148841(11)	
Ephemeris for O-C diagram (Berdnikov & Pastukhova 1995) 2430600.957 + 3.148946	

[1]Postma (2008); [2]Gieren (1989); [3]van Leeuwen (2007)

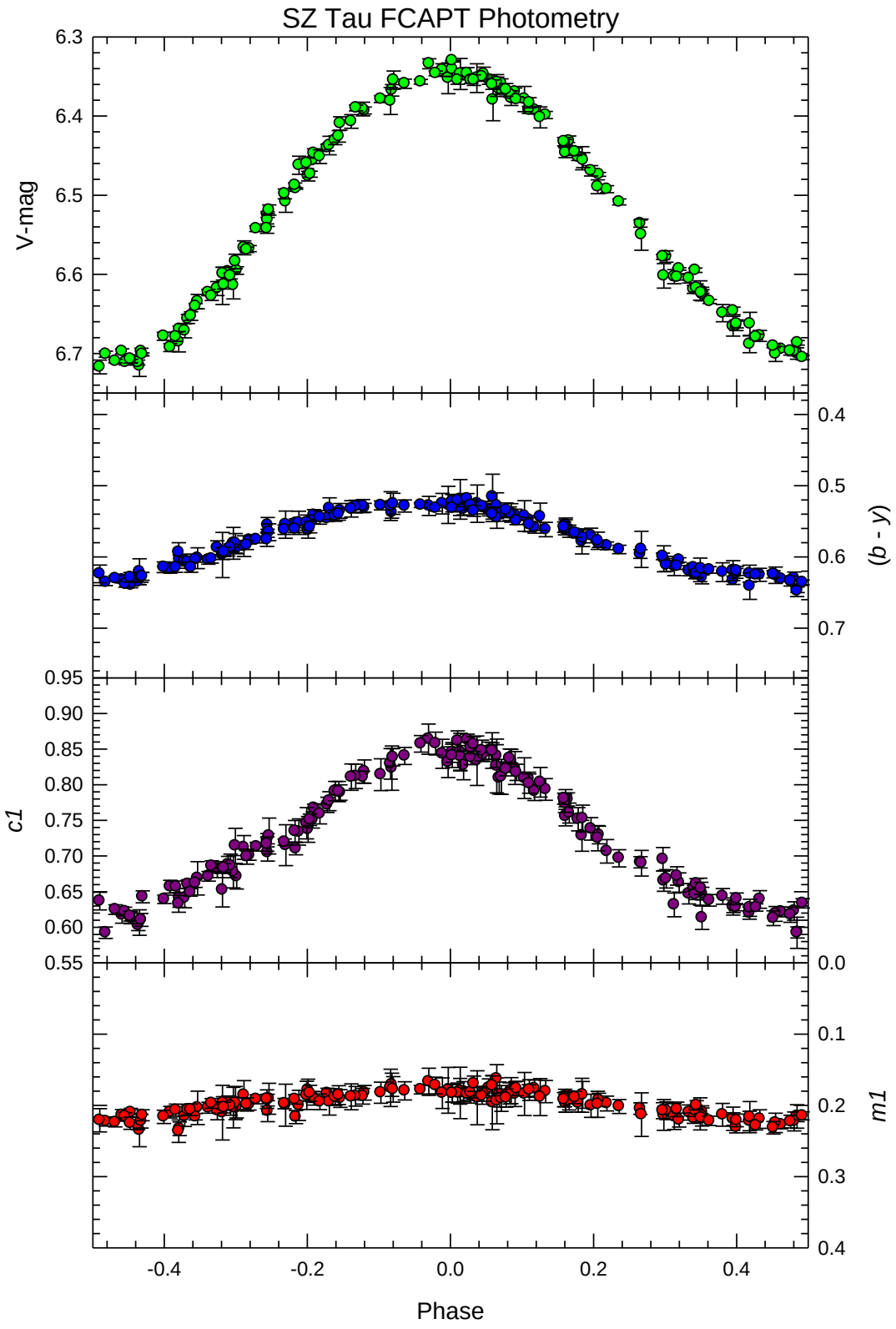

Figure 33 – The *uvby* data collected for SZ Tau. The *y*-band data have been transformed to standard *V*-band magnitudes, and phased to the newly calculated ephemeris given in Table 11.

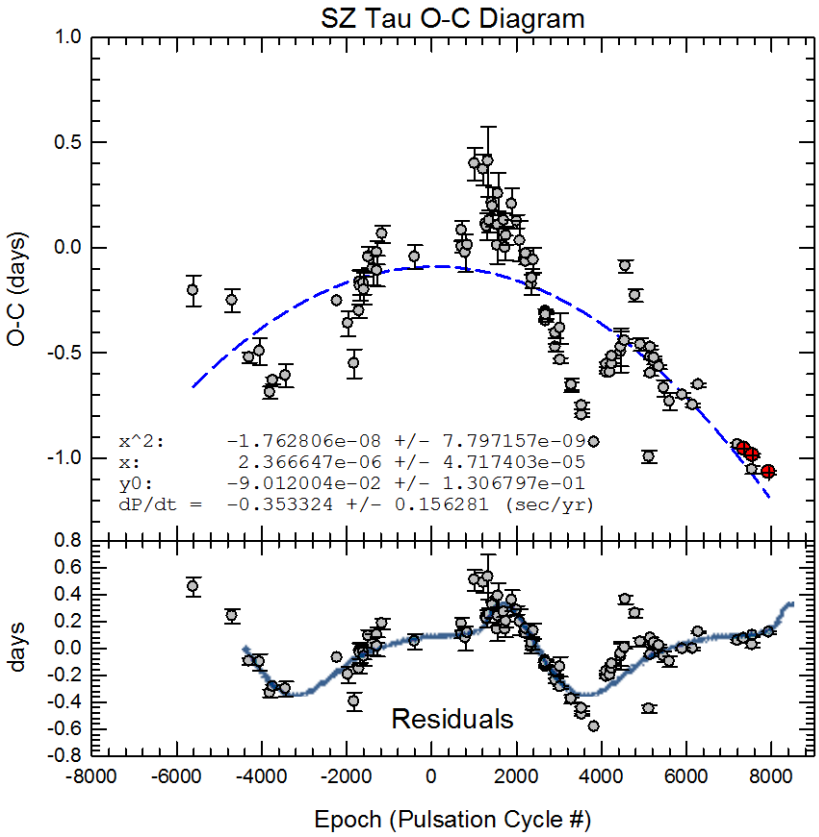

Figure 34 – The O-C diagram for SZ Tau, showing some very complex period behavior. There seems to be an overall trend of decreasing period (indicated by the fit), but with a possibly cyclic variability overlaid, as with SZ Cas and SV Vul. Further data is required to confirm the ~59-year cyclic behavior. Coefficients of the quadratic fit are given in the plot, along with the rate of period change (dP/dt). Points determined from this program are plotted as red filled and crossed circles.

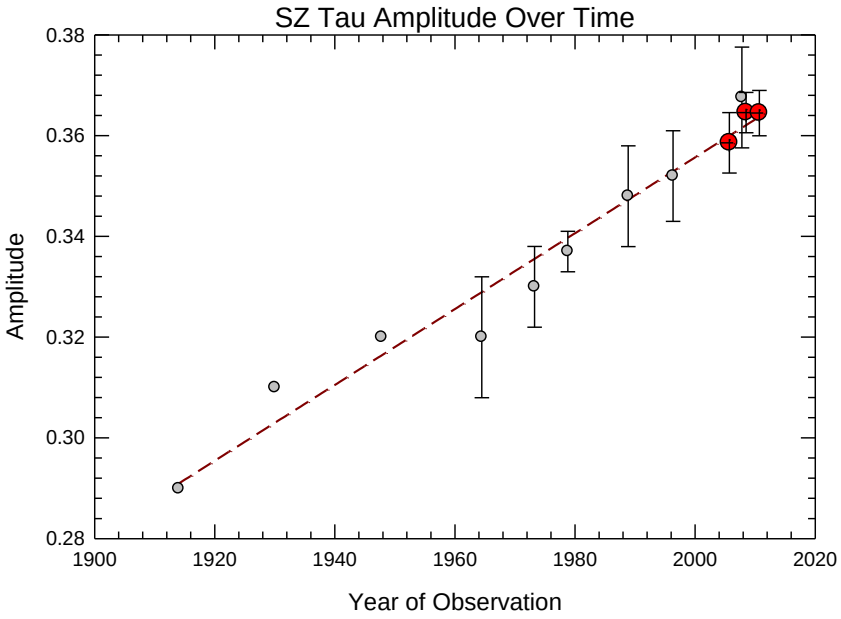

Figure 35 – The observed light amplitudes of SZ Tau are plotted vs. the mid-time of the observation set. Points measured as part of this program are indicated by red filled, crossed circles. A constant increasing trend is very obvious in the data. Hints of additional amplitude variability can be seen, but the sparseness of the data prevents firm conclusions.

2.11 VY Cyg

Along with SZ Cas, VY Cyg is one of the fainter Cepheids in our study and, as such, does not possess a rich observational history, like some of the brighter Cepheids. Klagyivik & Szabados (2009) infer that VY Cyg has an as yet unseen blue companion, based on its light amplitudes across different photometric bands when compared to other Cepheids. This would confirm the earlier results of Madore (1977) who suggested that VY Cyg has a B7 main sequence companion. VY Cyg has a revised *Hipparcos* parallax of π_{Hipp} = 0.05 ± 1.12 mas (van Leeuwen 2007). As with EU Tau and SV Vul, the distance of this Cepheid is far too large to allow for a usable trigonometric parallax measurement. Given in Table 12 is the calculated distance of VY Cyg, taking into account the absolute magnitude determined by Kovtyukh et al. (2010) and the dereddened (Kovtyukh et al. 2008) apparent magnitude observed as part of this program, adjusted for the presence of the hot companion (Madore 1977).

Table 12 – Relevant Stellar Properties of VY Cyg

Spectral Type	F6 – G1 Ib[1]
T_{eff} (K)	~5500 – 6300[2]
Mass (pulsational) ($M_{\odot}$)	~4.5[3]
Mass (evolutionary) ($M_{\odot}$)	~5[3]
Mean Luminosity ($L_{\odot}$)	~2000[3]
Mean Radius ($R_{\odot}$)	~49[4]
Distance (calculated – pc)	~1600 (see text)
Ephemeris (this study) 2455852.511 + 7.857125(33) × E	
Ephemeris for O-C diagram (Szabados 1980) 2443045.282 + 7.856982 × E	

[1]Luck et al. (2006); [2]Kovtyukh et al. (2010); [3]Gieren (1989); [4]Cogan (1978)

As part of this study, three fully-covered lightcurves of VY Cyg have been obtained (Fig. 36), from which times of maximum light and amplitudes were determined. Fig. 37 shows the O-C diagram for VY Cyg. A quadratic fit has been run through the data, assuming a linear increase in period, which is calculated to be dP/dt = +0.249 ± 0.003 sec/yr, placing VY Cyg in its third crossing of the instability strip, very similar to η Aql which is of similar period, amplitude and stellar properties

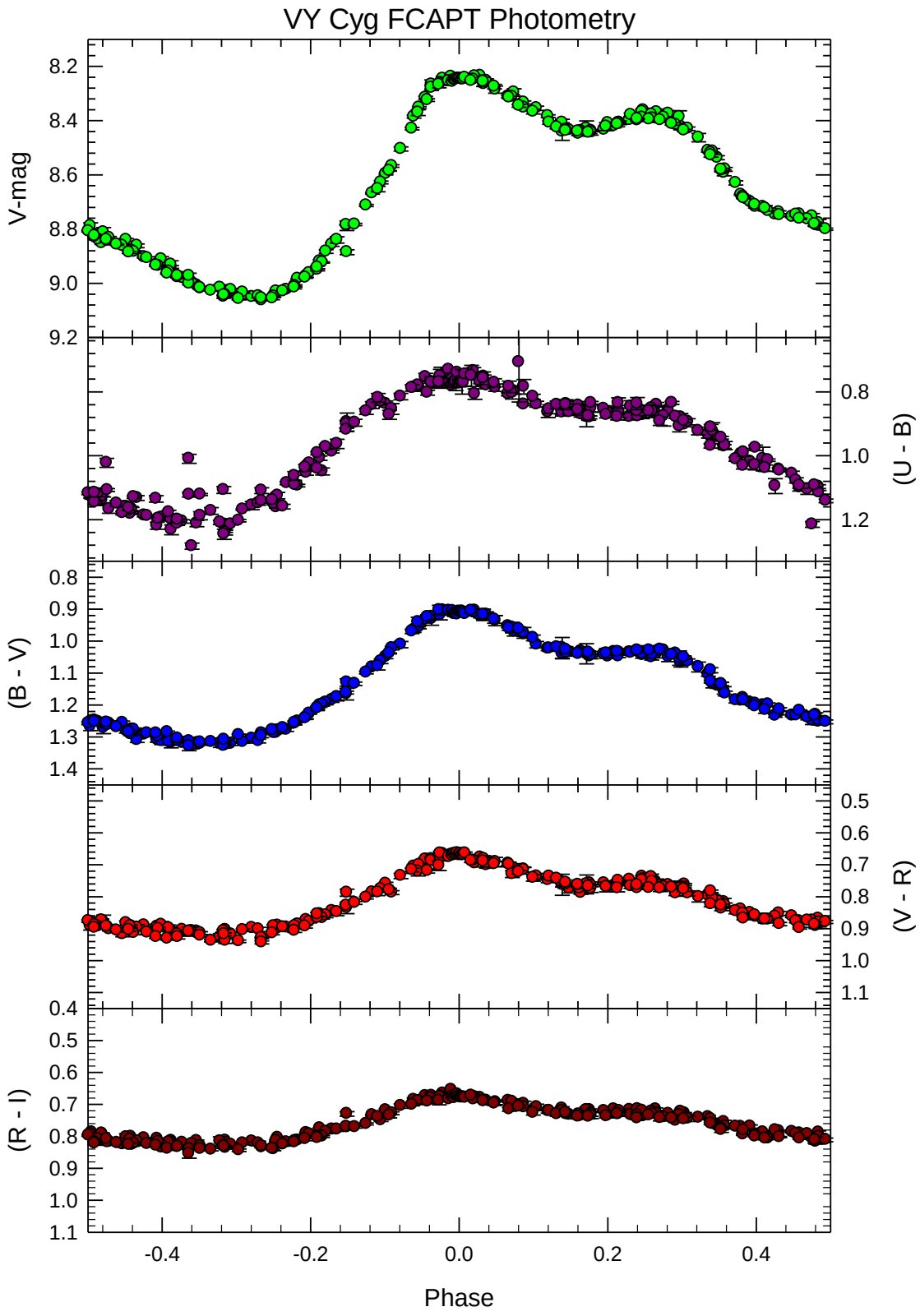

Figure 36 – The *UBVRI* data obtained for VY Cyg, phased to the new ephemeris determined in this study (given in Table 12).

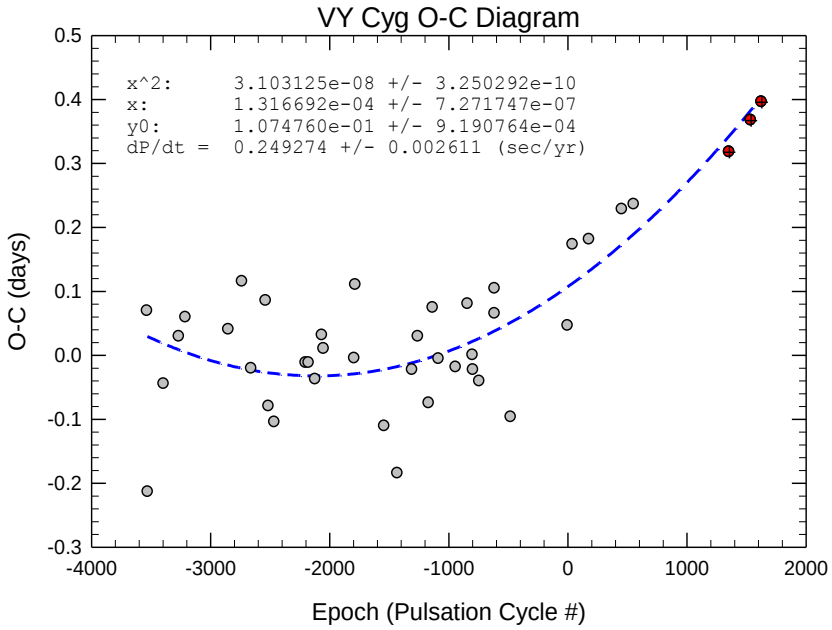

Figure 37 – The O-C diagram for VY Cyg. Our data provides further confirmation and characterization of the recent increasing period trend. Coefficients of the quadratic fit are given in the plot, along with the rate of period change (dP/dt). Points determined from this program are plotted as red filled and crossed circles.

The amplitude behavior of VY Cyg over time is shown in Fig. 38. A linear fit of the amplitudes is given, which indicates a steady period increase of ~0.6-mmag per year, but this is substantially influenced by lower amplitude values reported over a century ago. It is rational to assume that no linear trend in VY Cyg is confidently displayed in the data (coincidentally, as is also the case with η Aql). There is an appreciable spread in amplitudes reported in the past few decades, however, as with other Cepheids, the sparseness of the data precludes a deeper investigation of possible coherent variability in the amplitude over time.

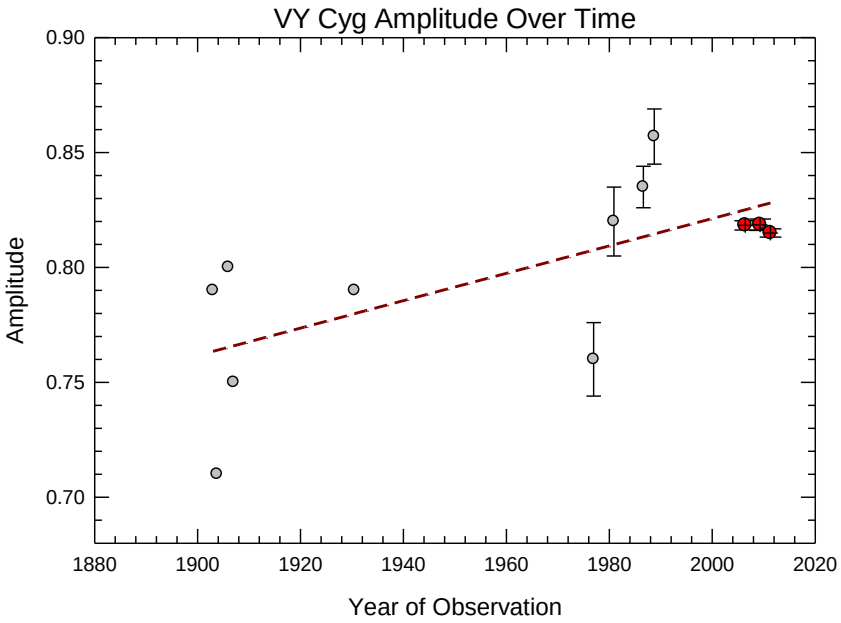

Figure 38 – The observed light amplitudes of VY Cyg are plotted vs. the mid-time of the observation set. Points measured as part of this program are indicated by red crosses. A constant increasing trend is assumed by the fit, but is not concrete since it mainly relies on the oldest, least accurate data. The amplitude measurements of the 1970s and 80s show a spread in amplitudes beyond the realm of observational error, but the lack of observations in the 1990s prevents a further investigation.

2.12 ζ Gem

The discovery of light variability in ζ Gem is attributed to Julius Schmidt in either 1844 or 1847, depending on the source (Allen (1899), p. 235; Henroteau (1925)). However, suspicions of variability were originally raised as early as 1790. Radial velocity variability was discovered independently by Belopolsky (1899) and Campbell (1899), and comparisons to δ Cep started shortly thereafter. In fact, for some time after, δ Cep and ζ Gem both enjoyed elevated status as the prototypes of two separate but related classes of variable stars – the δ Cep-type stars, or Cepheids, and the ζ Gem-type stars, or Geminids, to which other more symmetric Cepheids like SZ Tau and Polaris were assigned (Ludendorff (1916) and Henroteau (1925)). To date, no unresolvable companions have been detected, but ζ Gem does have a resolved F3.5 – 4 V companion, ζ Gem B, which lies ~1.4-arcmin from the Cepheid (Majaess et al. 2012). Majaess et al. have also concluded that ζ Gem is the member of a newly discovered cluster, making it an important calibrator Cepheid, for which fundamental stellar parameters, and distance, can be obtained in a variety of ways and then compared.

Table 13 – Relevant Stellar Properties of ζ Gem

Spectral Type	F7 – G3 Ib[1]
T_{eff} (K)	~5200 – 5800[2]
Mass (pulsational) ($M_{\odot}$)	~5.5[3]
Mass (evolutionary) ($M_{\odot}$)	~6[3]
Mean Luminosity ($L_{\odot}$)	~2900[4]
Mean Radius ($R_{\odot}$)	~65[3]
Distance (pc)	360^{+25}_{-22} [5]
Ephemeris (this study) 2451909.770 + 10.149401(101)	
Ephemeris for O-C diagram (Berdnikov et al. 2000) 2423838.469 + 10.1522686(135)	

[1]Kervella et al. (2001); [2]Luck et al. (2008); [3]Gieren (1989); [4]Mallik (1999); [5]Benedict et al. (2007)

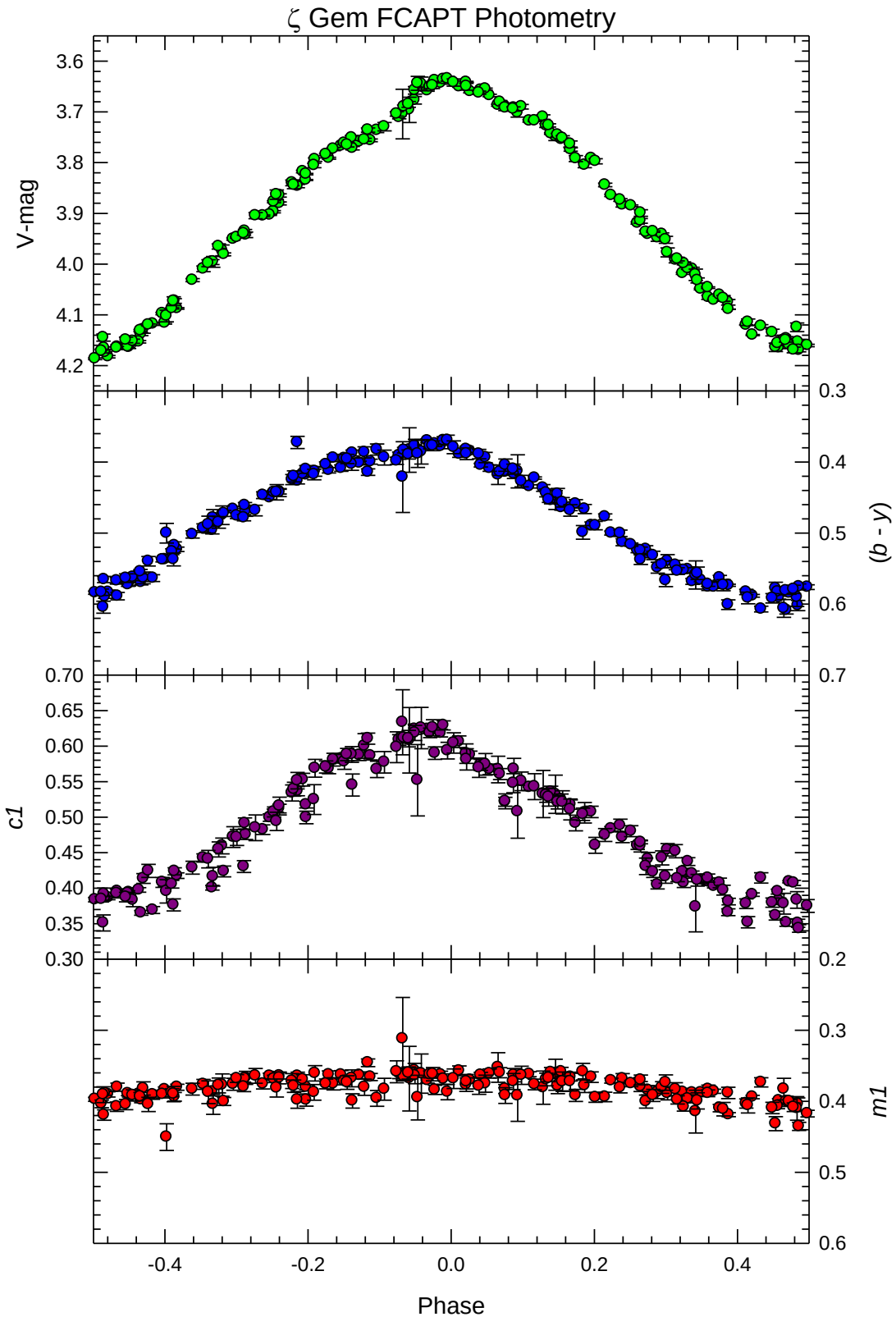

Figure 39 – The *uvby* data collected for ζ Gem. The *y*-band data have been transformed to standard *V*-band magnitudes, and phased to the newly calculated ephemeris given in Table 13.

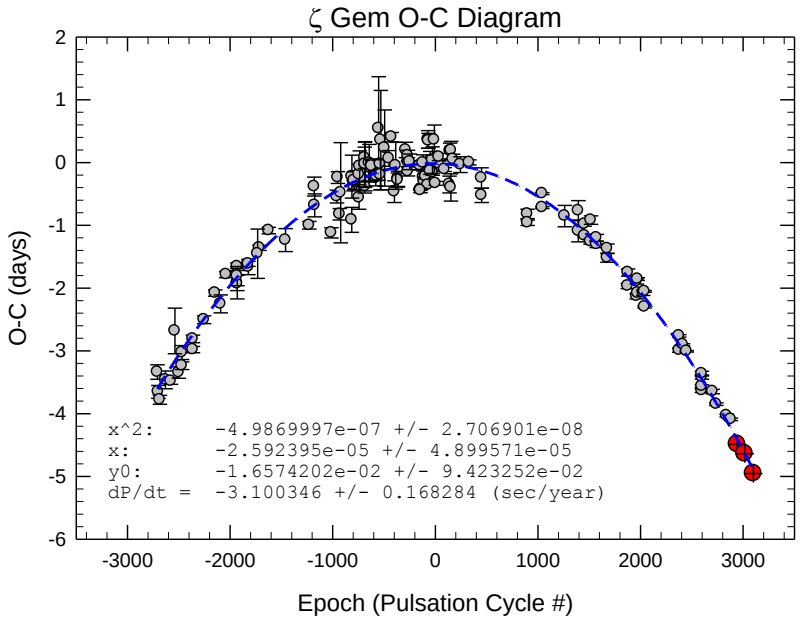

Figure 40 – The O-C diagram for ζ Gem, with the long-term, steadily decreasing period trend easily visible. No hints of further variability are evident. Coefficients of the quadratic fit are given in the plot, along with the rate of period change (dP/dt). Points determined from this program are plotted as red filled and crossed circles.

Three fully covered lightcurves have been obtained for ζ Gem in this program (Fig. 39). Fig. 40 shows the O-C diagram for ζ Gem, where the period is seen to have been undergoing a smooth, steady decline for the full ~160-yr dataset. No coherent variability shows up in the residuals to the quadratic fit, which gives a period change rate of dP/dt = –3.100 ± 0.011 sec/yr. This rate alone could place ζ Gem in either the second or fourth crossing of the instability strip. However, Turner (2010) has classified it as a fourth crossing Cepheid, since its light amplitude is below that expected for a second crossing Cepheid and its color is better matched to a fourth crossing Cepheid. The amplitude behavior of ζ Gem over time shows a probable linear increase, with the best fit giving ~1-mmag per year (0.01-mag per decade – see Fig. 41). On top of the linear trend, however, the more recent data shows a possible ~50-yr cycle to the amplitude. If this cycle is true, it will naturally take a couple decades of regular observation to definitively confirm.

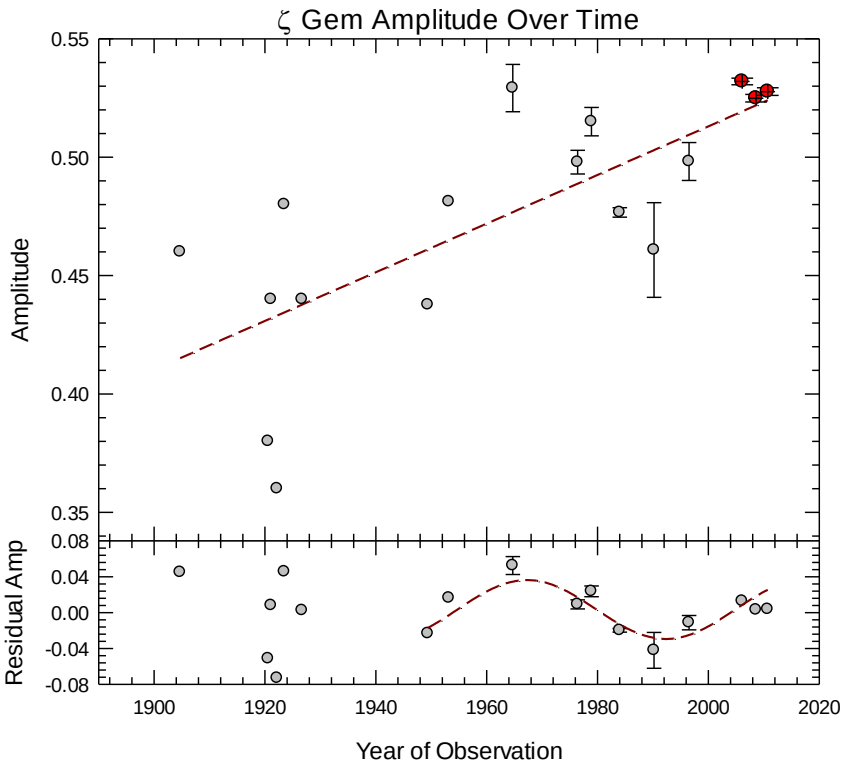

Figure 41 – The observed light amplitudes of ζ Gem are plotted vs. the mid-time of the observation set. Points measured as part of this program are indicated by red crosses. A constant increasing trend is assumed by the fit, but is not concrete since it is strongly influenced by the two low amplitudes around 1920. The amplitude measurements from the 1940s until recently show a possible cyclic behavior of ~50-years (see residuals), but further data is necessary to confirm.

2.13 β Dor

The radial velocity variability of β Dor was discovered by Palmer through observations taken in 1930/1904 (Applegate 1927). Wilson was the first to note, at an *American Astronomical Society* meeting, the similarities between β Dor and other Cepheids, suggesting that it might be a member of the class ([*the paper is listed in the ADS as*] N/A 1921). The first confirmation of brightness variability for β Dor is that of Shapley & Walton (1927). Unfortunately, with a declination below -62°, β Dor is a Cepheid that most ground-based telescopes in the northern hemisphere will be unable to observe. As such, no photometric observations have been carried out for β Dor as a part of this program. Nevertheless, it is one of the nearest and brightest Cepheids (see Table 14) which is a large advantage for spectroscopic studies, as a sufficient signal-to-noise value can be quickly obtained. Table 14 gives some important stellar properties for β Dor.

Table 14 – Relevant Stellar Properties of β Dor

Spectral Type	F4 – G4 Ia – II[1]
T_{eff} (K)	~5500[1]
Mass (pulsational) ($M_{\odot}$)	~6[3]
Mass (evolutionary) ($M_{\odot}$)	~7[3]
Mean Luminosity ($L_{\odot}$)	~3200[4]
Mean Radius ($R_{\odot}$)	~68[2]
Distance (calculated – pc)	318^{+18}_{-15} [5]
Ephemeris (Berdnikov et al. 2003) 2440905.3 + 9.8426 × E	
Ephemeris used for O-C Diagram 2425659.1126 + 9.8426 × E	

[1]Kervella et al. (2004); [2]Taylor & Booth (1998); [4]Turner (2010);
[3]Gieren (1989); [5]Benedict et al. (2007)

Although no new photometry was carried out for β Dor as part of this study, recent AAVSO observations exist. We acknowledge with thanks the 2012-2013 observations of β Dor, carried out by Neil Butterworth, and accessed through the *AAVSO International Database*. A single time of maximum light was obtained from the V-band data, and added to the O-C data presented by Berdnikov et al. (2003 – *data obtained by private communication*). Fig. 42 shows the O-C diagram for β Dor. A parabola is fit to the data, showing a slow, steady increase in the pulsation period of dP/dt = 0.468 ± 0.016 sec/yr. This rate of period increase places β Dor well within the third crossing of the instability strip, and represents a good fit to the dataset, although a second interpretation of the data is also possible, where the period underwent a sudden lengthening around Epoch 1800 (calendar year 1977), and has since held steady at 9.8426-days.

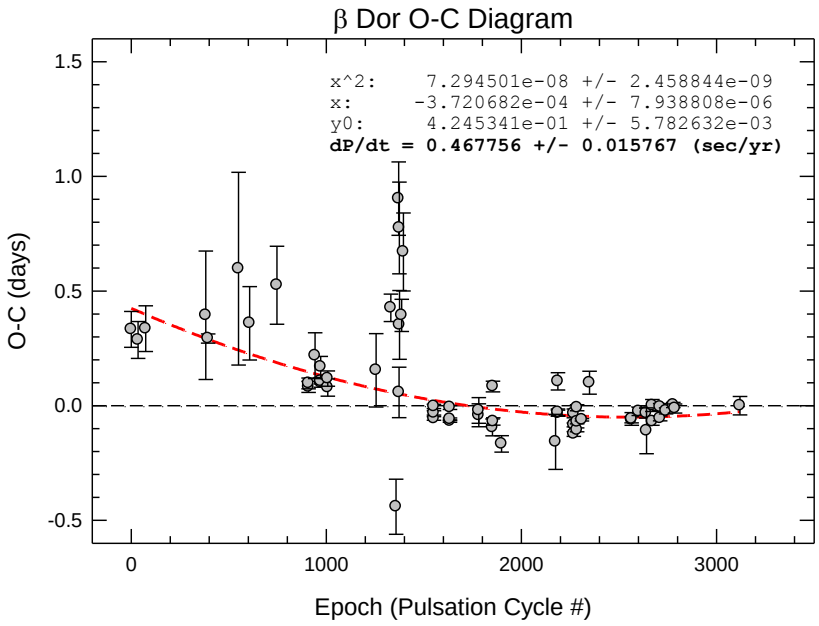

Figure 42 – The O-C diagram for β Dor, with the long-term, steadily increasing period trend shown. No hints of further variability are evident. Coefficients of the quadratic fit are given in the plot, along with the rate of period change (dP/dt). The latest data point is that determined from the 2012 – 2013 AAVSO data (Observer: Neil Butterworth).

2.14 A Brief Summary of Chapter 2

New *UBVRI* or *uvby* photometry has been gathered for ten Cepheids, to determine changes in pulsation period and light amplitude. Although no new photometry of the Cepheid β Dor could be gathered in this study, since it is a southern hemisphere target, an updated O-C diagram was built using available literature data and recent photometry gathered by AAVSO observer Neil Butterworth. Thus, the optical study currently contains period studies for eleven Cepheids, and amplitude studies for ten. Table 15 briefly describes the results. All eleven Cepheids display some form of period variability. Six of the eleven Cepheids (δ Cep, η Aql, Polaris, VY Cyg, ζ Gem and β Dor) show steady, persistent increases/decreases in period, and an additional two (EU Tau and SU Cas) display either a slow, steady period change or a sudden shift in period. The remaining three Cepheids (SV Vul, SZ Cas and SZ Tau) display a combination of steady period change and a cyclic variation in the rate of period change, as shown in the residual plots below their O-C diagrams.

The amplitude datasets are much sparser than the O-C diagrams, mainly because the phase-ranges around both maximum *and* minimum light must be well-covered. Nevertheless, there is only one Cepheid, η Aql, which shows no evidence of coherent amplitude variability. EU Tau displays a possible, albeit very small, decrease in amplitude. However, given the margins of error,

a steadily decreasing amplitude is unlikely. VY Cyg shows a large spread in recent amplitude values beyond the margin of errors, but a steadily changing amplitude is unlikely. For SV Vul, a long-term amplitude change is merely a possibility due to the large spread of early amplitude measures. However, the Cepheid does display a recent amplitude cycle of similar length (~30-yr) to variations also observed in its rate of period change. This is an interesting behavior, but one that will likely take years of additional data to completely understand. The amplitude of Polaris was once thought to be steadily declining, but is now increasing again and it is unknown if the amplitude will simply attain and hold some previous, larger value or if the Cepheid is undergoing an amplitude cycle. SZ Cas also shows an amplitude that recently declined but now appears to be growing. However, the data is too sparse to present a firm conclusion. SU Cas shows a slowly increasing amplitude, with a small possibility of cyclic behavior. Similarly, SZ Tau shows a reliable, long-term amplitude increase with only a small possibility of additional variations. Both δ Cep and ζ Gem show long-term increases in its amplitude, but with stronger evidence recent additional, cyclic behaviors.

Table 15 – Period / Amplitude Behaviors of Program Cepheids

Cepheid	Period (days)	Period Change (sec/yr)	Crossing	Long- and Short-term (right column, if present) Amplitude Change (mmag/yr)	
SU Cas	1.949	+0.0204 (or abrupt shift)	3rd	+0.8	Possible
EU Tau	2.102	–0.337 (or abrupt shift)	4th	–0.2 (tentative result; likely within errors)	
SZ Tau	3.149	–0.353 (with complex additional variability)	4th ?	+0.8	Hinted at, but recent data would not fit the expectations.
Polaris	3.972	+4.470	1st	+2.96 (current)	Previously declining, currently increasing – possible cycle.
δ Cep	5.366	–0.1006	2nd	+1.4	Possible
η Aql	7.177	+0.255	3rd	No coherent amp. variability	
VY Cyg	7.857	+0.249	3rd	+0.6 (unlikely)	Large spread in amplitude, but sparse data limit conclusions.
β Dor	9.843	+0.468	3rd	--	--
ζ Gem	10.149	–3.1003	4th	+1.03	Possible ~50-yr cycle.
SZ Cas	13.638	+39.187 (with possible additional cycle)	3rd (5th ?)	-0.96	Complex: possible recent increase after previous decline
SV Vul	44.993	–231.223 (with likely ~30-yr cycle)	2nd	+1.7 (possible)	A ~30-yr cycle, similar to the period behavior.

CHAPTER 3 – THE HIGH-ENERGY (UV – X-RAY) STUDIES

Several high-energy (specifically UV and X-ray, in this program) studies of Cepheids have been carried out in previous decades, using earlier-generation instruments, most notably *IUE*, *Einstein* and *ROSAT*. The results of these various studies lead us to question just what Cepheid atmospheres would look like when viewed through modern instruments, such as HST, Chandra and XMM. The current Cepheid sample for the high-energy study is unfortunately more limited than the optical study. Two main factors are primarily responsible for this.

First, although Cepheids are optically luminous, allowing the photometric observations to be efficiently carried out even with small telescopes, they are *far* less luminous in the UV and X-ray regimes. Achieving a minimally sufficient signal-to-noise (S/N) ratio at UV and X-ray wavelengths ordinarily requires kiloseconds of exposure time. Fortunately for this study (and numerous others), COS is one of the most sensitive UV spectrographs ever flown. Using roughly one half of an HST orbit per observation, after target acquisition (usually ~900–1100-sec), we were able to achieve S/N ratios of ~10 – 20 for the emission lines studied. For the X-ray images, however, exposure lengths of ~30 – 70-ksec (almost 20 hours) are necessary to secure useful data.

The second factor is the availability of UV and X-ray instruments. Villanova has guaranteed access to the ground-based telescopes used for the optical studies. When dealing with satellite instruments, the competition is very strong and the observing time is extremely precious. The exposure times required, the need for multiple observations of each target to achieve phase coverage, and the willingness of time allocation committees, all combine to dictate the pace at which the high-energy study can proceed. Nevertheless, we are extremely fortunate to have gathered as much data as we have over the past few years, and we are continually attempting to expand the Cepheid high-energy database.

3.1 Ultraviolet Studies with HST-COS

During 2009-13, we were awarded 29 HST orbits for COS spectroscopy of three Cepheids: two visits (2 orbits/visit) for Polaris, and 19 visits (1 orbit/visit) for δ Cep & β Dor and 6 visits (1 orbit/visit) for the ~35-day Cepheid ℓ Car. Table 15 summarizes the important information on the COS Cepheid observations carried out in time for inclusion in the current study. Our targets were well-acquired, and the spectra required no special processing. Thus, the data used in this study are the CALCOS pipeline-processed data available from the MAST archive (http://archive.stsci.edu). The original aim of the COS observations was to improve upon previous studies using the IUE satellite, since what appeared to be photospheric continuum flux added to uncertainties in emission line identification and flux measures. The hope was that COS, with its finer spectral

resolution, high-sensitivity and low noise, would return superior spectra for which much more precise measurements could be carried out. In addition, closely-spaced emission lines that were blended together in IUE spectra could be individually resolved in COS data and perhaps even less-prominent emission lines would be detected. Since the only reliable data in the ~1200 – 1600 Å region available for Cepheids (at the beginning of this project) was low-resolution (~1–2 Å) IUE spectra, it was quite frankly unknown exactly what the COS observations would show.

Table 16 – The HST-COS "Cepheid Inventory" To Date

Target Name	Dataset	Start Time (UT)	Stop Time (UT)	Exp Time	COS Grating	Central Wavelength
POLARIS	LB5001010	12/25/2009 8:56	12/25/2009 9:39	2364.384	G130M	1281.623
POLARIS	LB5001020	12/25/2009 10:18	12/25/2009 10:49	1400.064	G160M	1581.854
POLARIS	LB5001030	12/25/2009 10:54	12/25/2009 10:58	243	G185M	1914.848
POLARIS	LB5001040	12/25/2009 11:03	12/25/2009 11:07	244	G185M	1941.725
POLARIS	LB5001050	12/25/2009 11:11	12/25/2009 11:15	243	G185M	1883.428
POLARIS	LB5002010	12/27/2009 8:51	12/27/2009 9:33	2364.384	G130M	1281.646
POLARIS	LB5002020	12/27/2009 10:12	12/27/2009 10:43	1400.096	G160M	1581.87
POLARIS	LB5002030	12/27/2009 10:49	12/27/2009 10:53	243	G185M	1914.413
POLARIS	LB5002040	12/27/2009 10:57	12/27/2009 11:01	244	G185M	1941.38
POLARIS	LB5002050	12/27/2009 11:05	12/27/2009 11:09	243	G185M	1883.207
V-DEL-CEP	LBK809010	10/19/2010 0:12	10/19/2010 0:30	924.992	G130M	1291
V-DEL-CEP	LBK809020	10/19/2010 1:30	10/19/2010 1:48	923.968	G160M	1589
V-DEL-CEP	LBK817010	12/12/2010 6:12	12/12/2010 6:29	924.992	G130M	1291
V-DEL-CEP	LBK817020	12/12/2010 6:34	12/12/2010 6:52	923.904	G160M	1589
V-DEL-CEP	LBK818010	10/30/2010 16:24	10/30/2010 16:41	924.96	G130M	1291
V-DEL-CEP	LBK818020	10/30/2010 16:54	10/30/2010 17:11	923.968	G160M	1589
V-DEL-CEP	LBK819010	10/31/2010 4:04	10/31/2010 4:22	925.024	G130M	1291
V-DEL-CEP	LBK819020	10/31/2010 4:26	10/31/2010 4:44	924.032	G160M	1589
V-DEL-CEP	LBK820010	12/13/2010 23:42	12/14/2010 0:00	925.024	G130M	1291
V-DEL-CEP	LBK820020	12/14/2010 0:04	12/14/2010 1:13	924.032	G160M	1589
V-DEL-CEP	LBK821010	10/22/2010 1:41	10/22/2010 1:59	925.024	G130M	1291
V-DEL-CEP	LBK821020	10/22/2010 2:56	10/22/2010 3:14	924.032	G160M	1589
V-DEL-CEP	LBK822010	10/31/2010 2:28	10/31/2010 2:46	925.024	G130M	1291
V-DEL-CEP	LBK822020	10/31/2010 2:50	10/31/2010 3:08	924.032	G160M	1589
V-DEL-CEP	LBK823010	10/29/2010 22:59	10/29/2010 23:28	924.928	G130M	1291
V-DEL-CEP	LBK823020	10/29/2010 23:32	10/29/2010 23:50	923.936	G160M	1589
V-DEL-CEP-1	LBK815010	6/13/2011 16:50	6/13/2011 17:12	1152.032	G130M	1291
V-DEL-CEP-1	LBK815020	6/13/2011 17:17	6/13/2011 17:37	1024.032	G160M	1589
V-DEL-CEP	LC2307010	1/18/2013 18:29	1/18/2013 18:49	767.008	G130M	1291
V-DEL-CEP	LC2307020	1/18/2013 18:52	1/18/2013 20:12	763.072	G160M	1589
V-BET-DOR	LBK801010	3/17/2011 8:19	3/17/2011 8:37	927.04	G130M	1291
V-BET-DOR	LBK801020	3/17/2011 8:41	3/17/2011 8:59	927.008	G160M	1589
V-BET-DOR	LBK811010	3/17/2011 9:55	3/17/2011 10:13	927.04	G130M	1291
V-BET-DOR	LBK811020	3/17/2011 10:17	3/17/2011 10:35	927.04	G160M	1589
V-BET-DOR	LBK812010	2/16/2011 10:38	2/16/2011 10:56	927.04	G130M	1291
V-BET-DOR	LBK812020	2/16/2011 11:00	2/16/2011 11:18	927.008	G160M	1589

V-BET-DOR	LBK813010	2/27/2011 22:45	2/27/2011 23:03	927.04	G130M	1291
V-BET-DOR	LBK813020	2/27/2011 23:07	2/27/2011 23:25	927.04	G160M	1589
V-BET-DOR	LBK814010	11/14/2010 1:53	11/14/2010 2:10	927.04	G130M	1291
V-BET-DOR	LBK814020	11/14/2010 2:15	11/14/2010 2:33	926.944	G160M	1589
V-BET-DOR-1	LBK810010	6/23/2011 5:03	6/23/2011 6:08	1127.008	G130M	1291
V-BET-DOR-1	LBK810020	6/23/2011 6:12	6/23/2011 6:32	1036	G160M	1589
V-BET-DOR-1	LBK816010	8/3/2011 15:00	8/3/2011 15:21	1126.976	G130M	1291
V-BET-DOR-1	LBK816020	8/3/2011 15:26	8/3/2011 15:46	1036.032	G160M	1589

It was *well-known*, however, that IUE suffered from scattered optical light contamination, though it turned out to be much more of an issue than we had anticipated. Fig. 42 shows comparisons of representative IUE and COS spectra for each of the three Cepheids observed with COS at the time of writing. The differences are dramatic. The much finer resolution was expected, but as the figure shows, a great deal of what was originally considered continuum flux from the photosphere turned out to be scattered light. This was the reason that IUE spectra of the program Cepheids could unambiguously show *only* the strongest emission lines (if any). In the case of Polaris, as is shown in the top panel of Fig. 43, there was uncertainty as to whether *any* emission lines were present in the spectra; there was only the possible detection of the strong, but blended, oxygen/sulfur lines near ~1300 Å. The scattered light is not present in the COS spectra of Cepheids, however, which display a wealth of emission lines not detected in the archival IUE spectra (Figs. 43 and 44). These lines define rich and complex Cepheid atmospheres and, as is well known, offer excellent atmospheric diagnostic potential (Linsky et al. 1995 and references therein), since different line species originate in plasmas of specific temperatures. Also, emission line strengths and ratios, as well as line broadening and radial velocities, when measured over the stars' pulsation cycles, offer important atmospheric diagnostics. FUV emission line strengths and ratios (along with changes in radial velocity [RV] during pulsations) can also distinguish between supergiant (Cepheid) atmosphere emissions or unresolved main sequence companions (if present).

Emission line fluxes were measured by integrating the total flux beneath the emission line itself, subtracting off any neighboring continuum radiation (if present), with the *Specview* software tool (http://www.stsci.edu/institute/software_hardware/specview), published by the Space Telescope Science Institute. Emission line centers (for RV studies) were measured by fitting Gaussian profiles to each emission line, using the IRAF *splot* routine.

Although many important emission lines are present in the COS spectra, a few of importance were selected for the current study. Future plans for the UV study are to utilize the full set of observed emission lines to construct a differential emission measure for each spectrum. This details the full distribution of plasma temperatures within the atmosphere, and these distributions

can then be compared to those of other cool supergiants and even dwarfs. As discussed later, specific line ratios can also allow the stellar atmospheric density to be determined, but the Cepheid spectra do not display any of the most often used (hence, best understood) line pairings. This has forced us to search for less-commonly used density diagnostics, with the unavoidable consequence that these diagnostics will not be as well-studied. So great care must be taken to find usable (and, above all, reliable) density diagnostics, given the lines present in the COS FUV spectra of the Cepheids.

For this study, the following lines were selected because they represent a wide range of formation temperatures, and are relatively free from contamination via blending with nearby lines, offering a "pure" measurement of the emission line in question. The lines selected are:

- **O I 1358 Å** – selected in favor of the well-known O I triplet at ~1300 Å because the triplet are fluorescent lines excited by H Lyman-β radiation (Koncewicz & Jordan 2007) and also suffer from blending with (primarily) nearby S I lines. Therefore, the flux of the O triplet is directly related to the Lyman flux and not necessarily indicative of plasmas at the O I peak formation temperature of $1 - 2 \times 10^4$ K (Doyle et al. 1997).
- **Si IV 1394/1403 Å** – a well-known doublet with a peak formation temperature of $\sim 5 - 8 \times 10^4$ K (Linsky et al. 1995). This doublet represents an important link between the cooler, O I emitting plasmas and the hotter plasmas responsible for the N V and O V emission lines.
- **N V 1239/1243 Å** – another well-known doublet, but with a higher peak formation temperature of $\sim 1.5 - 2.5 \times 10^5$ K (Linsky et al. 1995). This doublet is very important because the lines are prominent in the spectra and occur at shorter wavelengths where photospheric continuum flux is essentially negligible. The N V doublet is the best measure of higher-temperature plasma variability in the UV range.
- **O V 1218 Å** – although not selected for a variability study due to its location on the red wing of the Lyman-α geocoronal-contaminated emission line, the line is clearly observed in the spectra (Fig. 43) and has a peak formation temperature of $\sim 2 - 4 \times 10^5$ K (Linsky et al. 1995). This places it among the hottest lines observable in the UV spectra of cool stars like the Cepheids, and its presence provides an important link to higher-temperature X-ray emissions.

Progress in the satellite-based high-energy studies has been much slower than for the optical studies. As a result, only δ Cep and β Dor currently have substantial phase coverage with COS, although important phase-gaps still exist in the β Dor dataset, and approved observations are still to be carried out to completely fill in the Cepheid's phase-space. As an illustration of the results

of the UV program thus far, the current COS light curves of δ Cep and β Dor are given in Figs. 45 & 46. In looking at these plots, a few features are immediately striking:

The specific phases at which line emissions begin to increase. The phase coverage of δ Cep has been more illustrative in terms of the rise in emission flux. However, preliminary conclusions can be extrapolated for β Dor from the currently available data, taking into account the findings of previous UV studies. In comparing the emission line fluxes to the included RV plots for δ Cep, we see good correlation between the phase where UV line emissions begin to peak and a "pre-piston phase" as given by the radial velocities. During this pre-piston phase, the photosphere has almost reached its minimum value, its recession is decelerating, and it is about to begin expanding again. Fokin et al. (1996) have shown that a shock should be propagating through the atmosphere of δ Cep at this phase (~$0.8 - 0.85\phi$). The emission line flux behavior, combined with the results of Fokin et al. (1996), give strong evidence in favor of a shock heating mechanism. As will be discussed later, RVs show that this phase range is also when atmospheric compression begins. This effect would further excite atmospheric plasmas.

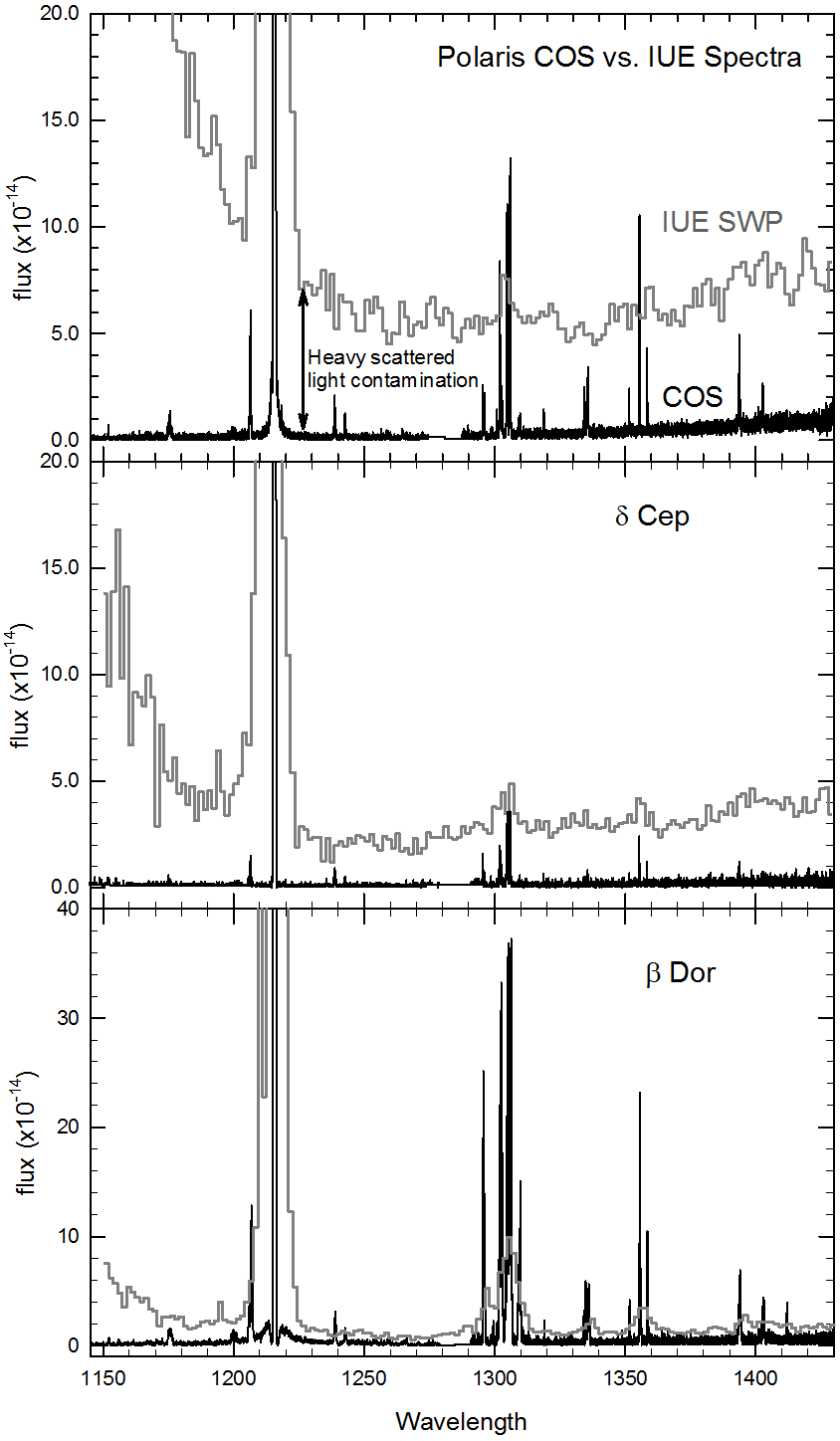

Figure 43 – Comparisons of IUE and HST/COS data for the three Cepheids observed with COS thus far. The *dramatic* improvement in data quality, particularly in the reduction of scattered light contamination, is easy to see.

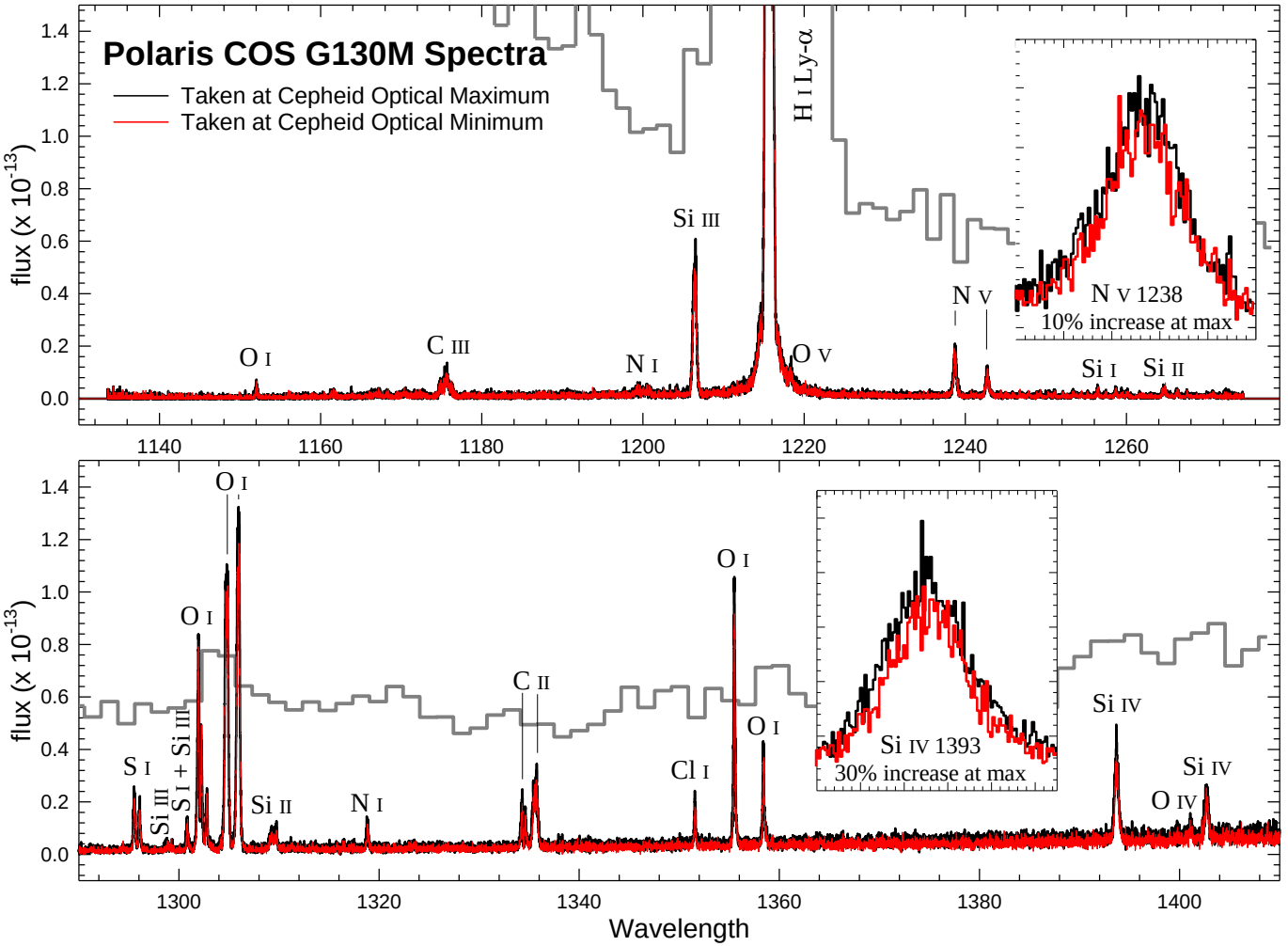

Figure 44 – A detailed view of the Polaris HST/COS FUV (G130M grating) spectra is shown. Again, the IUE data is shown as the dark gray spectrum. All visible emission lines are identified. The low level of emission line variability between the spectra is highlighted by inserts.

For β Dor, as mentioned, the conclusions are a bit more ambiguous, arising from the current (at the time of writing) lack of phase coverage to observe the rise in emission line flux. As seen in Fig. 46, the approach to maximum is partially observed for N V, but the cooler emission lines are only observed during phases of decreasing flux or at phases of quiescent emission. The phase coverage begins just after the piston phase has begun for β Dor, but it is still possible that the rise in emission line flux begins shortly after the deceleration of the photosphere, as it does in δ Cep. Hutchinson et al. (1975) report that a shock would be propagating through the atmosphere around this phase, based on five-filter UV photometry (in the ~1330 – 4250 Å range) taken by the *Wisconsin Experiment Package* (*WEP*) onboard *Orbiting Astronomical Observatory-2* (*OAO-2*).

The abruptness of the increase in emissions from δ Cep is indicative of a sudden heating or excitation mechanism. For example, over a phase-space of just 0.08ϕ, the O I flux increases by ~7× (numbered points 4 – 7 in Fig. 45) and the Si IV flux increases by ~10×. Such an abrupt, strong plasma excitation also points to a shock-related mechanism. The decrease in flux is also rapid (though not as rapid as the increase), as one would expect for a sudden heating event such as a shock. It's important to note that a possibly related behavior occurs in Mira variables (pulsating, asymptotic giant branch [AGB] stars), which have shown "cool" UV emission lines excited by their own pulsation-induced shocks (Wood & Karovska 2000 and references therein). The only UV lines observed in the Miras have cooler formation temperatures than the O I line studied in Cepheids, and no "warmer" lines are observed. This could be understood as a consequence of the Miras producing weaker shocks, since their pulsation periods are much longer than the Cepheids' and their velocity amplitudes are also smaller. It also appears that the line emissions disappear at certain phases, implying that there are no quiescent atmospheric emissions, only those excited by the shocks.

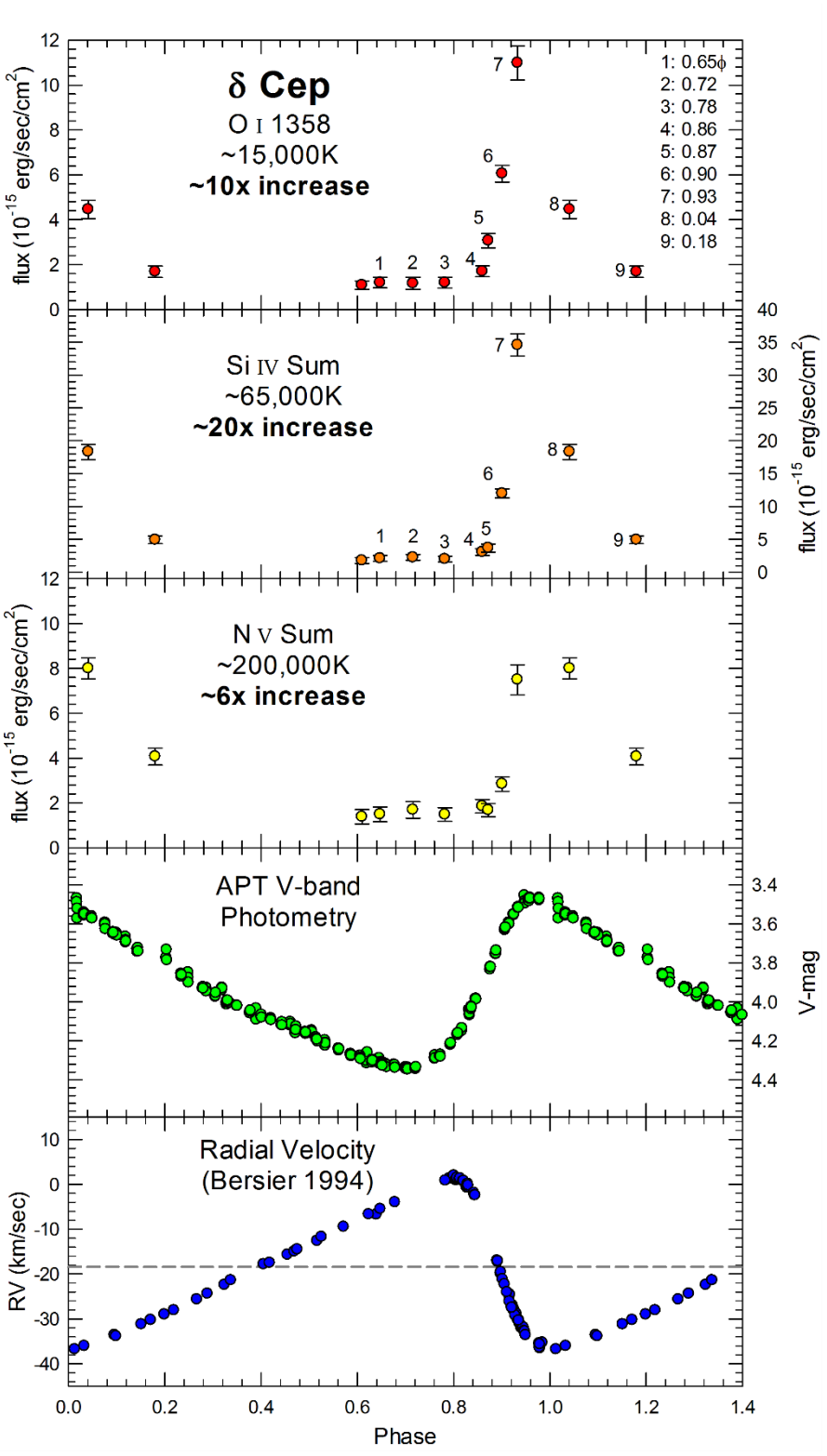

Figure 45 – Integrated fluxes of 3 important emission lines observed in δ Cep with COS - top three panels. The fourth panel (green points) is the V-band light curve from this program. The bottom panel plots the photospheric radial velocities. Spectra referred to later in the thesis are numbered, and the associated phases are given in the top plot.

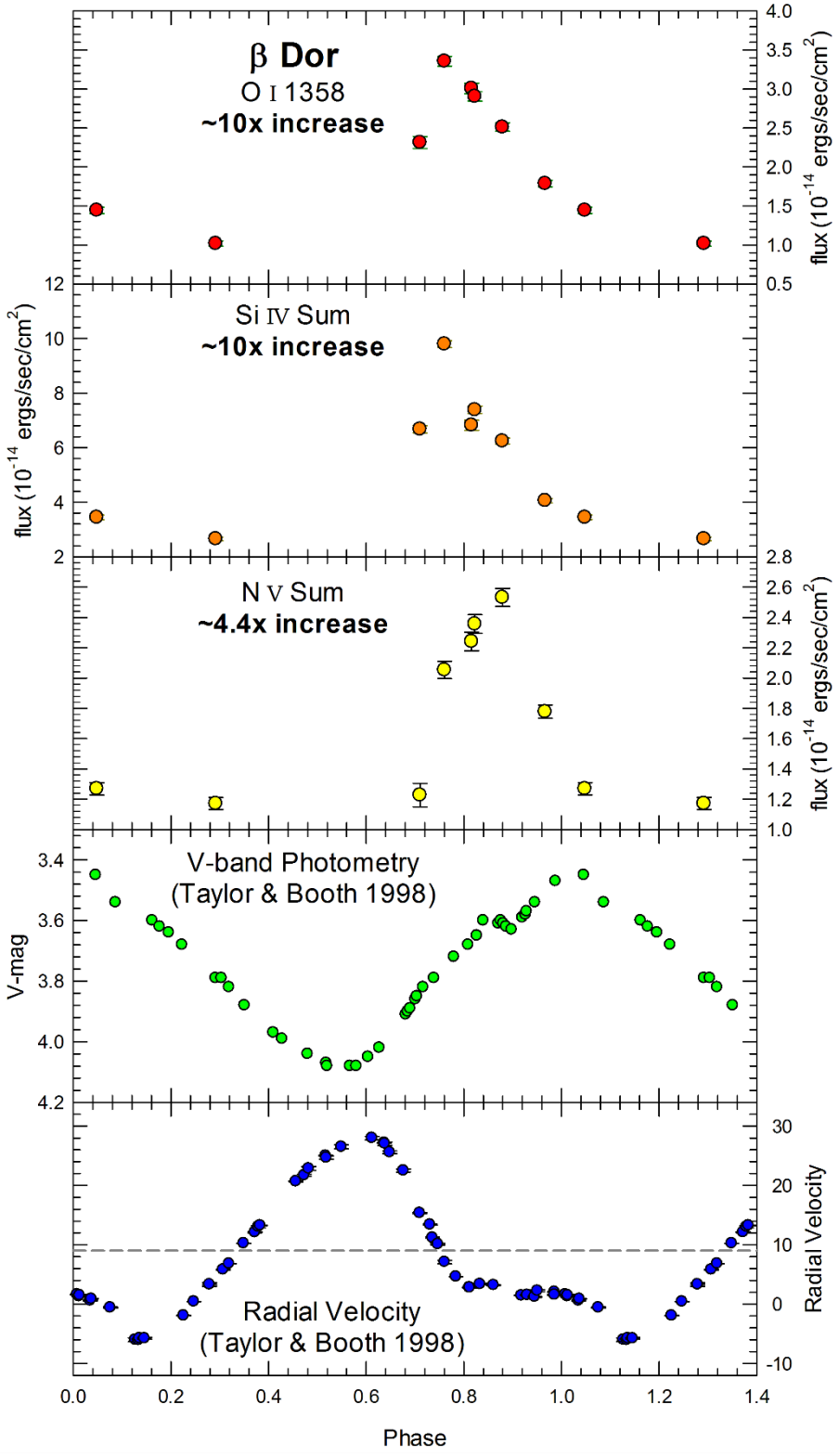

Figure 46 – The same arrangement as in Fig. 45, but for β Dor.

For β Dor, again the conclusions are mitigated by insufficient phase coverage, but the decrease in emission line flux appears much more gradual than in δ Cep. Also, the range of flux variability is much smaller in β Dor. This partially arises because β Dor is more active during quiescent phases than δ Cep. Since β Dor is a longer period Cepheid, and reaches lower temperatures, it is safe to assume that β Dor would possess a deeper, larger convective zone which could be responsible for the stronger quiescent emissions observed, on top of which additional compression/shock heating is present at the appropriate phases.

The phase-difference between the peak flux of the most energetic (highest peak formation temperature) emission feature observed – N V ~1240 Å – and the peak fluxes of the two cooler emission features. This aspect of the program requires robust phase-coverage, so neither Cepheid can have strict, quantitative conclusions drawn. However, in both Cepheids the lower temperature plasma emission lines appear to peak earlier than N V, the hottest emission line. The phase difference is a good bit larger in β Dor than it is in δ Cep. However, Böhm-Vitense & Love (1994) theorized that emissions from the hottest plasmas should peak first in the case of shock-heating, followed by line emissions from cooling plasmas in the post-shock regions. This is clearly an interesting behavior, and the newly approved HST-COS Cycle 20 observations will allow us to more strictly define the phase differences.

In a final evaluation of the overall intensity of atmospheric emissions from the Cepheids observed thus far, we plot spectra (scaled to account for differences in distance) representative of the range of emissions found for each star in Fig. 47. For Polaris, whose range of line variability appears small, only the spectrum with stronger emissions is plotted to prevent further crowding of the plot. As we have mentioned before, the true phase of maximum atmospheric emissions from Polaris has most likely been missed by our limited observations. The fluxes that we have measured for Polaris place it within the range observed in δ Cep, but further observations are needed to truly compare the two Cepheids' maximum emissions. To a certain degree, though, the range of emissions from δ Cep and β Dor are understood and can be compared. For N V emissions, β Dor is ~5× as strong as δ Cep at their maximum phases, and ~13× as strong at their respective minima. For Si IV emissions, β Dor is ~3× as strong as δ Cep at their maximum phases, and ~7× as strong at their respective minima. Finally, for O I emissions, β Dor is ~3× as strong as δ Cep at their maximum phases, and ~16× as strong at their respective minima. Since we presently have no reliable estimates of the sizes of the Cepheid atmospheres, we can use their photospheric radii to serve as an approximation of the ratio of their emitting areas. On average, β Dor has ~2.3× the emitting area of δ Cep. As one can see, this is perhaps enough to account for the difference in *maximum* emissions. However, a difference of emitting area is not enough to

account for the relative strength of *average* atmospheric emissions in β Dor, which can also indicate different balances of heating mechanisms at play in the Cepheids.

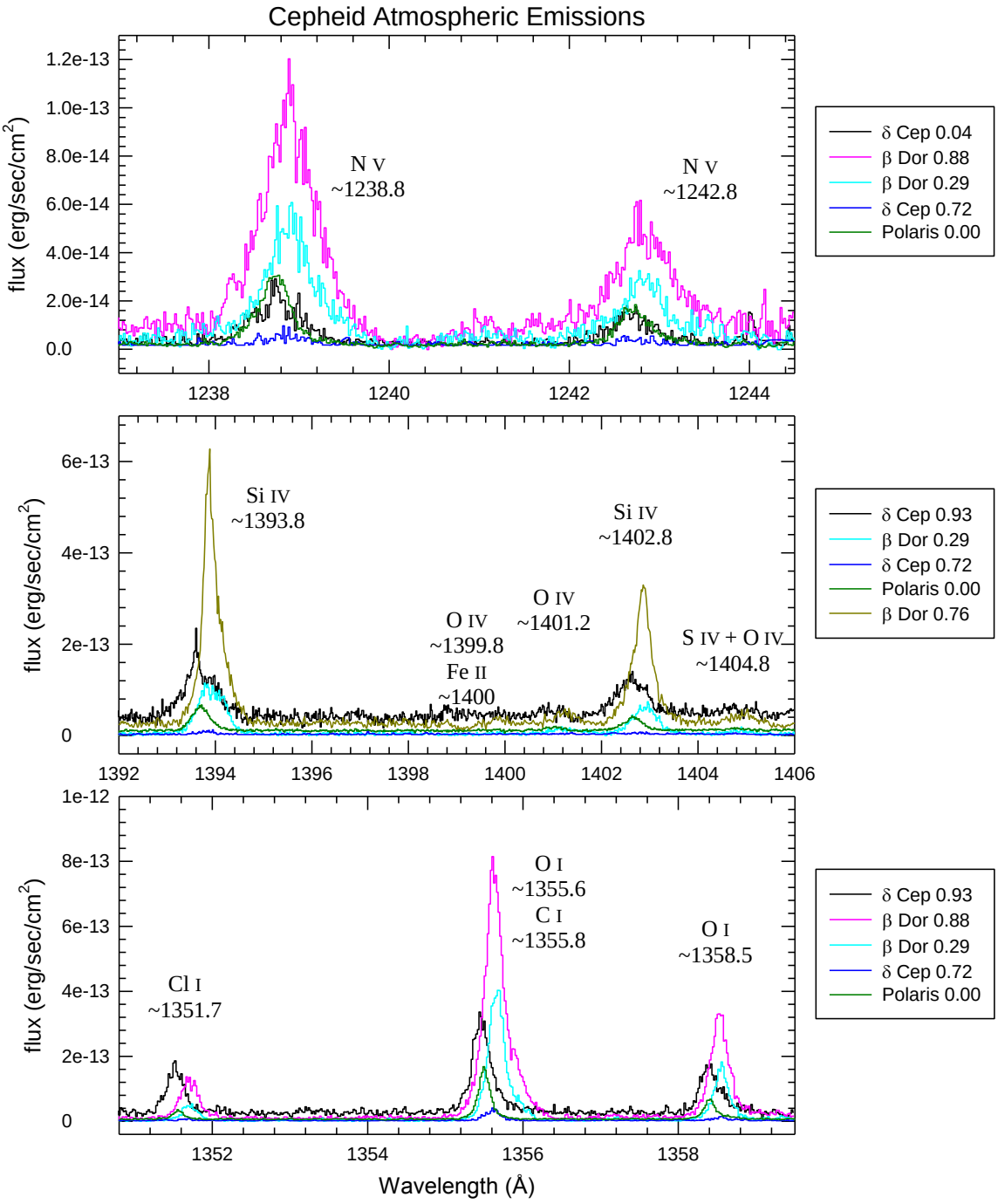

Figure 47 – A comparison of the COS spectra of all three Cepheids, giving an idea of their relative emission strengths and widths. As seen here, β Dor is easily the most active Cepheid. The phase of each Cepheid's spectrum is given in the legends.

In addition to what the emission line fluxes can tell us about the heating mechanism(s) at work in Cepheid atmospheres, the line profiles and radial velocities observed in the COS spectra can provide valuable, complementary information. Fig. 48 gives the profiles of the O I 1358 and Si IV 1394 emission lines observed in several spectra of δ Cep. The most potentially informative characteristic is the heavy asymmetry present in spectra 6, 7 and (for O I) 8, where the lines show a strong, additional blue-shifted emission component. This can be understood as the effect of an expanding shock emerging from the Cepheid photosphere. On the "near" side of the Cepheid atmosphere, the shock is approaching, producing the blue-shifted emission. In spectrum 8, the O I line still shows heavy asymmetry, but the Si IV line shows an extremely broad and even emission profile, indicative of a large velocity distribution but no additional blue-shifted feature. At this phase (0.04ϕ) we could be observing Si IV emission from a very turbulent post-shock region, where the high turbulence would be responsible for the velocity distribution, meaning that the shock has "passed by" the Si IV emitting region. The difference in O I and Si IV line profiles at this phase indicates that they are likely originating from different regions (heights) within the Cepheid atmosphere. The line profiles offer up further evidence in favor of shock-heating and compression being responsible for the enhanced emissions.

The radial velocities of the UV emission lines can give additional information on the workings of the δ Cep atmosphere, although we note there are COS wavelength calibration issues affecting their absolute accuracy (Aloisi et al. 2010). As such, the velocities can possess a larger than normal uncertainty, but the agreement in overall velocity trends between the three lines plotted gives confidence in the measures. In Fig. 48, the radial velocities (from top to bottom panels) of the O I, Si IV, N V emission lines and photosphere are plotted. As indicated in the figure, the emission line radial velocities have had the phase-specific photospheric radial velocity removed. For spectra where the Si IV and/or O I line showed asymmetry, two Gaussian profiles were fit to the line. The RV of the broad atmospheric emission is plotted, as opposed to the blue-shifted emission component discussed in the previous paragraph. The agreement between the Si IV and O I velocity behaviors and that of the N V line, which maintained a symmetric single-Gaussian profile throughout the observed phases, gives confidence in the double-Gaussian approach. As seen in the plot, the phases of increased flux ($0.85 - 0.04\phi$) correspond to phases where the stellar atmosphere is receding (compressing) relative to the photosphere. Specifics of key, selected phases are:

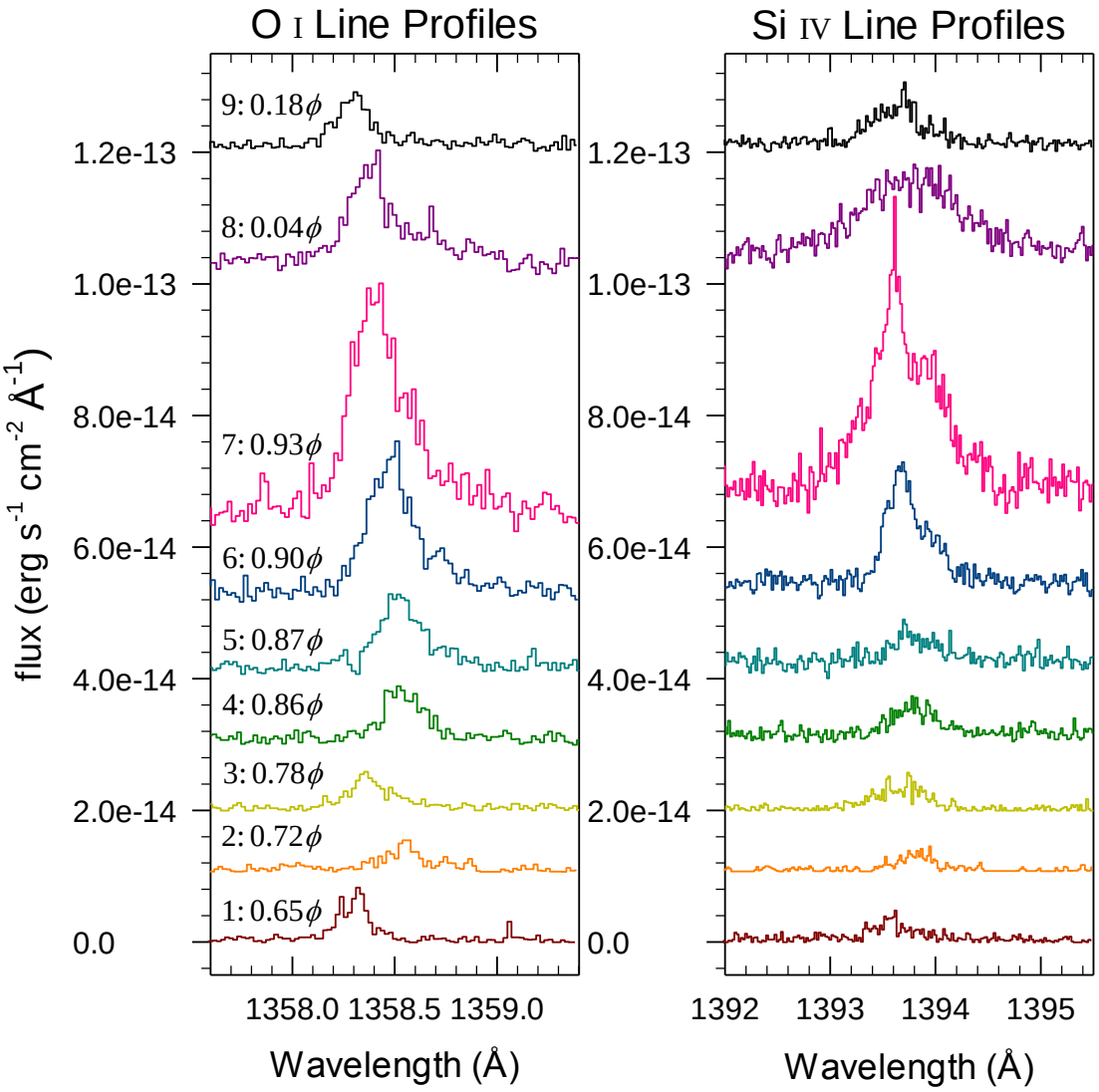

Figure 48 – The line profiles of O I (left) and Si IV (right) for δ Cep are shown. The different emission strengths can be seen, along with the asymmetries present in several phases, caused by the emergence of an additional blueward emission feature during phases where a shock is propagating through the atmosphere.

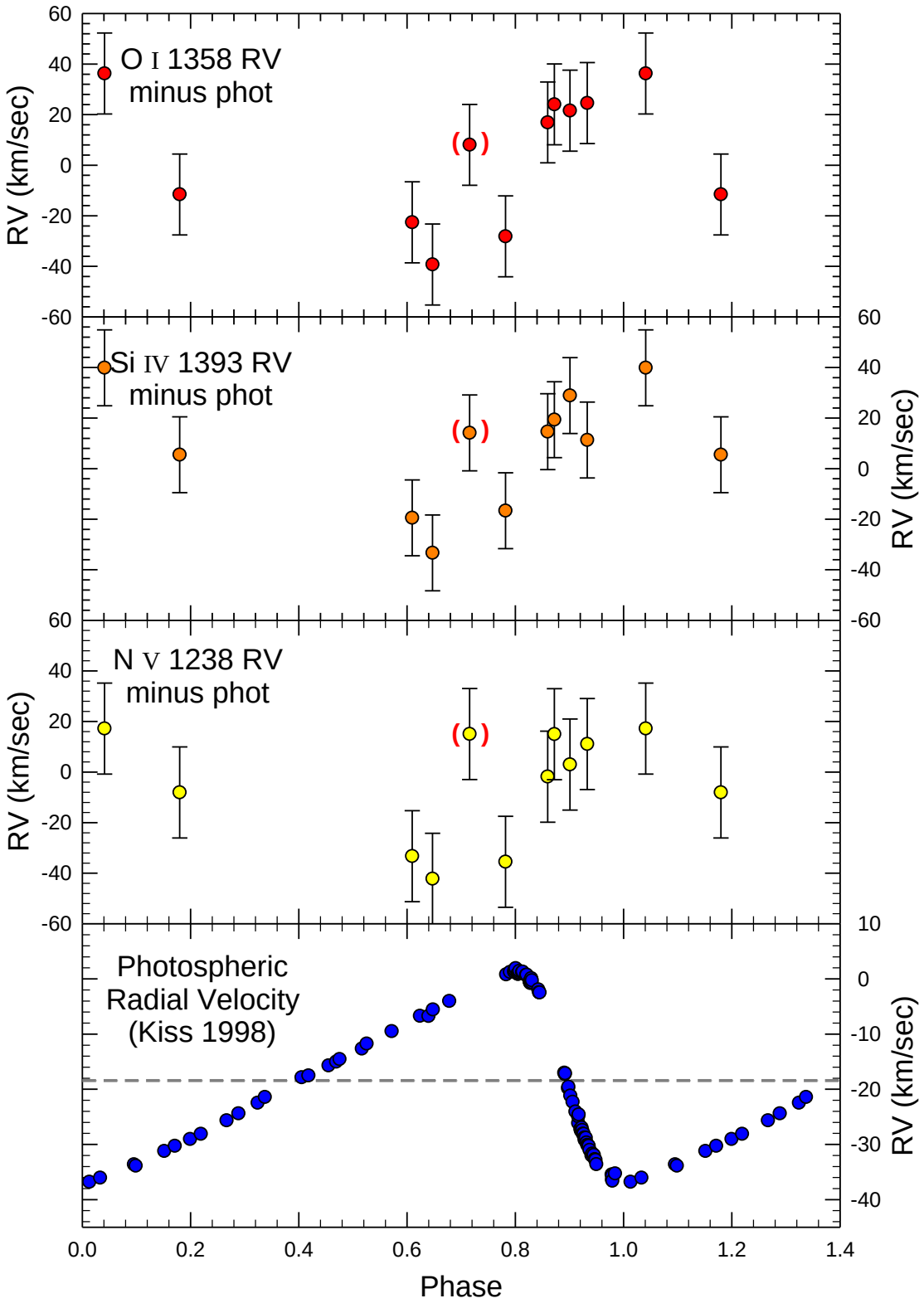

Figure 49 – Radial velocities determined for the COS-observed emission lines of δ Cep are shown vs. phase. The emission line velocities have the photospheric velocities (bottom panel) removed.

The bracketed RV is from a spectrum with a possible wavelength discrepancy, but the lack of continuum flux prevents us from confirming via photospheric or ISM absorption lines.

- $\phi \approx 0.86 - 0.87$: At these phases, the recession of the photosphere begins decelerating as it approaches minimum radius. While the photospheric recession is decelerating, the atmosphere recedes at a faster pace, as indicated by the emission line velocities. Thus, this phase-range is when the atmospheric compression begins. This is also the phase-range where Fokin et al. (1996) predict that a shock should emerge from the photosphere.
- $\phi \approx 0.90$: The photosphere has reached minimum radius (the photospheric velocity is at its mean value here), before expanding again – the start of the piston phase. While the stellar surface is no longer receding, the atmosphere is collapsing down onto it with appreciable velocity. The line profiles broaden at this phase, the result of atmospheric compression. Also, a blueward emission component becomes visible, indicating that an outward propagating shock is now passing by the line formation region of the atmosphere. This phase is most likely rather complex, in terms of atmospheric heating/excitation.
- $\phi \approx 0.93$: The photosphere has now begun expanding again, but the atmosphere continues receding relative to it, leading to even stronger atmospheric compression and line broadening. Line asymmetry is very pronounced at this phase. Line emissions from both the compressed atmospheric plasmas, and the shocked plasmas, are at their strongest levels at this phase.
- $\phi \approx 0.04$: Just after maximum visual brightness, at this phase the photosphere is undergoing its most rapid expansion and while the atmosphere continues to recede. Emission line fluxes are decreasing at this phase, yet line profiles are broader than in any other phase. The O I line profile still displays a strong blueward emission component. However, the Si IV line profile is very even and symmetric. The markedly different emission line profiles (with rather different peak formation temperatures) could indicate that they originate at different levels (heights) within the atmosphere. At this phase, shocked plasmas still exist in the O I line formation region, but we appear to be observing Si IV emissions from a turbulent post-shock region.
- At all phases, the N V lines display symmetric line profiles lacking any additional emission components, though they undergo the same radial velocity changes as the cooler lines. The phase lag, where peak N V emission appears to occur later than peak Si IV emission which, in turn, is slightly later in phase than O I, could indicate the time necessary for the shock to reach the different atmospheric levels, but could also indicate the time required to achieve higher levels of ionization. Finally, cooler O I emission could also occur at multiple heights within the atmosphere, leading to longer observation of shocked material, whereas emissions from the hotter lines are more localized.

Because of the incomplete understanding of the balance of heating mechanisms at work in Cepheid atmospheres, it was decided to place them within the context of somewhat similar stars. The most natural comparison to be made is with the so-called "Hybrid-atmosphere supergiants" (simply *Hybrids* hereafter): stars that display cool winds *and* heated atmospheres. The Hybrids are similar to the Cepheids in spectral type and luminosity, but show no definitive evidence of significant variability or pulsations. To some extent, Hybrids can be seen as an example of how Cepheids might behave if they didn't undergo the radial pulsations which define them as a class of variable star. Fortunately, HST medium- to high-resolution UV spectra have been obtained for a number of Hybrids. We compared these spectra to better illustrate the atmospheres present in each class of supergiant. The Hybrids, for which UV spectra were obtained and plotted, are given in Table 16. Data sources marked as STIS are pipeline-processed spectra obtained from the MAST archive, where STIS STARCAT come from a database of further refined spectra maintained by Thomas Ayres (http://casa.colorado.edu/~ayres/StarCAT/).

Table 17 – Spectral Types and Data Sources for Hybrids and Cepheids

Star	Spectral Type	Data Source
Representative Hybrids		
α TrA	K4 II	STIS
α Aqr	G2 Ib	STIS
β Aqr	G0 Ib	STIS STARCAT
β Cam	G0 Ib	STIS STARCAT
β Dra	G2 II	STIS
Cepheids		
β Dor	F4–G4 Ia–II	COS
δ Cep	F5–G1 Ib	COS
Polaris	F7–F8 Ib–II	COS

The results of the comparisons including β Dor are shown in Figs. 50 and 51, and those including δ Cep are shown in Figs. 52 and 53. The "very active supergiants" β Cam and β Dra (Reimers et al. 1996) are easily the strongest emitters when it comes to the hottest plasmas (N V and O IV emissions). No matter what line is being studied, δ Cep and Polaris are much less active than all other supergiants plotted, but β Dor does attain nearly Hybrid-levels of activity from hotter plasmas. For S IV emissions, β Dor ranges from less active than all supergiants at its minimum to more active than the Hybrids but less active than the very active supergiants at maximum. For the cool O I emissions, however, β Dor reaches the highest activity level of the supergiants plotted, due in part to its noticeably broadened profile. This can be taken as further indication of its likely turbulent atmosphere's strong velocity gradient.

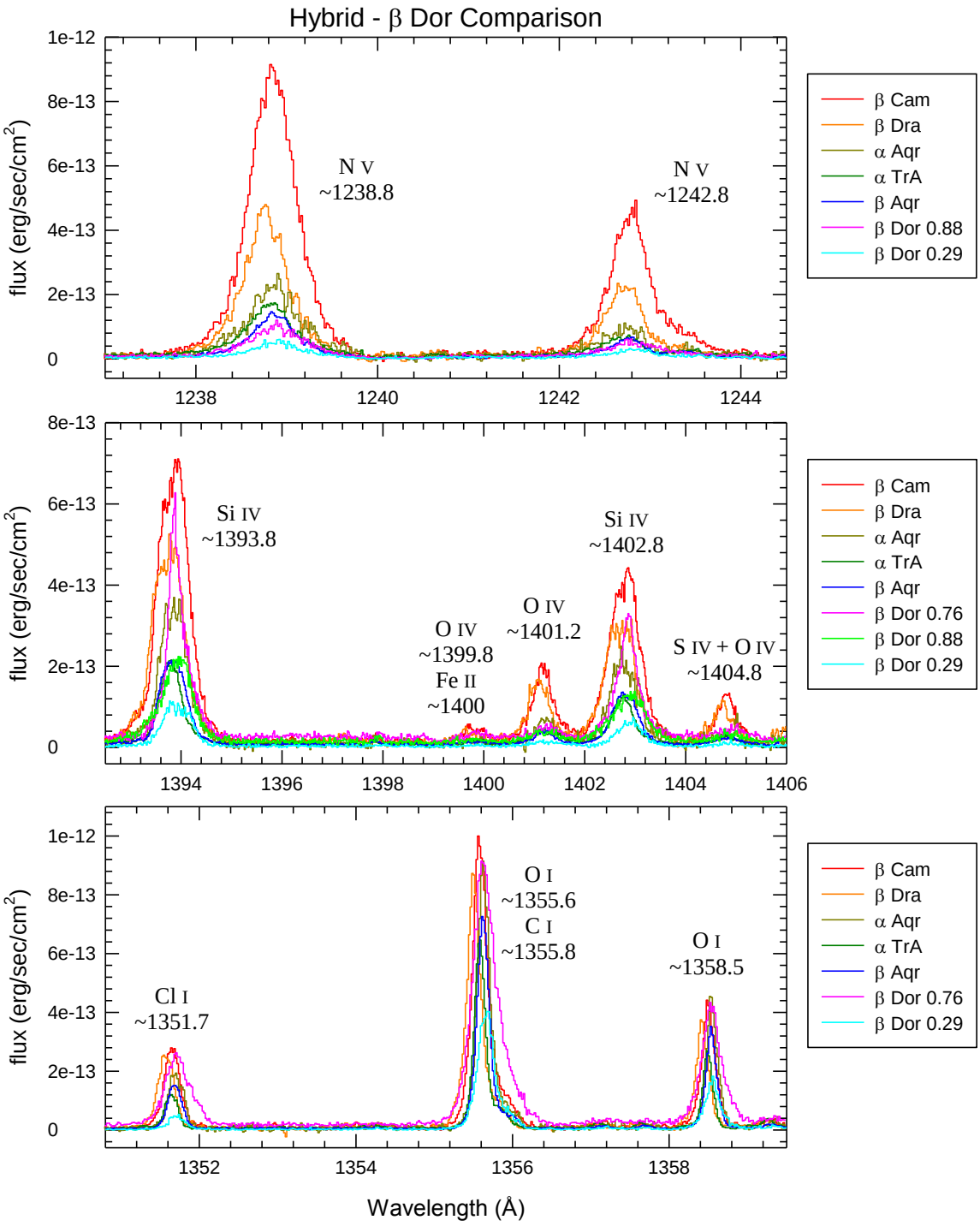

Figure 50 – Comparison of UV spectral regions of: the very active supergiants (β Cam and β Dra), the Hybrids (α and β Aqr and α TrA), and the Cepheid β Dor at its varying emission levels. The phase of each β Dor spectrum is given in the legend.

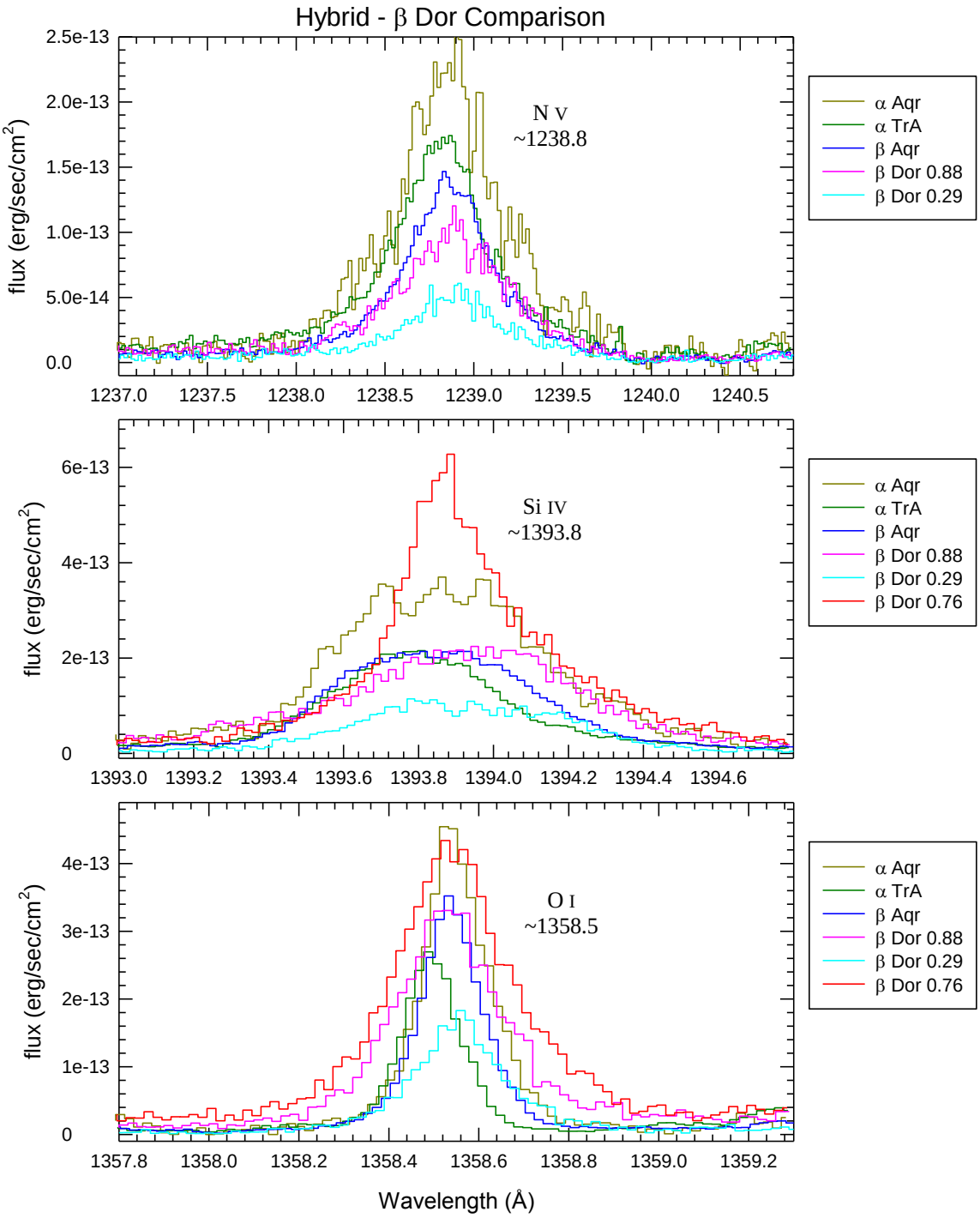

Figure 51 – A closer view of individual emission lines in the supergiants, with the very active supergiants removed for ease of viewing. At or near maximum, one can easily see the broadness of β Dor's O I emissions, and the asymmetry of the O I and Si IV lines when compared to the Hybrids. The phase of each β Dor spectrum is given in the legend.

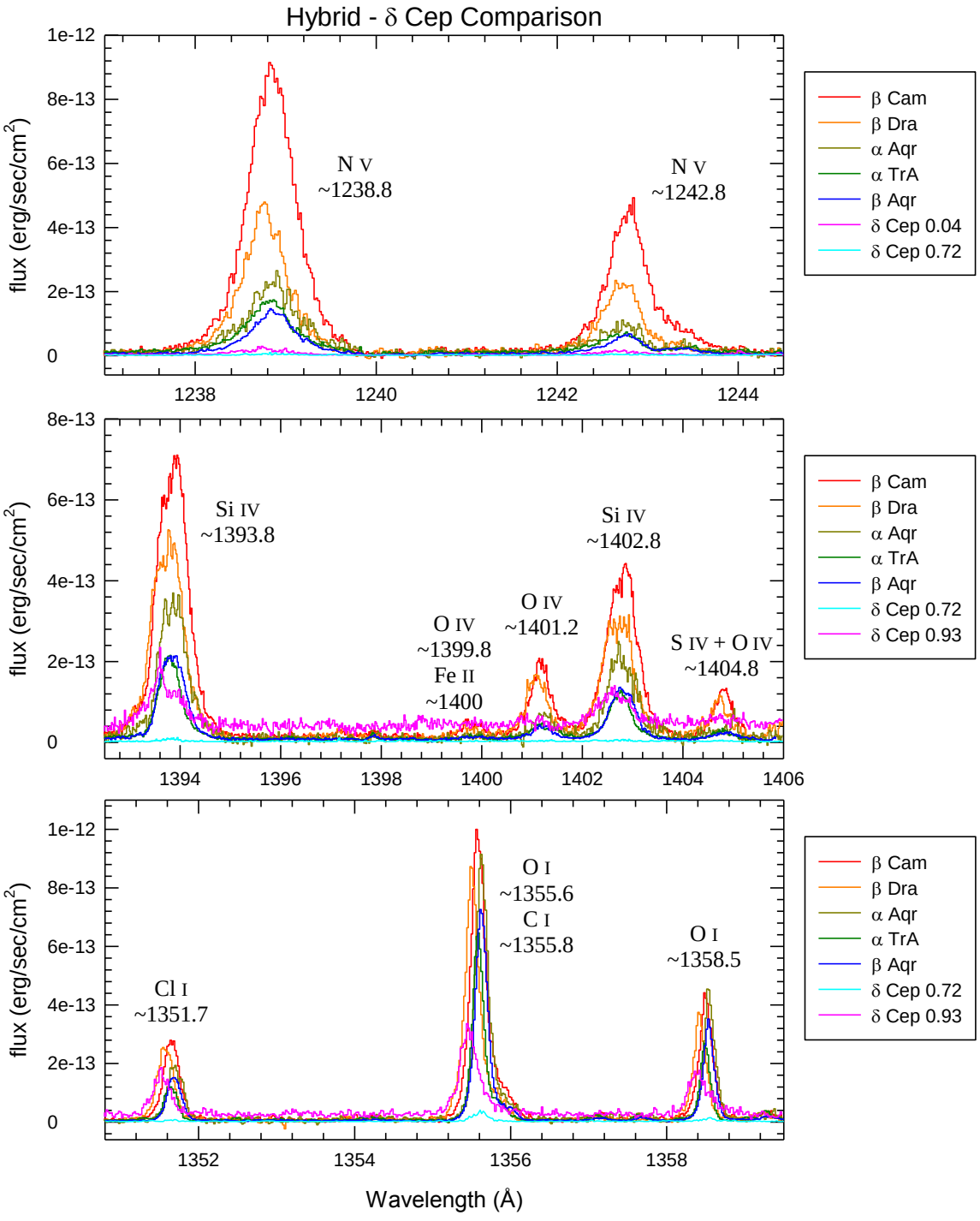

Figure 52 – The same convention as Fig. 50, but with δ Cep instead of β Dor.

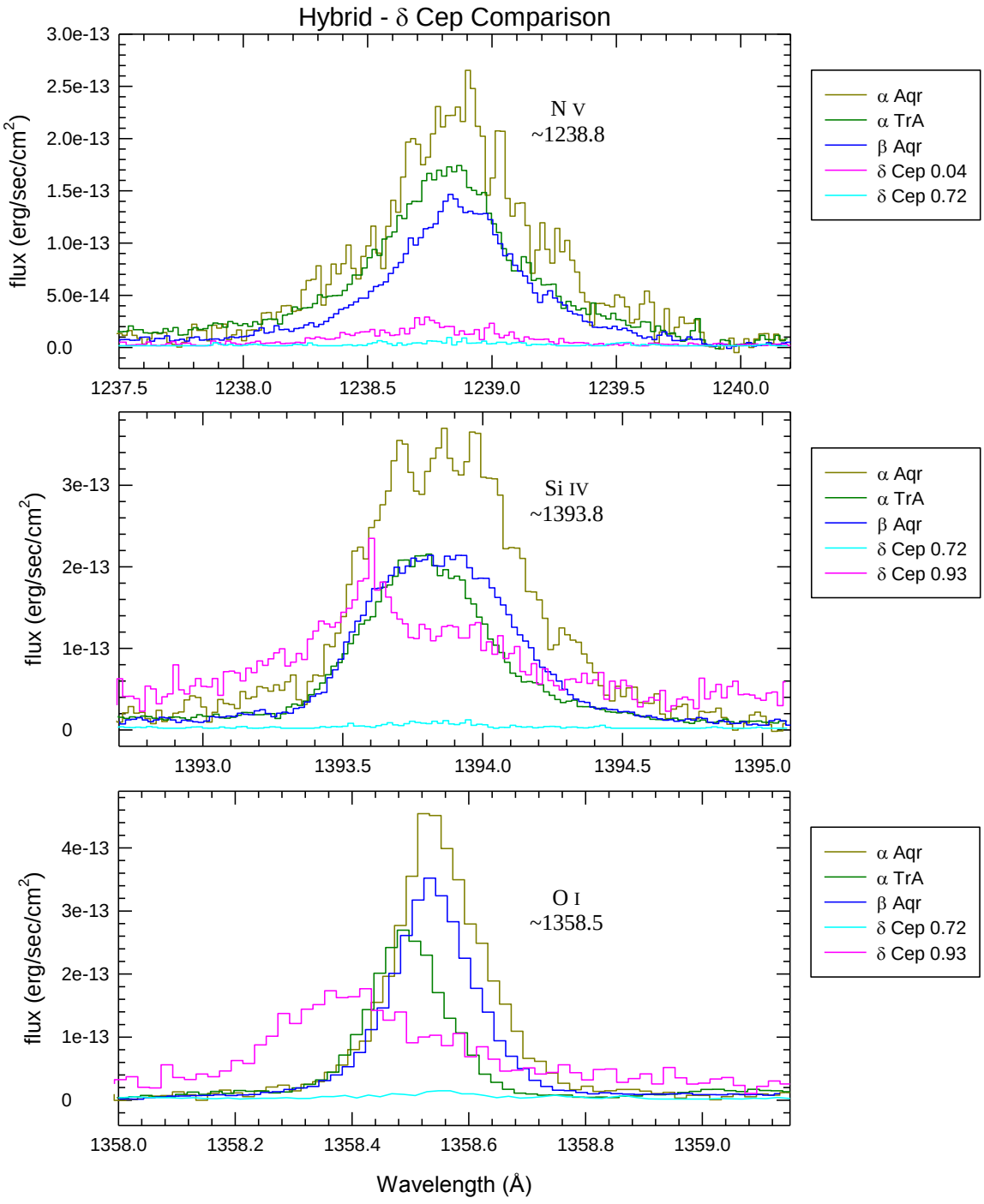

Figure 53 – The same convention as Fig. 51, but with δ Cep instead of β Dor.

When comparing δ Cep to the other supergiants, however, equal comparisons can never be made. It is obvious that, at the plasma temperatures probed by the UV emissions, the atmosphere of δ Cep (and the comparably active Polaris as seen in Fig. 47) is far less active than either the Hybrids or the very active supergiants, no matter which phase of the Cepheid is being observed. At maximum emission, δ Cep does have similarly broad emission lines compared to the Hybrids, but still with much less overall intensity, again in stark contrast to the behavior of β Dor. The Hybrids raise further questions about the specific heating mechanisms at work in the Cepheids.

Most recently, in light of the pulsation-induced variability and likely compression of the atmosphere, attempts have been made to find suitable electron density-sensitive emission line ratios to gain further physical insights into the Cepheid and other supergiant atmospheres. A handful of well-studied ratios exist in the literature, making use of such emission lines as, e.g. C III (1909 Å), Si III (1892 Å) and O IV (~1400 Å). Very unfortunately, either the spectra available for the program stars do not cover the wavelengths at which these emission lines occur (C III 1909 Å or Si III 1892 Å), or the lines are not strong enough to allow an unambiguous measurement (O IV ~1400 Å). Thus, none of the usual density measures could successfully be applied, and a search for less well-known density ratios was carried out. Making use of the latest CHIANTI atomic database (http://www.chiantidatabase.org/) available at the time of writing (v7.1.3), investigations were carried out for a ratio of Si III line fluxes:

$$R_{Si\ III} = \frac{f(1298.894 + 1298.948)}{f(1206.502)}$$

Measurements of all Hybrid spectra show very low densities, as do *almost* all Cepheid spectra. Spectrum 6 of δ Cep (Fig. 45), where the flux is steeply rising, shows a much higher density of $N_e \approx 3.2 \times 10^{10}$ cm^{-3}. For reference, at similar plasma temperatures to those probed by the Si III ratio above, quiet regions of the Sun have measured densities of ~5×10^{10} cm^{-3} and active regions have densities of ~1×10^{10} cm^{-3} (Dupree et al. 1976), and other studies (e.g. Keenan et al. 1989) have found solar densities to match that measured for δ Cep.

It must be noted, though, that issues have been raised with using the Si III 1206.502 Å line in density diagnostics. Dufton et al. (1983) calculated that, for the Sun, the 1206 line would be far too optically thick to give an accurate density. Although we believe that, in the supergiants, the line would essentially be optically thin and suitable in that regard, there is also the temperature sensitivity to take into account when using a ground state transition like 1206 with other subordinate features from higher levels. As such, we view the result as confirmation of increased atmospheric density during the phase of rising flux, but are still investigating the usefulness of the Si III ratio in returning an accurate, numerical density measure.

3.2 X-ray Studies with XMM-Newton and the Chandra X-ray Observatory

UV line emissions with formation temperatures of 10^6 K (MK) and hotter are rare, typically weak, and only appear in the most active of stars. The best example of this would likely be the coronal Fe XXI 1354 Å emission line (see Linsky et al. 1995 for a discussion of the line). This line has a peak formation temperature of ~1 × 10^7 K, but is a relatively weak line and is also blended with a neighboring C I line. None of the COS Cepheid spectra that we obtained unambiguously displayed the Fe XXI emission line. Thus, to detect and study Cepheids at MK temperatures, X-ray observations are needed. Though X-ray activity in Cepheids was considered possible (from, e.g., pulsation-induced shocks) in the mid-1990s (Sasselov & Lester 1994), the failure of previous efforts to detect X-rays with pointed Einstein and ROSAT observations reinforced the theory that Cepheids are not (at least significant) X-ray sources. Even with *log* $L_X \approx 29$ erg/s, the problem with detecting X-rays from Cepheids is that they (except for Polaris at ~133 pc – van Leeuwen 2007) are relatively far away at d > 250 pc. Thus, based on the null detections, Cepheids could only have relatively weak X-ray fluxes ($f_X \leq 10^{-14}$ ergs/s/cm$^{2)}$. Though Polaris was detected on the 3σ level in a *Röntgen Satellite* (ROSAT)/High Resolution Imager (HRI) archival image (the detection was not discovered until several years after the observation was carried out – see Evans et al. 2007), definitive detection of X-rays from Polaris and other "nearby" Cepheids had to wait for the arrival of powerful X-ray observatories such as XMM-Newton (XMM) and Chandra.

Accordingly, we successfully obtained Chandra (PI: Evans) and XMM-Newton (PI: Guinan) observations of multiple Cepheids – Polaris, δ Cep, β Dor, SU Cas and ***ℓ*** Car have been observed to date (Table 17). The Chandra data reduction for Polaris is discussed in Evans et al. (2010). The XMM observations were fully re-processed from raw data with XMM-SAS (Scientific Analysis System) and filtered for any background flaring events. The data were then modeled using the *Sherpa* modeling and fitting package (distributed as part of the *Chandra Interactive Analysis of Observations* (*CIAO*) suite). *MEKAL* models (http://cxc.harvard.edu/sherpa/ahelp/xsmekal.html) were used for the final one- and two-temperature (1T and 2T) fitting and flux calculations. The models calculate synthetic X-ray energy distributions for a given plasma temperature, utilizing a database of emission line parameters for various elements, known to prominently occur at X-ray wavelengths. The nearest 3 Cepheids (and so far the only Cepheids detected) – Polaris, δ Cep & β Dor – display X-ray luminosities of *log* $L_X \approx 28.6 – 29.2$ ergs/s (Table 17 gives the relevant information for the detections). Neither the short period Cepheid SU Cas (P = 1.95-d; d = 395 ± 30 pc) nor the long period, luminous Cepheid ***ℓ*** Car (P = 35.5-d; d = 498 ± 55 pc: Benedict et al. 2007) were detected. Upper X-ray luminosity limits of *log* $L_X < 29.6$ and 29.5 ergs/s were estimated for ***ℓ*** Car and SU Cas, respectively, based on exposure times, background count rates

and stellar distances. Therefore, it is still possible that SU Cas and ℓ Car are X-ray sources with similar levels of activity to the Cepheids detected thus far, but are too distant to be detected above the background of the XMM exposures. However, the failure to detect two of our targets underscores a long-standing ambiguity present in the X-ray studies of Cepheids.

Since the initial detections of the three Cepheids at X-ray wavelengths first occurred, the argument has been made that unresolved companions were perhaps responsible for the activity being mistakenly assigned to Cepheids (see Evans et al. 2010). This is a definite possibility that needs to be taken into account, since Cepheids are young stars (~50 – 200 Myr) and any main-sequence G-K-M companions (if present) would be coronal X-ray sources with X-ray luminosities similar to that of the Cepheids (see Guinan & Engle 2009 and references therein). To within the accuracy of the instruments (4-arcsec per pixel for the XMM images), the X-ray detections are centered on the locations of the Cepheids themselves to within a single pixel, as shown in Figs. 55 – 57. Given the spatial resolution of the XMM detectors, this alone does not rule out nearby companions, but it is nevertheless the best positional confirmation that can be achieved with the instrument. Further confirmation comes from our HST/COS results, which show plasmas up to 10^5 K that are variable with the Cepheids' pulsation periods – indicating that plasmas approaching soft X-ray emitting temperatures exist in Cepheid atmospheres. Also, our X-ray observations of δ Cep show variability possibly correlated with the stars' pulsation periods, as with the FUV emission lines (see Fig. 54). While we feel confident that the Cepheids are indeed producing the detected X-ray activity, further observations will allow us to investigate the phase dependence of the X-ray emissions on pulsation period. In addition to providing more conclusive proof that Cepheids themselves are X-ray sources (and not hypothetical young coronal companions, as previously mentioned), the additional X-ray observations will also shed more light on the origin and variability of hot (MK) Cepheid plasmas, and what its exact relationship is (if any) to the warm UV-emitting plasmas. There are different mechanisms that could produce X-ray variability in Cepheids, and again it can benefit the study to put their high-energy properties into a stellar context.

Table 18 – Observation Log for Cepheid X-ray Data Used in Here

Cepheid	Observation	Start Time UT Julian Date Phase	Stop Time UT Julian Date Phase	Grouping	1 kT (keV)	log N_H	flux (0.3-2.5 keV)	2 kT (keV)	Normalizations	flux (0.3-2.5 keV)	2 kT Lx
δ Cep	603740901	1/20/2010 18:04	1/21/2010 12:37	25-channel	0.609	20.5	4.261E-15	0.151 + 0.655	1.329E-6 + 1.343E-6	5.342E-15	4.737E+28
	XMM-pn	2455217.253	2455218.026								
		0.054	0.12								
δ Cep	0603741001_I	1/22/2010 18:05	1/23/2010 14:17	25-channel	1.357	20.5	1.338E-14	0.404 + 1.610	2.232E-6 + 7.033E-6	1.508E-14	1.337E+29
	XMM-pn	2455219.254	2455220.095								
		0.43	0.50								
	0603741001_II	0.51	0.58	25-channel	0.586	20.5	6.761E-15	0.489 + 2.104	1.699E-6 + 3.320E-6	8.420E-15	7.466E+28
δ Cep	552410401	6/5/2008 14:26	6/5/2008 21:53	25-channel	0.654	20.5	5.719E-15	0.619 + 4.000	1.591E-6 + 2.569E-6	6.886E-15	6.106E+28
	XMM-pn	2454623.101	2454623.412								
		0.33	0.39								
δ Cep	0723540301_I	6/28/2013 6:34	6/29/2013 13:49	25-channel	0.963	20.5	4.460E-15	0.321 + 1.328	1.435E-6 + 1.473E-6	5.634E-15	4.996E+28
	XMM-pn	2456471.774	2456473.076								
		0.84	0.96								
	0723540301_II	0.96	0.08	25-channel	0.486	20.5	4.374E-15	0.408 + 1.378	1.392E-6 + 8.998E-7	4.921E-15	4.363E+28
δ Cep	0723540401_I	7/2/2013 6:17	7/3/2013 7:51	25-channel	0.613	20.5	3.825E-15	0.613 + 0.741	1.388E-6 + 2.138E-14	3.825E-15	3.392E+28
	XMM-pn	2456475.762	2456476.827								
		0.58	0.68								
	0723540401_II	0.68	0.78	25-channel	0.468	20.5	5.526E-15	0.016 + 0.482	3.202 + 1.999E-6	6.112E-15	5.419E+28
β Dor	603740801	2/1/2006 9:09	2/2/2006 3:54	25-channel	0.297	20.4	9.545E-15	0.266 + 2.129	3.121E-6 + 5.609E-6	1.306E-14	1.576E+29
	XMM-pn	2455230.25	2455230.66								
		0.41	0.45								

β Dor	603741101	3/23/2006 4:26	3/23/2006 23:40	25-channel	0.325	20.4	7.954E-15	0.298 + 1.302	2.865E-6 + 1.946E-6	9.544E-15	1.152E+29
	XMM-pn	2455280.08	2455280.49								
		0.47	0.51								
β Dor	552410101	6/22/2004 6:35	6/22/2004 17:49	25-channel	0.528	20.4	5.159E-15	0.480 + 4.000	1.391E-6 + 2.784E-6	6.480E-15	7.821E+28
	XMM-pn	2454640.774	2454641.242								
		0.52	0.56								
Polaris	503140101	2/23/2008 21:51	2/24/2008 2:25	25-channel	0.390	20.0	2.800E-14	0.085 + 0.591	3.584E-5 + 9.276E-6	3.749E-14	7.919E+28
	XMM-pn	2454520.410	2454520.601								
		0.21	0.26								
Polaris	503140401	4/29/2008 8:04	4/29/2008 13:00	25-channel	0.477	20.0	2.975E-14	0.107 + 0.543	9.282E-6 + 9.812E-6	3.313E-14	6.998E+28
	XMM-pn	2454585.836	2454586.042								
		0.68	0.74								
Polaris	654780201	5/1/2010 9:12	5/1/2010 19:43	10-channel	0.495	20.0	3.011E-14	0.136 + 0.502	7.676E-7 + 1.087E-5	3.051E-14	6.445E+28
	XMM-MOS	2455317.883	2455318.322								
		0.97	0.08								
Polaris	6431 (Chandra)	2/9/2006 1:01	2/9/2006 3:47					0.57 + 0.12		3.800E-14	8.027E+28
		2453775.542	2453775.658								
		0.71	0.73								
ℓ Car	603740301	4/2/2010 11:38	5/2/2010 3:01								
		2455231.985	2455232.626								
		0.639	0.968								
SU Cas	603740501	8/2/2010 10:32	9/2/2010 2:32								
		2455235.939	2455236.606								
		0.932	0.951								

*log N_H – number of neutral Hydrogen atoms per cubic cm between us and the target (column density) – calculated using the online tool at http://archive.stsci.edu/euve/ism/ismform.html

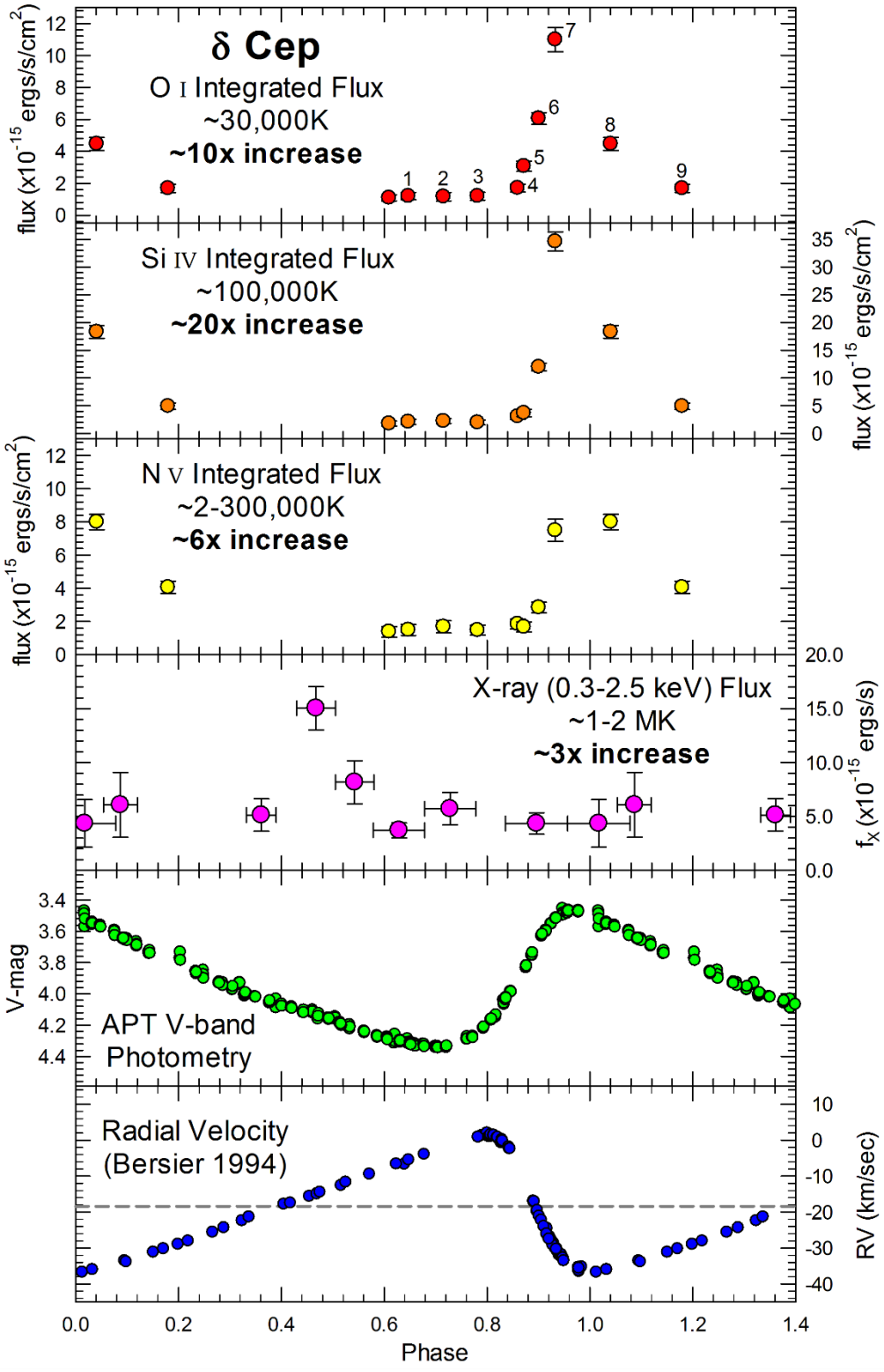

Figure 54 – The top four panels give the UV emission line fluxes and the X-ray fluxes measured vs. pulsational phase for δ Cep. The bottom two panels give the V-band photometry and photospheric radial velocities, as previously seen. The X-ray activity appears to decrease when the UV activity increases which, if confirmed, would give valuable insight into the stellar dynamics.

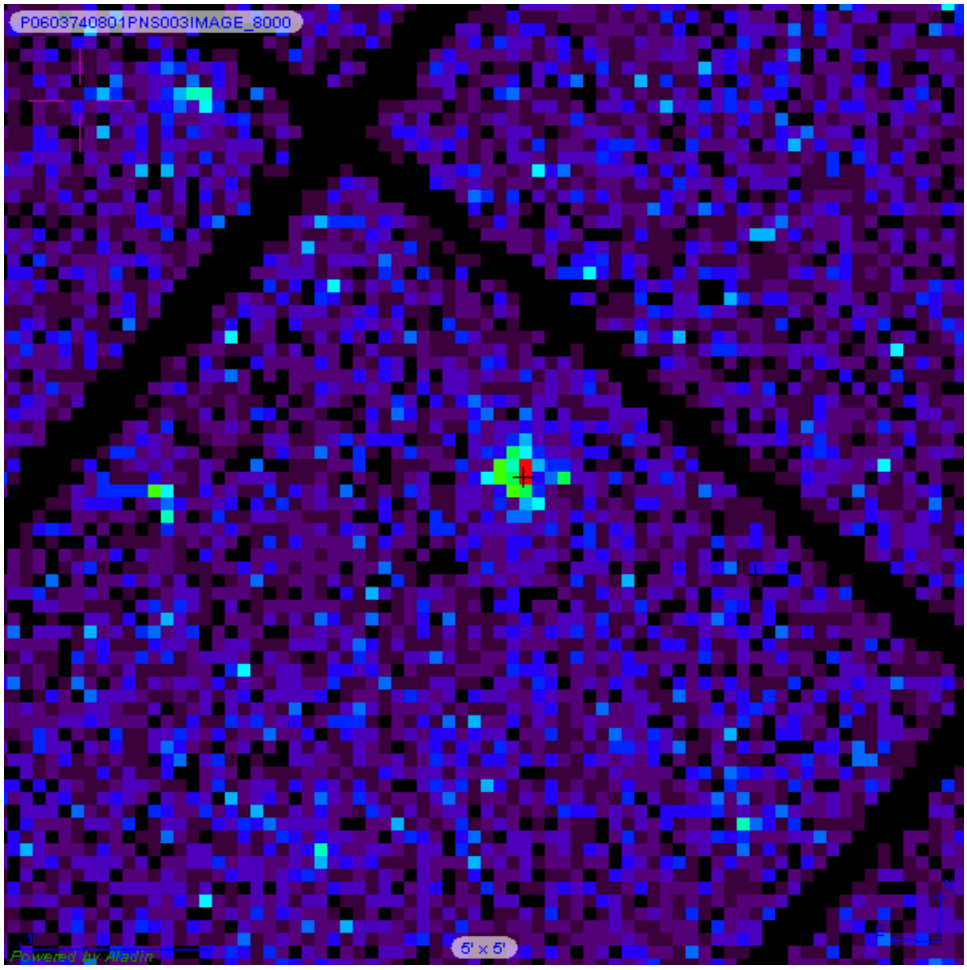

Figure 55 – A 5×5 arcmin section of XMM observation 801 of β Dor is shown. Near the center, the X-ray source can be seen, with the black cross at the center indicating the coordinates of the Cepheid.

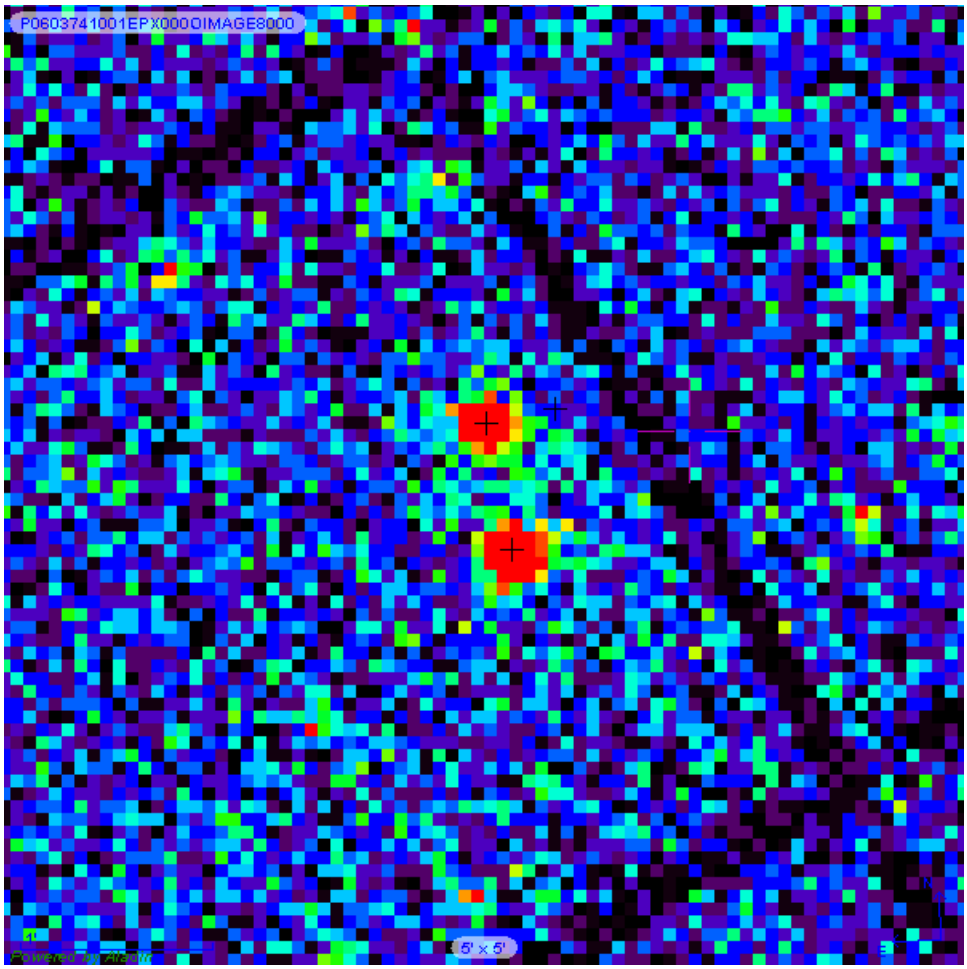

Figure 56 – A 5×5 arcmin section of XMM observation 1001 of δ Cep is shown. Near the center, two X-ray sources are seen, with the black cross at the center of the northern source indicating the coordinates of the Cepheid, and the black cross at the center of the southern source indicating the coordinates of the Cepheid's long-known hotter binary companion (see Section 2.3).

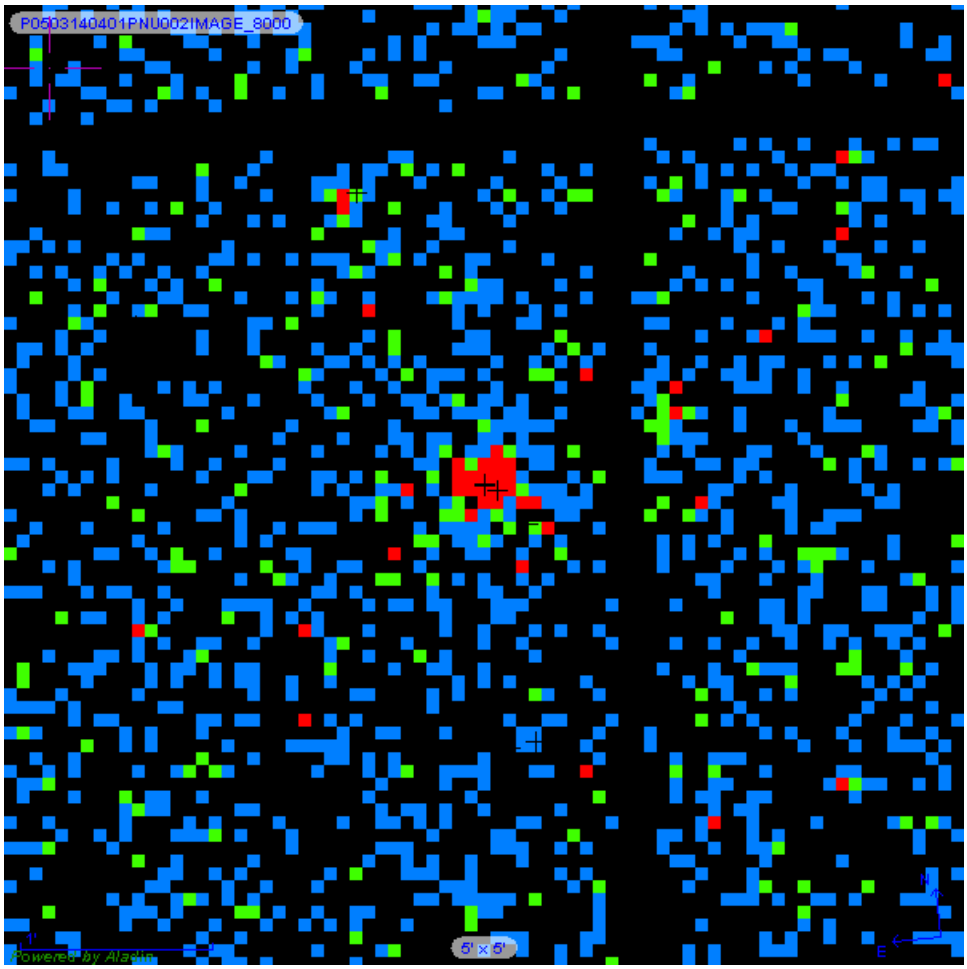

Figure 57 – A 5×5 arcmin section of XMM observation 401 of Polaris is shown. Near the center, the X-ray source can be seen, with the black cross at the center indicating the coordinates of the Cepheid. The black cross below and to the right of the center cross marks the location of a distant background star, originally thought to be a companion to the Cepheid, but recently disproven as such (Evans et al. 2010).

Figs. 58 (Polaris), 59 (β Dor) and 60 (δ Cep) give the energy distributions obtained from our XMM observations, along with the best-fitting 2T MEKAL models for each observation (parameters given in Table 17). Fig. 61 gives only the 2T models of each Cepheid for an easier comparison. As one can see, the background-subtracted count rates that we encounter are somewhat low, due to the distances of the Cepheids. Because of this, uncertainties on the X-ray measures are between ~20 – 40%, so the plasma temperatures and fluxes derived from the data have a bit of "leeway" associated with them. However, the general X-ray properties of the three Cepheids are similar. The energy distributions show all three Cepheids to have peak overall emissions in the 0.6 – 0.8 keV range. By contrast, observations of young, cool main sequence stars show their emissions to consistently peak in the 0.9 – 1.0 keV range. This is a small difference, especially in light of the larger errors associated with the Cepheid observations, but it is noticeable and consistent. The softer X-ray emissions of the Cepheids give evidence that they are the source of the activity, instead of main sequence companions. As with the UV data, X-ray observations of other supergiants can be used to put the Cepheid detections in context.

Fig. 62 shows a plot adapted from Ayres, Brown & Harper (2003), in which various "groups" of cool, X-ray emitting stars are mapped according to their ratios of X-ray and C IV 1550Å luminosities to their bolometric luminosities. The three detected Cepheids have been plotted as the purple, diagonal striped boxes. There does seem to be a division between the two shorter-period Cepheids δ Cep and Polaris – which are also of more similar spectral type – and the longer period, slightly later spectral type Cepheid β Dor. The higher level of UV activity in β Dor is the main segregator between the Cepheids and, of course, observations of additional Cepheids are warranted to determine if this segregation holds true. However, the results are still interesting. Polaris and δ Cep are among the more "UV deficient" stars plotted, and border on Group 5, labeled by Ayres et al. as a region of cool, inactive giants, whereas β Dor lies between Group 5 and the GK supergiants and Hybrids that make up Group 6. The very active supergiants discussed in the UV studies occupy Group 2, and cool, main sequence stars (including the Sun marked by the solar symbol) occupy Group 1. Fig. 63 shows the same general figure (this time adapted from Ayres 2011), but now some of the groups of stars have been replaced with giants and supergiants of different spectral type. Polaris and δ Cep fall very close to the two other F-type supergiants measured, although perhaps a bit X-ray deficient (but confirming this would require measurements of additional stars), whereas β Dor is currently UV deficient when compared to other early-G supergiants. As with O I and Si IV, only the descending branch of the C IV activity curve has been observed for β Dor. However, it would be surprising if the approved observations show the true maximum of C IV activity in β Dor to rival the levels observed in other, non-

pulsating (and Hybrid) G-type supergiants. As shown previously in Fig. 51, however, the lower-temperature UV emissions of β Dor can match and even exceed other supergiants. This implies that the pulsations of Cepheids may inhibit an overall atmospheric heating mechanism (perhaps convective strength), and the shocks they generate can excite cooler atmospheric emissions enough to compensate for this deficiency, but the shocks are not strong enough to recover the "missing" higher-temperature activity. Again, in Fig. 63 (as in Fig. 62) the cool, main sequence stars are plotted in the yellow wedge. It can be seen how much more active (when taking into account bolometric luminosity) the cool main sequence stars are, as compared to most cool supergiants and the Cepheids.

As example, from a first glance at the hottest atmospheric emissions, the mean L_X values observed for Cepheids are on the order of 30 – 60× that of the mean solar value (adopting $L_X \approx 1 \times 10^{29}$ ergs/s for Cepheids and average $\langle L_X \rangle_\odot \approx 2 \times 10^{27}$ ergs/s from DeWarf et al. 2010). However, Cepheid surface X-ray fluxes (F_X) and L_X/L_{bol} ratios, compared to the Sun, are much smaller (e.g. *log* (L_X/L_{bol}) ≈ -7.7 [δ Cep] and -6.3 [Sun]). For further example, in the case of δ Cep (adopting a radius of R = 44.5 $R_\odot$, L ≈ 2,000 $L_\odot$ (Matthews et al. 2012), the average surface X-ray flux is $F_X \approx 8.3 \times 10^2$ ergs/s/cm^2. The corresponding mean value for the Sun is $\langle F_X \rangle_\odot \approx 4.1 \times 10^5$ ergs/s/cm^2. Thus, the average X-ray surface flux of the Sun is ~500× stronger than that of the Cepheid. There is an even more dramatic difference when the fact that the Sun is a middle-aged main sequence star is taken into account, since the UV and X-ray activity of cool, main sequence stars declines over time. The X-ray surface flux (or L_X/L_{bol} values) of cool main sequence stars at similar ages to those of the Cepheids could be as much as ~100,000× stronger than the Cepheids.

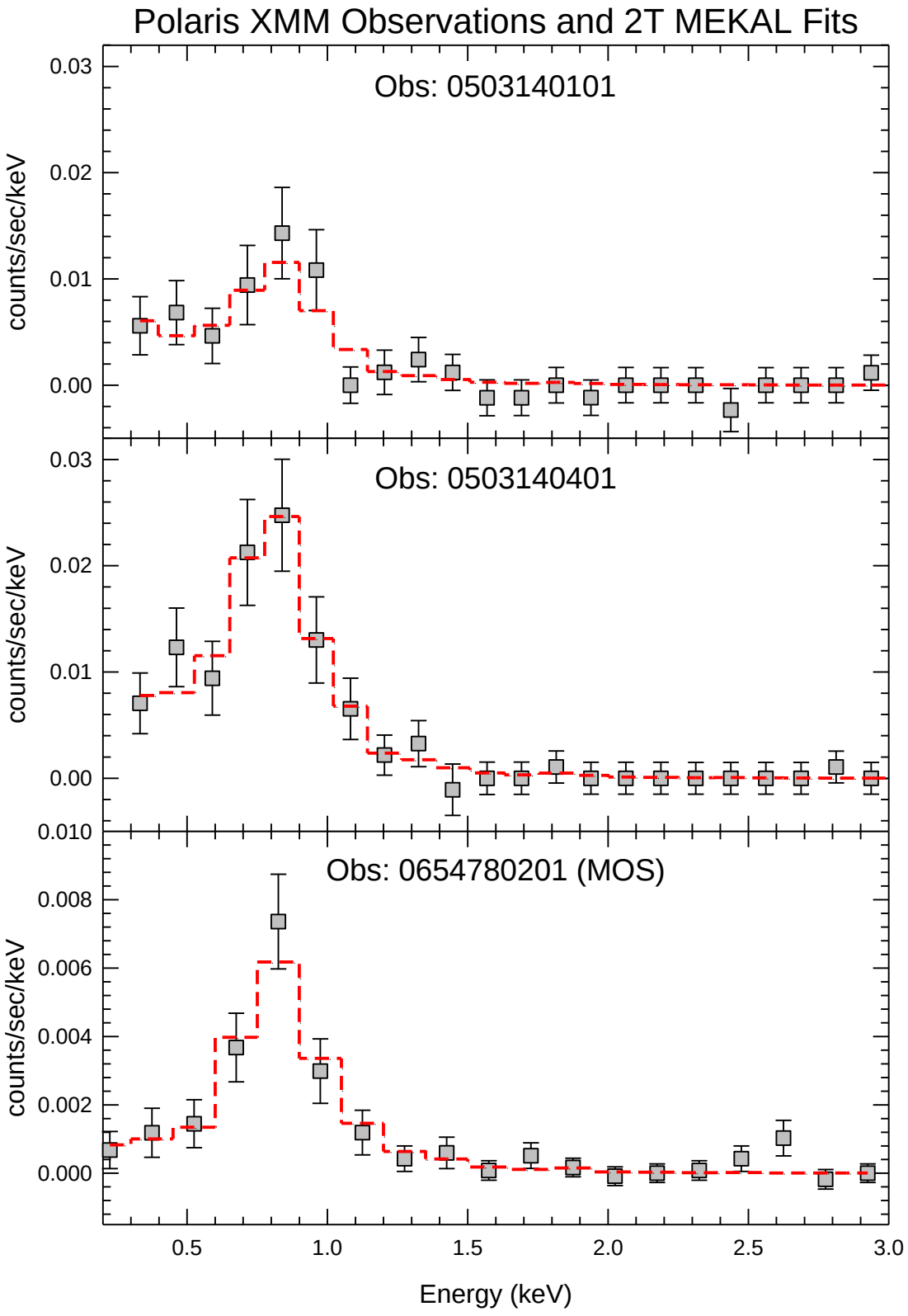

Figure 58 – The three XMM observations of Polaris are shown, along with the best fitting two-temperature MEKAL models.

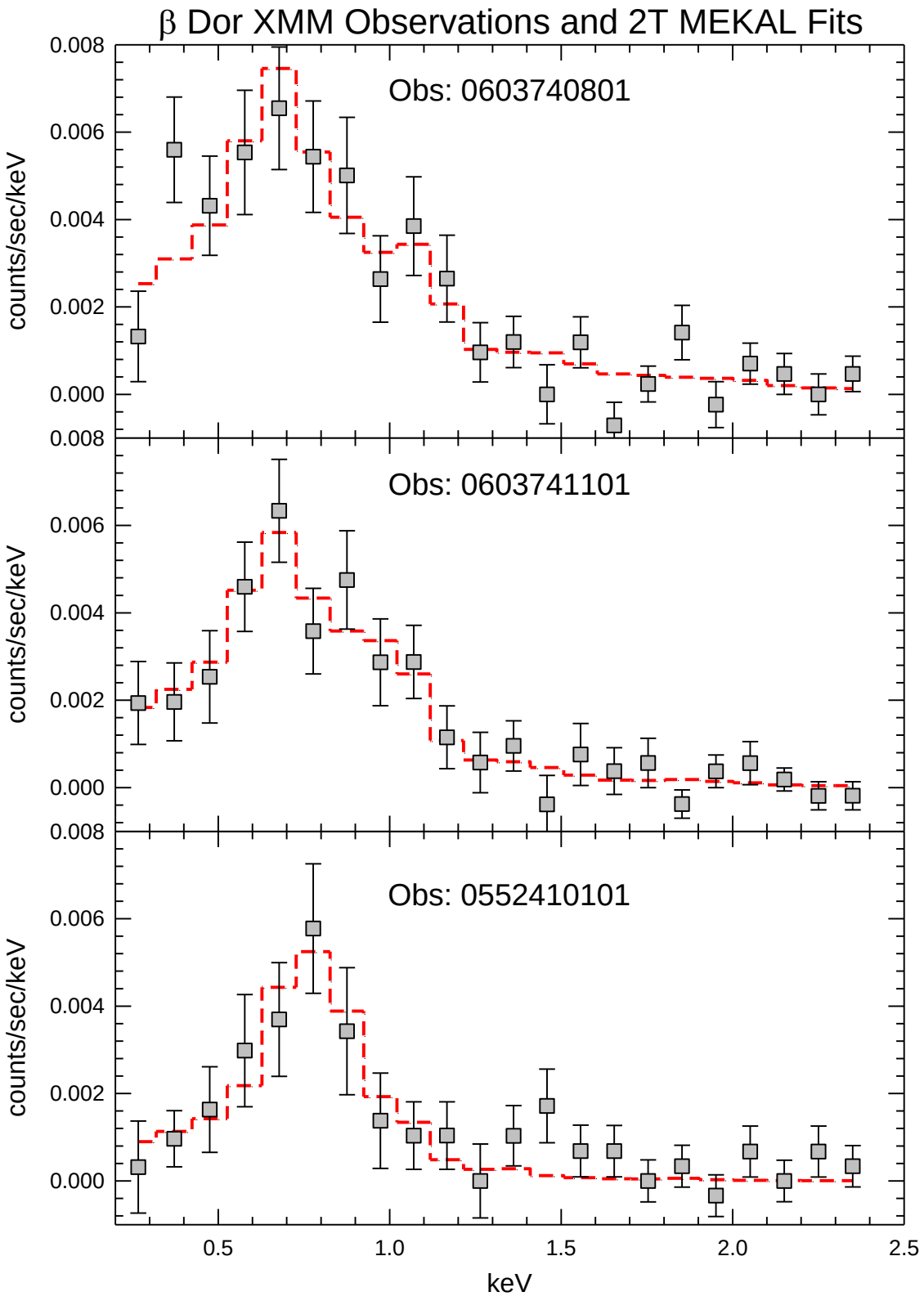

Figure 59 – Same convention as Fig. 58, but for β Dor.

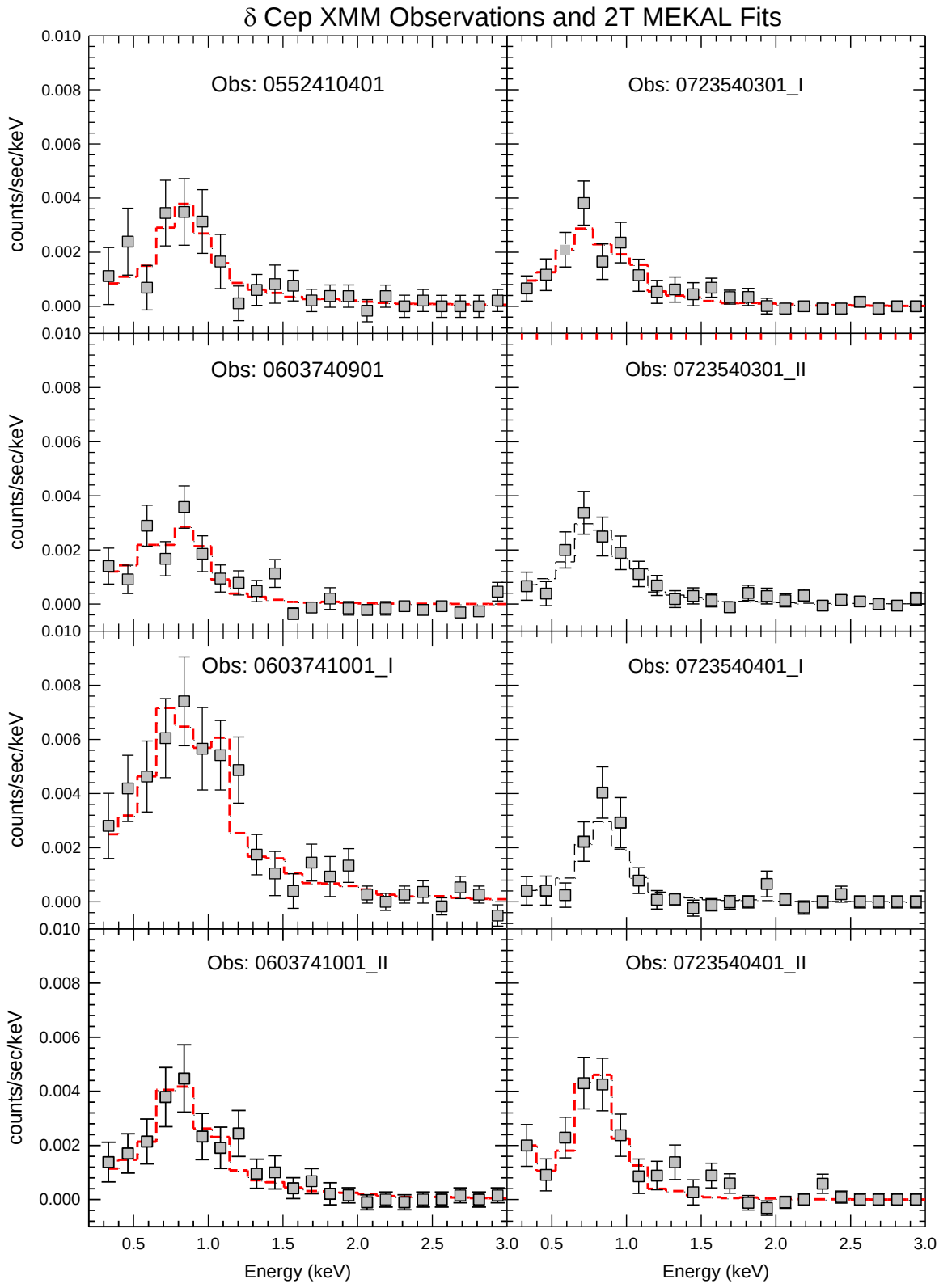

Figure 60 – Same convention as Fig. 58, but for δ Cep.

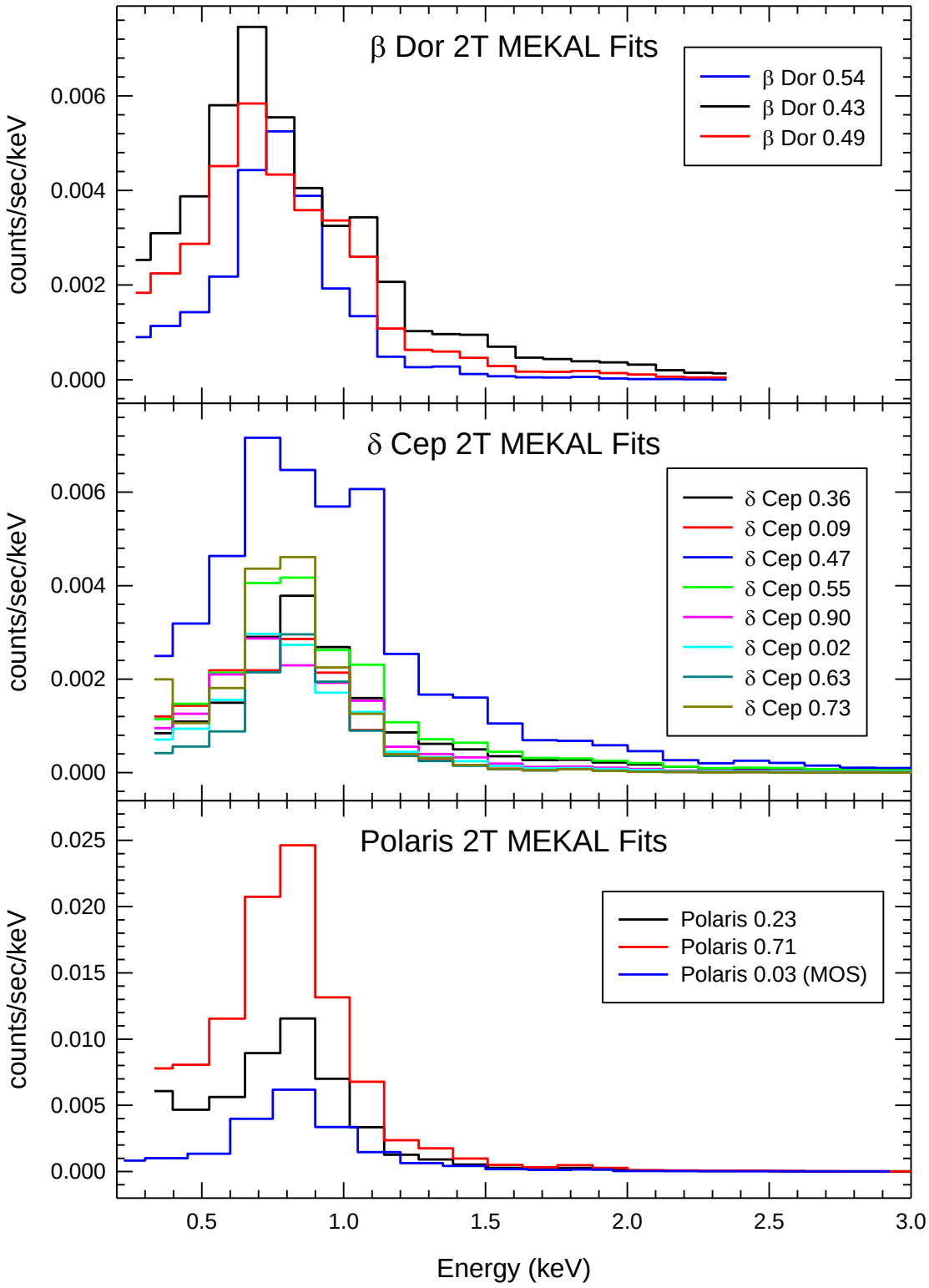

Figure 61 – For ease of comparison, this figure shows only the models from Figs. 58, 59 and 60. The phases of the individual X-ray distributions for each Cepheid are given in the legends.

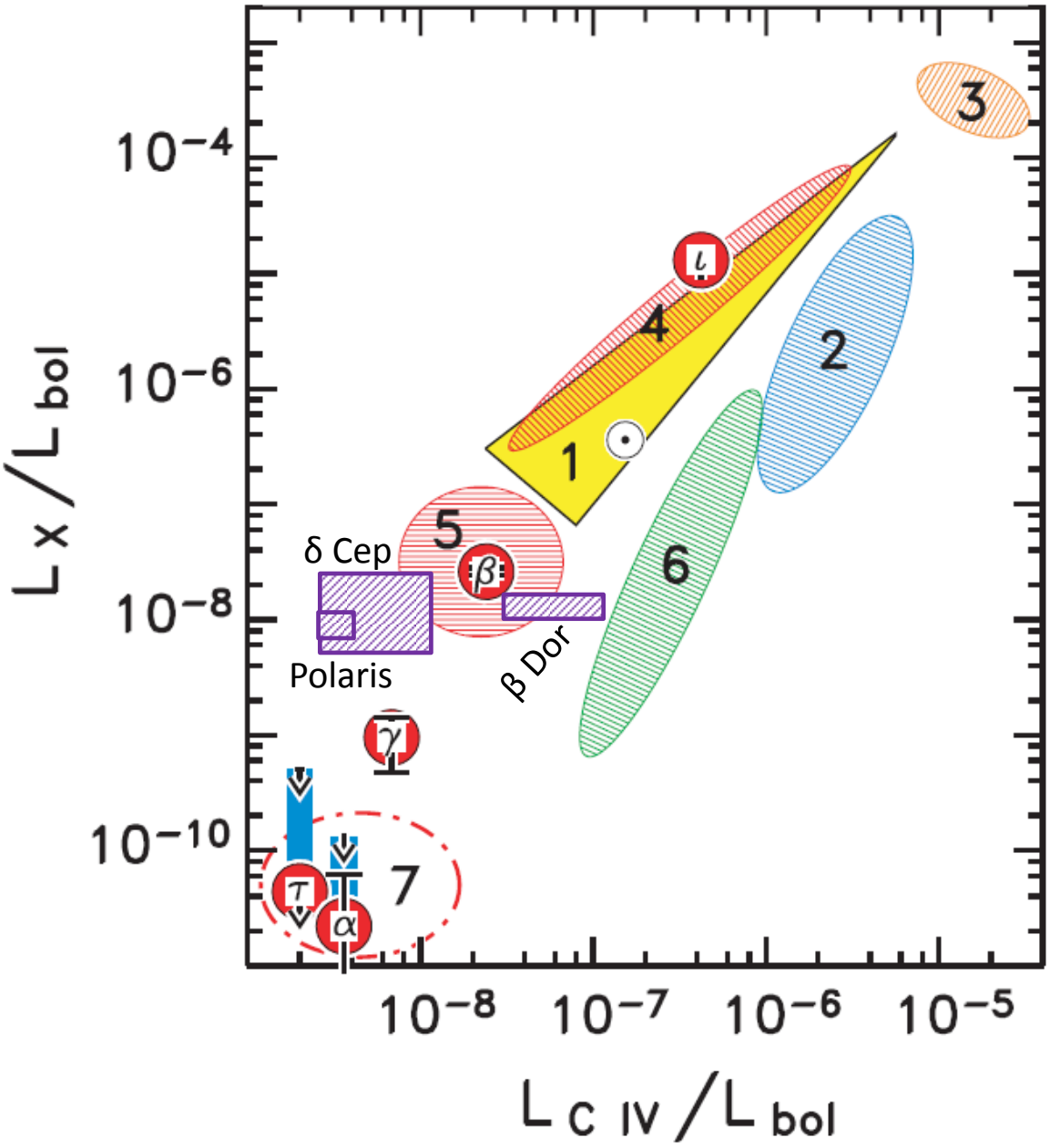

Figure 62 – A cool stars atmospheric comparison plot, adapted from Ayres, Brown & Harper (2003). One can see the separation of β Dor from δ Cep and Polaris, placing it closer to Group 6, which includes the Hybrids. Further details are given in the text. The numbered groups represent (1) GK dwarfs (the circled dot marks the average solar ratio), (2) "X-ray deficient" Hertzsprung gap giants and the “very active supergiants” β Cam and β Dra, (3) hyperactive RS CVn binaries, (4) active clump (G8-K0) giants, (5) inactive but still coronal K0 giants, (6) GK supergiants (the lower activity Hybrids are located here), and (7) noncoronal (≥K1) red giants. Filled red circles mark α Boo ("α" – K1.5 III), τ Tau (" τ " – K5 III), and three comparison stars: ι Cap (" ι " – G8 III), β Gem (" β " K0 III), and γ Dra (" γ " – K5 III). Vertical blue bars connect earlier ROSAT upper limits with newer Chandra measurements.

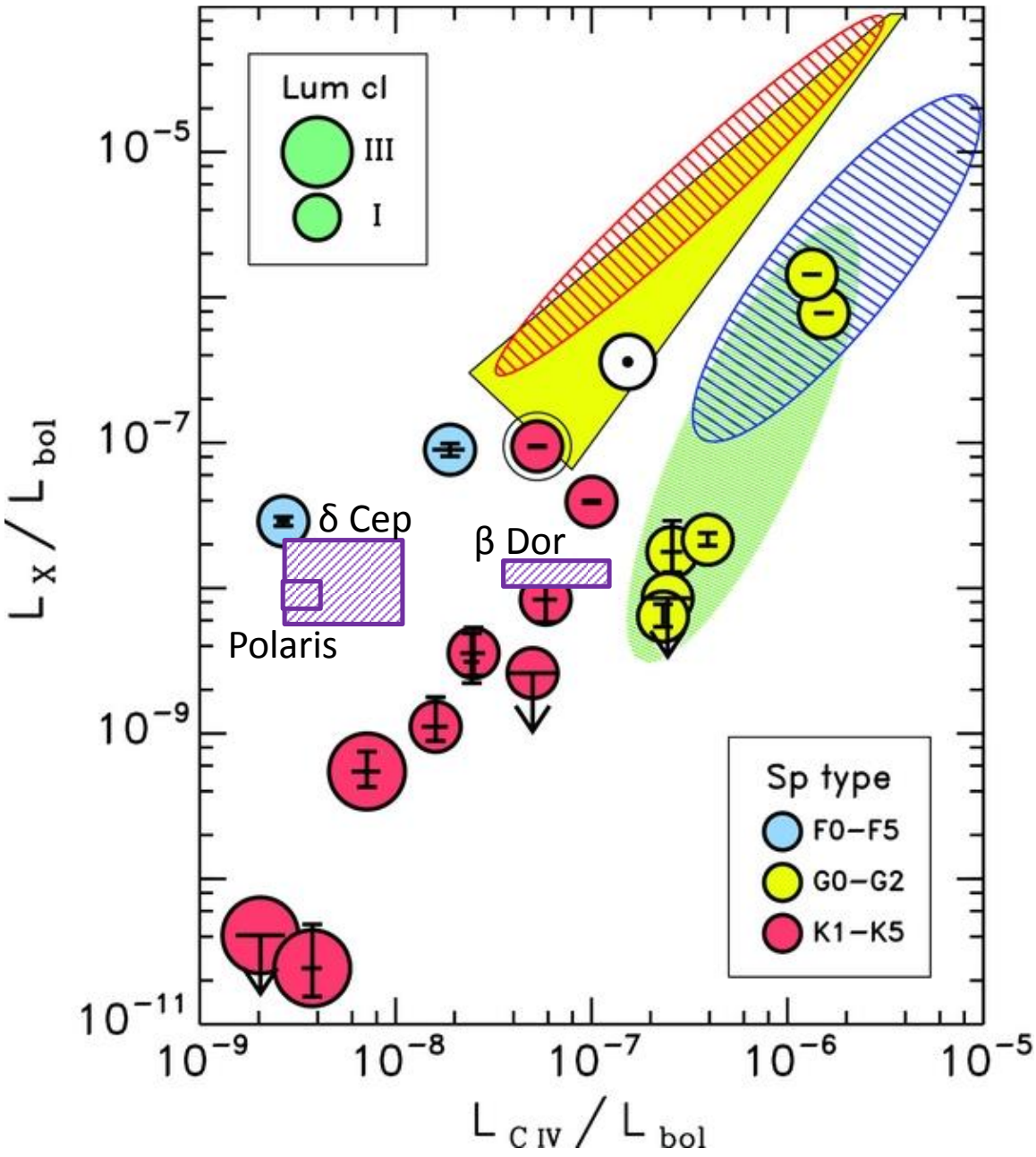

Figure 63 – The same as Fig. 62, except now the separation of supergiant spectral types is shown (adapted from Ayres 2011). Here δ Cep and Polaris are shown to fittingly lie near other F-type supergiants, whereas the somewhat later spectral type β Dor is between the F-type and G-type supergiants, in the range of K-type supergiants.

3.3 A Brief Summary of Chapter 3

Multiple, high resolution UV (~1150 – 1750 Å) spectra have been obtained for Polaris, δ Cep and β Dor with *HST*-COS to characterize the effects of the stars' pulsations on their atmospheric

emissions from heated plasmas. Only two phases of Polaris' pulsations have been observed thus far, compared to multiple observations of δ Cep and β Dor. The crucial pulsation phases of δ Cep were observed with greater efficiently, though, resulting in a more complete understanding of its atmospheric variability. The emission curve given in Fig. 45 shows an abrupt, strong increase in emission line fluxes beginning at phase = 0.86ϕ. This is just before the start of the Cepheid's piston phase, where the star begins to expand again. The change from stellar recession to expansion is expected to compress the atmosphere of the Cepheid, and generate a shock, which would propagate through the atmospheric plasmas. The phasing of the increase in flux strongly supports this expectation. In addition, radial velocities show that the atmosphere continues to recede at phases where the photosphere begins expanding, resulting in atmospheric compression. Finally, emission line profiles during the piston phases show an additional, blue-shifted feature originating from excited plasmas at the bow of the propagating shock, and increasing line broadening from phases $0.83 - 0.01\phi$ show increased emissions from compressed plasmas and also turbulent plasmas in the wake of the shock.

For β Dor, the phases of rising emission flux (and possibly maximum flux) have not yet been observed, but important similarities and differences are already apparent when compared to δ Cep. Fig. 46 shows the current emission curve for β Dor. An overall similar behavior to δ Cep is seen, with enhanced atmospheric emissions around the piston phase, but there are specifics that distinguish the two Cepheids. In δ Cep, it appears that N V, the hottest emission line plotted, peaks in activity at a slightly later phase than the cooler lines. For β Dor, however, the phase difference is dramatic, with the peaks separated by ~0.1ϕ or more. Preliminary conclusions about the relative activity levels of the Cepheids can also be drawn. Polaris' emission line fluxes are approximate to the average fluxes of δ Cep. This can be expected since the two Cepheids are very similar in terms of both average surface temperature and size, but the more interesting question is the effect of pulsations on the stellar atmospheres, since Polaris' pulsations are so weak in comparison to those of δ Cep. However, with just two COS spectra of Polaris, investigating the effects of pulsation must await further data. The δ Cep and β Dor datasets are more complete, and when comparing maximum O I, Si IV and N V fluxes, β Dor has ~6×, ~3× and ~5× stronger emissions, respectively. With our current understanding of the quiescent levels of O I, Si IV and N V fluxes for β Dor, it is ~16×, ~7× and ~13× more active than δ Cep. Clearly, β Dor possesses a much higher level of persistent atmospheric emissions, yet a smaller amplitude of variability when compared to δ Cep. This would seem to indicate weaker shock activity in β Dor.

Polaris, δ Cep and β Dor have also been successfully detected and measured at X-ray wavelengths. Table 18 gives the observation specifics, the determined plasma temperatures and X-ray activity levels. Figs. 58 – 61 give the reduced data, and show that the three Cepheids display similar X-ray energy distributions, with peak emissions in the 0.6 – 0.9 keV range. As with the UV data, δ Cep has had more complete pulsation phase coverage at X-ray wavelengths, and shows a fairly consistent activity level with the exception of phase $\approx 0.45\phi$ (Fig. 54). At this phase, there is a ~3× jump in the X-ray flux and the peak X-ray emission broadens out to include higher energies (up to ~1.2 keV). Analyses of this data (background counts, nearby sources…) confirm that the increased flux comes from the location of δ Cep itself, and is not the result of a data artifact or error of some sort. Additional X-ray data have been proposed to confirm the increased activity at this phase, and also cover the missing phases directly beforehand.

CHAPTER 4 – SUMMARY & CONCLUSIONS

Apart from the scientific conclusions of this program, there is an overall ethos that this study will hopefully convey, and it is that likely no class of object in astronomy has "given up all of its secrets" just yet. For a long time, Cepheids were prized for the stability and predictability of their light curves. Objects like Polaris and V473 Lyr, that displayed either cyclic or long-term amplitude variability, were seen as anomalous. However, this study shows that perhaps these objects are more common than previously thought.

Similarly, in the high-energy (X-ray – UV) regime, the important discoveries of previous IUE studies were never followed up with modern UV instruments, nor were the non-detections with previous-generation X-ray instruments. In fact, even though Polaris *was* detected in a pointed 1997 ROSAT-HRI exposure, the detection went unpublished (and, it would seem, unknown) for roughly a decade, until an archival search by the author "re-discovered" it. Now, recent studies at these wavelengths have the potential to redefine our understanding of supergiant atmospheres under the influence of radial pulsations.

From the two studies contained within this thesis, the conclusions are as follows.

4.1 Summary of Findings from the Optical Studies

The several years of regular photometric monitoring carried out as part of this study, when combined with literature data, clearly indicate variations in the light amplitudes of Cepheids on various timescales. This is, of course, in addition to the well-known and documented period changes of Cepheids previously documented. To summarize:

δ Cep – The prototype of Cepheids shows a well-documented decreasing period, but also an increasing light amplitude over the past ~100 years. The amplitude change shows an overall linearly increasing trend. Shorter timescale periodicity is hinted at, but the sparseness of the data prevents a conclusive find.

η Aql – The first-discovered Cepheid shows a well-documented, increasing period, but its amplitude shows no coherent trend. In all likelihood, to within the errors and calibrations of the data, the amplitude of this Cepheid appears constant over the past ~100 years.

EU Tau – This short-period (~2.1-day) Cepheid has recently begun to show period variation, either in the form of a smooth, consistent decrease or in the form of a rapid shift to a shorter pulsation period. The recent lack of regular photometric observations prevents a firm conclusion at this time. The overall trend in the light amplitude measures of EU Tau hints at a possible amplitude decrease over time, however, all measures lie within acceptable errors of each other and the amplitude can easily have remained constant.

Polaris – The North Star shows a (mostly) smooth, decreasing pulsation period, except for an apparent abrupt shift in period around 1963 – 1964. This roughly coincides with the beginning of Polaris' decline in light amplitude (visual or *V*-band) from ~0.12- to 0.025-mag. After having reached a minimum amplitude of ~0.025-mag around the year 2000, recent observations show the amplitude to again be increasing. For example, preliminary reductions of the most recent V-band photometry acquired but not included in this thesis, yields a light amplitude of ~0.067-mag, thus continuing the recent trend of increasing light amplitude. Further data will be needed to discern whether we are witnessing the beginning of an amplitude cycle for Polaris, or if it is simply returning to earlier, larger amplitude levels.

SU Cas – The shortest-period (~1.95-day) Cepheid studied, the new O-C points indicate that the period is increasing but, as with EU Tau, additional data is needed to confirm a continued period increase, instead of a possible sudden lengthening of the period. The light amplitudes of SU Cas show a possible increase over time, but if the older, less accurate observations are excluded, then the trend becomes rather small, approaching the level of scatter allowed by observational error.

SV Vul – The longest-period (~45-day) Cepheid in our study, SV Vul displays a substantial, consistent decrease in period over time. Additionally, SV Vul displays an apparent ~30-year cyclic variability in both light amplitude and pulsation period: an interesting behavior that we will of course continue to monitor.

SZ Cas – This Cepheid has for years displayed a well-documented increasing period. On top of this trend, there appeared to be evidence of a lengthy cyclic behavior, as well. However, the more recent data (including those of this study) indicate that the period may now be holding steady. The amplitude behavior of this Cepheid is intriguing, having decreased by over 10% in the span of a couple decades. New data show that the light amplitude may again be increasing.

SZ Tau – This Cepheid displays a very complex O-C diagram, likely characterized by constant long-term period decrease, but with substantial additional variability on shorter timescales, with a possible ~59-year period. Measures of SZ Tau's amplitude show that it has steadily increased by ~20% over the past century.

VY Cyg – The new O-C points given in this study confirm the recent evidence that the period of this Cepheid is increasing. The quality of the older data makes it hard to determine if this has been a long-term, subtle increase, or if it has only recently begun. VY Cyg is unfortunately deficient in modern light amplitude measures; however, the spread of the existing measures is larger than the observational errors, suggesting that light amplitude variations may be in progress.

ζ Gem – This well-studied Cepheid shows a steadily decreasing pulsation period over time with no evidence of additional, secondary period variability. The light amplitudes of this Cepheid display an increase over time, as well as (for the past ~60 years) a possible ~40-year cyclic variability.

β Dor – This Cepheid shows a slow, steadily increasing pulsation period over time with no additional coherent period variability. A light amplitude variability study has not yet been conducted for this Cepheid.

4.2 Implications of the Optical Study

As part of this study, ten Cepheids have been (and continue to be) observed. Of these, eight of the Cepheids display evidence of light amplitude variability, by way of either long-term increasing/decreasing trends or possible decades-long light amplitude cycles. All ten Cepheids display coherent changes in pulsation period, and three Cepheids show signs of additional cyclic period variability. Of course, the Cepheids studied here represent but a small fraction of the known galactic Cepheids, so this number cannot be taken as indicative of Cepheids as a whole. Changes in the pulsation period of a Cepheid can be expected, as studies of larger samples of Cepheids (e.g. Turner et al. 2006) have shown such changes to be commonplace. However, our findings do indicate that Cepheid light amplitudes may not be as fixed as previously thought.

Light amplitude changes in Cepheids, although still regarded as a rare phenomenon, is not a completely alien concept. As mentioned, the Blazhko effect in RR Lyr stars – cyclic modulations of their pulsational periods and amplitudes – has been known for over a century, and has been observed in an increasing fraction of RR Lyr stars over time. In fact, when all ground- and space-based surveys are taken into account (especially recent studies with the *Kepler* satellite), as much as 50% of all fundamental mode RR Lyr stars display the Blazhko effect (Kolenberg 2012). This is obviously a significant fraction of RR Lyr stars, for whom the κ-mechanism is primarily driving their radial pulsations, as it does with the Cepheids. The pulsations of both classes of variable stars are driven by the same primary mechanism, but many of their stellar properties (Mass, T_{eff}, Luminosity, etc.) are very different. However, because the Blazhko effect is a pulsation-related phenomenon, it is not so unreasonable to speculate that Cepheids are also capable of displaying the effect.

At present, no studies have been undertaken to monitor a substantial fraction of galactic Cepheids to search for Blazhko-type variabilities, although the Optical Gravitational Lensing Experiment (*OGLE*) has formed an extensive Cepheid inventory for the Magellanic Clouds. A study of the most recent *completed* phase – OGLE-III – found ~4% of fundamental mode

Cepheids, and ~28% of first overtone Cepheids, to undergo Blazhko-type variability (Soszynski et al. 2008). These percentages are lower than those for RR Lyr stars; however, the longer periods of Cepheids make it more difficult to adequately cover individual pulsation cycles. With multiple pulsations usually being merged together to form a single well-covered light curve, searching for Blazhko-type variability will be much more difficult. Additionally, Cepheids have not benefitted as much as RR Lyr stars have from the modern era of ultra-precise, continuous space-based photometric programs (e.g. there is only one confirmed Cepheid in the entire *Kepler* satellite field of view – V1154 Cyg) which are extremely well-suited to revealing period and amplitude modulations. A near-complete survey of Blazhko-type variability in Cepheids will have to wait for either a future space-based photometric mission or a multi-site, high-cadence ground-based survey program – neither of which are likely in the near future. The recently launched (at the time writing) BRITE-Constellation (http://www.brite-constellation.at/) nano-satellites are designed to carry out very-high-precision photometry, and Cepheid targets have already been approved for observations. However, as the satellites are designed to observe very bright objects, at present only ~6 Cepheids are approved for BRITE-Constellation photometry.

Even with the "high standards" set for Cepheids to reveal Blazhko-type variability, the percentages of "Blazhko Cepheids" found in OGLE-III data is both revealing and encouraging. For RR Lyr stars, the occurrence rate for the effect is ~1.5× higher in the OGLE Galactic Bulge fields than in the LMC. This originally suggested a metallicity dependence, which was found to not be true for Galactic RR Lyr (Smolec 2005), but it is still correct that Blazhko RR Lyr stars occur more frequently in the galaxy than in the LMC. Testing whether this applies to Blazhko Cepheids, as mentioned, will be difficult, to say the least. However, the results of our optical study support the conclusion that Blazhko-type variability in galactic Cepheids may be a more common occurrence than previously thought. The importance of such a finding, given the use of Cepheids as standard candles, easily warrants further investigation.

4.3 The High-Energy (UV and X-ray) Study

The UV and X-ray studies of Cepheids have definitely had their ups and downs. On one hand, the quality of the HST-COS spectra and the scientific potential contained within, especially when compared to the previously available IUE data (see Figs. 43 and 44), can be described without exaggeration as amazing. The X-ray data and evidence of variability, when combined with the UV observations, reveal Cepheid atmospheres of such complexity that it appears new ground is being broken, and perhaps Cepheids cannot even be treated as a group, but instead need to be studied and understood on a case-by-case basis, or at least placed into subgroups based on pulsation period and spectral type range (as Figs. 62 and 63 might imply). On the other hand, the

competitive nature of applying for satellite observing time, and the number/length of observations required, have combined to slow the progress of the high-energy study. The current empirical findings of the high-energy study are as follows:

UV fluxes – Both β Dor and δ Cep display moderate-to-strong variability in the intensities of their atmospheric UV emission lines. Since the observations have been gathered over the course of months, and even years, there can be no doubt that the phasing dictates a pulsation-driven variability (as opposed to a transient event such as a flare, which could possibly be argued for if the data were taken consecutively over a short span of time). Although β Dor has stronger *overall* UV line emissions, δ Cep displays a much larger range of variability. This conclusion is currently mitigated by the poorer phase coverage of β Dor, but future approved HST-COS observations of β Dor have been phase-constrained to further our understanding of this Cepheid's range of UV activity.

UV phasing – δ Cep shows a much more abrupt rise in emission flux (although, phases where the flux of the cooler emission lines of β Dor are expected to rise have not yet been observed), which would be in agreement with the photospheric RV curves of the Cepheids. Specifically, δ Cep goes from minimum radius to maximum outward velocity in just ~0.1ϕ (~0.54-days), while β Dor takes ~0.4ϕ (~3.9-days) to do the same (see Figs. 45 and 46). Based on the current data, β Dor also takes longer to return to quiescent emission levels. The phase at which emission flux in δ Cep begins to increase (~0.85ϕ) is shortly after the recession of the Cepheid photosphere has begun to decelerate. This theoretically coincides with the formation of a shock in δ Cep and its propagation through the stellar atmosphere. With the present phase coverage, conclusions cannot be drawn for the specific phase at which line emissions begin to strengthen in β Dor. However, phase-lags can be seen in both Cepheids, where the hottest emission feature – the N V 1240Å doublet – peaks later in phase than either of the cooler lines. This behavior could arise from N V forming in a different level of the Cepheid atmosphere, where the lag represents the time needed for the shock to reach the N V emitting region, or it could represent the additional time needed for the shocked plasmas to excite a highly ionized species such as N V. The lag is more pronounced in β Dor, a possible consequence of β Dor having a more extended atmosphere than δ Cep, or perhaps a consequence of specific atmospheric parameters such as density/pressure, relative abundances or shock strengths. Detailed atmospheric modeling is needed to better understand this issue.

UV line profiles and velocities – These data have only been shown for δ Cep, since both the rise and fall of its emissions have been observed. The profiles and velocities are very informative, revealing a correlation between atmospheric compression (as indicated by relative atmospheric

and photospheric velocities) and a broadening of the line profiles during enhanced emissions, indicating increased density/pressure. The appearance of an additional, blue-shifted emission component in the phases of rising emission flux is clear indication of an outward-propagating shock moving through the atmosphere. Also, increased line width during declining emissions could be a consequence of the high turbulent velocity gradient present in a post-shock atmosphere.

Results from the X-ray study are not as detailed; a consequence of the low signal strength of the Cepheids at these wavelengths, preventing the higher spectral resolution observations and thorough phase coverage from which the UV study has greatly benefitted. Nonetheless, new ground has been broken by the detections of Cepheids at X-ray wavelengths. Five Cepheids were observed, with three detections (Polaris, δ Cep and β Dor) and two non-detections (SU Cas and ℓ Car), which can be understood given the greater distances of the undetected targets and the detected Cepheid X-ray luminosities of $\langle \log L_X \rangle \approx 10^{29}$ erg/sec. Although the low count rates prevent highly detailed energy distributions from being built (Figs. 58 – 60), the three detected Cepheids show generally similar X-ray luminosities ($\langle \log L_X \rangle \approx 10^{29}$ erg/sec) and plasma temperatures ($kT \approx 0.3 - 0.7$ keV). When viewing Fig. 61, it could be argued that β Dor has slightly softer X-ray emission than either δ Cep or Polaris, but with the current inventory and quality of data, this conclusion remains somewhat ambiguous. X-ray data from all three Cepheids show variability. For Polaris, the level of variability is low, as would be expected for this low light- and RV-amplitude Cepheid, but within the observational errors, so no formal conclusion on phased variability can yet be made. β Dor has insufficient phase-coverage to conclusively determine variability. δ Cep, on the other hand, shows a level of X-ray variability beyond the errors, and has much better pulsational phase coverage. Further data is needed, and has been proposed for, but at present δ Cep shows evidence of phased X-ray variability, although the active/quiet phases are completely at odds with the UV activity.

4.4 Implications of the High-Energy Study

The first question raised is exactly how Cepheids are generating the high-energy activity and variability. A very plausible (and promising) mechanism for the variable, pulsation-phase dependent UV – FUV and observed (possibly phase-dependent) X-ray emissions is discussed by Sasselov & Lester (1994). They concluded that Cepheids should have outer atmospheres heated by acoustic (or magnetic) wave dissipation, in addition to the transient heating by pulsation dynamics. From this theory (and observations of the He I 10,830 Å line), they predict average X-ray surface fluxes (0.05 – 1 keV) in the range of $F_X \approx 600 - 11{,}000$ ergs/cm^2/sec. Taking into account the large stellar radii of Cepheids, this suggests average L_X values of ~10^{29} erg/s for

Cepheids with P ≤ 10-days, in good agreement with what we have observed in Polaris, β Dor and δ Cep. This study was carried out in 1994, before X-rays were discovered from Cepheids (although, as mentioned, pointed X-ray observations of the brighter (more nearby) Cepheids were carried out by Einstein and ROSAT). Our limited X-ray results seem to confirm these theoretical expectations. Sasselov & Lester (1994) also estimated that the X-ray luminosities of Cepheids could vary by a factor of ~2.5× over the pulsation period, due to propagating shocks within the stellar atmosphere. Indeed, as shown in Fig 54, the X-ray observations to date for δ Cep vary by at least a factor of ~2. Additional phase coverage is needed to fully explore the X-ray maximum (during $\phi \approx 0.5$) and determine the actual range of X-ray emissions. Sasselov & Lester further concluded that Cepheids should not possess solar-type "coronae", as it would likely be difficult to support a hot outer atmosphere overlying the extensive warm chromosphere that the (supergiant) Cepheids would possess.

The dual-mechanism explanation, in which pulsations modify an underlying, persistent heating source, appears more likely when examining the UV variability of the Cepheids. For δ Cep there is a steady quiescent chromosphere at $\phi \approx 0.6 - 0.8$, which is additionally heated by shock/compression behavior. For β Dor, the phase coverage is not yet extensive enough to either support or deny a dual-mechanism explanation. In terms of the X-ray activity and variability, this explanation could be further supported by the non-detection of RR Lyr in a deep Chandra X-ray image (PI: Guinan). The observation places an upper limit of $log\ L_X \approx 28.0$, which is well below the Cepheid detections. There is the small possibility of RR Lyr being a rather strong X-ray variable, but the non-detection is otherwise fairly conclusive. RR Lyr has a much shorter period than the observed Cepheids *and* much larger RV amplitude, which combined would initiate much stronger shocks. However, RR Lyr has a spectral type of A8 – F7, which is earlier than the Cepheids, giving RR Lyr a much shallower convective zone (or none at all). Since many stellar atmospheres in the cool half of the H-R diagram are heated by acoustic/magnetic activity originating in the convective zone, this would imply that a minimum convective zone depth/strength is required to produce the quiescent UV / X-ray activity, which propagating shocks can then modulate. Also, Bono et al. (1999) showed that, for a Cepheid model of similar properties to δ Cep, convective flux increases during phases of compression ($\phi \approx 0.5 - 0.9$) and sharply decreases after. Stronger convection within the Cepheid could lead to a stronger dynamo and increased magnetic activity (and X-ray activity), explaining the observed X-ray variability in δ Cep. However, one can reasonably assume the varying magnetic field would also affect the UV emissions. This does not seem to be the case, although full phase coverage of the Cepheids at UV / X-ray wavelengths would be needed to definitively rule out such behavior. At present, though,

the data implies that different mechanisms govern the UV and X-ray variabilities. Proposed XMM observations of δ Cep will provide full phase coverage and help resolve this issue. If the X-ray variability is not necessarily caused by modulation of the magnetic field, then perhaps the structure of the magnetic field is responsible.

Numerous studies have been carried out to detect magnetic fields around Cepheids, and most have either failed or returned ambiguous results. Recently, however, a survey of cool supergiants has detected a weak magnetic field in the Cepheid η Aql (Grunhut et al. 2010). However, neither δ Cep nor ζ Gem were found to have Zeeman signatures, but the high incidence of supergiant magnetic field detections in the study led the authors to conclude that perhaps all cool supergiants possess magnetic fields, but of varying degrees of complexity that could mitigate their detection. This is in accord with an earlier theory suggested by Ayres, Brown & Harper (2003) to explain the atmospheric activity and magnetic fields of red giants, shown in Fig. 64. Ayres suggested that the extended chromospheres of red giants would result in "buried coronae" where the magnetic structures responsible for X-ray activity exist entirely within the extended chromospheres. The low surface gravity Cepheids could also possess extended warm chromospheres, as pointed out by Sasselov & Lester, and their internal structures and convective zone placements could also lead to magnetic structures nearer the stellar surface. The variable ionization and compression of the Cepheid chromospheres would cause differing levels of X-ray absorption, and thus varying levels of X-ray emission. However, this scenario remains speculative; an extrapolation of that proposed for red giants, which happens to loosely fit the observations so far for Cepheids. True confirmation of buried coronae in Cepheids will have to await not only additional data, to get a full picture of X-ray activity and variability, and its relation (if any) to the UV emissions, but also a more detailed model of Cepheid atmospheres and internal structure. This may have to be done on a Cepheid-by-Cepheid basis since Cepheids can have a range of masses, temperatures and luminosities.

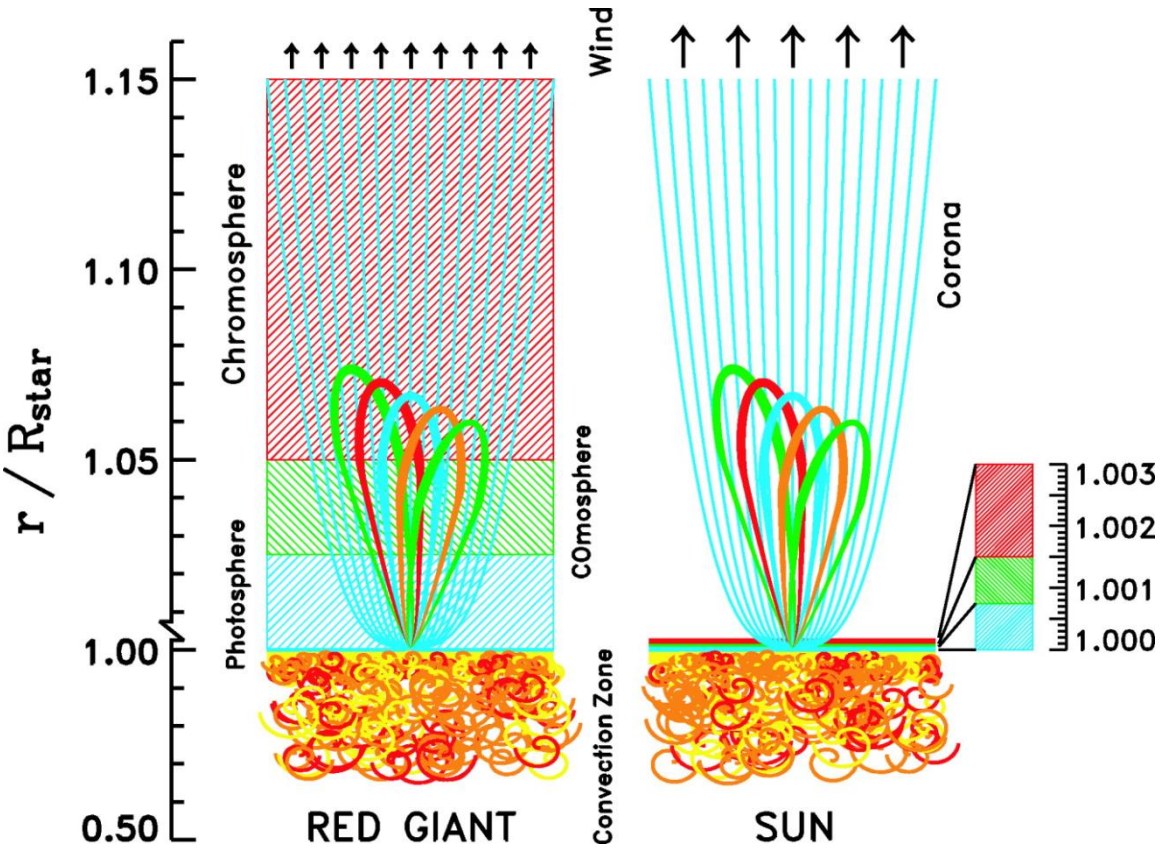

Figure 64 – A cartoon illustration from Ayres, Brown & Harper (2003) depicting the "buried coronae" of red giants. In a cool, main sequence star like the Sun, magnetic structures exist well above the relatively cooler regions of the stellar (solar) atmosphere, and X-ray activity is easily seen. The larger red giants have magnetic structures which scale in height to the Sun, but their low gravities result in much larger, X-ray absorbing chromospheres.

4.5 Future Work

The work that will be carried out in the future is, first and foremost, the continued expansion of the Cepheid database at optical, UV and X-ray wavelengths. As seen in Fig. 65, the Cepheids observed here occupy a large range of the instability strip, but they do not uniformly cover that range, and are simply too few to represent Cepheids as a stellar class. All Cepheids for which optical data have been presented here continue to be observed with the aim of obtaining well-covered light curves of the Cepheids as regularly as observational constraints permit. This will allow us to further refine Cepheid period behaviors – e.g. long-term changes and possible cyclic changes – and characterize amplitude variability, and the possibility of Blazhko effects in Cepheids. Although the optical study has shown amplitude variability in several Cepheids, the full characterization of a Blazhko-type effect in Cepheids other than V473 Lyr is the final

(hopeful) goal. Unfortunately, many more years of data will likely be required to meet this goal, but it is a challenge that we are up to.

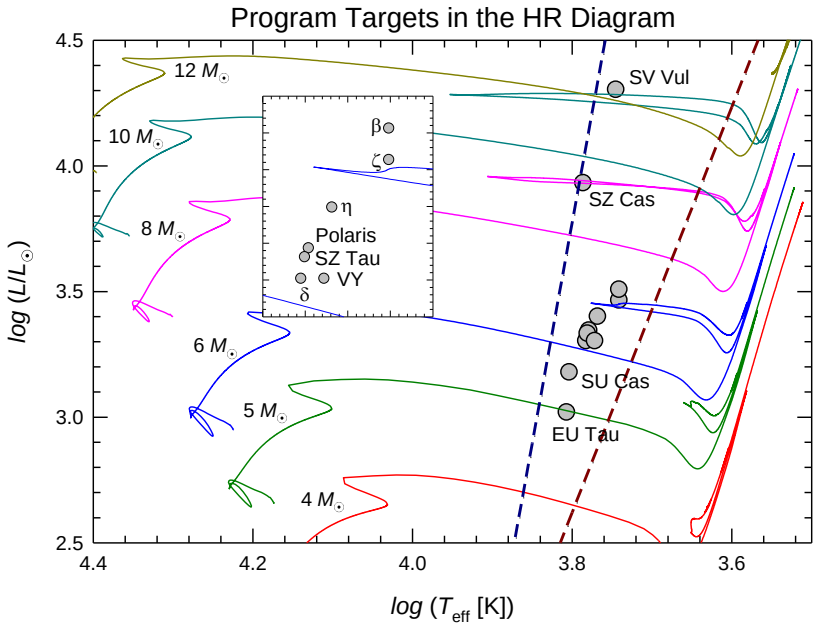

Figure 65 - The Cepheids included in this study are plotted on an HR diagram. SAtlas evolutionary tracks are also plotted (with the initial masses indicated) along with the blue and red edges of the Cepheid instability strip. The sub-plot is included to allow the close group of Cepheids to be spread out for easier identification.

At UV wavelengths, we have recently been approved for additional HST-COS observations of β Dor, to better fill in the activity curve, and for new observations of ℓ Car to precisely understand the large levels of UV activity IUE data have shown for it. HST is currently the only instrument capable of high-resolution UV – FUV spectroscopy, and no future servicing missions will be performed. The only future mission compatible with this study would be the World Space Observatory – Ultraviolet (WSO-UV), currently planned for launch in 2016. However, the possibility of a US Guest Observer program for WSO-UV is uncertain. At present, the pressure is on to observe Cepheids at a variety of periods and pulsation amplitudes so we can begin to understand how UV activity manifests itself and differs across as wide a range of Cepheids as possible. This will give us much greater knowledge of how cool supergiant stellar atmospheres are affected by radial pulsations. Additionally, we plan to observe a sample of non-variable supergiants within the Cepheid instability strip, to provide a more complete understanding of cool supergiant atmospheres as a whole.

The future of the X-ray study is more uncertain. As stated previously, accurate X-ray measures of the Cepheids require long exposure times, and observing time on X-ray satellites such as Chandra and XMM is highly competitive. Also, both are somewhat aged satellites, with Chandra currently in the 13th year of its mission and XMM in the 12th. We have recently been approved for a new Chandra observation of β Dor to search for X-ray variability, and have proposed for an additional XMM observation of δ Cep to confirm its X-ray variability. However, the XMM non-detections of two Cepheids pose a possibly serious problem in that the background levels of the XMM detectors may be high enough to prevent the detections of any Cepheids much more distant than β Dor. If true, then Chandra (with its very low background levels) will be the only satellite capable of extending the X-ray inventory to new, more distant Cepheids. A future proposal is planned to carry out exploratory observations of not only new and varied Cepheids but also (as with the UV study) selected non-variable supergiants within the Cepheid instability strip. The only future program-compatible, planned X-ray mission is ASTRO-H, with a proposed launch date of 2015 and operations planned to begin in 2016, but (again) the status of a US Guest Investigator program is unknown. Until ASTRO-H successfully launches, and such a program is approved, it appears time is running short for Cepheid X-ray studies.

Outside of acquiring more data, the current high-energy dataset is of such complexity that it of course warrants further study. The detailed models required to completely exploit the scientific potential of the data is beyond the scope of this thesis. However, recent collaborations have been made to facilitate this endeavor. To better understand the structure of dynamic stellar atmospheres, program collaborator Hilding Neilson (and his own pre-existing collaborators) are developing a new hydrodynamic stellar atmosphere code based on the Sasselov & Raga (1992) hydrodynamic pulsation code and the SAtlas stellar atmospheres code (Lester & Neilson 2008), also taking into account the newest atmospheric emission line data of CHIANTI. This new code will compute the atmospheric structure and emergent radiation of the stars including the effects of pulsation, full LTE opacities and atmospheric extension. This code will model these three aspects together, along with the shock physics necessary to understand Cepheid photospheres. Combinations of two of the three effects have been presented in previous articles, but not all three (Nardetto et al. 2007; Marengo et al. 2002). The code will allow a direct comparison of synthetic and observed spectra as a function of pulsation phase to constrain the role of shocks (as can the comparison of pulsating Cepheid models and spectra to those of non-pulsating supergiants), while differences between synthetic and observed spectra can provide a measure of the role of magnetic heating and shed light on the driving mechanism of Cepheid and supergiant winds. The formation of emission lines in the post-shock regions can be assessed using traditional emission measure

analyses (using the CHIANTI IDL procedures), which has more recently been evaluated and improved by considering nonstandard processes including effects associated with the breakdown of statistical equilibria (Judge et al. 1995, and subsequent work). We will also measure the thermal ($\rho v T$) and hydrodynamic (ρv^2) energy content of the shocks determined by the post-shock temperatures and outflow velocities, respectively. Finally, discrepancies between the shock models and the observations can tell us the role that magnetic heating plays while outflow velocities will hopefully shed light on the important topic of mass loss in Cepheids.

There is still much to be done before we can claim a total understanding of the secret lives of Cepheids. The first step, taken here, is to recognize that these secret lives exist, and can only be understood through dedicated, persistent study and extensive, rewarding collaborations.

REFERENCES:

Aerts, C., Christensen-Dalsgaard, J., & Kurtz, D. W. 2010, aste.book, - http://adsabs.harvard.edu/abs/2010aste.book.....A

Allen, R. H. 1899, QB802, - http://adsabs.harvard.edu/abs/1899QB802.A4

Aloisi, A., Ake, T., Bostroem, A., Bohlin, R., Cox, C., Diaz, R., Dixon, V., Ghavamian, P., Goudfrooij, P., Hartig, G., Hodge, P., Keyes, C., Kriss, G., Lallo, M., Lennon, D., Massa, D., Niemi, S., Oliveira, C., Osten, R., Proffitt, C. R., Sahnow, D., Smith, E., Wheeler, T., Wolfe, M., York, B., Zheng, W., Green, J., Froning, C., Beland, S., Burgh, E., France, K., Osterman, S., Penton, S., McPhate, J., & Delker, T. 2010, hstc.work, - http://adsabs.harvard.edu/abs/2010hstc.workE...3A

Andrievsky, S. M., Luck, R. E., & Kovtyukh, V. V. 2005, AJ, 130, 1880 - http://adsabs.harvard.edu/abs/2005AJ....130.1880A

Andrievsky, S. M., Kovtyukh, V. V., & Usenko, I. A. 1996, A&A, 305, 551 - http://adsabs.harvard.edu/abs/1996A%26A...305..551A

Applegate, D. 1927, LicOB, 13, 12 - http://adsabs.harvard.edu/abs/1927LicOB..13...12A

Arellano Ferro, A. 1983, ApJ, 274, 755 - http://adsabs.harvard.edu/abs/1983ApJ...274..755A

Ayres, T. R. 2011, ApJ, 738, 120 - http://adsabs.harvard.edu/abs/2011ApJ...738..120A

Ayres, T. R., Brown, A., & Harper, G. M. 2003, ApJ, 598, 610 - http://adsabs.harvard.edu/abs/2003ApJ...598..610A

Baade, W. 1956, PASP, 68, 5 - http://adsabs.harvard.edu/abs/1956PASP...68....5B

Baade, W. 1944, ApJ, 100, 137 - http://adsabs.harvard.edu/abs/1944ApJ...100..137B

Baade, W. 1926, AN, 228, 359 - http://adsabs.harvard.edu/abs/1926AN....228..359

Baker, N., & Kippenhahn, R. 1962, ZA, 54, 114 - http://adsabs.harvard.edu/abs/1962ZA.....54..114B

Becker, S. A. 1981, ApJ, 248, 298 - http://adsabs.harvard.edu/abs/1981ApJ...248..298B

Bejgman, I. L., & Stepanov, A. E. 1981, SvAL, 7, 96 - http://adsabs.harvard.edu/abs/1981SvAL....7...96B

Belopolsky, A. 1899, AN, 149, 239 - http://adsabs.harvard.edu/abs/1899AN....149..239B

Belopolsky, A. 1895, ApJ, 1, 160 - http://adsabs.harvard.edu/abs/1895ApJ.....1..160B

Belopolsky, A. 1894, AN, 136, 281 - http://adsabs.harvard.edu/abs/1894AN....136..281B

Benedict, G. F., McArthur, B. E., Feast, M. W., Barnes, T. G., Harrison, T. E., Patterson, R. J., Menzies, J. W., Bean, J. L., & Freedman, W. L. 2007, AJ, 133, 1810 - http://adsabs.harvard.edu/abs/2007AJ....133.1810B

Benedict, G. F., McArthur, B. E., Fredrick, L. W., Harrison, T. E., Slesnick, C. L., Rhee, J., Patterson, R. J., Skrutskie, M. F., Franz, O. G., Wasserman, L. H., Jefferys, W. H., Nelan, E., van Altena, W., Shelus, P. J., Hemenway, P. D., Duncombe, R. L., Story, D., Whipple, A. L., & Bradley, A. J. 2002, AJ, 124, 1695 - http://adsabs.harvard.edu/abs/2002AJ....124.1695B

Berdnikov, L. N. 2008, yCat, 2285, 0 - http://adsabs.harvard.edu/abs/2008yCat.2285....0B

Berdnikov, L., Mattei, J. A., & Beck, S. J. 2003, JAVSO, 31, 146 - http://adsabs.harvard.edu/abs/2003JAVSO..31..146B

Berdnikov, L. N., Ignatova, V. V., Caldwell, J. A. R., & Koen, C. 2000, NewA, 4, 625 - http://adsabs.harvard.edu/abs/2000NewA....4..625B

Berdnikov, L. N., & Pastukhova, E. N. 1995, AstL, 21, 369 - http://adsabs.harvard.edu/abs/1995AstL...21..369B

Berdnikov, L. N. 1994, AstL, 20, 232 - http://adsabs.harvard.edu/abs/1994AstL...20..232B

Berdnikov, L. N. 1992, SvAL, 18, 130 - http://adsabs.harvard.edu/abs/1992SvAL...18..130B

Berdnikov, L. N. 1986, PZ, 22, 369 - http://adsabs.harvard.edu/abs/1986PZ.....22..369B

Bersier, D., Burki, G., & Kurucz, R. L. 1997, A&A, 320, 228 - http://adsabs.harvard.edu/abs/1997A%26A...320..228B

Bertelli, G., Nasi, E., Girardi, L., & Marigo, P. 2009, A&A, 508, 355 - http://adsabs.harvard.edu/abs/2009A%26A...508..355B

Bezdenezhnyj, V. P. 2007, OAP, 20, 17 - http://adsabs.harvard.edu/abs/2007OAP....20...17B

Blazhko, S. 1907, AN, 175, 325 - http://adsabs.harvard.edu/abs/1907AN....175..325B

Bohm-Vitense, E. 1958, ZA, 46, 108 - http://adsabs.harvard.edu/abs/1958ZA.....46..108B

Bohm-Vitense, E., & Love, S. G. 1994, ApJ, 420, 401 - http://adsabs.harvard.edu/abs/1994ApJ...420..401B

Bono, G., Marconi, M., & Stellingwerf, R. F. 2000a, A&A, 360, 245 - http://adsabs.harvard.edu/abs/2000A%26A...360..245B

Bono, G., Castellani, V., & Marconi, M. 2000b, ApJ, 529, 293 - http://adsabs.harvard.edu/abs/2000ApJ...529..293B

Bono, G., Marconi, M., & Stellingwerf, R. F. 1999, ApJS, 122, 167 - http://adsabs.harvard.edu/abs/1999ApJS..122..167B

Bowen, G. H. 1988, ApJ, 329, 299 - http://adsabs.harvard.edu/abs/1988ApJ...329..299B

Bruntt, H., Evans, N. R., Stello, D., Penny, A. J., Eaton, J. A., Buzasi, D. L., Sasselov, D. D., Preston, H. L., & Miller-Ricci, E. 2008, ApJ, 683, 433 - http://adsabs.harvard.edu/abs/2008ApJ...683..433B

Brunt, D. 1913, Obs, 36, 59 - http://adsabs.harvard.edu/abs/1913Obs....36...59

Budding, E., Demircan, O., Ellis, R., Huchra, J., Kahn, S., Rieke, G., & Stetson, P. B. 2007, iap..book, - http://adsabs.harvard.edu/abs/2007iap..book.....B

Buscombe, W., & Foster, B. E. 2001, yCat, 3223, 0 - http://adsabs.harvard.edu/abs/2001yCat.3223....0B

Buscombe, W., & Foster, B. E. 1995, msct.book, - http://adsabs.harvard.edu/abs/1995msct.book.....B

Campbell, W. W. 1899, ApJ, 9, 86 - http://adsabs.harvard.edu/abs/1899ApJ.....9...86C

Canfield, R. C. 2003, AdSpR, 32, 985 - http://adsabs.harvard.edu/abs/2003AdSpR..32..985C

Caputo, F., Bono, G., Fiorentino, G., Marconi, M., & Musella, I. 2005, ApJ, 629, 1021 - http://adsabs.harvard.edu/abs/2005ApJ...629.1021C

Carroll, B. W., & Ostlie, D. A. 2006, ima..book, - http://adsabs.harvard.edu/abs/2006ima..book.....C

Chabrier, G., & Kuker, M. 2006, A&A, 446, 1027 - http://adsabs.harvard.edu/abs/2006A%26A...446.1027C

Cogan, B. C. 1978, ApJ, 221, 635 - http://adsabs.harvard.edu/abs/1978ApJ...221..635C

Cox, J. P. 1985, cto..conf, 126 - http://adsabs.harvard.edu/abs/1985cto..conf..126C

Cox, A. N. 1979, ApJ, 229, 212 - http://adsabs.harvard.edu/abs/1979ApJ...229..212C

Cox, J. P. 1974, RPPh, 37, 563 - http://adsabs.harvard.edu/abs/1974RPPh...37..563C

Cox, J. P. 1963, ApJ, 138, 487 - http://adsabs.harvard.edu/abs/1963ApJ...138..487C

Cox, J. P., Cox, A. N., Olsen, K. H., King, D. S., & Eilers, D. D. 1966, ApJ, 144, 1038 - http://adsabs.harvard.edu/abs/1966ApJ...144.1038C

Cuntz, M., Rammacher, W., Ulmschneider, P., Musielak, Z. E., & Saar, S. H. 1999, ApJ, 522, 1053 - http://adsabs.harvard.edu/abs/1999ApJ...522.1053C

Cuntz, M., & Ulmschneider, P. 1988, A&A, 193, 119 - http://adsabs.harvard.edu/abs/1988A%26A...193..119C

Cuntz, M. 1990, ApJ, 353, 255 - http://adsabs.harvard.edu/abs/1990ApJ...353..255C

Davis, J. J., Tracey, J. C., Engle, S. G., & Guinan, E. F. 2002, AAS, 34, #117.11 - http://adsabs.harvard.edu/abs/2002AAS...20111711D

de la Fuente Marcos, R., & de la Fuente Marcos, C. 2009, NewA, 14, 180 - http://adsabs.harvard.edu/abs/2009NewA...14..180D

de Zeeuw, P. T., Hoogerwerf, R., de Bruijne, J. H. J., Brown, A. G. A., & Blaauw, A. 1999, AJ, 117, 354 - http://adsabs.harvard.edu/abs/1999AJ....117..354D

DeWarf, L. E., Datin, K. M., & Guinan, E. F. 2010, ApJ, 722, 343 - http://adsabs.harvard.edu/abs/2010ApJ...722..343D

Derekas, A., Szabo, G. M., Berdnikov, L., Szabo, R., Smolec, R., Kiss, L. L., Szabados, L., Chadid, M., Evans, N. R., Kinemuchi, K., Nemec, J. M., Seader, S. E., Smith, J. C., & Tenenbaum, P. 2012, MNRAS, 425, 1312 - http://adsabs.harvard.edu/abs/2012MNRAS.425.1312D

Doschek, G. A., Feldman, U., Mariska, J. T., & Linsky, J. L. 1978, ApJ, 226, L35 - http://adsabs.harvard.edu/abs/1978ApJ...226L..35D

Doyle, J. G., O'Shea, E., Erdelyi, R., Dere, K. P., Socker, D. G., & Keenan, F. P. 1997, SoPh, 173, 243 - http://adsabs.harvard.edu/abs/1997SoPh..173..243D

Dufton, P. L., Hibbert, A., Kingston, A. E., & Doschek, G. A. 1983, The Astrophysical Journal, 274, 420 - http://adsabs.harvard.edu/abs/1983ApJ...274..420D

Dupree, A. K., Foukal, P. V., & Jordan, C. 1976, The Astrophysical Journal, 209, 621 - http://adsabs.harvard.edu/abs/1976ApJ...209..621D

Eddington, A. S. 1919, Obs, 42, 338 - http://adsabs.harvard.edu/abs/1919Obs....42..338E

Eddington, A. S. 1918, MNRAS, 79, 2 - http://adsabs.harvard.edu/abs/1918MNRAS..79R...2E

Eddington, A. S. 1918, MNRAS, 79, 2 - http://adsabs.harvard.edu/abs/1918MNRAS..79Q...2E

Eddington, A. S. 1917, Obs, 40, 290 - http://adsabs.harvard.edu/abs/1917Obs....40..290E

Eddington, A. S., Sir 1941, MNRAS, 101, 182 - http://adsabs.harvard.edu/abs/1941MNRAS.101..182E

Engle, S. G., Guinan, E. F., & Koch, R. H. 2004, AAS, 36, 744 - http://adsabs.harvard.edu/abs/2004AAS...204.0609E

Engle, S. G., & Guinan, E. F. 2012, JASS, 29, 181 - http://adsabs.harvard.edu/abs/2012JASS...29..181E

Engle, S. G., Guinan, E. F., Depasquale, J., & Evans, N. 2009, AIPC, 1135, 192 - http://adsabs.harvard.edu/abs/2009AIPC.1135..192E

Evans, N. R. 1991, ApJ, 372, 597 - http://adsabs.harvard.edu/abs/1991ApJ...372..597E

Evans, N. R., Bond, H., Schaefer, G., Karovska, M., Mason, B., DePasquale, J., Pillitteri, I., Guinan, E., & Engle, S. 2011, AAS, #230.02 - http://adsabs.harvard.edu/abs/2011AAS...21823002R

Evans, N. R., Guinan, E., Engle, S., Wolk, S. J., Schlegel, E., Mason, B. D., Karovska, M., & Spitzbart, B. 2010, AJ, 139, 1968 - http://adsabs.harvard.edu/abs/2010AJ....139.1968E

Evans, N. R., Schaefer, G., Bond, H. E., Nelan, E., Bono, G., Karovska, M., Wolk, S., Sasselov, D., Guinan, E., Engle, S., Schlegel, E., & Mason, B. 2007, IAUS, 240, 102 - http://adsabs.harvard.edu/abs/2007IAUS..240..102E

Fawzy, D. E., Cuntz, M., & Rammacher, W. 2012, MNRAS, 426, 1916 - http://adsabs.harvard.edu/abs/2012MNRAS.426.1916F

Fernie, J. D., Kamper, K. W., & Seager, S. 1993, ApJ, 416, 820 - http://adsabs.harvard.edu/abs/1993ApJ...416..820F

Fernie, J. D. 1987, PASP, 99, 1093 - http://adsabs.harvard.edu/abs/1987PASP...99.1093F

Fokin, A. B., Gillet, D., & Breitfellner, M. G. 1996, A&A, 307, 503 - http://adsabs.harvard.edu/abs/1996A%26A...307..503F

Freedman, W. L., Madore, B. F., Gibson, B. K., Ferrarese, L., Kelson, D. D., Sakai, S., Mould, J. R., Kennicutt, R. C., Jr., Ford, H. C., Graham, J. A., Huchra, J. P., Hughes, S. M. G., Illingworth, G. D., Macri, L. M., & Stetson, P. B. 2001, ApJ, 553, 47 - http://adsabs.harvard.edu/abs/2001ApJ...553...47F

Fricke, K., Stobie, R. S., & Strittmatter, P. A. 1972, ApJ, 171, 593 - http://adsabs.harvard.edu/abs/1972ApJ...171..593F

Gastine, T., & Dintrans, B. 2011, A&A, 528, A6 - http://adsabs.harvard.edu/abs/2011A%26A...528A...6G

Gieren, W. P., Fouque, P., & Gomez, M. I. 1997, ApJ, 488, 74 - http://adsabs.harvard.edu/abs/1997ApJ...488...74G

Gieren, W. P. 1989, A&A, 225, 381 - http://adsabs.harvard.edu/abs/1989A%26A...225..381G

Gieren, W. P., Moffett, T. J., Barnes, T. G., III, Frueh, M. L., & Matthews, J. M. 1990, AJ, 99, 1196 - http://adsabs.harvard.edu/abs/1990AJ.....99.1196G

Goodricke, J., & Bayer, J. 1786, RSPT, 76, 48 - http://adsabs.harvard.edu/abs/1786RSPT...76...48G

Grunhut, J. H., Wade, G. A., Hanes, D. A., & Alecian, E. 2010, MNRAS, 408, 2290 - http://adsabs.harvard.edu/abs/2010MNRAS.408.2290G

Guinan, E. F. 1972, PASP, 84, 56 - http://adsabs.harvard.edu/abs/1972PASP...84...56G

Guinan, E. F. 1966, IBVS, 170, 1 - http://adsabs.harvard.edu/abs/1966IBVS..170....1G

Guinan, E. F., & Engle, S. G. 2009, IAUS, 258, 395 - http://adsabs.harvard.edu/abs/2009IAUS..258..395G

Haisch, B. M., & Linsky, J. L. 1976, ApJ, 205, L39 - http://adsabs.harvard.edu/abs/1976ApJ...205L..39H

Hayes, D. S., Genet, R. M., & Crawford, D. L. 1988, IAPPP, 34, 44 - http://adsabs.harvard.edu/abs/1988IAPPP..34...44H

Henroteau, F. 1925, PDO, 9, 105 - http://adsabs.harvard.edu/abs/1925PDO.....9..105H

Herbig, G. H. 1960, ApJ, 131, 632 - http://adsabs.harvard.edu/abs/1960ApJ...131..632H

Hertzsprung, E. 1926, BAN, 3, 115 - http://adsabs.harvard.edu/abs/1926BAN.....3..115H

Hertzsprung, E. 1911, AN, 189, 89 - http://adsabs.harvard.edu/abs/1911AN....189...89H

Hertzsprung, E. 1909, AN, 179, 373 - http://adsabs.harvard.edu/abs/1909AN....179..373H

Hoyle, F., & Lyttleton, R. A. 1943, MNRAS, 103, 21 - http://adsabs.harvard.edu/abs/1943MNRAS.103...21H

Hubble, E. P. 1925, Obs, 48, 139 - http://adsabs.harvard.edu/abs/1925Obs....48..139H

Hutchinson, J. L., Lillie, C. F., & Hill, S. J. 1975, AJ, 80, 1044 - http://adsabs.harvard.edu/abs/1975AJ.....80.1044H

Ivanov, G. R. 1984, Ap&SS, 105, 369 - http://adsabs.harvard.edu/abs/1984Ap%26SS.105..369I

Jeans, J. H. 1925, MNRAS, 85, 797 - http://adsabs.harvard.edu/abs/1925MNRAS..85..797J

Jordan, C. 1987, PhST, 17, 104 - http://adsabs.harvard.edu/abs/1987PhST...17..104J

Judge, P. G., Woods, T. N., Brekke, P., & Rottman, G. J. 1995, ApJ, 455, L85 - http://adsabs.harvard.edu/abs/1995ApJ...455L..85J

Keenan, F. P., Dufton, P. L., Kingston, A. E., & Cook, J. W. 1989, The Astrophysical Journal, 340, 1135 - http://adsabs.harvard.edu/abs/1989ApJ...340.1135K

Kervella, P., Coude du Foresto, V., Perrin, G., Scholler, M., Traub, W. A., & Lacasse, M. G. 2001, A&A, 367, 876 - http://adsabs.harvard.edu/abs/2001A%26A...367..876K

Kervella, P., Nardetto, N., Bersier, D., Mourard, D., & Coude du Foresto, V. 2004, A&A, 416, 941 - http://adsabs.harvard.edu/abs/2004A%26A...416..941K

Klagyivik, P., & Szabados, L. 2009, A&A, 504, 959 - http://adsabs.harvard.edu/abs/2009A%26A...504..959K

Kolenberg, K. 2012, JAVSO, 40, 481 - http://adsabs.harvard.edu/abs/2012JAVSO..40..481K

Koncewicz, R., & Jordan, C. 2007, MNRAS, 374, 220 - http://adsabs.harvard.edu/abs/2007MNRAS.374..220K

Kovtyukh, V. V., Andrievsky, S. M., Usenko, I. A., & Klochkova, V. G. 1996, A&A, 316, 155 - http://adsabs.harvard.edu/abs/1996A%26A...316..155K

Kovtyukh, V. V., Chekhonadskikh, F. A., Luck, R. E., Soubiran, C., Yasinskaya, M. P., & Belik, S. I. 2010, MNRAS, 408, 1568 - http://adsabs.harvard.edu/abs/2010MNRAS.408.1568K

Kovtyukh, V. V., Soubiran, C., Luck, R. E., Turner, D. G., Belik, S. I., Andrievsky, S. M., & Chekhonadskikh, F. A. 2008, MNRAS, 389, 1336 - http://adsabs.harvard.edu/abs/2008MNRAS.389.1336K

Kraft, R. P. 1960, ApJ, 131, 330 - http://adsabs.harvard.edu/abs/1960ApJ...131..330K

Kraft, R. P. 1957, ApJ, 125, 336 - http://adsabs.harvard.edu/abs/1957ApJ...125..336K

Kukarkin, B. V. 1975, pust.book, - http://adsabs.harvard.edu/abs/1975pust.book.....K

Leavitt, H. S. 1908, AnHar, 60, 87 - http://adsabs.harvard.edu/abs/1908AnHar..60...87L

Leavitt, H. S., & Pickering, E. C. 1912, HarCi, 173, 1 - http://adsabs.harvard.edu/abs/1912HarCi.173....1L

Lester, J. B., & Neilson, H. R. 2008, A&A, 491, 633 - http://adsabs.harvard.edu/abs/2008A%26A...491..633L

Linsky, J. L., Wood, B. E., Judge, P., Brown, A., Andrulis, C., & Ayres, T. R. 1995, ApJ, 442, 381 - http://adsabs.harvard.edu/abs/1995ApJ...442..381L

Luck, R. E., & Andrievsky, S. M. 2004, AJ, 128, 343 - http://adsabs.harvard.edu/abs/2004AJ....128..343L

Luck, R. E., Andrievsky, S. M., Fokin, A., & Kovtyukh, V. V. 2008, AJ, 136, 98 - http://adsabs.harvard.edu/abs/2008AJ....136...98L

Luck, R. E., Kovtyukh, V. V., & Andrievsky, S. M. 2006, AJ, 132, 902 - http://adsabs.harvard.edu/abs/2006AJ....132..902L

Luck, R. E., Kovtyukh, V. V., & Andrievsky, S. M. 2001, A&A, 373, 589 - http://adsabs.harvard.edu/abs/2001A%26A...373..589L

Ludendorff, H. 1916, AN, 203, 361 - http://adsabs.harvard.edu/abs/1916AN....203..361L

Madore, B. F. 1977, MNRAS, 178, 505 - http://adsabs.harvard.edu/abs/1977MNRAS.178..505M

Majaess, D., Turner, D., & Gieren, W. 2012, ApJ, 747, 145 - http://adsabs.harvard.edu/abs/2012ApJ...747..145M

Majaess, D., Turner, D., Gieren, W., Balam, D. & Lane, D. 2012, ApJ, 748, L9 - http://adsabs.harvard.edu/abs/2012ApJ...748L...9M

Mallik, S. V. 1999, A&A, 352, 495 - http://adsabs.harvard.edu/abs/1999A%26A...352..495M

Marengo, M., Sasselov, D. D., Karovska, M., Papaliolios, C., & Armstrong, J. T. 2002, ApJ, 567, 1131 - http://adsabs.harvard.edu/abs/2002ApJ...567.1131M

Matthews, L. D., Marengo, M., Evans, N. R., & Bono, G. 2012, ApJ, 744, 53 - http://adsabs.harvard.edu/abs/2012ApJ...744...53M

Milone, E. F., Wilson, W. J. F., & Volk, K. 1999, AJ, 118, 3016 - http://adsabs.harvard.edu/abs/1999AJ....118.3016M

N/A 1921, PA, 29, 76 - http://adsabs.harvard.edu/abs/1921PA.....29...76

Nardetto, N., Mourard, D., Mathias, P., Fokin, A., & Gillet, D. 2007, A&A, 471, 661 - http://adsabs.harvard.edu/abs/2007A%26A...471..661N

Neilson, H. R., Cantiello, M., & Langer, N. 2011, A&A, 529, L9 - http://adsabs.harvard.edu/abs/2011A%26A...529L....9N

Neilson, H. R., Nardetto, N., Ngeow, C.-C., Fouque, P., & Storm, J. 2012, A&A, 541, A134 - http://adsabs.harvard.edu/abs/2012A%26A...541A.134N

Neilson, H. R., Engle, S. G., Guinan, E., & Langer, N. 2012, AAS, 219, #152.02 - http://adsabs.harvard.edu/abs/2012AAS...21915202N

Neilson, H. R., Engle, S. G., Guinan, E., Langer, N., Wasatonic, R. P., & Williams, D. B. 2012, ApJ, 745, L32 - http://adsabs.harvard.edu/abs/2012ApJ...745L..32N

Nordgren, T. E., Armstrong, J. T., Germain, M. E., Hindsley, R. B., Hajian, A. R., Sudol, J. J. & Hummel, C. A. 2000, ApJ, 543, 972 - http://adsabs.harvard.edu/abs/2000ApJ...543..972N

Noyes, R. W., Hartmann, L. W., Baliunas, S. L., Duncan, D. K., & Vaughan, A. H. 1984, ApJ, 279, 763 - http://adsabs.harvard.edu/abs/1984ApJ...279..763N

Parker, E. N. 2009, SSRv, 144, 15 - http://adsabs.harvard.edu/abs/2009SSRv..144...15P

Pena, J. H., Arellano Ferro, A., Pena-Miller, R., Alvarez, M., Rosas, Y., Garcia, H., Munoz, G., Vargas, B., Sareyan, J. P., Guerrero, C. A., & Renteria, A. 2010, RMxAA, 46, 291 - http://adsabs.harvard.edu/abs/2010RMxAA..46..291P

Pigott, E. 1785, RSPT, 75, 127 - http://adsabs.harvard.edu/abs/1785RSPT...75..127P

Plummer, H. C. 1913, MNRAS, 73, 661 - http://adsabs.harvard.edu/abs/1913MNRAS..73..661P

Plummer, H. G. 1914, MNRAS, 74, 660 - http://adsabs.harvard.edu/abs/1914MNRAS..74..660P

Pop, A., & Codreanu, S. 2001, Ap&SS, 275, 247 - http://adsabs.harvard.edu/abs/2001Ap%26SS.275..247P

Postma, J. E. 2008, MsT, 1 - http://adsabs.harvard.edu/abs/2008MsT.....1P

Prugniel, P., Soubiran, C., Koleva, M., & Le Borgne, D. 2007, yCat, 3251, 0 - http://adsabs.harvard.edu/abs/2007yCat.3251....0P

Rastorguev, A. S., & Dambis, A. K. 2011, AstBu, 66, 47 - http://adsabs.harvard.edu/abs/2011AstBu..66...47R

Redfield, S., Linsky, J. L., Ake, T. B., Ayres, T. R., Dupree, A. K., Robinson, R. D., Wood, B. E., & Young, P. R. 2002, ApJ, 581, 626 - http://adsabs.harvard.edu/abs/2002ApJ...581..626R

Reimers, D., Huensch, M., Schmitt, J. H. M. M., & Toussaint, F. 1996, A&A, 310, 813 - http://adsabs.harvard.edu/abs/1996A%26A...310..813R

Remage Evans, N. 2011, arXiv, arXiv:1112.1046 - http://adsabs.harvard.edu/abs/2011arXiv1112.1046R

Riess, A. G., Macri, L., Casertano, S., Lampeitl, H., Ferguson, H. C., Filippenko, A. V., Jha, S. W., Li, W., & Chornock, R. 2011, ApJ, 730, 119 - http://adsabs.harvard.edu/abs/2011ApJ...730..119R

Russell, H. N. 1913, Obs, 36, 324 - http://adsabs.harvard.edu/abs/1913Obs....36..324R

Sasselov, D. D., & Raga, A. 1992, ASPC, 26, 549 - http://adsabs.harvard.edu/abs/1992ASPC...26..549S

Sasselov, D. D., & Lester, J. B. 1994, ApJ, 423, 795 - http://adsabs.harvard.edu/abs/1994ApJ...423..795S

Schmidt, E. G., & Parsons, S. B. 1984, ApJ, 279, 202 - http://adsabs.harvard.edu/abs/1984ApJ...279..202S

Schmidt, E. G., & Parsons, S. B. 1984, ApJ, 279, 215 - http://adsabs.harvard.edu/abs/1984ApJ...279..215S

Schmidt, E. G., & Parsons, S. B. 1982, ApJS, 48, 185 - http://adsabs.harvard.edu/abs/1982ApJS...48..185S

Schwarzschild, K. 1910, AN, 185, 133 - http://adsabs.harvard.edu/abs/1910AN....185..133S

Schwarzschild, K. 1900, AN, 152, 65 - http://adsabs.harvard.edu/abs/1900AN....152...65S

Shapley, H., & Walton, M. L. 1927, HarCi, 316, 1 - http://adsabs.harvard.edu/abs/1927HarCi.316....1S

Shapley, H. 1914, ApJ, 40, 448 - http://adsabs.harvard.edu/abs/1914ApJ....40..448S

Shapley, H. 1927, HarCi, 314, 1 - http://adsabs.harvard.edu/abs/1927HarCi.314....1S

Skumanich, A. 1972, ApJ, 171, 565 - http://adsabs.harvard.edu/abs/1972ApJ...171..565S

Smolec, R. 2005, AcA, 55, 59 - http://adsabs.harvard.edu/abs/2005AcA....55...59S

Soszynski, I., Poleski, R., Udalski, A., Szymanski, M. K., Kubiak, M., Pietrzynski, G., Wyrzykowski, L., Szewczyk, O., & Ulaczyk, K. 2010, AcA, 60, 17 - http://adsabs.harvard.edu/abs/2010AcA....60...17S

Soszynski, I., Poleski, R., Udalski, A., Szymanski, M. K., Kubiak, M., Pietrzynski, G., Wyrzykowski, L., Szewczyk, O., & Ulaczyk, K. 2008, AcA, 58, 163 - http://adsabs.harvard.edu/abs/2008AcA....58..163S

Spreckley, S. A., & Stevens, I. R. 2008, MNRAS, 388, 1239 - http://adsabs.harvard.edu/abs/2008MNRAS.388.1239S

Storm, J., Gieren, W., Fouque, P., Barnes, T. G., Soszynski, I., Pietrzynski, G., Nardetto, N., & Queloz, D. 2011, A&A, 534, A95 - http://adsabs.harvard.edu/abs/2011A%26A...534A..95S

Stothers, R. B. 2009, ApJ, 696, L37 - http://adsabs.harvard.edu/abs/2009ApJ...696L..37S

Stothers, R. B. 2006, ApJ, 652, 643 - http://adsabs.harvard.edu/abs/2006ApJ...652..643S

Sutmann, G., & Ulmschneider, P. 1995, A&A, 294, 232 - http://adsabs.harvard.edu/abs/1995A%26A...294..232S

Szabados, L. 2010, OAP, 23, 106 - http://adsabs.harvard.edu/abs/2010OAP....23..106S

Szabados, L. 2003, ASPC, 298, 237 - http://adsabs.harvard.edu/abs/2003ASPC..298..237S

Szabados, L. 1991, CoKon, 96, 123 - http://adsabs.harvard.edu/abs/1991CoKon..96..123S

Szabados, L. 1981, CoKon, 77, 1 - http://adsabs.harvard.edu/abs/1981CoKon..77....1S

Szabados, L. 1980, CoKon, 76, 1 - http://adsabs.harvard.edu/abs/1980CoKon..76....1S

Szabados, L. 1977, CoKon, 70, 1 - http://adsabs.harvard.edu/abs/1977CoKon..70....1S

Tammann, G. A., Sandage, A., & Reindl, B. 2003, A&A, 404, 423 - http://adsabs.harvard.edu/abs/2003A%26A...404..423T

Taylor, M. M., & Booth, A. J. 1998, MNRAS, 298, 594 - http://adsabs.harvard.edu/abs/1998MNRAS.298..594T

Turner, D. G., & Berdnikov, L. N. 2004, A&A, 423, 335 - http://adsabs.harvard.edu/abs/2004A%26A...423..335T

Turner, D. G., Kovtyukh, V. V., Usenko, I. A., & Gorlova, N. I. 2013, ApJ, 762, L8 - http://adsabs.harvard.edu/abs/2013ApJ...762L...8T

Turner, D. G., Majaess, D. J., Lane, D. J., Balam, D. D., Gieren, W. P., Storm, J., Forbes, D. W., Havlen, R. J., & Alessi, B. 2012, MNRAS, 422, 2501 - http://adsabs.harvard.edu/abs/2012MNRAS.422.2501T

Turner, D. G., Savoy, J., Derrah, J., Abdel-Sabour Abdel-Latif, M., & Berdnikov, L. N. 2005, PASP, 117, 207 - http://adsabs.harvard.edu/abs/2005PASP..117..207T

Turner, D. G. 2010, Ap&SS, 326, 219 - http://adsabs.harvard.edu/abs/2010Ap%26SS.326..219T

Turner, D. G. 1998, JAVSO, 26, 101 - http://adsabs.harvard.edu/abs/1998JAVSO..26..101T

Turner, D. G. 1992, AJ, 104, 1865 - http://adsabs.harvard.edu/abs/1992AJ....104.1865T

Turner, D. G., Abdel-Sabour Abdel-Latif, M., & Berdnikov, L. N. 2006, PASP, 118, 410 - http://adsabs.harvard.edu/abs/2006PASP..118..410T

Turner, D. G., Bryukhanov, I. S., Balyuk, I. I., Gain, A. M., Grabovsky, R. A., Grigorenko, V. D., Klochko, I. V., Kosa-Kiss, A., Kosinsky, A. S., Kushmar, I. J., Mamedov, V. T., Narkevich, N. A., Pogosyants, A. J., Semenyuta, A. S., Sergey, I. M., Schukin, V. V., Strigelsky, J. B., Tamello, V. G., Lane, D. J., & Majaess, D. J. 2007, PASP, 119, 1247 - http://adsabs.harvard.edu/abs/2007PASP..119.1247T

Turner, D. G., & Burke, J. F. 2002, AJ, 124, 2931 - http://adsabs.harvard.edu/abs/2002AJ....124.2931T

Valle, G., Marconi, M., Degl'Innocenti, S., & Prada Moroni, P. G. 2009, A&A, 507, 1541 - http://adsabs.harvard.edu/abs/2009A%26A...507.1541V

van Leeuwen, F. 2013, A&A, 550, L3 - http://adsabs.harvard.edu/abs/2013A%26A...550L...3V

van Leeuwen, F. 2008, yCat, 1311, 0 - http://adsabs.harvard.edu/abs/2008yCat.1311....0F

van Leeuwen, F. 2007, ASSL, 350, - http://adsabs.harvard.edu/abs/2007ASSL..350.....V

van Leeuwen, F., Feast, M. W., Whitelock, P. A., & Laney, C. D. 2007, MNRAS, 379, 723 - http://adsabs.harvard.edu/abs/2007MNRAS.379..723V

Wesselink, A. J. 1946, BAN, 10, 91 - http://adsabs.harvard.edu/abs/1946BAN....10...91

Wielen, R., Jahreis, H., Dettbarn, C., Lenhardt, H., & Schwan, H. 2000, A&A, 360, 399 - http://adsabs.harvard.edu/abs/2000A%26A...360..399W

Wood, B. E., & Karovska, M. 2000, ApJ, 535, 304 - http://adsabs.harvard.edu/abs/2000ApJ...535..304W

Yoon, S.-C., & Langer, N. 2005, A&A, 443, 643 - http://adsabs.harvard.edu/abs/2005A%26A...443..643Y

Zhevakin, S. A. 1963, ARA&A, 1, 367 - http://adsabs.harvard.edu/abs/1963ARA%26A...1..367Z

Zombeck, M. 2007, hsaa.book, - http://adsabs.harvard.edu/abs/2007hsaa.book.....Z

APPENDIX A: CEPHEID PHOTOMETRIC DATA OBTAINED AS PART OF THIS PROGRAM

Photometry of δ Cep

HJD	Phase	V-mag	V-err	HJD	Phase	U-B	U-B err	HJD	Phase	B-V	B-V err
2454437.5956	-0.2357	4.3136	0.0026	2454437.5926	-0.2362	0.6518	0.0060	2454437.5941	-0.2360	0.8588	0.0062
2454439.5928	0.1365	3.6690	0.0056	2454439.5941	0.1367	0.3887	0.0216	2454439.5928	0.1365	0.5839	0.0104
2454440.5858	0.3215	3.9369	0.0015	2454440.5856	0.3215	0.5173	0.0081	2454440.5857	0.3215	0.7411	0.0058
2454447.5794	-0.3752	4.2614	0.0029	2454447.5806	-0.3750	0.6512	0.0043	2454447.5793	-0.3752	0.8752	0.0035
2454449.5797	-0.0024	3.4627	0.0206	2454449.5795	-0.0025	0.3408	0.0429	2454449.5797	-0.0024	0.4522	0.0270
2454450.5797	0.1839	3.7435	0.0051	2454450.5795	0.1839	0.4299	0.0150	2454450.5797	0.1839	0.6358	0.0064
2454452.6001	-0.4396	4.1927	0.0008	2454452.6000	-0.4396	0.6393	0.0033	2454452.6001	-0.4396	0.8575	0.0028
2454454.5902	-0.0687	3.6357	0.0080	2454454.5914	-0.0685	0.3344	0.0223	2454454.5901	-0.0687	0.5130	0.0192
2454458.6295	-0.3160	4.3210	0.0038	2454458.6293	-0.3160	0.6698	0.0066	2454458.6294	-0.3160	0.8739	0.0075
2454459.6007	-0.1350	4.0087	0.0061	2454459.6005	-0.1350	0.4212	0.0188	2454459.6007	-0.1350	0.6829	0.0087
2454460.6012	0.0514	3.5319	0.0044	2454460.6010	0.0514	0.3427	0.0241	2454460.6011	0.0514	0.4928	0.0098
2454465.5856	-0.0197	3.4726	0.0097	2454465.5854	-0.0197	0.3114	0.0393	2454465.5855	-0.0197	0.4432	0.0161
2454466.5860	0.1667	3.7179	0.0030	2454466.5858	0.1667	0.4135	0.0243	2454466.5860	0.1667	0.6152	0.0090
2454623.9115	0.4845	4.0934	0.0069	2454623.9125	0.4847	0.5818	0.0075	2454623.9114	0.4845	0.8290	0.0102
2454624.9073	-0.3299	4.2869	0.0101	2454624.9096	-0.3295	0.6965	0.0045	2454624.9072	-0.3299	0.8948	0.0110
2454625.9096	-0.1431	4.0377	0.0132	2454625.9119	-0.1427	0.4678	0.0181	2454625.9095	-0.1431	0.6995	0.0203
2454626.9007	0.0416	3.5028	0.0736	2454626.9005	0.0415	0.3168	0.1136	2454626.9006	0.0416	0.4855	0.1044
2454628.8954	0.4133	4.0524	0.0255	2454628.8952	0.4133	0.5968	0.0100	2454628.8953	0.4133	0.7961	0.0272
2454630.8915	-0.2147	4.2666	0.0064	2454630.8914	-0.2147	0.6220	0.0067	2454630.8915	-0.2147	0.8435	0.0091
2454631.8927	-0.0282	3.4735	0.0338	2454631.8925	-0.0282	0.3129	0.0547	2454631.8926	-0.0282	0.4578	0.0472
2454634.8826	-0.4710	4.1342	0.0059	2454634.8837	-0.4708	0.6428	0.0085	2454634.8825	-0.4710	0.8499	0.0103
2454636.8754	-0.0996	3.8125	0.0075	2454636.8752	-0.0997	0.3607	0.0195	2454636.8753	-0.0996	0.5974	0.0164
2454637.9466	0.1000	3.5949	0.0221	2454637.9464	0.1000	0.3873	0.0198	2454637.9465	0.1000	0.5456	0.0281
2454638.8721	0.2725	3.8548	0.0283	2454638.8719	0.2724	0.4832	0.0229	2454638.8720	0.2724	0.6989	0.0339
2454640.8664	-0.3559	4.2744	0.0198	2454640.8712	-0.3550	0.6568	0.0127	2454640.8688	-0.3554	0.8617	0.0228

2455098.6395	-0.0493	3.5439	0.0031	2455098.6394	-0.0493	0.3202	0.0300	2455098.6395	-0.0493	0.4703	0.0115
2455098.8061	-0.0182	3.4698	0.0098	2455098.8059	-0.0183	0.3162	0.0282	2455098.8060	-0.0182	0.4468	0.0147
2455099.6796	0.1445	3.6712	0.0174	2455099.6794	0.1445	0.3933	0.0283	2455099.6795	0.1445	0.5873	0.0251
2455099.8098	0.1688	3.7231	0.0083	2455099.8096	0.1688	0.3957	0.0177	2455099.8097	0.1688	0.6079	0.0111
2455100.6797	0.3309	3.9503	0.0098	2455100.6795	0.3309	0.4961	0.0188	2455100.6796	0.3309	0.7481	0.0099
2455100.8049	0.3542	3.9894	0.0057	2455100.8047	0.3542	0.5408	0.0110	2455100.8049	0.3543	0.7592	0.0064
2455101.8009	-0.4601	4.1662	0.0051	2455101.8007	-0.4602	0.6152	0.0068	2455101.8008	-0.4602	0.8436	0.0056
2455102.6697	-0.2982	4.3076	0.0037	2455102.6695	-0.2983	0.6399	0.0111	2455102.6696	-0.2983	0.8748	0.0098
2455102.7986	-0.2742	4.3196	0.0036	2455102.7984	-0.2743	0.6272	0.0052	2455102.7986	-0.2742	0.8799	0.0044
2455106.7864	0.4689	4.0959	0.0071	2455106.7862	0.4689	0.5972	0.0116	2455106.7863	0.4689	0.8225	0.0090
2455131.7559	0.1220	3.6400	0.0047	2455131.7557	0.1220	0.3726	0.0261	2455131.7558	0.1220	0.5682	0.0131
2455133.7727	0.4978	4.1171	0.0079	2455133.7725	0.4978	0.6057	0.0094	2455133.7726	0.4978	0.8312	0.0087
2455134.7810	-0.3143	4.3066	0.0058	2455134.7808	-0.3143	0.6630	0.0104	2455134.7810	-0.3143	0.8879	0.0103
2455135.7811	-0.1279	3.9710	0.0016	2455135.7809	-0.1279	0.4214	0.0131	2455135.7810	-0.1279	0.6597	0.0042
2455136.7802	0.0583	3.5396	0.0107	2455136.7800	0.0583	0.3263	0.0237	2455136.7801	0.0583	0.5041	0.0139
2455143.7567	0.3584	3.9866	0.0033	2455143.7565	0.3583	0.5265	0.0077	2455143.7566	0.3584	0.7666	0.0068
2455144.7438	-0.4577	4.1803	0.0026	2455144.7449	-0.4575	0.6064	0.0024	2455144.7438	-0.4577	0.8490	0.0032
2455145.7524	-0.2697	4.3230	0.0037	2455145.7535	-0.2695	0.6619	0.0052	2455145.7523	-0.2697	0.8749	0.0049
2455146.7367	-0.0863	3.7385	0.0118	2455146.7378	-0.0861	0.3430	0.0261	2455146.7366	-0.0863	0.5586	0.0177
2455151.7214	-0.1574	4.1278	0.0068	2455151.7212	-0.1574	0.4719	0.0093	2455151.7214	-0.1574	0.7403	0.0095
2455468.8625	-0.0577	3.5880	0.0058	2455468.8623	-0.0578	0.2636	0.0332	2455468.8624	-0.0577	0.4836	0.0086
2455469.8524	0.1267	3.6395	0.0091	2455469.8522	0.1267	0.3709	0.0277	2455469.8523	0.1267	0.5750	0.0101
2455470.8496	0.3126	3.9216	0.0090	2455470.8506	0.3128	0.4550	0.0090	2455470.8495	0.3126	0.7337	0.0107
2455471.8477	0.4986	4.1325	0.0074	2455471.8476	0.4986	0.5523	0.0085	2455471.8477	0.4986	0.8203	0.0075
2455476.8328	0.4275	4.0543	0.0066	2455476.8326	0.4275	0.5565	0.0078	2455476.8328	0.4276	0.7966	0.0079
2455477.8317	-0.3863	4.2534	0.0037	2455477.8315	-0.3863	0.6369	0.0067	2455477.8317	-0.3863	0.8640	0.0050
2455478.8278	-0.2007	4.2579	0.0035	2455478.8288	-0.2005	0.5306	0.0030	2455478.8277	-0.2007	0.8274	0.0043

2455479.8259	-0.0147	3.4598	0.0058	2455479.8258	-0.0147	0.2990	0.0374	2455479.8259	-0.0147	0.4438	0.0124
2455480.8224	0.1710	3.7180	0.0116	2455480.8222	0.1710	0.3776	0.0215	2455480.8223	0.1710	0.6115	0.0154
2455481.8206	0.3570	3.9785	0.0029	2455481.8204	0.3570	0.5003	0.0195	2455481.8205	0.3570	0.7636	0.0049
2455482.8167	-0.4573	4.1735	0.0006	2455482.8165	-0.4574	0.6105	0.0096	2455482.8166	-0.4574	0.8388	0.0063
2455488.8022	-0.3419	4.2813	0.0050	2455488.8033	-0.3417	0.6661	0.0053	2455488.8034	-0.3417	0.8781	0.0051
2455492.8071	0.4044	4.0341	0.0058	2455492.8069	0.4044	0.5646	0.0185	2455492.8070	0.4044	0.7843	0.0097
2455493.7961	-0.4113	4.2234	0.0036	2455493.7959	-0.4113	0.6438	0.0093	2455493.7960	-0.4113	0.8642	0.0054
2455495.7963	-0.0386	3.5080	0.0040	2455495.7962	-0.0386	0.3188	0.0224	2455495.7963	-0.0386	0.4529	0.0059
2455498.7913	-0.4805	4.1397	0.0038	2455498.7911	-0.4805	0.5898	0.0089	2455498.7913	-0.4804	0.8403	0.0063
2455499.7861	-0.2951	4.3109	0.0060	2455499.7872	-0.2949	0.6147	0.0060	2455499.7860	-0.2951	0.8810	0.0075
2455501.7758	0.0757	3.5584	0.0083	2455502.7734	0.2616	0.4184	0.0107	2455501.7758	0.0757	0.5080	0.0131
2455502.7736	0.2617	3.8492	0.0084	2455503.7702	0.4474	0.5650	0.0081	2455502.7735	0.2616	0.6962	0.0085
2455503.7704	0.4474	4.0703	0.0041	2455504.7687	-0.3666	0.6450	0.0064	2455503.7703	0.4474	0.8109	0.0073
2455504.7676	-0.3668	4.2629	0.0068	2455506.7628	0.0051	0.3137	0.0261	2455504.7676	-0.3668	0.8764	0.0087
2455506.7656	0.0056	3.4644	0.0101	2455508.7574	0.3767	0.4885	0.0094	2455506.7642	0.0053	0.4493	0.0161
2455508.7576	0.3768	4.0027	0.0015	2455510.7521	-0.2515	0.6259	0.0038	2455508.7575	0.3768	0.7787	0.0063
2455510.7523	-0.2515	4.3192	0.0031	2455511.7497	-0.0656	0.3313	0.0237	2455510.7522	-0.2515	0.8726	0.0042
2455511.7498	-0.0656	3.6148	0.0078	2455512.7461	0.1200	0.3340	0.0193	2455511.7498	-0.0656	0.5041	0.0247
2455512.7463	0.1201	3.6349	0.0040	2455513.7464	0.3065	0.4628	0.0073	2455512.7462	0.1201	0.5566	0.0100
2455513.7465	0.3065	3.9130	0.0042	2455515.7437	-0.3213	0.6444	0.0078	2455513.7465	0.3065	0.7305	0.0070
2455515.7439	-0.3213	4.2962	0.0067	2455516.7379	-0.1361	0.3991	0.0162	2455515.7438	-0.3213	0.8734	0.0084
2455516.7381	-0.1360	4.0154	0.0058	2455532.6060	-0.1790	0.5079	0.0084	2455516.7381	-0.1360	0.6895	0.0087
2455532.6062	-0.1790	4.1985	0.0037	2455532.6851	-0.1643	0.4582	0.0140	2455532.6061	-0.1790	0.7854	0.0039
2455532.6853	-0.1643	4.1480	0.0034	2455533.5938	0.0050	0.3076	0.0636	2455532.6852	-0.1643	0.7549	0.0081
2455533.5940	0.0051	3.4631	0.0044	2455862.6716	0.3291	0.5273	0.0073	2455533.5939	0.0051	0.4426	0.0056
2455862.6718	0.3292	3.9454	0.0048	2455865.6121	-0.1229	0.4116	0.0161	2455862.6717	0.3291	0.7361	0.0058
2455865.6113	-0.1231	3.9479	0.0047	2455866.5960	0.0604	0.3642	0.0151	2455865.6112	-0.1231	0.6473	0.0085

2455866.5962	0.0605	3.5297	0.0046	2455867.5953	0.2467	0.4690	0.0202	2455866.5962	0.0605	0.4819	0.0056
2455867.5955	0.2467	3.8237	0.0048	2455868.5949	0.4329	0.5862	0.0089	2455867.5954	0.2467	0.6749	0.0078
2455868.5950	0.4330	4.0575	0.0014	2455881.5649	-0.1501	0.4587	0.0050	2455868.5950	0.4330	0.8013	0.0030
2455881.5651	-0.1500	4.0841	0.0023	2455881.5798	-0.1473	0.4551	0.0141	2455881.5651	-0.1500	0.7125	0.0035
2455881.5800	-0.1473	4.0662	0.0026	2455881.5946	-0.1445	0.4413	0.0064	2455881.5799	-0.1473	0.7114	0.0043
2455881.5948	-0.1445	4.0545	0.0033	2455881.6095	-0.1418	0.4362	0.0135	2455881.5947	-0.1445	0.7006	0.0052
2455881.6097	-0.1417	4.0402	0.0042	2455881.6244	-0.1390	0.4287	0.0077	2455881.6096	-0.1417	0.6987	0.0069
2455881.6246	-0.1390	4.0255	0.0036	2455881.6393	-0.1362	0.4173	0.0093	2455881.6245	-0.1390	0.6893	0.0044
2455881.6395	-0.1362	4.0084	0.0047	2455881.6539	-0.1335	0.4129	0.0020	2455881.6394	-0.1362	0.6861	0.0073
2455881.6541	-0.1335	3.9959	0.0056	2455881.6685	-0.1308	0.4136	0.0092	2455881.6541	-0.1335	0.6806	0.0058
2455881.6687	-0.1307	3.9808	0.0021	2455881.6832	-0.1280	0.4107	0.0057	2455881.6687	-0.1307	0.6726	0.0056
2455881.6833	-0.1280	3.9622	0.0076	2455881.6978	-0.1253	0.4064	0.0085	2455881.6833	-0.1280	0.6657	0.0087
2455881.6980	-0.1253	3.9496	0.0025	2455881.7125	-0.1226	0.3926	0.0164	2455881.6980	-0.1253	0.6482	0.0061
2455881.7127	-0.1225	3.9351	0.0048	2455881.7272	-0.1198	0.3862	0.0083	2455881.7127	-0.1225	0.6463	0.0061
2455881.7274	-0.1198	3.9171	0.0030	2455882.7385	0.0686	0.3482	0.0101	2455881.7273	-0.1198	0.6407	0.0066
2455882.7387	0.0687	3.5467	0.0059	2455888.7206	0.1834	0.4150	0.0201	2455882.7386	0.0686	0.5016	0.0065
2455888.7209	0.1834	3.7327	0.0025	2455892.6967	-0.0757	0.3329	0.0126	2455888.7208	0.1834	0.6285	0.0045
2455892.6969	-0.0756	3.6782	0.0051	2455893.7072	0.1127	0.3696	0.0104	2455892.6968	-0.0756	0.5418	0.0128
2455893.7074	0.1127	3.6233	0.0062	2455900.6873	0.4134	0.5663	0.0066	2455893.7073	0.1127	0.5509	0.0072
2455900.6875	0.4134	4.0396	0.0048	2455911.6608	0.4583	0.5911	0.0063	2455900.6874	0.4134	0.7927	0.0068
2455911.6610	0.4584	4.0806	0.0023	2455912.6201	-0.3629	0.6577	0.0056	2455911.6609	0.4584	0.8116	0.0054
2455912.6203	-0.3629	4.2621	0.0061	2455919.5647	-0.0688	0.3442	0.0165	2455912.6202	-0.3629	0.8832	0.0077
2455919.5649	-0.0687	3.6346	0.0062	2455919.5793	-0.0660	0.3317	0.0183	2455919.5648	-0.0687	0.5022	0.0125
2455919.5816	-0.0656	3.6206	0.0063	2455919.5944	-0.0632	0.3344	0.0118	2455919.5805	-0.0658	0.5072	0.0098
2455919.5946	-0.0632	3.6030	0.0111	2455919.6066	-0.0610	0.3326	0.0126	2455919.5946	-0.0632	0.4904	0.0152
2455919.6068	-0.0609	3.5938	0.0103	2455919.6213	-0.0582	0.3053	0.0177	2455919.6067	-0.0609	0.4928	0.0126
2455919.6215	-0.0582	3.5778	0.0056	2455922.6358	-0.4965	0.5951	0.0057	2455919.6214	-0.0582	0.4911	0.0056

2455922.6360	-0.4964	4.1270	0.0054	2455926.6210	0.2462	0.4516	0.0113	2455922.6359	-0.4964	0.8262	0.0065
2455926.6211	0.2462	3.8209	0.0048	2455927.6222	0.4328	0.5737	0.0143	2455926.6211	0.2462	0.6892	0.0083
2455927.6223	0.4328	4.0375	0.0060	2455931.6089	0.1757	0.3997	0.0097	2455927.6223	0.4328	0.8152	0.0090
2455931.6091	0.1757	3.7166	0.0021					2455931.6090	0.1757	0.6286	0.0046

Photometry of δ Cep, cont…

HJD	Phase	V-R	V-R err	HJD	Phase	R-I	R-I err
2454623.9116	0.4846	0.8475	0.0133	2454623.9118	0.4846	0.4449	0.0182
2454624.9074	-0.3299	0.8906	0.0133	2454624.9076	-0.3298	0.4568	0.0213
2454625.9097	-0.1431	0.8115	0.0306	2454625.9099	-0.1431	0.3999	0.0298
2454626.9008	0.0416	0.6316	0.1148	2454626.9010	0.0416	0.3114	0.1183
2454628.8955	0.4133	0.8242	0.0368	2454628.8957	0.4134	0.4223	0.0388
2454630.8917	-0.2147	0.8686	0.0130	2454630.8919	-0.2147	0.4471	0.0157
2454631.8928	-0.0281	0.6187	0.0376	2454631.8930	-0.0281	0.3017	0.0322
2454634.8827	-0.4710	0.8436	0.0104	2454634.8829	-0.4709	0.4573	0.0132
2454636.8755	-0.0996	0.7132	0.0159	2454636.8757	-0.0996	0.3449	0.0187
2454637.9467	0.1000	0.6852	0.0240	2454637.9469	0.1001	0.3425	0.0154
2454638.8722	0.2725	0.7897	0.0339	2454638.8724	0.2725	0.4029	0.0381
2454640.8665	-0.3559	0.8592	0.0332	2454640.8667	-0.3558	0.4639	0.0394
2455098.6397	-0.0492	0.6392	0.0147	2455098.6399	-0.0492	0.3083	0.0179
2455098.8062	-0.0182	0.6168	0.0112	2455098.8064	-0.0182	0.2922	0.0067
2455099.6797	0.1446	0.7060	0.0267	2455099.6799	0.1446	0.3626	0.0325
2455099.8099	0.1688	0.7150	0.0091	2455099.8101	0.1689	0.3659	0.0079
2455100.6798	0.3309	0.7976	0.0147	2455100.6800	0.3310	0.4048	0.0113
2455100.8050	0.3543	0.7972	0.0098	2455100.8052	0.3543	0.4187	0.0084
2455101.8010	-0.4601	0.8341	0.0063	2455101.8012	-0.4601	0.4423	0.0075

2455102.6711	-0.2980	0.8716	0.0120	2455102.6713	-0.2979	0.4458	0.0148
2455102.7988	-0.2742	0.8655	0.0043	2455102.7989	-0.2742	0.4518	0.0037
2455106.7865	0.4689	0.8297	0.0105	2455106.7867	0.4690	0.4382	0.0095
2455131.7560	0.1220	0.6839	0.0093	2455131.7562	0.1221	0.3430	0.0087
2455133.7728	0.4979	0.8295	0.0112	2455133.7730	0.4979	0.4465	0.0096
2455134.7811	-0.3142	0.8777	0.0105	2455134.7813	-0.3142	0.4600	0.0121
2455135.7812	-0.1279	0.7493	0.0051	2455135.7814	-0.1278	0.3802	0.0063
2455136.7803	0.0583	0.6346	0.0162	2455136.7805	0.0584	0.3161	0.0164
2455143.7568	0.3584	0.7916	0.0094	2455143.7570	0.3584	0.4198	0.0095
2455144.7440	-0.4576	0.8426	0.0040	2455144.7442	-0.4576	0.4436	0.0044
2455145.7525	-0.2697	0.8528	0.0057	2455145.7527	-0.2697	0.4529	0.0047
2455146.7368	-0.0863	0.6751	0.0133	2455146.7370	-0.0862	0.3376	0.0091
2455151.7215	-0.1574	0.7938	0.0089	2455151.7217	-0.1573	0.4094	0.0075
2455468.8626	-0.0577	0.6324	0.0083	2455468.8628	-0.0577	0.3048	0.0098
2455469.8525	0.1268	0.6848	0.0109	2455469.8527	0.1268	0.3427	0.0078
2455470.8497	0.3126	0.7778	0.0119	2455470.8499	0.3126	0.4063	0.0100
2455471.8479	0.4986	0.8250	0.0085	2455471.8481	0.4987	0.4364	0.0092
2455476.8329	0.4276	0.8102	0.0108	2455476.8331	0.4276	0.4323	0.0127
2455477.8318	-0.3863	0.8584	0.0070	2455477.8320	-0.3862	0.4547	0.0083
2455478.8279	-0.2007	0.8286	0.0038	2455478.8281	-0.2006	0.4406	0.0048
2455479.8261	-0.0146	0.6120	0.0090	2455479.8263	-0.0146	0.2867	0.0101
2455480.8225	0.1710	0.7142	0.0151	2455480.8227	0.1711	0.3588	0.0147
2455481.8207	0.3571	0.7908	0.0090	2455481.8209	0.3571	0.4168	0.0099
2455482.8168	-0.4573	0.8476	0.0022	2455482.8170	-0.4573	0.4427	0.0055
2455488.8023	-0.3419	0.8648	0.0057	2455488.8025	-0.3419	0.4536	0.0050
2455492.8072	0.4044	0.8116	0.0069	2455492.8074	0.4044	0.4269	0.0051
2455493.7962	-0.4113	0.8532	0.0073	2455493.7964	-0.4113	0.4506	0.0078

2455495.7965	-0.0385	0.6257	0.0089	2455495.7967	-0.0385	0.2863	0.0159
2455498.7914	-0.4804	0.8334	0.0042	2455498.7916	-0.4804	0.4434	0.0021
2455499.7862	-0.2950	0.8576	0.0082	2455499.7864	-0.2950	0.4483	0.0096
2455501.7760	0.0758	0.6490	0.0141	2455501.7761	0.0758	0.3168	0.0154
2455502.7737	0.2617	0.7618	0.0091	2455502.7739	0.2617	0.3878	0.0057
2455503.7705	0.4474	0.8195	0.0057	2455503.7707	0.4475	0.4345	0.0047
2455504.7678	-0.3667	0.8593	0.0076	2455504.7679	-0.3667	0.4492	0.0054
2455506.7644	0.0054	0.6110	0.0125	2455506.7633	0.0051	0.2903	0.0178
2455508.7577	0.3768	0.8131	0.0051	2455508.7579	0.3768	0.4182	0.0051
2455510.7524	-0.2515	0.8705	0.0049	2455510.7526	-0.2514	0.4505	0.0052
2455511.7500	-0.0656	0.6559	0.0093	2455511.7502	-0.0655	0.3113	0.0094
2455512.7464	0.1201	0.6888	0.0080	2455512.7466	0.1201	0.3422	0.0100
2455513.7467	0.3065	0.7853	0.0058	2455513.7469	0.3065	0.4056	0.0047
2455515.7440	-0.3213	0.8583	0.0084	2455515.7442	-0.3213	0.4594	0.0066
2455516.7383	-0.1360	0.7643	0.0068	2455516.7384	-0.1360	0.3856	0.0085
2455532.6063	-0.1790	0.8205	0.0040	2455532.6065	-0.1789	0.4245	0.0019
2455532.6854	-0.1642	0.8072	0.0039	2455532.6856	-0.1642	0.4113	0.0024
2455533.5941	0.0051	0.6192	0.0055	2455533.5943	0.0051	0.2939	0.0052
2455862.6718	0.3292	0.7970	0.0059	2455862.6720	0.3292	0.4151	0.0039
2455865.6113	-0.1231	0.7487	0.0054	2455865.6114	-0.1230	0.3780	0.0073
2455866.5963	0.0605	0.6474	0.0064	2455866.5964	0.0605	0.3171	0.0048
2455867.5955	0.2467	0.7607	0.0056	2455867.5957	0.2467	0.3860	0.0058
2455868.5951	0.4330	0.8311	0.0035	2455868.5952	0.4330	0.4313	0.0053
2455881.5652	-0.1500	0.7904	0.0045	2455881.5653	-0.1500	0.4069	0.0046
2455881.5800	-0.1473	0.7815	0.0030	2455881.5802	-0.1472	0.4031	0.0031
2455881.5949	-0.1445	0.7834	0.0067	2455881.5950	-0.1445	0.3968	0.0064
2455881.6098	-0.1417	0.7768	0.0053	2455881.6099	-0.1417	0.3948	0.0038

2455881.6246	-0.1390	0.7713	0.0041	2455881.6248	-0.1389	0.3922	0.0049
2455881.6396	-0.1362	0.7630	0.0063	2455881.6397	-0.1361	0.3914	0.0066
2455881.6542	-0.1334	0.7657	0.0067	2455881.6543	-0.1334	0.3871	0.0052
2455881.6688	-0.1307	0.7597	0.0032	2455881.6689	-0.1307	0.3864	0.0047
2455881.6834	-0.1280	0.7515	0.0079	2455881.6835	-0.1280	0.3776	0.0049
2455881.6981	-0.1253	0.7551	0.0035	2455881.6982	-0.1252	0.3733	0.0042
2455881.7128	-0.1225	0.7531	0.0084	2455881.7129	-0.1225	0.3776	0.0074
2455881.7274	-0.1198	0.7378	0.0052	2455881.7276	-0.1198	0.3727	0.0050
2455882.7387	0.0687	0.6529	0.0120	2455882.7389	0.0687	0.3096	0.0122
2455888.7209	0.1835	0.7202	0.0049	2455888.7210	0.1835	0.3609	0.0049
2455892.6969	-0.0756	0.6567	0.0080	2455892.6971	-0.0756	0.3329	0.0099
2455893.7074	0.1127	0.6821	0.0075	2455893.7075	0.1127	0.3441	0.0047
2455900.6875	0.4134	0.8189	0.0075	2455900.6877	0.4135	0.4316	0.0063
2455911.6610	0.4584	0.8345	0.0057	2455911.6611	0.4584	0.4278	0.0082
2455912.6203	-0.3629	0.8583	0.0074	2455912.6204	-0.3628	0.4601	0.0050
2455919.5649	-0.0687	0.6601	0.0076	2455919.5650	-0.0687	0.3246	0.0104
2455919.5806	-0.0658	0.6615	0.0101	2455919.5796	-0.0660	0.3160	0.0112
2455919.5947	-0.0632	0.6539	0.0117	2455919.5948	-0.0632	0.3128	0.0101
2455919.6069	-0.0609	0.6510	0.0114	2455919.6070	-0.0609	0.3162	0.0140
2455919.6215	-0.0582	0.6572	0.0092	2455919.6217	-0.0581	0.2988	0.0087
2455922.6360	-0.4964	0.8478	0.0065	2455922.6361	-0.4964	0.4338	0.0039
2455926.6212	0.2462	0.7505	0.0086	2455926.6214	0.2463	0.3917	0.0088
2455927.6224	0.4328	0.8066	0.0098	2455927.6225	0.4328	0.4227	0.0108
2455931.6091	0.1757	0.7170	0.0067	2455931.6092	0.1757	0.3588	0.0071

Photometry of η Aql

HJD	Phase	V-mag	V-err	HJD	Phase	U-B	U-B err	HJD	Phase	B-V	B-V err
2454623.8857	0.2292	3.7495	0.0174	2454623.8860	0.2292	0.4789	0.0199	2454623.8858	0.2292	0.8047	0.0235
2454625.8694	-0.4944	4.0584	0.0210	2454625.8697	-0.4944	0.6830	0.0176	2454625.8695	-0.4944	0.9514	0.0246
2454626.8750	-0.3543	4.2333	0.0040	2454626.8752	-0.3543	0.7556	0.0047	2454626.8750	-0.3543	1.0183	0.0046
2454627.8737	-0.2151	4.1733	0.0126	2454627.8739	-0.2151	0.5786	0.0156	2454627.8737	-0.2151	0.9398	0.0161
2454628.8784	-0.0751	3.6784	0.0111	2454628.8786	-0.0751	0.3893	0.0326	2454628.8784	-0.0751	0.6897	0.0233
2454630.8659	0.2018	3.7484	0.0115	2454630.8661	0.2018	0.4931	0.0238	2454630.8660	0.2018	0.7816	0.0161
2454631.8599	0.3403	3.7627	0.0160	2454631.8602	0.3403	0.5411	0.0137	2454631.8600	0.3403	0.8170	0.0173
2454634.9098	-0.2348	4.2332	0.0101	2454634.9100	-0.2347	0.6800	0.0097	2454634.9099	-0.2348	0.9591	0.0109
2454636.8961	0.0420	3.5217	0.0227	2454636.8963	0.0420	0.3654	0.0306	2454636.8961	0.0420	0.6261	0.0344
2454638.9073	0.3222	3.7592	0.0139	2454638.9076	0.3223	0.5174	0.0165	2454638.9074	0.3222	0.8106	0.0205
2454643.9336	0.0225	3.4871	0.0178	2454643.9338	0.0226	0.3725	0.0260	2454643.9337	0.0226	0.6116	0.0202
2454648.8659	-0.2902	4.2592	0.0054	2454648.8661	-0.2902	0.7303	0.0105	2454648.8660	-0.2902	1.0154	0.0061
2454733.6930	-0.4710	4.0718	0.0106	2454733.6933	-0.4709	0.7301	0.0063	2454733.6931	-0.4709	0.9719	0.0117
2454734.6956	-0.3313	4.2543	0.0023	2454734.6959	-0.3312	0.7674	0.0111	2454734.6957	-0.3313	1.0093	0.0026
2454737.6951	0.0867	3.5780	0.0030	2454737.6953	0.0867	0.4031	0.0320	2454737.6951	0.0867	0.6589	0.0042
2454738.7153	0.2288	3.7501	0.0065	2454738.7156	0.2289	0.4983	0.0124	2454738.7154	0.2288	0.8016	0.0081
2454741.6762	-0.3586	4.2165	0.0028	2454741.6765	-0.3586	0.7782	0.0107	2454741.6763	-0.3586	1.0125	0.0058
2455098.7215	0.3897	3.8754	0.0055	2455098.7218	0.3898	0.5918	0.0207	2455098.7216	0.3898	0.8737	0.0091
2455099.6100	-0.4865	4.0787	0.0043	2455099.6102	-0.4864	0.6830	0.0150	2455099.6100	-0.4865	0.9518	0.0045
2455099.6477	-0.4812	4.0746	0.0016	2455099.6490	-0.4810	0.6877	0.0043	2455099.6478	-0.4812	0.9655	0.0038
2455099.7313	-0.4696	4.0812	0.0075	2455099.7316	-0.4695	0.7206	0.0086	2455099.7314	-0.4696	0.9690	0.0082
2455100.6088	-0.3473	4.2484	0.0026	2455100.6090	-0.3473	0.7551	0.0038	2455100.6088	-0.3473	1.0116	0.0030
2455100.7239	-0.3313	4.2476	0.0044	2455100.7242	-0.3312	0.7770	0.0093	2455100.7240	-0.3312	1.0163	0.0073
2455101.6848	-0.1974	4.1294	0.0062	2455101.6851	-0.1973	0.5789	0.0150	2455101.6849	-0.1974	0.9053	0.0112
2455102.6090	-0.0686	3.6543	0.0048	2455102.6072	-0.0689	0.3688	0.0296	2455102.6081	-0.0687	0.6642	0.0082

2455102.7213	-0.0530	3.5866	0.0120	2455102.7215	-0.0529	0.3544	0.0262	2455102.7213	-0.0530	0.6262	0.0191
2455133.6527	0.2568	3.7685	0.0029	2455133.6529	0.2569	0.5197	0.0085	2455133.6527	0.2568	0.8070	0.0044
2455134.6521	0.3961	3.9132	0.0019	2455134.6524	0.3961	0.6100	0.0155	2455134.6522	0.3961	0.8760	0.0071
2455136.6452	-0.3262	4.2535	0.0055	2455136.6454	-0.3262	0.7575	0.0089	2455136.6452	-0.3262	1.0197	0.0092
2455137.6444	-0.1870	4.1141	0.0029	2455137.6447	-0.1870	0.5487	0.0053	2455137.6445	-0.1870	0.8840	0.0045
2455138.6440	-0.0477	3.5579	0.0057	2455138.6443	-0.0477	0.3490	0.0302	2455138.6441	-0.0477	0.6176	0.0074
2455139.6431	0.0915	3.5839	0.0040	2455139.6434	0.0915	0.4044	0.0122	2455139.6432	0.0915	0.6634	0.0051
2455141.6423	0.3700	3.8287	0.0086	2455141.6426	0.3701	0.5140	0.0543	2455141.6424	0.3701	0.8404	0.0117
2455143.6450	-0.3509	4.2309	0.0024	2455143.6453	-0.3509	0.8021	0.0055	2455143.6451	-0.3509	1.0100	0.0051
2455144.6407	-0.2122	4.1795	0.0069	2455144.6410	-0.2121	0.6452	0.0088	2455144.6408	-0.2122	0.9338	0.0098
2455146.6396	0.0663	3.5446	0.0096	2455146.6398	0.0664	0.3857	0.0281	2455146.6396	0.0663	0.6509	0.0136
2455508.5890	0.4980	4.0595	0.0012	2455508.5893	0.4981	0.6794	0.0076	2455508.5891	0.4980	0.9506	0.0042
2455513.5866	0.1943	3.7499	0.0044	2455513.5869	0.1944	0.4950	0.0130	2455513.5867	0.1944	0.7727	0.0067
2455516.5857	-0.3878	4.2044	0.0008	2455516.5860	-0.3877	0.7682	0.0077	2455516.5858	-0.3878	1.0020	0.0052
2455826.8136	-0.1626	4.0397	0.0100	2455826.8138	-0.1626	0.5278	0.0141	2455826.8136	-0.1626	0.7967	0.0141
2455827.8105	-0.0237	3.5147	0.0106	2455827.8108	-0.0237	0.3887	0.0778	2455827.8106	-0.0237	0.5870	0.0238
2455828.7796	0.1113	3.6196	0.0205	2455828.7798	0.1113	0.4207	0.0269	2455828.7796	0.1113	0.7011	0.0280
2455840.7593	-0.2195	4.2057	0.0035	2455840.7596	-0.2195	0.6511	0.0049	2455840.7594	-0.2195	0.9207	0.0045
2455842.7536	0.0583	3.5371	0.0090	2455842.7539	0.0584	0.3983	0.0221	2455842.7537	0.0583	0.6427	0.0157
2455843.7499	0.1972	3.7463	0.0072	2455843.7502	0.1972	0.5191	0.0056	2455843.7500	0.1972	0.7718	0.0080
2455844.7578	0.3376	3.7876	0.0042	2455844.7580	0.3376	0.5523	0.0057	2455844.7578	0.3376	0.8048	0.0057
2455845.7454	0.4752	4.0403	0.0066	2455845.7456	0.4752	0.6979	0.0071	2455845.7455	0.4752	0.9298	0.0079
2455846.7423	-0.3859	4.2054	0.0032	2455846.7426	-0.3859	0.7649	0.0071	2455846.7424	-0.3859	0.9951	0.0054
2455847.7385	-0.2471	4.2581	0.0027	2455847.7399	-0.2469	0.7115	0.0058	2455847.7386	-0.2471	0.9558	0.0058
2455848.7359	-0.1081	3.8300	0.0048	2455848.7362	-0.1081	0.4342	0.0173	2455848.7360	-0.1081	0.7312	0.0066
2455849.7336	0.0309	3.5156	0.0066	2455849.7339	0.0309	0.3809	0.0230	2455849.7337	0.0309	0.6146	0.0149
2455854.7336	-0.2725	4.2693	0.0014	2455854.7338	-0.2724	0.7449	0.0029	2455854.7337	-0.2724	0.9766	0.0025

2455855.5865	-0.1536	3.9784	0.0042	2455855.5868	-0.1536	0.4577	0.0097	2455855.5866	-0.1536	0.8074	0.0047
2455856.5858	-0.0144	3.4988	0.0042	2455856.5861	-0.0143	0.3482	0.0129	2455856.5859	-0.0144	0.5964	0.0134
2455857.5849	0.1248	3.6486	0.0066	2455857.5852	0.1249	0.4194	0.0190	2455857.5850	0.1248	0.7141	0.0120
2455858.5841	0.2641	3.7700	0.0029	2455858.5844	0.2641	0.5074	0.0083	2455858.5842	0.2641	0.8048	0.0034
2455861.5818	-0.3183	4.2733	0.0025	2455861.5821	-0.3182	0.7622	0.0044	2455861.5819	-0.3183	1.0127	0.0026
2455862.5706	-0.1805	4.0873	0.0017	2455862.5708	-0.1805	0.5395	0.0039	2455862.5706	-0.1805	0.8611	0.0027
2455862.5852	-0.1785	4.0754	0.0028	2455862.5855	-0.1784	0.5325	0.0060	2455862.5853	-0.1784	0.8635	0.0047
2455862.5999	-0.1764	4.0690	0.0039	2455862.6001	-0.1764	0.5263	0.0073	2455862.6000	-0.1764	0.8542	0.0067
2455862.6146	-0.1744	4.0575	0.0019	2455862.6149	-0.1743	0.5219	0.0083	2455862.6147	-0.1744	0.8516	0.0063
2455862.6293	-0.1723	4.0524	0.0024	2455862.6296	-0.1723	0.5239	0.0042	2455862.6294	-0.1723	0.8462	0.0035
2455864.6530	0.1097	3.6188	0.0032	2455864.6532	0.1097	0.4196	0.0121	2455864.6531	0.1097	0.6914	0.0110
2455865.5790	0.2387	3.7718	0.0045	2455865.5792	0.2387	0.4964	0.0089	2455865.5790	0.2387	0.7943	0.0064

Photometry of η Aql, cont…

HJD	Phase	V-R	V-R err	HJD	Phase	R-I	R-I err
2454623.8859	0.2292	0.6292	0.0248	2454623.8861	0.2293	0.4401	0.0215
2454625.8696	-0.4944	0.7119	0.0270	2454625.8698	-0.4943	0.5025	0.0336
2454626.8751	-0.3543	0.7316	0.0042	2454626.8753	-0.3542	0.5265	0.0056
2454627.8738	-0.2151	0.7192	0.0168	2454627.8741	-0.2151	0.5564	0.0166
2454628.8785	-0.0751	0.5682	0.0219	2454628.8788	-0.0751	0.4037	0.0364
2454630.8660	0.2018	0.6188	0.0229	2454630.8663	0.2018	0.4391	0.0339
2454631.8601	0.3403	0.6401	0.0183	2454631.8603	0.3403	0.4392	0.0117
2454634.9099	-0.2348	0.7137	0.0132	2454634.9102	-0.2347	0.4863	0.0158
2454636.8962	0.0420	0.5257	0.0304	2454636.8965	0.0420	0.3477	0.0265
2454638.9074	0.3222	0.6445	0.0199	2454638.9077	0.3223	0.4384	0.0285
2454643.9337	0.0226	0.5055	0.0185	2454643.9340	0.0226	0.3579	0.0344

2454648.8660	-0.2902	0.7215	0.0079	2454648.8663	-0.2902	0.5058	0.0130
2454733.6931	-0.4709	0.7077	0.0121	2454733.6934	-0.4709	0.4559	0.0130
2454734.6957	-0.3313	0.7466	0.0076	2454734.6960	-0.3312	0.4812	0.0133
2454737.6952	0.0867	0.5615	0.0066	2454737.6955	0.0867	0.3599	0.0123
2454738.7155	0.2288	0.6229	0.0115	2454738.7157	0.2289	0.4136	0.0178
2454741.6763	-0.3586	0.7413	0.0036	2454741.6766	-0.3586	0.4806	0.0040
2455098.7217	0.3898	0.6634	0.0109	2455098.7219	0.3898	0.4291	0.0155
2455099.6101	-0.4865	0.7194	0.0068	2455099.6103	-0.4864	0.4703	0.0151
2455099.6478	-0.4812	0.7162	0.0065	2455099.6481	-0.4812	0.4621	0.0141
2455099.7315	-0.4695	0.7167	0.0101	2455099.7317	-0.4695	0.4489	0.0202
2455100.6089	-0.3473	0.7499	0.0049	2455100.6091	-0.3473	0.4942	0.0099
2455100.7240	-0.3312	0.7307	0.0078	2455100.7243	-0.3312	0.4805	0.0104
2455101.6850	-0.1973	0.6824	0.0084	2455101.6852	-0.1973	0.4509	0.0109
2455102.6081	-0.0687	0.5477	0.0092	2455102.6073	-0.0688	0.3523	0.0108
2455102.7214	-0.0529	0.5226	0.0194	2455102.7227	-0.0528	0.3667	0.0153
2455133.6528	0.2568	0.6285	0.0061	2455133.6531	0.2569	0.4041	0.0131
2455134.6522	0.3961	0.6736	0.0115	2455134.6525	0.3961	0.4354	0.0168
2455136.6453	-0.3262	0.7412	0.0130	2455136.6456	-0.3262	0.4794	0.0135
2455137.6445	-0.1870	0.6805	0.0055	2455138.6444	-0.0477	0.3371	0.0192
2455138.6441	-0.0477	0.5453	0.0109	2455139.6435	0.0915	0.3665	0.0117
2455139.6433	0.0915	0.5562	0.0082	2455141.6427	0.3701	0.4192	0.0270
2455141.6425	0.3701	0.6650	0.0143	2455143.6454	-0.3509	0.4900	0.0101
2455143.6452	-0.3509	0.7215	0.0072	2455144.6422	-0.2120	0.4760	0.0117
2455144.6409	-0.2122	0.6951	0.0080	2455146.6399	0.0664	0.3543	0.0154
2455146.6397	0.0663	0.5324	0.0122	2455508.5894	0.4981	0.4756	0.0136
2455508.5892	0.4980	0.7209	0.0025	2455513.5870	0.1944	0.4159	0.0133
2455513.5867	0.1944	0.6329	0.0086	2455516.5861	-0.3877	0.4943	0.0121

2455516.5858	-0.3878	0.7316	0.0070	2455826.8139	-0.1626	0.3982	0.0141
2455826.8137	-0.1626	0.7005	0.0141	2455827.8109	-0.0237	0.3232	0.0292
2455827.8107	-0.0237	0.4908	0.0223	2455828.7800	0.1113	0.3589	0.0281
2455828.7797	0.1113	0.5871	0.0293	2455840.7597	-0.2195	0.4502	0.0123
2455840.7595	-0.2195	0.7190	0.0048	2455842.7540	0.0584	0.3513	0.0243
2455842.7538	0.0584	0.5082	0.0183	2455843.7503	0.1972	0.4025	0.0244
2455843.7500	0.1972	0.6121	0.0187	2455844.7581	0.3376	0.4235	0.0058
2455844.7579	0.3376	0.6526	0.0062	2455845.7458	0.4752	0.4590	0.0114
2455845.7455	0.4752	0.6863	0.0113	2455846.7427	-0.3859	0.4704	0.0191
2455846.7424	-0.3859	0.7350	0.0101	2455847.7400	-0.2469	0.4744	0.0053
2455847.7387	-0.2471	0.7187	0.0058	2455848.7363	-0.1081	0.3736	0.0132
2455848.7361	-0.1081	0.6041	0.0116	2455849.7340	0.0309	0.3408	0.0231
2455849.7338	0.0309	0.5205	0.0162	2455854.7340	-0.2724	0.4711	0.0069
2455854.7337	-0.2724	0.7399	0.0066	2455855.5869	-0.1536	0.4380	0.0079
2455855.5866	-0.1536	0.6528	0.0044	2455856.5862	-0.0143	0.3537	0.0181
2455856.5860	-0.0144	0.5103	0.0050	2455857.5853	0.1249	0.3847	0.0207
2455857.5851	0.1249	0.5762	0.0113	2455858.5845	0.2641	0.4142	0.0196
2455858.5843	0.2641	0.6305	0.0095	2455861.5822	-0.3182	0.4739	0.0068
2455861.5819	-0.3183	0.7397	0.0036	2455862.5710	-0.1804	0.4157	0.0077
2455862.5707	-0.1805	0.6825	0.0051	2455862.5856	-0.1784	0.4165	0.0077
2455862.5854	-0.1784	0.6705	0.0050	2455862.6003	-0.1764	0.4135	0.0094
2455862.6000	-0.1764	0.6733	0.0057	2455862.6150	-0.1743	0.4205	0.0125
2455862.6147	-0.1744	0.6658	0.0058	2455862.6297	-0.1723	0.4163	0.0087
2455862.6294	-0.1723	0.6615	0.0072	2455864.6534	0.1097	0.3630	0.0173
2455864.6531	0.1097	0.5712	0.0080	2455865.5793	0.2387	0.4350	0.0191
2455865.5791	0.2387	0.6354	0.0064				

Photometry of EU Tau

HJD	Phase	V-mag	V-err	HJD	Phase	U-B	U-B err	HJD	Phase	B-V	B-V err
2454439.8995	0.2252	8.0471	0.0029	2454439.8993	0.2251	0.4397	0.0042	2454439.8994	0.2252	0.6788	0.0035
2454440.8767	-0.3099	8.1773	0.0018	2454440.8765	-0.3100	0.4429	0.0049	2454440.8767	-0.3099	0.7159	0.0021
2454447.8994	0.0305	7.9251	0.0035	2454447.8993	0.0305	0.4074	0.0162	2454447.8994	0.0305	0.6121	0.0055
2454448.8949	-0.4959	8.2249	0.0007	2454448.8947	-0.4960	0.4688	0.0046	2454448.8949	-0.4959	0.7532	0.0020
2454449.9033	-0.0163	7.9278	0.0024	2454449.9031	-0.0164	0.4035	0.0115	2454449.9032	-0.0163	0.6164	0.0057
2454450.8903	0.4532	8.2017	0.0014	2454450.8902	0.4532	0.4760	0.0046	2454450.8903	0.4532	0.7361	0.0035
2454451.9579	-0.0390	7.9093	0.0029	2454451.9577	-0.0391	0.3848	0.0099	2454451.9578	-0.0390	0.6124	0.0067
2454452.8615	0.3909	8.1638	0.0003	2454452.8614	0.3908	0.4623	0.0050	2454452.8615	0.3909	0.7345	0.0033
2454453.8663	-0.1312	7.9863	0.0017	2454453.8662	-0.1312	0.4084	0.0038	2454453.8663	-0.1312	0.6367	0.0030
2454454.8773	0.3497	8.1365	0.0020	2454454.8771	0.3496	0.4593	0.0091	2454454.8772	0.3497	0.7227	0.0042
2454458.9014	0.2639	8.0721	0.0053	2454458.9012	0.2638	0.4365	0.0114	2454458.9013	0.2638	0.7087	0.0074
2454459.8868	-0.2674	8.1326	0.0047	2454459.8866	-0.2675	0.4389	0.0125	2454459.8867	-0.2675	0.7010	0.0075
2454460.8781	0.2041	8.0252	0.0018	2454460.8779	0.2040	0.4237	0.0073	2454460.8780	0.2041	0.6768	0.0033
2454461.9041	-0.3078	8.1833	0.0041	2454461.9039	-0.3079	0.4431	0.0070	2454461.9040	-0.3079	0.7218	0.0069
2454464.9022	0.1183	7.9413	0.0074	2454464.9020	0.1182	0.4180	0.0208	2454464.9021	0.1182	0.6484	0.0133
2454465.8949	-0.4095	8.2130	0.0032	2454465.8947	-0.4096	0.4683	0.0062	2454465.8949	-0.4095	0.7586	0.0033
2454475.8352	0.3188	8.1091	0.0050	2454475.8350	0.3187	0.4449	0.0092	2454475.8351	0.3187	0.7119	0.0053
2454476.8260	-0.2100	8.0741	0.0038	2454476.8258	-0.2100	0.4187	0.0061	2454476.8259	-0.2100	0.6810	0.0053
2454480.8116	-0.3141	8.1924	0.0033	2454480.8115	-0.3142	0.4517	0.0069	2454480.8116	-0.3141	0.7183	0.0062
2454481.8149	0.1631	7.9995	0.0050	2454481.8147	0.1630	0.4332	0.0204	2454481.8148	0.1631	0.6629	0.0100
2454483.8133	0.1137	7.9537	0.0131	2454483.8131	0.1136	0.4145	0.0169	2454483.8132	0.1136	0.6372	0.0168
2454484.8017	-0.4162	8.2347	0.0028	2454484.8015	-0.4162	0.4639	0.0062	2454484.8016	-0.4162	0.7383	0.0039
2454485.8403	0.0779	7.9416	0.0049	2454485.8401	0.0778	0.4146	0.0048	2454485.8403	0.0779	0.6338	0.0056
2454486.7951	-0.4680	8.2285	0.0089	2454486.7949	-0.4680	0.4719	0.0071	2454486.7950	-0.4680	0.7515	0.0103

2454494.7853	0.3327	8.1165	0.0095	2454494.7851	0.3326	0.4552	0.0089	2454494.7853	0.3327	0.7258	0.0103
2454495.8039	-0.1827	8.0293	0.0077	2454495.8038	-0.1828	0.4132	0.0087	2454495.8039	-0.1827	0.6606	0.0103
2454496.8152	0.2983	8.0838	0.0048	2454496.8151	0.2983	0.4469	0.0089	2454496.8152	0.2983	0.7081	0.0064
2454503.7894	-0.3843	8.2003	0.0043	2454503.7892	-0.3844	0.4603	0.0081	2454503.7893	-0.3843	0.7558	0.0060
2454504.7525	0.0738	7.9219	0.0164	2454504.7523	0.0737	0.4157	0.0199	2454504.7524	0.0738	0.6262	0.0223
2454505.7879	-0.4337	8.2149	0.0111	2454505.7877	-0.4337	0.4736	0.0100	2454505.7878	-0.4337	0.7603	0.0137
2454506.7576	0.0276	7.9064	0.0082	2454506.7575	0.0276	0.4135	0.0090	2454506.7576	0.0276	0.6216	0.0111
2454508.7604	-0.0197	7.9072	0.0019	2454508.7602	-0.0198	0.3982	0.0180	2454508.7603	-0.0198	0.6065	0.0102
2454509.7758	0.4633	8.1900	0.0048	2454509.7756	0.4632	0.4490	0.0085	2454509.7757	0.4632	0.7569	0.0080
2454838.7356	-0.0605	7.9349	0.0015	2454838.7354	-0.0606	0.3964	0.0081	2454838.7355	-0.0606	0.6184	0.0032
2454838.8983	0.0169	7.8909	0.0100	2454838.8981	0.0168	0.4206	0.0141	2454838.8983	0.0169	0.6465	0.0141
2454839.7321	0.4135	8.1848	0.0028	2454839.7319	0.4134	0.4575	0.0073	2454839.7321	0.4135	0.7362	0.0067
2454839.8892	0.4882	8.2355	0.0021	2454839.8880	0.4877	0.4476	0.0142	2454839.8892	0.4882	0.7502	0.0061
2454840.7334	-0.1102	7.9546	0.0042	2454840.7332	-0.1103	0.4100	0.0085	2454840.7333	-0.1103	0.6195	0.0067
2454841.7330	0.3653	8.1555	0.0089	2454841.7328	0.3652	0.4532	0.0167	2454841.7330	0.3653	0.7246	0.0106
2454842.7285	-0.1612	8.0283	0.0020	2454842.7283	-0.1613	0.4208	0.0047	2454842.7284	-0.1613	0.6399	0.0034
2454842.8937	-0.0826	7.9450	0.0034	2454842.8935	-0.0827	0.3917	0.0106	2454842.8936	-0.0827	0.6122	0.0059
2454844.7177	-0.2150	8.1004	0.0066	2454844.7175	-0.2151	0.4060	0.0062	2454844.7177	-0.2150	0.6723	0.0071
2454844.8817	-0.1370	7.9935	0.0028	2454844.8815	-0.1371	0.3971	0.0111	2454844.8816	-0.1370	0.6530	0.0029
2454845.8660	0.3312	8.1191	0.0017	2454845.8658	0.3311	0.4505	0.0081	2454845.8659	0.3312	0.7163	0.0021
2454846.7192	-0.2630	8.1261	0.0047	2454846.7190	-0.2630	0.4207	0.0074	2454846.7191	-0.2630	0.6950	0.0051
2454846.8826	-0.1852	8.0245	0.0033	2454846.8824	-0.1853	0.4038	0.0040	2454846.8825	-0.1853	0.6572	0.0050
2454847.7108	0.2087	8.0293	0.0019	2454847.7106	0.2086	0.4287	0.0034	2454847.7107	0.2087	0.6689	0.0038
2454847.8734	0.2861	8.0840	0.0020	2454847.8742	0.2864	0.4365	0.0053	2454847.8733	0.2860	0.7040	0.0029
2454849.7037	0.1567	7.9978	0.0019	2454849.7035	0.1566	0.4252	0.0025	2454849.7036	0.1566	0.6558	0.0021
2454849.8797	0.2404	8.0506	0.0100	2454849.8796	0.2404	0.4345	0.0141	2454849.8797	0.2404	0.7031	0.0141
2454856.7018	0.4855	8.2144	0.0010	2454856.7016	0.4854	0.4738	0.0047	2454856.7017	0.4854	0.7495	0.0027

2454856.8472	-0.4454	8.1989	0.0084	2454856.8470	-0.4455	0.4779	0.0080	2454856.8471	-0.4454	0.7617	0.0106
2454859.8448	-0.0195	7.9180	0.0100	2454859.8405	-0.0215	0.3962	0.0078	2454859.8427	-0.0205	0.6080	0.0113
2454860.8363	0.4521	8.1730	0.0013	2454860.8341	0.4511	0.4608	0.0047	2454860.8352	0.4516	0.7539	0.0035
2454861.8356	-0.0725	7.9299	0.0023	2454861.8354	-0.0726	0.3919	0.0071	2454861.8356	-0.0725	0.6189	0.0023
2454862.8307	0.4008	8.1718	0.0009	2454862.8285	0.3998	0.4613	0.0051	2454862.8296	0.4003	0.7387	0.0009
2454863.8321	-0.1229	7.9739	0.0005	2454863.8308	-0.1235	0.3819	0.0039	2454863.8320	-0.1229	0.6444	0.0005
2454864.8193	0.3467	8.1118	0.0037	2454864.8170	0.3456	0.4469	0.0045	2454864.8182	0.3462	0.7364	0.0057
2454865.8245	-0.1751	8.0258	0.0032	2454865.8244	-0.1752	0.3985	0.0157	2454865.8245	-0.1751	0.6515	0.0113
2454876.7912	0.0414	7.9174	0.0045	2454876.7921	0.0418	0.4137	0.0089	2454876.7912	0.0414	0.6212	0.0051
2455614.7979	0.0888	7.9333	0.0016	2455618.7943	-0.0102	0.3827	0.0053	2455614.7978	0.0888	0.6354	0.0095
2455615.7929	-0.4379	8.2173	0.0033	2455622.7536	-0.1269	0.3913	0.0131	2455615.7929	-0.4379	0.7637	0.0038
2455618.7945	-0.0101	7.9099	0.0062	2455624.7560	-0.1744	0.4048	0.0127	2455618.7944	-0.0102	0.6081	0.0082
2455622.7538	-0.1268	7.9846	0.0005	2455625.7375	0.2925	0.4372	0.0119	2455622.7537	-0.1268	0.6370	0.0028
2455624.7562	-0.1743	8.0129	0.0053	2455629.7458	0.1991	0.4297	0.0072	2455624.7562	-0.1743	0.6566	0.0059
2455625.7377	0.2926	8.0840	0.0015	2455630.7451	-0.3256	0.4304	0.0091	2455625.7377	0.2926	0.7137	0.0017
2455629.7460	0.1992	8.0050	0.0041	2455631.7340	0.1448	0.4158	0.0090	2455629.7460	0.1992	0.6858	0.0076
2455630.7453	-0.3255	8.1811	0.0112	2455634.7478	-0.4216	0.4520	0.0030	2455630.7453	-0.3255	0.7562	0.0117
2455631.7342	0.1449	7.9795	0.0067	2455637.7228	-0.0065	0.4081	0.0126	2455631.7341	0.1449	0.6583	0.0074
2455634.7480	-0.4215	8.2188	0.0003	2455638.7248	0.4701	0.4734	0.0092	2455634.7479	-0.4216	0.7639	0.0009
2455637.7230	-0.0064	7.8886	0.0164	2455639.7268	-0.0532	0.3660	0.0101	2455637.7229	-0.0064	0.6280	0.0174
2455638.7240	0.4698	8.1885	0.0081	2455643.7082	-0.1594	0.3957	0.0162	2455638.7239	0.4697	0.7522	0.0088
2455639.7260	-0.0536	7.9234	0.0012	2455644.7087	0.3165	0.4389	0.0132	2455639.7259	-0.0537	0.6324	0.0054
2455643.7084	-0.1593	7.9997	0.0043	2455646.7128	0.2698	0.4143	0.0300	2455643.7083	-0.1594	0.6553	0.0072
2455644.7089	0.3166	8.1140	0.0033	2455647.7101	-0.2558	0.4162	0.0124	2455644.7088	0.3165	0.7231	0.0051
2455646.7130	0.2699	8.0732	0.0001	2455648.7064	0.2181	0.4294	0.0102	2455646.7129	0.2698	0.7076	0.0057
2455647.7103	-0.2557	8.1199	0.0124	2455649.7033	-0.3077	0.4369	0.0072	2455647.7102	-0.2558	0.7155	0.0140
2455648.7065	0.2181	8.0324	0.0030	2455652.6974	0.1165	0.4293	0.0161	2455648.7065	0.2181	0.6798	0.0034

2455649.7035	-0.3076	8.1682	0.0042	2455663.6668	0.3343	0.4471	0.0060	2455649.7034	-0.3077	0.7331	0.0055
2455652.6975	0.1165	7.9559	0.0128	2455664.6616	-0.1925	0.4007	0.0053	2455652.6975	0.1165	0.6433	0.0174
2455663.6670	0.3344	8.1164	0.0127	2455672.6445	-0.3953	0.4573	0.0141	2455663.6670	0.3344	0.7205	0.0136
2455664.6619	-0.1924	8.0567	0.0017	2455944.8622	0.0904	0.4203	0.0080	2455664.6619	-0.1924	0.6714	0.0017
2455672.6448	-0.3951	8.2150	0.0100					2455672.6447	-0.3952	0.7553	0.0141
2455944.8625	0.0906	7.9251	0.0082					2455944.8625	0.0906	0.6411	0.0106

Photometry of EU Tau, cont…

HJD	Phase	V-R	V-R err	HJD	Phase	R-I	R-I err
2454439.8995	0.2252	0.8739	0.0039	2454439.8997	0.2253	0.4438	0.0049
2454440.8768	-0.3099	0.9100	0.0025	2454440.8769	-0.3099	0.4613	0.0021
2454447.8995	0.0306	0.8383	0.0038	2454447.8996	0.0306	0.4139	0.0019
2454448.8950	-0.4959	0.9196	0.0019	2454448.8951	-0.4958	0.4815	0.0041
2454449.9034	-0.0162	0.8347	0.0030	2454449.9035	-0.0162	0.4191	0.0028
2454450.8904	0.4533	0.9177	0.0027	2454450.8905	0.4533	0.4696	0.0035
2454451.9579	-0.0390	0.8308	0.0050	2454451.9581	-0.0389	0.4145	0.0064
2454452.8616	0.3909	0.9222	0.0047	2454452.8617	0.3910	0.4734	0.0050
2454453.8664	-0.1311	0.8542	0.0025	2454453.8665	-0.1311	0.4299	0.0033
2454454.8773	0.3497	0.9082	0.0039	2454454.8775	0.3498	0.4665	0.0045
2454458.9014	0.2639	0.8923	0.0091	2454458.9016	0.2640	0.4564	0.0097
2454459.8868	-0.2674	0.9023	0.0075	2454459.8869	-0.2674	0.4622	0.0116
2454460.8782	0.2042	0.8786	0.0048	2454460.8783	0.2042	0.4473	0.0070
2454461.9042	-0.3078	0.9105	0.0043	2454461.9043	-0.3078	0.4701	0.0024
2454464.9023	0.1183	0.8570	0.0103	2454464.9024	0.1184	0.4292	0.0131
2454465.8950	-0.4095	0.9314	0.0042	2454465.8951	-0.4095	0.4823	0.0049

2454475.8352	0.3188	0.8978	0.0070	2454475.8353	0.3188	0.4629	0.0064
2454476.8260	-0.2100	0.8828	0.0079	2454476.8262	-0.2099	0.4460	0.0091
2454480.8117	-0.3141	0.9154	0.0040	2454480.8118	-0.3140	0.4679	0.0073
2454481.8149	0.1631	0.8705	0.0066	2454481.8151	0.1632	0.4418	0.0058
2454483.8133	0.1137	0.8610	0.0137	2454483.8134	0.1137	0.4333	0.0092
2454484.8018	-0.4161	0.9177	0.0061	2454484.8019	-0.4161	0.4756	0.0103
2454485.8404	0.0779	0.8485	0.0088	2454485.8405	0.0780	0.4334	0.0105
2454486.7951	-0.4680	0.9318	0.0094	2454486.7952	-0.4679	0.4785	0.0040
2454494.7854	0.3328	0.9041	0.0136	2454494.7855	0.3328	0.4621	0.0124
2454495.8040	-0.1827	0.8755	0.0102	2454495.8041	-0.1826	0.4361	0.0112
2454496.8153	0.2984	0.8982	0.0066	2454496.8154	0.2984	0.4616	0.0074
2454503.7894	-0.3843	0.9179	0.0099	2454503.7896	-0.3842	0.4770	0.0120
2454504.7525	0.0738	0.8467	0.0247	2454504.7527	0.0739	0.4214	0.0217
2454505.7880	-0.4336	0.9281	0.0163	2454505.7881	-0.4336	0.4826	0.0161
2454506.7577	0.0277	0.8432	0.0097	2454506.7578	0.0277	0.4201	0.0103
2454508.7604	-0.0197	0.8424	0.0031	2454508.7606	-0.0196	0.4225	0.0128
2454509.7758	0.4633	0.9258	0.0058	2454509.7760	0.4634	0.4751	0.0070
2454838.7356	-0.0605	0.8404	0.0015	2454838.7357	-0.0605	0.4186	0.0062
2454838.8984	0.0169	0.8457	0.0141	2454838.8985	0.0170	0.4280	0.0141
2454839.7322	0.4135	0.9196	0.0055	2454839.7323	0.4136	0.4761	0.0087
2454839.8883	0.4878	0.9328	0.0043	2454839.8884	0.4878	0.4676	0.0040
2454840.7334	-0.1102	0.8447	0.0085	2454840.7336	-0.1101	0.4172	0.0105
2454841.7331	0.3653	0.9093	0.0104	2454841.7332	0.3654	0.4698	0.0069
2454842.7285	-0.1612	0.8551	0.0051	2454842.7287	-0.1611	0.4292	0.0055
2454842.8937	-0.0826	0.8423	0.0078	2454842.8939	-0.0825	0.4157	0.0092
2454844.7178	-0.2150	0.8792	0.0099	2454844.7179	-0.2149	0.4452	0.0100
2454844.8828	-0.1365	0.8649	0.0091	2454844.8829	-0.1364	0.4298	0.0122

2454845.8660	0.3312	0.9108	0.0034	2454845.8662	0.3313	0.4717	0.0060
2454846.7192	-0.2630	0.8958	0.0056	2454846.7194	-0.2629	0.4510	0.0094
2454846.8827	-0.1852	0.8609	0.0040	2454846.8828	-0.1851	0.4378	0.0031
2454847.7108	0.2087	0.8764	0.0044	2454847.7109	0.2088	0.4453	0.0049
2454847.8734	0.2861	0.9005	0.0023	2454847.8736	0.2862	0.4586	0.0041
2454849.7037	0.1567	0.8682	0.0026	2454849.7039	0.1568	0.4430	0.0118
2454849.8788	0.2400	0.8837	0.0100	2454849.8768	0.2390	0.4620	0.0042
2454856.7018	0.4855	0.9215	0.0057	2454856.7019	0.4855	0.4835	0.0071
2454856.8473	-0.4453	0.9327	0.0107	2454856.8474	-0.4453	0.4824	0.0110
2454859.8428	-0.0205	0.8562	0.0104	2454859.8409	-0.0214	0.4243	0.0037
2454860.8354	0.4517	0.9276	0.0031	2454860.8345	0.4513	0.4771	0.0063
2454861.8357	-0.0725	0.8485	0.0048	2454861.8358	-0.0724	0.4190	0.0077
2454862.8308	0.4008	0.9271	0.0029	2454862.8309	0.4009	0.4802	0.0046
2454863.8321	-0.1229	0.8612	0.0014	2454863.8312	-0.1233	0.4289	0.0066
2454864.8183	0.3462	0.8963	0.0085	2454864.8174	0.3458	0.4708	0.0089
2454865.8246	-0.1751	0.8739	0.0054	2454865.8247	-0.1750	0.4363	0.0059
2454876.7923	0.0419	0.8531	0.0059	2454876.7924	0.0420	0.4219	0.0070
2455614.7979	0.0888	0.8430	0.0053	2455618.7947	-0.0100	0.4213	0.0096
2455615.7940	-0.4374	0.9377	0.0039	2455622.7540	-0.1267	0.4239	0.0081
2455618.7945	-0.0101	0.8362	0.0110	2455624.7564	-0.1742	0.4450	0.0185
2455622.7539	-0.1267	0.8508	0.0045	2455625.7379	0.2927	0.4608	0.0106
2455624.7563	-0.1743	0.8693	0.0108	2455629.7462	0.1993	0.4571	0.0050
2455625.7378	0.2926	0.8980	0.0029	2455630.7476	-0.3244	0.4656	0.0051
2455629.7461	0.1992	0.8660	0.0053	2455631.7343	0.1450	0.4323	0.0151
2455630.7464	-0.3249	0.8992	0.0123	2455634.7482	-0.4214	0.4736	0.0052
2455631.7342	0.1449	0.8769	0.0107	2455637.7232	-0.0063	0.4199	0.0065
2455634.7480	-0.4215	0.9536	0.0049	2455638.7252	0.4703	0.4872	0.0057

2455637.7230	-0.0064	0.8418	0.0166	2455639.7262	-0.0535	0.4274	0.0114
2455638.7240	0.4698	0.9383	0.0095	2455643.7086	-0.1592	0.4362	0.0107
2455639.7260	-0.0536	0.8549	0.0094	2455644.7091	0.3167	0.4703	0.0076
2455643.7084	-0.1593	0.8571	0.0048	2455646.7131	0.2699	0.4485	0.0096
2455644.7089	0.3166	0.9063	0.0043	2455647.7105	-0.2556	0.4635	0.0075
2455646.7130	0.2699	0.8987	0.0060	2455648.7067	0.2182	0.4511	0.0139
2455647.7104	-0.2557	0.9083	0.0130	2455649.7037	-0.3075	0.4739	0.0162
2455648.7066	0.2182	0.8958	0.0109	2455652.6977	0.1166	0.4369	0.0061
2455649.7036	-0.3076	0.9067	0.0137	2455663.6672	0.3345	0.4511	0.0297
2455652.6976	0.1166	0.8724	0.0129	2455664.6621	-0.1923	0.4672	0.0067
2455663.6671	0.3344	0.9415	0.0299	2455672.6450	-0.3951	0.4868	0.0141
2455664.6620	-0.1923	0.8745	0.0017	2455944.8627	0.0907	0.4325	0.0107
2455672.6448	-0.3951	0.9257	0.0141				
2455944.8626	0.0906	0.8546	0.0119				

Photometry of SU Cas

HJD	Phase	V-mag	V-err	HJD	Phase	b-y	b-y err
2453665.8510	0.1845	5.8525	0.0019	2453665.8510	0.1845	0.4764	0.0037
2453666.7856	-0.3361	6.1195	0.0015	2453666.7855	-0.3361	0.5281	0.0031
2453667.8076	0.1882	5.8478	0.0049	2453667.8076	0.1882	0.4757	0.0059
2453668.8027	-0.3013	6.1061	0.0042	2453668.8026	-0.3014	0.5248	0.0052
2453669.7148	0.1666	5.8366	0.0047	2453669.7148	0.1666	0.4719	0.0062
2453669.8349	0.2282	5.8966	0.0041	2453669.8348	0.2281	0.4885	0.0057
2453670.7114	-0.3222	6.1176	0.0040	2453670.7113	-0.3222	0.5404	0.0042
2453670.8371	-0.2577	6.0577	0.0029	2453670.8370	-0.2577	0.5175	0.0045
2453671.7097	0.1900	5.8619	0.0020	2453671.7096	0.1899	0.4747	0.0055
2453671.9694	0.3232	5.9882	0.0031	2453671.9693	0.3231	0.5163	0.0051
2453672.7050	-0.2994	6.0928	0.0023	2453672.7049	-0.2995	0.5225	0.0044
2453672.8326	-0.2340	6.0141	0.0030	2453672.8325	-0.2340	0.4975	0.0047
2453673.7028	0.2124	5.8762	0.0047	2453673.7028	0.2124	0.4793	0.0062
2453673.8241	0.2747	5.9389	0.0014	2453673.8240	0.2746	0.4983	0.0021
2453673.9641	0.3465	6.0028	0.0031	2453673.9641	0.3465	0.5206	0.0052
2453674.7041	-0.2739	6.0697	0.0019	2453674.7041	-0.2739	0.5220	0.0042
2453674.8296	-0.2095	5.9690	0.0059	2453674.8295	-0.2096	0.4861	0.0079
2453674.9622	-0.1415	5.8467	0.0060	2453674.9621	-0.1416	0.4652	0.0073
2453675.8243	0.3007	5.9636	0.0021	2453675.8243	0.3007	0.5032	0.0025
2453677.8180	0.3235	5.9827	0.0017	2453677.8180	0.3235	0.5117	0.0032
2453678.8119	-0.1666	5.9046	0.0061	2453678.8118	-0.1667	0.4785	0.0087
2453679.6847	0.2811	5.9470	0.0012	2453679.6846	0.2811	0.4980	0.0045
2453679.8058	0.3432	6.0022	0.0008	2453679.8058	0.3432	0.5190	0.0019

2453680.6845	-0.2060	5.9601	0.0048	2453680.6844	-0.2060	0.4925	0.0061
2453680.8061	-0.1436	5.8550	0.0060	2453680.8060	-0.1437	0.4649	0.0085
2453684.6734	-0.1597	5.8973	0.0034	2453684.6734	-0.1597	0.4673	0.0055
2453684.7917	-0.0990	5.8003	0.0059	2453684.7916	-0.0991	0.4573	0.0068
2453688.6583	-0.1155	5.8080	0.0018	2453688.6583	-0.1155	0.4497	0.0033
2453688.7819	-0.0520	5.7464	0.0048	2453688.7819	-0.0521	0.4395	0.0073
2453688.8870	0.0019	5.7383	0.0026	2453688.8869	0.0018	0.4409	0.0067
2453689.6550	0.3959	6.0376	0.0027	2453689.6549	0.3958	0.5235	0.0036
2453690.6530	-0.0922	5.7930	0.0041	2453690.6529	-0.0922	0.4418	0.0105
2453692.7715	-0.0054	5.7379	0.0036	2453692.7714	-0.0055	0.4425	0.0060
2453692.9067	0.0640	5.7529	0.0049	2453692.9066	0.0639	0.4532	0.0085
2453693.6520	0.4463	6.0747	0.0030	2453693.6520	0.4463	0.5371	0.0038
2453693.7711	-0.4926	6.1068	0.0019	2453693.7710	-0.4927	0.5448	0.0022
2453694.6439	-0.0449	5.7402	0.0043	2453694.6438	-0.0449	0.4522	0.0049
2453694.7688	0.0192	5.7439	0.0035	2453694.7687	0.0192	0.4409	0.0039
2453695.6426	0.4675	6.0847	0.0036	2453695.6425	0.4674	0.5357	0.0062
2453695.7646	-0.4699	6.1123	0.0026	2453695.7645	-0.4700	0.5397	0.0028
2453695.8943	-0.4034	6.1338	0.0022	2453695.8942	-0.4035	0.5451	0.0033
2453699.6324	-0.4858	6.1172	0.0042	2453699.6324	-0.4858	0.5352	0.0052
2453699.7511	-0.4249	6.1401	0.0025	2453699.7511	-0.4249	0.5393	0.0038
2453699.8871	-0.3551	6.1351	0.0046	2453699.8871	-0.3551	0.5396	0.0069
2453700.7588	0.0921	5.7691	0.0043	2453700.7588	0.0921	0.4567	0.0067
2453701.6358	-0.4580	6.1256	0.0063	2453701.6357	-0.4581	0.5303	0.0086
2453702.6603	0.0675	5.7582	0.0074	2453702.6603	0.0675	0.4442	0.0077
2453702.7466	0.1118	5.7910	0.0045	2453702.7466	0.1118	0.4570	0.0064
2453702.8927	0.1868	5.8570	0.0022	2453702.8927	0.1867	0.4793	0.0056
2453703.6492	-0.4252	6.1618	0.0029	2453703.6491	-0.4252	0.5452	0.0067

2453703.7597	-0.3685	6.1297	0.0026	2453703.7596	-0.3685	0.5423	0.0041
2453705.6176	-0.4154	6.1392	0.0029	2453705.6176	-0.4154	0.5356	0.0031
2453705.7344	-0.3555	6.1287	0.0017	2453705.7343	-0.3555	0.5393	0.0021
2453705.8799	-0.2808	6.0799	0.0018	2453705.8798	-0.2809	0.5163	0.0019
2453706.6176	0.0976	5.7762	0.0042	2453706.6176	0.0976	0.4533	0.0056
2453706.7320	0.1563	5.8203	0.0005	2453706.7319	0.1562	0.4700	0.0009
2453706.8692	0.2267	5.8857	0.0047	2453706.8691	0.2266	0.4812	0.0055
2454764.7114	-0.1037	5.8109	0.0085	2454764.7114	-0.1037	0.4489	0.0090
2454766.7058	-0.0806	5.7760	0.0035	2454766.7057	-0.0806	0.4448	0.0067
2454766.9464	0.0429	5.7541	0.0107	2454766.9464	0.0429	0.4288	0.0109
2454767.7043	0.4317	6.0665	0.0091	2454767.7042	0.4316	0.5338	0.0115
2454767.9270	-0.4541	6.1236	0.0024	2454767.9269	-0.4542	0.5458	0.0036
2454768.9566	0.0741	5.7587	0.0031	2454768.9566	0.0741	0.4402	0.0044
2454770.9604	0.1020	5.7689	0.0052	2454770.9603	0.1020	0.4528	0.0067
2454771.6923	0.4775	6.1027	0.0092	2454771.6922	0.4774	0.5350	0.0106
2454771.9508	-0.3899	6.1407	0.0014	2454771.9507	-0.3900	0.5448	0.0037
2454772.6892	-0.0111	5.7439	0.0058	2454772.6891	-0.0112	0.4441	0.0072
2454775.6898	-0.4718	6.1143	0.0067	2454775.6897	-0.4719	0.5390	0.0083
2454775.9058	-0.3610	6.1332	0.0046	2454775.9058	-0.3610	0.5349	0.0062
2454778.6774	0.0608	5.7552	0.0010	2454778.6773	0.0608	0.4429	0.0040
2454783.6670	-0.3795	6.1528	0.0011	2454783.6670	-0.3795	0.5347	0.0044
2454785.6565	-0.3589	6.1438	0.0038	2454785.6564	-0.3590	0.5473	0.0046
2454788.6458	0.1746	5.8520	0.0066	2454788.6457	0.1745	0.4631	0.0078
2454789.6458	-0.3124	6.1045	0.0024	2454789.6457	-0.3125	0.5326	0.0045
2454790.6407	0.1980	5.8691	0.0087	2454790.6406	0.1979	0.4802	0.0106
2454791.6447	-0.2870	6.0899	0.0126	2454791.6446	-0.2870	0.5253	0.0149
2454794.8744	0.3698	6.0257	0.0012	2454794.8743	0.3698	0.5246	0.0014

2454801.8492	-0.0521	5.7472	0.0024	2454801.8491	-0.0522	0.4440	0.0044
2454802.6127	0.3396	6.0041	0.0020	2454802.6127	0.3396	0.5194	0.0022
2454802.8480	0.4603	6.0909	0.0028	2454802.8480	0.4603	0.5340	0.0033
2454803.6090	-0.1493	5.8661	0.0080	2454803.6089	-0.1494	0.4757	0.0090
2454810.6095	0.4419	6.0772	0.0045	2454810.6094	0.4418	0.5476	0.0082
2454811.6064	-0.0467	5.7539	0.0025	2454811.6063	-0.0468	0.4470	0.0031
2454821.8059	0.1856	5.8528	0.0008	2454821.8059	0.1856	0.4760	0.0047
2454822.7736	-0.3180	6.1108	0.0042	2454822.7735	-0.3180	0.5391	0.0043
2454829.7872	0.2800	5.9431	0.0043	2454829.7871	0.2799	0.4919	0.0052
2454830.7767	-0.2124	5.9800	0.0042	2454830.7766	-0.2125	0.4962	0.0051
2455184.6074	0.3016	5.9739	0.0027	2455184.6074	0.3016	0.5124	0.0032
2455184.7715	0.3858	6.0463	0.0025	2455184.7715	0.3858	0.5222	0.0029
2455189.6040	-0.1351	5.8349	0.0022	2455189.6040	-0.1352	0.4663	0.0046
2455189.7569	-0.0567	5.7524	0.0085	2455189.7569	-0.0567	0.4342	0.0091
2455191.7584	-0.0299	5.7319	0.0008	2455191.7584	-0.0300	0.4382	0.0024
2455195.7657	0.0258	5.7420	0.0019	2455195.7656	0.0257	0.4399	0.0033
2455197.5788	-0.0441	5.7368	0.0017	2455197.5787	-0.0442	0.4388	0.0029
2455197.7377	0.0374	5.7343	0.0054	2455197.7377	0.0374	0.4431	0.0061
2455198.5790	0.4690	6.0911	0.0006	2455198.5790	0.4690	0.5320	0.0017
2455198.7473	-0.4447	6.1295	0.0008	2455198.7481	-0.4443	0.5399	0.0009
2455199.5797	-0.0176	5.7385	0.0052	2455199.5797	-0.0177	0.4320	0.0052
2455199.7440	0.0666	5.7474	0.0029	2455199.7440	0.0666	0.4552	0.0039
2455200.5800	0.4955	6.1086	0.0013	2455200.5799	0.4954	0.5427	0.0022
2455200.7444	-0.4202	6.1407	0.0014	2455200.7443	-0.4202	0.5449	0.0026
2455202.5809	-0.4780	6.1126	0.0027	2455202.5808	-0.4781	0.5488	0.0037
2455202.7218	-0.4058	6.1368	0.0008	2455202.7227	-0.4053	0.5480	0.0009
2455204.7204	-0.3805	6.1310	0.0015	2455204.7204	-0.3805	0.5500	0.0023

2455208.5857	-0.3976	6.1403	0.0025	2455208.5847	-0.3981	0.5539	0.0042
2455208.7056	-0.3361	6.1320	0.0011	2455208.7055	-0.3362	0.5402	0.0019
2455209.7018	0.1750	5.8517	0.0012	2455209.7018	0.1749	0.4680	0.0031
2455210.6985	-0.3137	6.1129	0.0032	2455210.6984	-0.3138	0.5364	0.0032
2455211.6990	0.1995	5.8713	0.0034	2455211.6990	0.1995	0.4734	0.0075
2455212.5938	-0.3415	6.1273	0.0014	2455212.5937	-0.3415	0.5315	0.0015
2455213.7139	0.2332	5.8968	0.0021	2455213.7139	0.2331	0.5001	0.0080
2455236.6477	-0.0019	5.7316	0.0018	2455236.6476	-0.0019	0.4336	0.0055
2455240.6386	0.0454	5.7484	0.0050	2455240.6386	0.0454	0.4499	0.0065
2455241.6321	-0.4449	6.1300	0.0034	2455241.6320	-0.4450	0.5456	0.0038
2455532.6529	-0.1522	5.8759	0.0021	2455532.6528	-0.1522	0.4671	0.0058
2455535.8084	0.4666	6.0855	0.0041	2455535.8084	0.4666	0.5419	0.0041
2455536.6790	-0.0868	5.7863	0.0001	2455536.6789	-0.0869	0.4454	0.0080
2455536.8099	-0.0196	5.7402	0.0084	2455536.8098	-0.0197	0.4330	0.0108
2455538.8048	0.0037	5.7401	0.0035	2455538.8047	0.0037	0.4326	0.0052
2455539.7994	-0.4860	6.1185	0.0020	2455539.7994	-0.4860	0.5384	0.0020
2455543.6258	0.4769	6.0907	0.0012	2455543.6257	0.4768	0.5430	0.0019
2455543.7913	-0.4382	6.1277	0.0034	2455543.7913	-0.4382	0.5499	0.0041
2455544.6206	-0.0128	5.7405	0.0019	2455544.6205	-0.0128	0.4391	0.0021
2455544.7884	0.0733	5.7516	0.0020	2455544.7884	0.0733	0.4521	0.0038
2455545.6177	0.4987	6.1043	0.0026	2455545.6177	0.4987	0.5492	0.0035
2455545.7850	-0.4154	6.1418	0.0008	2455545.7850	-0.4155	0.5447	0.0022
2455546.7825	0.0963	5.7800	0.0040	2455546.7824	0.0962	0.4516	0.0048
2455580.7065	0.4992	6.1068	0.0012	2455580.7065	0.4992	0.5396	0.0030
2455581.7078	0.0128	5.7283	0.0022	2455581.7077	0.0128	0.4464	0.0093
2455582.7082	-0.4740	6.1231	0.0010	2455582.7081	-0.4740	0.5400	0.0068
2455583.6969	0.0332	5.7468	0.0018	2455583.6969	0.0332	0.4388	0.0032

2455584.7000	-0.4522	6.1297	0.0035	2455584.6999	-0.4522	0.5468	0.0055
2455585.6913	0.0564	5.7563	0.0045	2455585.6913	0.0563	0.4451	0.0048
2455588.6864	-0.4072	6.1322	0.0062	2455588.6864	-0.4072	0.5443	0.0064
2455597.6949	0.2142	5.8724	0.0127	2455597.6948	0.2141	0.4931	0.0130
2455598.6434	-0.2993	6.1087	0.0064	2455598.6433	-0.2993	0.5304	0.0087
2455603.6376	0.2628	5.9313	0.0014	2455603.6376	0.2627	0.4946	0.0032
2455604.6451	-0.2204	5.9986	0.0057	2455604.6451	-0.2204	0.5038	0.0067
2455605.6299	0.2848	5.9524	0.0027	2455605.6299	0.2848	0.5017	0.0031
2455607.6265	0.3090	5.9741	0.0060	2455607.6265	0.3090	0.5156	0.0103
2455608.6316	-0.1753	5.9161	0.0006	2455608.6315	-0.1754	0.4790	0.0032
2455883.9138	0.0435	5.7536	0.0040	2455883.9137	0.0435	0.4437	0.0057
2455888.9019	-0.3976	6.1408	0.0021	2455888.9018	-0.3976	0.5482	0.0034
2455893.8869	0.1597	5.8280	0.0019	2455893.8878	0.1602	0.4720	0.0020
2455900.8273	-0.2799	6.0813	0.0043	2455900.8272	-0.2800	0.5223	0.0066
2455911.8080	0.3532	6.0152	0.0018	2455911.8079	0.3531	0.5111	0.0027
2455921.7735	0.4654	6.0860	0.0023	2455921.7735	0.4654	0.5452	0.0026
2455922.7676	-0.0246	5.7440	0.0014	2455922.7675	-0.0246	0.4393	0.0035
2455925.7620	-0.4885	6.1185	0.0020	2455925.7619	-0.4885	0.5320	0.0032
2455926.7580	0.0225	5.7427	0.0039	2455926.7579	0.0224	0.4352	0.0045
2455927.7547	-0.4662	6.1308	0.0014	2455927.7546	-0.4663	0.5416	0.0036
2455944.6660	0.2092	5.8776	0.0042	2455944.6659	0.2092	0.4788	0.0072

Photometry of SU Cas, cont…

HJD	Phase	c1	c1 err	HJD	Phase	m1	m1 err
2453665.8508	0.1844	0.9410	0.0064	2453665.8509	0.1844	0.1576	0.0058

2453666.7853	-0.3362	0.7814	0.0055	2453666.7854	-0.3362	0.1813	0.0049
2453667.8074	0.1881	0.9510	0.0088	2453667.8075	0.1881	0.1557	0.0075
2453668.8025	-0.3014	0.7840	0.0066	2453668.8026	-0.3014	0.1750	0.0062
2453669.7152	0.1668	0.9575	0.0147	2453669.7147	0.1665	0.1587	0.0098
2453669.8346	0.2280	0.9125	0.0092	2453669.8347	0.2281	0.1597	0.0074
2453670.7111	-0.3223	0.7726	0.0099	2453670.7113	-0.3222	0.1640	0.0059
2453670.8369	-0.2578	0.8071	0.0069	2453670.8370	-0.2577	0.1685	0.0066
2453671.7094	0.1898	0.9386	0.0095	2453671.7096	0.1899	0.1626	0.0080
2453671.9691	0.3230	0.8452	0.0067	2453671.9693	0.3231	0.1584	0.0073
2453672.7048	-0.2996	0.7923	0.0071	2453672.7049	-0.2995	0.1750	0.0071
2453672.8323	-0.2341	0.8425	0.0082	2453672.8325	-0.2340	0.1735	0.0065
2453673.7026	0.2123	0.9231	0.0097	2453673.7027	0.2124	0.1651	0.0086
2453673.8238	0.2745	0.8884	0.0097	2453673.8240	0.2746	0.1613	0.0062
2453673.9639	0.3464	0.8300	0.0062	2453673.9640	0.3464	0.1615	0.0069
2453674.7039	-0.2740	0.8051	0.0077	2453674.7040	-0.2740	0.1714	0.0066
2453674.8294	-0.2096	0.8689	0.0105	2453674.8295	-0.2096	0.1708	0.0098
2453674.9619	-0.1417	0.9456	0.0120	2453674.9620	-0.1416	0.1523	0.0112
2453675.8241	0.3006	0.8677	0.0063	2453675.8242	0.3007	0.1651	0.0045
2453677.8178	0.3234	0.8500	0.0101	2453677.8179	0.3235	0.1654	0.0056
2453678.8117	-0.1667	0.9079	0.0130	2453678.8118	-0.1667	0.1570	0.0119
2453679.6844	0.2810	0.8749	0.0057	2453679.6846	0.2811	0.1686	0.0064
2453679.8056	0.3431	0.8364	0.0082	2453679.8057	0.3432	0.1622	0.0052
2453680.6842	-0.2061	0.8842	0.0091	2453680.6844	-0.2060	0.1597	0.0081
2453680.8058	-0.1438	0.9411	0.0102	2453680.8060	-0.1437	0.1565	0.0112
2453684.6732	-0.1598	0.9096	0.0096	2453684.6733	-0.1598	0.1694	0.0084
2453684.7914	-0.0992	0.9698	0.0068	2453684.7915	-0.0991	0.1485	0.0080
2453688.6581	-0.1156	0.9620	0.0064	2453688.6582	-0.1155	0.1606	0.0056

2453688.7817	-0.0522	1.0055	0.0111	2453688.7818	-0.0521	0.1563	0.0099
2453688.8867	0.0017	1.0176	0.0122	2453688.8868	0.0018	0.1498	0.0115
2453689.6547	0.3957	0.8161	0.0042	2453689.6549	0.3958	0.1703	0.0049
2453690.6527	-0.0923	0.9652	0.0159	2453690.6529	-0.0922	0.1658	0.0167
2453692.7712	-0.0056	1.0009	0.0082	2453692.7714	-0.0055	0.1579	0.0083
2453692.9064	0.0638	1.0160	0.0143	2453692.9066	0.0639	0.1411	0.0125
2453693.6518	0.4462	0.7740	0.0083	2453693.6519	0.4462	0.1729	0.0071
2453693.7715	-0.4924	0.7609	0.0045	2453693.7710	-0.4927	0.1734	0.0038
2453694.6437	-0.0450	1.0099	0.0115	2453694.6438	-0.0449	0.1385	0.0078
2453694.7685	0.0191	1.0182	0.0112	2453694.7686	0.0191	0.1525	0.0069
2453695.6424	0.4674	0.7766	0.0088	2453695.6425	0.4674	0.1766	0.0087
2453695.7643	-0.4701	0.7731	0.0030	2453695.7645	-0.4700	0.1763	0.0031
2453695.8947	-0.4032	0.7729	0.0044	2453695.8942	-0.4035	0.1662	0.0044
2453699.6322	-0.4859	0.7659	0.0089	2453699.6323	-0.4858	0.1832	0.0072
2453699.7509	-0.4250	0.7570	0.0051	2453699.7510	-0.4249	0.1815	0.0053
2453699.8869	-0.3552	0.7739	0.0121	2453699.8870	-0.3552	0.1678	0.0110
2453700.7586	0.0920	0.9925	0.0144	2453700.7587	0.0920	0.1531	0.0112
2453701.6356	-0.4581	0.7567	0.0092	2453701.6357	-0.4581	0.1894	0.0106
2453702.6601	0.0674	1.0088	0.0062	2453702.6602	0.0675	0.1605	0.0081
2453702.7464	0.1117	0.9897	0.0092	2453702.7465	0.1117	0.1558	0.0082
2453702.8925	0.1866	0.9314	0.0106	2453702.8926	0.1867	0.1546	0.0088
2453703.6766	-0.4111	0.7274	0.0079	2453703.6490	-0.4253	0.1711	0.0092
2453705.6180	-0.4152	0.7655	0.0066	2453703.7596	-0.3685	0.1705	0.0056
2453705.7342	-0.3556	0.7676	0.0044	2453705.6175	-0.4154	0.1810	0.0036
2453705.8796	-0.2810	0.8006	0.0067	2453705.7343	-0.3555	0.1731	0.0028
2453706.6174	0.0975	0.9970	0.0073	2453705.8798	-0.2809	0.1746	0.0051
2453706.7318	0.1562	0.9674	0.0097	2453706.6175	0.0976	0.1547	0.0073

2453706.8690	0.2266	0.9180	0.0079	2453706.7319	0.1562	0.1544	0.0026
2454764.7112	-0.1038	0.9631	0.0163	2453706.8691	0.2266	0.1621	0.0076
2454766.7056	-0.0807	0.9718	0.0079	2454764.7113	-0.1037	0.1656	0.0101
2454766.9462	0.0428	0.9982	0.0135	2454766.7057	-0.0806	0.1672	0.0090
2454767.7041	0.4316	0.7893	0.0195	2454766.9463	0.0428	0.1745	0.0124
2454767.9267	-0.4543	0.7418	0.0076	2454767.7042	0.4316	0.1726	0.0151
2454768.9564	0.0740	1.0028	0.0079	2454767.9268	-0.4542	0.1764	0.0050
2454770.9601	0.1019	1.0052	0.0061	2454768.9565	0.0740	0.1627	0.0063
2454771.6920	0.4773	0.7743	0.0129	2454770.9603	0.1020	0.1514	0.0085
2454771.9505	-0.3901	0.7536	0.0051	2454771.6922	0.4774	0.1802	0.0141
2454772.6889	-0.0113	1.0093	0.0075	2454771.9507	-0.3900	0.1741	0.0054
2454775.6895	-0.4720	0.7688	0.0085	2454772.6891	-0.0112	0.1527	0.0085
2454775.9056	-0.3611	0.7571	0.0095	2454775.6896	-0.4719	0.1779	0.0108
2454778.6771	0.0607	1.0029	0.0084	2454775.9057	-0.3611	0.1824	0.0095
2454783.6668	-0.3796	0.7849	0.0078	2454778.6772	0.0607	0.1634	0.0066
2454785.6562	-0.3591	0.7557	0.0074	2454783.6669	-0.3796	0.1690	0.0069
2454788.6455	0.1744	0.9404	0.0089	2454785.6563	-0.3590	0.1674	0.0071
2454789.6455	-0.3126	0.7842	0.0080	2454788.6456	0.1745	0.1748	0.0097
2454790.6404	0.1978	0.9433	0.0221	2454789.6456	-0.3125	0.1683	0.0066
2454791.6444	-0.2872	0.7666	0.0225	2454790.6406	0.1979	0.1552	0.0158
2454794.8741	0.3697	0.8248	0.0082	2454791.6446	-0.2870	0.1810	0.0217
2454801.8489	-0.0523	0.9888	0.0083	2454794.8742	0.3697	0.1629	0.0038
2454802.6125	0.3395	0.8346	0.0110	2454801.8490	-0.0522	0.1528	0.0060
2454802.8491	0.4608	0.7776	0.0042	2454802.6126	0.3395	0.1669	0.0040
2454803.6087	-0.1495	0.9301	0.0089	2454802.8483	0.4604	0.1795	0.0038
2454810.6093	0.4418	0.7990	0.0127	2454803.6088	-0.1495	0.1478	0.0103
2454811.6062	-0.0468	0.9917	0.0139	2454810.6094	0.4418	0.1497	0.0112

2454821.8057	0.1855	0.9509	0.0210	2454811.6063	-0.0468	0.1505	0.0101
2454822.7733	-0.3181	0.7670	0.0093	2454821.8058	0.1856	0.1574	0.0119
2454829.7870	0.2799	0.8661	0.0096	2454822.7734	-0.3181	0.1718	0.0046
2454830.7764	-0.2126	0.8605	0.0094	2454829.7871	0.2799	0.1762	0.0072
2455184.6072	0.3015	0.8727	0.0086	2454830.7766	-0.2125	0.1604	0.0079
2455184.7713	0.3857	0.8158	0.0095	2455184.6073	0.3016	0.1513	0.0068
2455189.6038	-0.1353	0.9626	0.0053	2455184.7714	0.3857	0.1653	0.0068
2455189.7567	-0.0568	0.9956	0.0150	2455189.6039	-0.1352	0.1462	0.0064
2455191.7582	-0.0301	1.0080	0.0078	2455189.7568	-0.0568	0.1668	0.0115
2455195.7654	0.0256	1.0218	0.0098	2455191.7583	-0.0300	0.1539	0.0048
2455197.5785	-0.0443	1.0120	0.0064	2455195.7655	0.0257	0.1539	0.0051
2455197.7375	0.0373	1.0057	0.0109	2455197.5786	-0.0442	0.1559	0.0042
2455198.5788	0.4689	0.7821	0.0076	2455197.7376	0.0374	0.1557	0.0089
2455198.7479	-0.4444	0.7651	0.0049	2455198.5789	0.4689	0.1806	0.0031
2455199.5795	-0.0178	1.0195	0.0089	2455198.7481	-0.4443	0.1776	0.0024
2455199.7438	0.0665	1.0195	0.0056	2455199.5796	-0.0177	0.1594	0.0076
2455200.5798	0.4954	0.7738	0.0040	2455199.7439	0.0666	0.1397	0.0048
2455200.7441	-0.4203	0.7444	0.0049	2455200.5799	0.4954	0.1707	0.0031
2455202.5806	-0.4782	0.7514	0.0068	2455200.7442	-0.4203	0.1783	0.0038
2455202.7220	-0.4057	0.7497	0.0074	2455202.5807	-0.4782	0.1707	0.0062
2455204.7202	-0.3806	0.7482	0.0049	2455202.7226	-0.4054	0.1725	0.0015
2455208.5841	-0.3984	0.7545	0.0042	2455204.7203	-0.3805	0.1663	0.0031
2455208.7053	-0.3363	0.7561	0.0071	2455208.5842	-0.3984	0.1639	0.0057
2455209.7016	0.1748	0.9401	0.0133	2455208.7054	-0.3362	0.1746	0.0046
2455210.6982	-0.3139	0.7572	0.0053	2455209.7017	0.1749	0.1667	0.0064
2455211.6988	0.1994	0.9157	0.0170	2455210.6984	-0.3138	0.1728	0.0039
2455212.5935	-0.3416	0.7606	0.0106	2455211.6989	0.1995	0.1673	0.0124

2455213.7137	0.2330	0.9190	0.0203	2455212.5936	-0.3416	0.1811	0.0059
2455236.6474	-0.0020	1.0227	0.0150	2455213.7138	0.2331	0.1453	0.0160
2455240.6384	0.0453	1.0100	0.0107	2455236.6475	-0.0020	0.1570	0.0081
2455241.6318	-0.4451	0.7663	0.0075	2455240.6385	0.0454	0.1436	0.0082
2455532.6526	-0.1523	0.9327	0.0111	2455241.6319	-0.4450	0.1670	0.0050
2455535.8082	0.4665	0.7763	0.0032	2455532.6527	-0.1523	0.1575	0.0095
2455536.6787	-0.0870	0.9760	0.0099	2455535.8083	0.4665	0.1637	0.0044
2455536.8097	-0.0198	1.0150	0.0160	2455536.6789	-0.0869	0.1577	0.0117
2455538.8045	0.0036	1.0060	0.0128	2455536.8098	-0.0197	0.1604	0.0141
2455539.7992	-0.4862	0.7583	0.0043	2455538.8047	0.0037	0.1656	0.0086
2455543.6255	0.4767	0.7674	0.0063	2455539.7993	-0.4861	0.1806	0.0030
2455543.7911	-0.4383	0.7645	0.0030	2455543.6256	0.4768	0.1733	0.0030
2455544.6203	-0.0129	1.0075	0.0083	2455543.7912	-0.4383	0.1671	0.0048
2455544.7882	0.0732	1.0109	0.0117	2455544.6204	-0.0129	0.1576	0.0053
2455545.6175	0.4986	0.7515	0.0053	2455544.7883	0.0732	0.1479	0.0064
2455545.7848	-0.4156	0.7295	0.0059	2455545.6176	0.4987	0.1720	0.0053
2455546.7822	0.0961	0.9861	0.0066	2455545.7849	-0.4155	0.1815	0.0037
2455580.7063	0.4991	0.7720	0.0038	2455546.7823	0.0962	0.1634	0.0055
2455581.7080	0.0129	1.0247	0.0124	2455580.7064	0.4991	0.1744	0.0042
2455582.7079	-0.4741	0.7637	0.0088	2455581.7076	0.0127	0.1357	0.0132
2455583.6967	0.0331	1.0079	0.0164	2455582.7081	-0.4740	0.1778	0.0096
2455584.6997	-0.4523	0.7550	0.0068	2455583.6968	0.0332	0.1616	0.0085
2455585.6911	0.0562	1.0070	0.0164	2455584.6999	-0.4522	0.1706	0.0074
2455588.6862	-0.4073	0.7643	0.0060	2455585.6912	0.0563	0.1530	0.0116
2455597.6947	0.2141	0.9339	0.0107	2455588.6863	-0.4072	0.1725	0.0071
2455598.6431	-0.2994	0.7850	0.0087	2455597.6948	0.2141	0.1439	0.0150
2455603.6374	0.2626	0.8888	0.0073	2455598.6433	-0.2993	0.1687	0.0107

2455604.6449	-0.2205	0.8422	0.0071	2455603.6375	0.2627	0.1651	0.0051
2455605.6297	0.2847	0.8818	0.0073	2455604.6450	-0.2205	0.1638	0.0078
2455607.6263	0.3089	0.8667	0.0131	2455605.6298	0.2847	0.1648	0.0041
2455608.6314	-0.1755	0.9042	0.0084	2455607.6264	0.3090	0.1503	0.0147
2455883.9136	0.0434	1.0158	0.0091	2455608.6315	-0.1754	0.1538	0.0046
2455888.9016	-0.3977	0.7581	0.0092	2455883.9137	0.0435	0.1519	0.0088
2455893.8880	0.1603	0.9531	0.0085	2455888.9018	-0.3976	0.1693	0.0058
2455900.8270	-0.2801	0.8003	0.0061	2455893.8881	0.1603	0.1577	0.0031
2455911.8077	0.3530	0.8293	0.0098	2455900.8271	-0.2800	0.1703	0.0083
2455921.7733	0.4653	0.7846	0.0068	2455911.8078	0.3531	0.1788	0.0054
2455922.7673	-0.0248	1.0192	0.0168	2455921.7734	0.4654	0.1598	0.0033
2455925.7617	-0.4886	0.7597	0.0107	2455922.7674	-0.0247	0.1505	0.0079
2455926.7577	0.0223	1.0125	0.0085	2455925.7618	-0.4886	0.1893	0.0047
2455927.7544	-0.4664	0.7582	0.0082	2455926.7579	0.0224	0.1626	0.0062
2455944.6657	0.2091	0.9222	0.0086	2455927.7546	-0.4663	0.1775	0.0060
				2455944.6659	0.2092	0.1658	0.0096

Photometry of SV Vul

HJD	Phase	V-mag	V-err	HJD	Phase	b-y	b-y err
2453302.6632	0.1866	6.9934	0.0044	2453302.6632	0.1866	0.9925	0.0138
2453303.6658	0.2089	6.9912	0.0100	2453303.6652	0.2089	1.0316	0.0112
2453309.6579	0.3421	7.1843	0.0039	2453309.6578	0.3421	1.1531	0.0046
2453310.6572	0.3643	7.2132	0.0026	2453310.6571	0.3643	1.1607	0.0033
2453311.6572	0.3865	7.2451	0.0013	2453311.6572	0.3865	1.1854	0.0016
2453312.6421	0.4084	7.2717	0.0044	2453312.6421	0.4084	1.1907	0.0044
2453313.6312	0.4304	7.3027	0.0028	2453313.6311	0.4304	1.2001	0.0037
2453318.6246	-0.4586	7.4440	0.0013	2453318.6246	-0.4586	1.2383	0.0021
2453319.6429	-0.4360	7.4748	0.0009	2453319.6428	-0.4360	1.2275	0.0012
2453320.5875	-0.4150	7.5030	0.0020	2453320.5874	-0.4150	1.2326	0.0044
2453336.6094	-0.0589	6.8461	0.0028	2453336.6093	-0.0589	0.8590	0.0063
2453340.5663	0.0291	6.7230	0.0050	2453340.5663	0.0291	0.8585	0.0059
2453341.5662	0.0513	6.7477	0.0017	2453341.5662	0.0513	0.8826	0.0025
2453348.5663	0.2069	6.9681	0.0024	2453348.5662	0.2069	1.0558	0.0054
2453349.5665	0.2291	7.0026	0.0052	2453349.5665	0.2291	1.0652	0.0057
2453350.5667	0.2513	7.0366	0.0017	2453350.5666	0.2513	1.0941	0.0038
2453351.5668	0.2736	7.0787	0.0042	2453351.5667	0.2735	1.0938	0.0068
2453354.5741	0.3404	7.1765	0.0018	2453354.5740	0.3404	1.1387	0.0022
2453355.5744	0.3626	7.1966	0.0100	2453355.5744	0.3626	1.1649	0.0141
2453357.5681	0.4069	7.2471	0.0100	2453357.5681	0.4069	1.2166	0.0141
2453462.9773	-0.2503	7.7311	0.0010	2453462.9772	-0.2503	1.2344	0.0015
2453464.9716	-0.2060	7.7431	0.0027	2453464.9716	-0.2060	1.2132	0.0035
2453466.9764	-0.1614	7.6350	0.0006	2453466.9764	-0.1614	1.1825	0.0023

2453476.9552	0.0604	6.7665	0.0008	2453476.9551	0.0604	0.8825	0.0039
2453480.9372	0.1489	6.9038	0.0065	2453480.9372	0.1489	0.9812	0.0077
2453481.9453	0.1713	6.9353	0.0027	2453481.9452	0.1713	1.0017	0.0067
2453483.9402	0.2156	6.9976	0.0071	2453483.9401	0.2156	1.0550	0.0076
2453487.9229	0.3042	7.1333	0.0023	2453487.9229	0.3042	1.1212	0.0044
2453488.9163	0.3262	7.1641	0.0005	2453488.9162	0.3262	1.1364	0.0034
2453490.9110	0.3706	7.2254	0.0052	2453490.9109	0.3706	1.1735	0.0053
2453494.8978	0.4592	7.3432	0.0036	2453494.8977	0.4592	1.1980	0.0060
2453496.9678	-0.4948	7.4016	0.0015	2453496.9678	-0.4948	1.2169	0.0027
2453500.8863	-0.4077	7.5140	0.0032	2453500.8863	-0.4077	1.2295	0.0036
2453501.8999	-0.3852	7.5393	0.0006	2453501.8998	-0.3852	1.2340	0.0007
2453502.9547	-0.3618	7.5746	0.0012	2453502.9546	-0.3618	1.2441	0.0014
2453503.8878	-0.3410	7.6132	0.0024	2453503.8878	-0.3410	1.2362	0.0040
2453504.9458	-0.3175	7.6496	0.0022	2453504.9458	-0.3175	1.2445	0.0023
2453506.9488	-0.2730	7.7124	0.0012	2453506.9488	-0.2730	1.2423	0.0019
2453507.8752	-0.2524	7.7372	0.0031	2453507.8752	-0.2524	1.2364	0.0033
2453509.8785	-0.2079	7.7467	0.0010	2453509.8776	-0.2079	1.2203	0.0018
2453510.8642	-0.1860	7.7258	0.0018	2453510.8642	-0.1860	1.1932	0.0020
2453511.8510	-0.1640	7.6810	0.0018	2453511.8509	-0.1640	1.1630	0.0022
2453512.8515	-0.1418	7.5859	0.0032	2453512.8515	-0.1418	1.1238	0.0035
2453513.8455	-0.1197	7.4293	0.0017	2453513.8454	-0.1197	1.0546	0.0066
2453520.8344	0.0356	6.7168	0.0125	2453520.8343	0.0356	0.8578	0.0188
2453524.8253	0.1243	6.8527	0.0041	2453524.8253	0.1243	0.9528	0.0087
2453525.8204	0.1465	6.8943	0.0040	2453525.8203	0.1465	0.9804	0.0080
2453526.8126	0.1685	6.9267	0.0006	2453526.8125	0.1685	0.9988	0.0018
2453527.8153	0.1908	6.9546	0.0004	2453527.8152	0.1908	1.0259	0.0028
2453528.8092	0.2129	6.9865	0.0037	2453528.8091	0.2129	1.0453	0.0039

2453529.8140	0.2352	7.0190	0.0024	2453529.8140	0.2352	1.0658	0.0039
2453530.8089	0.2573	7.0503	0.0044	2453530.8088	0.2573	1.0876	0.0046
2453531.8032	0.2794	7.0889	0.0018	2453531.8031	0.2794	1.1018	0.0023
2453532.8025	0.3016	7.1177	0.0008	2453532.8025	0.3016	1.1199	0.0025
2453533.7979	0.3238	7.1431	0.0025	2453533.7978	0.3238	1.1409	0.0027
2453534.7927	0.3459	7.1735	0.0038	2453534.7926	0.3459	1.1607	0.0046
2453535.7990	0.3682	7.2110	0.0031	2453535.7989	0.3682	1.1684	0.0045
2453536.7925	0.3903	7.2482	0.0025	2453536.7925	0.3903	1.1844	0.0041
2453537.7868	0.4124	7.2666	0.0020	2453537.7868	0.4124	1.1990	0.0056
2453538.7815	0.4345	7.3081	0.0026	2453538.7815	0.4345	1.2003	0.0030
2453539.7809	0.4567	7.3398	0.0029	2453539.7809	0.4567	1.2130	0.0039
2453543.7881	-0.4542	7.4395	0.0007	2453543.7880	-0.4542	1.2483	0.0034
2453547.7617	-0.3659	7.5786	0.0027	2453547.7616	-0.3659	1.2433	0.0033
2453548.7608	-0.3437	7.6137	0.0047	2453548.7608	-0.3437	1.2486	0.0059
2453549.7485	-0.3217	7.6590	0.0008	2453549.7484	-0.3217	1.2433	0.0038
2453550.7515	-0.2994	7.6795	0.0026	2453550.7515	-0.2994	1.2514	0.0047
2453551.7555	-0.2771	7.7155	0.0028	2453551.7554	-0.2771	1.2386	0.0031
2453552.7501	-0.2550	7.7364	0.0011	2453552.7500	-0.2550	1.2474	0.0015
2453554.7388	-0.2108	7.7196	0.0062	2453554.7387	-0.2108	1.2291	0.0082
2453555.7409	-0.1885	7.7406	0.0039	2453555.7409	-0.1885	1.2007	0.0060
2453556.7318	-0.1665	7.6970	0.0017	2453556.7317	-0.1665	1.1755	0.0025
2453557.7370	-0.1442	7.6023	0.0003	2453557.7369	-0.1442	1.1379	0.0009
2453558.7268	-0.1222	7.4514	0.0017	2453558.7267	-0.1222	1.0830	0.0019
2453560.7539	-0.0771	6.9863	0.0056	2453560.7539	-0.0771	0.9163	0.0065
2453561.7239	-0.0556	6.7990	0.0017	2453561.7238	-0.0556	0.8589	0.0025
2453563.7169	-0.0113	6.6999	0.0068	2453563.7168	-0.0113	0.8417	0.0112
2453565.7177	0.0332	6.7204	0.0069	2453565.7177	0.0332	0.8634	0.0097

2453567.7025	0.0773	6.7799	0.0163	2453567.7024	0.0773	0.9075	0.0205
2453627.6464	0.4096	7.2619	0.0020	2453627.6463	0.4096	1.2077	0.0026
2453628.7497	0.4341	7.3004	0.0017	2453628.7496	0.4341	1.2129	0.0029
2453629.6303	0.4537	7.3208	0.0029	2453629.6303	0.4537	1.2241	0.0038
2453631.6282	0.4981	7.3762	0.0010	2453631.6281	0.4981	1.2334	0.0023
2453632.7195	-0.4776	7.4145	0.0040	2453632.7195	-0.4776	1.2360	0.0041
2453634.7084	-0.4334	7.4810	0.0066	2453634.7083	-0.4334	1.2446	0.0074
2453636.7089	-0.3890	7.5382	0.0032	2453636.7089	-0.3890	1.2413	0.0033
2453637.6230	-0.3687	7.5588	0.0064	2453637.6229	-0.3687	1.2590	0.0066
2453638.7148	-0.3444	7.6104	0.0019	2453638.7148	-0.3444	1.2495	0.0022
2453639.7616	-0.3211	7.6448	0.0076	2453639.7615	-0.3211	1.2616	0.0085
2453641.6193	-0.2798	7.6981	0.0043	2453641.6193	-0.2798	1.2550	0.0045
2453642.7127	-0.2555	7.7192	0.0023	2453642.7126	-0.2555	1.2647	0.0034
2453643.6357	-0.2350	7.7363	0.0033	2453643.6356	-0.2350	1.2537	0.0035
2453644.7072	-0.2112	7.7402	0.0026	2453644.7072	-0.2112	1.2439	0.0032
2453648.6665	-0.1232	7.4535	0.0050	2453648.6665	-0.1232	1.0706	0.0053
2453652.6993	-0.0336	6.7282	0.0055	2453652.6992	-0.0336	0.8326	0.0057
2453653.6256	-0.0130	6.7023	0.0096	2453653.6256	-0.0130	0.8275	0.0112
2453655.6238	0.0314	6.7201	0.0062	2453655.6238	0.0314	0.8666	0.0077
2453657.6127	0.0756	6.7929	0.0021	2453657.6126	0.0756	0.9016	0.0031
2453667.6150	0.2979	7.1261	0.0028	2453667.6149	0.2979	1.1153	0.0054
2453668.6583	0.3211	7.1528	0.0019	2453668.6582	0.3211	1.1463	0.0025
2453669.6445	0.3430	7.1879	0.0023	2453669.6444	0.3430	1.1558	0.0031
2453671.6471	0.3876	7.2494	0.0030	2453671.6471	0.3876	1.1835	0.0038
2453672.5955	0.4086	7.2842	0.0019	2453672.5954	0.4086	1.1880	0.0030
2453673.5947	0.4308	7.3113	0.0033	2453673.5947	0.4308	1.2042	0.0033
2453674.5943	0.4531	7.3385	0.0013	2453674.5943	0.4531	1.2133	0.0026

2453679.5913	-0.4359	7.4825	0.0004	2453679.5912	-0.4359	1.2295	0.0029
2453680.5908	-0.4137	7.5130	0.0027	2453680.5908	-0.4137	1.2342	0.0031
2453688.5870	-0.2359	7.7380	0.0022	2453688.5870	-0.2359	1.2432	0.0033
2453690.5866	-0.1915	7.7338	0.0008	2453690.5866	-0.1915	1.2117	0.0014
2453691.6006	-0.1690	7.6826	0.0054	2453691.6005	-0.1690	1.1876	0.0060
2453694.5691	-0.1030	7.2445	0.0013	2453694.5690	-0.1030	1.0013	0.0035
2453695.5686	-0.0808	7.0063	0.0044	2453695.5686	-0.0808	0.9107	0.0071
2454257.8701	0.4168	7.2550	0.0125	2454257.8700	0.4168	1.1777	0.0133
2454258.8574	0.4387	7.2907	0.0048	2454258.8573	0.4387	1.1756	0.0062
2454259.8671	0.4611	7.3125	0.0031	2454259.8670	0.4611	1.1865	0.0059
2454260.8501	0.4830	7.3427	0.0022	2454260.8500	0.4830	1.1982	0.0035
2454261.8621	-0.4945	7.3750	0.0068	2454261.8621	-0.4945	1.2060	0.0069
2454264.8406	-0.4283	7.4560	0.0037	2454264.8405	-0.4283	1.2222	0.0043
2454265.8428	-0.4060	7.4816	0.0030	2454265.8427	-0.4060	1.2257	0.0044
2454266.8502	-0.3837	7.5178	0.0046	2454266.8501	-0.3837	1.2209	0.0054
2454268.8487	-0.3392	7.5921	0.0066	2454268.8498	-0.3392	1.2197	0.0067
2454269.8522	-0.3169	7.6347	0.0079	2454269.8522	-0.3169	1.2310	0.0091
2454270.8360	-0.2951	7.6616	0.0025	2454270.8359	-0.2951	1.2432	0.0032
2454272.8346	-0.2507	7.7064	0.0075	2454272.8345	-0.2507	1.2363	0.0082
2454273.8510	-0.2281	7.7276	0.0007	2454273.8510	-0.2281	1.2266	0.0031
2454275.8470	-0.1837	7.7264	0.0077	2454275.8469	-0.1837	1.2100	0.0089
2454276.8256	-0.1619	7.6957	0.0055	2454276.8256	-0.1619	1.1850	0.0067
2454277.8396	-0.1394	7.6208	0.0115	2454277.8396	-0.1394	1.1507	0.0131
2454278.8156	-0.1177	7.5031	0.0050	2454278.8155	-0.1177	1.0943	0.0077
2454279.8272	-0.0952	7.3089	0.0049	2454279.8272	-0.0952	1.0183	0.0056
2454280.8169	-0.0732	7.0855	0.0157	2454280.8169	-0.0732	0.9343	0.0175
2454281.8222	-0.0509	6.8751	0.0162	2454281.8222	-0.0509	0.8591	0.0257

2454282.8111	-0.0289	6.7653	0.0038	2454282.8110	-0.0289	0.8318	0.0040
2454284.8274	0.0159	6.7045	0.0082	2454284.8273	0.0159	0.8286	0.0119
2454285.8187	0.0379	6.7247	0.0083	2454285.8186	0.0379	0.8516	0.0132
2454370.7160	-0.0752	7.1357	0.0025	2454370.7159	-0.0752	0.9541	0.0041
2454373.6457	-0.0101	6.7150	0.0005	2454373.6457	-0.0101	0.8218	0.0041
2454380.6932	0.1466	6.8899	0.0158	2454380.6931	0.1466	0.9644	0.0198
2454381.6383	0.1676	6.8632	0.0070	2454381.6383	0.1676	0.9759	0.0320
2454382.6818	0.1908	6.9469	0.0219	2454382.6817	0.1908	0.9877	0.0459
2454388.6703	0.3239	7.1199	0.0027	2454388.6703	0.3239	1.1263	0.0035
2454390.6573	0.3680	7.1828	0.0043	2454390.6573	0.3680	1.1492	0.0046
2454391.6192	0.3894	7.2103	0.0009	2454391.6191	0.3894	1.1747	0.0029
2454392.6555	0.4125	7.2429	0.0022	2454392.6554	0.4124	1.1788	0.0041
2454393.6177	0.4338	7.2740	0.0011	2454393.6176	0.4338	1.1880	0.0016
2454394.6452	0.4567	7.3044	0.0019	2454394.6452	0.4567	1.1989	0.0021
2454737.6343	0.0798	6.7605	0.0057	2454737.6343	0.0798	0.8905	0.0098
2454747.6247	0.3019	7.0937	0.0025	2454747.6247	0.3019	1.1105	0.0036
2454749.6423	0.3467	7.1517	0.0045	2454749.6423	0.3467	1.1506	0.0047
2454753.6465	0.4357	7.2807	0.0024	2454753.6464	0.4357	1.1999	0.0030
2454755.6287	0.4798	7.3479	0.0017	2454755.6286	0.4798	1.2099	0.0023
2454757.6114	-0.4762	7.3996	0.0011	2454757.6113	-0.4762	1.2273	0.0020
2454759.6099	-0.4317	7.4600	0.0036	2454759.6098	-0.4317	1.2322	0.0043
2454761.6228	-0.3870	7.5045	0.0024	2454761.6227	-0.3870	1.2556	0.0027
2454763.6215	-0.3426	7.5708	0.0003	2454763.6214	-0.3426	1.2631	0.0007
2454765.6290	-0.2980	7.6529	0.0008	2454765.6289	-0.2980	1.2456	0.0012
2454767.6280	-0.2535	7.7087	0.0024	2454767.6279	-0.2535	1.2475	0.0033
2454771.6388	-0.1644	7.7200	0.0014	2454771.6387	-0.1644	1.1983	0.0030
2454775.6235	-0.0758	7.1640	0.0083	2454775.6234	-0.0758	0.9559	0.0122

2454785.5945	0.1458	6.8738	0.0039	2454785.5945	0.1458	0.9667	0.0057
2454985.8817	-0.4027	7.5200	0.0049	2454985.8816	-0.4027	1.2222	0.0074
2454989.8728	-0.3140	7.6321	0.0036	2454989.8719	-0.3140	1.2272	0.0062
2454997.8479	-0.1367	7.6041	0.0034	2454997.8478	-0.1367	1.1406	0.0038
2454998.8419	-0.1146	7.4731	0.0034	2454998.8418	-0.1146	1.0885	0.0047
2454999.9182	-0.0907	7.2777	0.0070	2454999.9181	-0.0907	0.9993	0.0112
2455004.9125	0.0203	6.7376	0.0168	2455004.9125	0.0203	0.8320	0.0277
2455006.8737	0.0639	6.7883	0.0057	2455006.8737	0.0639	0.8691	0.0157
2455098.7335	0.1055	6.8588	0.0102	2455098.7334	0.1055	0.9119	0.0259
2455099.7450	0.1280	6.8789	0.0144	2455099.7458	0.1280	0.9442	0.0151
2455100.7376	0.1501	6.9014	0.0063	2455100.7375	0.1501	0.9703	0.0111
2455101.7538	0.1726	6.9383	0.0041	2455101.7529	0.1726	0.9946	0.0069
2455102.7367	0.1945	6.9770	0.0006	2455102.7358	0.1945	1.0116	0.0116
2455106.7264	0.2832	7.0876	0.0111	2455106.7263	0.2832	1.0896	0.0124
2455109.6904	0.3490	7.1759	0.0125	2455109.6904	0.3490	1.1551	0.0263
2455133.5951	-0.1197	7.5187	0.0020	2455133.5951	-0.1197	1.1047	0.0031
2455134.5945	-0.0975	7.3416	0.0070	2455134.5944	-0.0975	1.0364	0.0106
2455136.5932	-0.0530	6.9060	0.0055	2455136.5932	-0.0530	0.8717	0.0074
2455137.5925	-0.0308	6.7807	0.0044	2455137.5924	-0.0308	0.8425	0.0048
2455138.5921	-0.0086	6.7359	0.0036	2455138.5920	-0.0086	0.8303	0.0058
2455139.5913	0.0136	6.7254	0.0046	2455139.5913	0.0136	0.8353	0.0076
2455143.5931	0.1025	6.8414	0.0085	2455143.5930	0.1025	0.9053	0.0117
2455144.5889	0.1247	6.8619	0.0064	2455144.5888	0.1247	0.9367	0.0095
2455146.5878	0.1691	6.9180	0.0053	2455146.5878	0.1691	0.9880	0.0072
2455151.5863	0.2802	7.0672	0.0032	2455151.5871	0.2802	1.0945	0.0033
2455295.9908	0.4897	7.3662	0.0011	2455295.9907	0.4897	1.2148	0.0014
2455296.9876	-0.4882	7.3994	0.0025	2455296.9875	-0.4882	1.2158	0.0028

2455297.9867	-0.4660	7.4334	0.0054	2455297.9857	-0.4660	1.2175	0.0063
2455298.9823	-0.4438	7.4599	0.0036	2455298.9822	-0.4438	1.2260	0.0042
2455299.9800	-0.4216	7.4820	0.0042	2455299.9808	-0.4216	1.2275	0.0049
2455300.9778	-0.3995	7.5054	0.0056	2455300.9777	-0.3995	1.2386	0.0060
2455301.9763	-0.3773	7.5379	0.0034	2455301.9754	-0.3773	1.2352	0.0047
2455314.9776	-0.0883	7.2735	0.0072	2455314.9775	-0.0883	1.0023	0.0183
2455315.9661	-0.0663	7.0509	0.0078	2455315.9660	-0.0663	0.9176	0.0136
2455317.9495	-0.0223	6.7400	0.0070	2455317.9494	-0.0223	0.8315	0.0091
2455319.9868	0.0230	6.7074	0.0053	2455319.9868	0.0230	0.8426	0.0087
2455320.9495	0.0444	6.7288	0.0072	2455320.9494	0.0444	0.8577	0.0108
2455321.9213	0.0660	6.7627	0.0068	2455321.9213	0.0660	0.8799	0.0094
2455323.9637	0.1114	6.8290	0.0043	2455323.9636	0.1114	0.9329	0.0051
2455326.9085	0.1769	6.9518	0.0069	2455326.9084	0.1769	0.9903	0.0107
2455328.9404	0.2220	6.9933	0.0048	2455328.9412	0.2220	1.0390	0.0055
2455335.9252	0.3773	7.2165	0.0025	2455335.9251	0.3773	1.1639	0.0029
2455337.9468	0.4222	7.2777	0.0034	2455337.9468	0.4222	1.1916	0.0041
2455463.7800	0.2189	7.0197	0.0047	2455463.7791	0.2189	1.0396	0.0072
2455464.7555	0.2406	7.0505	0.0111	2455464.7563	0.2406	1.0697	0.0131
2455465.7727	0.2632	7.0813	0.0081	2455465.7727	0.2632	1.0833	0.0102
2455495.6278	-0.0732	7.0557	0.0057	2455495.6278	-0.0732	0.9152	0.0071
2455498.6708	-0.0056	6.7114	0.0162	2455498.6708	-0.0056	0.8345	0.0210
2455499.5942	0.0149	6.7032	0.0027	2455499.5942	0.0149	0.8464	0.0078
2455501.5933	0.0593	6.7574	0.0041	2455501.5933	0.0593	0.8807	0.0057
2455502.5926	0.0816	6.7912	0.0020	2455502.5925	0.0816	0.9022	0.0052
2455503.5922	0.1038	6.8284	0.0049	2455503.5922	0.1038	0.9223	0.0057
2455504.5915	0.1260	6.8635	0.0060	2455504.5914	0.1260	0.9553	0.0064
2455508.6042	0.2152	6.9982	0.0074	2455508.6042	0.2152	1.0504	0.0093

2455509.6056	0.2374	7.0416	0.0025	2455509.6056	0.2374	1.0639	0.0035
2455510.6050	0.2596	7.0663	0.0017	2455510.6041	0.2596	1.0813	0.0029
2455511.6027	0.2818	7.0993	0.0043	2455511.6027	0.2818	1.1049	0.0045
2455513.6019	0.3262	7.1526	0.0021	2455513.6019	0.3262	1.1379	0.0025
2455516.6011	0.3929	7.2605	0.0049	2455516.6010	0.3929	1.1733	0.0060
2455517.6006	0.4151	7.2786	0.0050	2455517.6006	0.4151	1.1889	0.0079
2455518.6005	0.4373	7.2990	0.0030	2455518.6013	0.4374	1.2007	0.0031
2455519.6001	0.4596	7.3328	0.0042	2455519.6000	0.4596	1.2093	0.0068
2455523.5762	-0.4521	7.4399	0.0029	2455523.5761	-0.4521	1.2315	0.0033
2455530.5747	-0.2965	7.6619	0.0018	2455530.5747	-0.2965	1.2400	0.0022
2455532.5747	-0.2521	7.7109	0.0013	2455532.5746	-0.2521	1.2429	0.0021
2455702.8369	-0.4679	7.4495	0.0060	2455702.8368	-0.4679	1.2227	0.0068
2455704.8441	-0.4233	7.5057	0.0031	2455704.8440	-0.4233	1.2445	0.0053
2455706.8238	-0.3793	7.5578	0.0007	2455706.8237	-0.3793	1.2544	0.0021
2455710.8259	-0.2903	7.7228	0.0139	2455710.8257	-0.2903	1.2493	0.0144
2455712.8106	-0.2462	7.7208	0.0030	2455712.8105	-0.2462	1.2564	0.0046
2455716.7980	-0.1576	7.6094	0.0063	2455716.7979	-0.1576	1.1609	0.0069
2455722.7974	-0.0242	6.7362	0.0050	2455722.7973	-0.0242	0.8404	0.0093
2455730.7643	0.1528	6.9670	0.0087	2455730.7642	0.1528	1.0222	0.0166
2455732.7539	0.1970	7.0250	0.0073	2455732.7538	0.1970	1.0480	0.0113
2455734.7651	0.2417	7.0985	0.0040	2455734.7650	0.2417	1.0896	0.0056
2455736.7470	0.2858	7.1448	0.0166	2455736.7468	0.2858	1.1193	0.0174
2455738.9257	0.3342	7.1801	0.0045	2455738.9256	0.3342	1.1715	0.0050
2455740.7563	0.3749	7.2763	0.0085	2455740.7561	0.3749	1.1765	0.0110
2455824.6474	0.2394	7.0542	0.0036	2455824.6473	0.2394	1.0885	0.0038
2455830.8020	0.3762	7.2298	0.0100	2455830.8019	0.3762	1.1891	0.0141
2455835.7882	0.4871	7.3889	0.0100	2455835.7881	0.4870	1.2055	0.0141

2455839.7766	-0.4243	7.4973	0.0100	2455839.7765	-0.4243	1.2433	0.0141
2455840.7742	-0.4021	7.5422	0.0100	2455840.7741	-0.4021	1.2399	0.0141
2455842.7686	-0.3578	7.6073	0.0100	2455842.7685	-0.3578	1.2511	0.0141
2455843.7649	-0.3357	7.6276	0.0100	2455843.7648	-0.3357	1.2459	0.0141
2455845.7604	-0.2913	7.6749	0.0100	2455845.7603	-0.2913	1.2721	0.0141
2455846.7574	-0.2692	7.7045	0.0100	2455846.7572	-0.2692	1.2529	0.0141
2455847.7537	-0.2470	7.7154	0.0100	2455847.7536	-0.2470	1.2381	0.0141
2455848.7510	-0.2248	7.7144	0.0100	2455848.7509	-0.2248	1.2449	0.0141
2455849.7488	-0.2027	7.7043	0.0100	2455849.7487	-0.2027	1.2324	0.0141
2455851.7430	-0.1583	7.5850	0.0100	2455851.7428	-0.1583	1.1435	0.0141
2455854.5877	-0.0951	7.0493	0.0026	2455854.5876	-0.0951	0.9236	0.0040
2455855.6018	-0.0726	6.8380	0.0028	2455855.6016	-0.0726	0.8566	0.0056
2455856.6010	-0.0504	6.7450	0.0030	2455856.6009	-0.0504	0.8250	0.0039
2455857.6295	-0.0275	6.7166	0.0049	2455857.6294	-0.0275	0.8356	0.0125
2455858.5994	-0.0060	6.7137	0.0054	2455858.5993	-0.0060	0.8410	0.0069
2455861.5971	0.0607	6.8006	0.0077	2455861.5970	0.0607	0.8985	0.0079
2455862.6551	0.0842	6.8340	0.0072	2455862.6550	0.0842	0.9291	0.0091
2455864.6685	0.1289	6.8998	0.0024	2455864.6684	0.1289	0.9833	0.0038
2455865.5944	0.1495	6.9345	0.0029	2455865.5943	0.1495	1.0070	0.0054

Photometry of SV Vul, cont…

HJD	Phase	c1	c1 err	HJD	Phase	m1	m1 err
2453302.6651	0.1867	0.6529	0.0217	2453302.6638	0.1866	0.1908	0.0215
2453303.6644	0.2089	0.5637	0.0368	2453303.6648	0.2089	0.2051	0.0124
2453309.6576	0.3421	0.4044	0.0035	2453309.6578	0.3421	0.2669	0.0054

2453310.6570	0.3643	0.3922	0.0091	2453310.6571	0.3643	0.2875	0.0064
2453311.6570	0.3865	0.3620	0.0123	2453311.6571	0.3865	0.2782	0.0064
2453312.6419	0.4084	0.3442	0.0061	2453312.6420	0.4084	0.2997	0.0049
2453313.6309	0.4304	0.3653	0.0106	2453313.6311	0.4304	0.2988	0.0057
2453318.6244	-0.4586	0.3248	0.0054	2453318.6245	-0.4586	0.3134	0.0028
2453319.6427	-0.4360	0.3203	0.0030	2453319.6428	-0.4360	0.3357	0.0025
2453320.5873	-0.4150	0.2897	0.0067	2453320.5874	-0.4150	0.3379	0.0061
2453336.6091	-0.0589	0.8501	0.0240	2453336.6092	-0.0589	0.1116	0.0175
2453340.5661	0.0291	0.9467	0.0114	2453340.5662	0.0291	0.0834	0.0083
2453341.5660	0.0513	0.8567	0.0212	2453341.5661	0.0513	0.1052	0.0104
2453348.5660	0.2069	0.5394	0.0133	2453348.5661	0.2069	0.2029	0.0101
2453349.5663	0.2291	0.4881	0.0050	2453349.5664	0.2291	0.2323	0.0065
2453350.5664	0.2513	0.4848	0.0164	2453350.5666	0.2513	0.2301	0.0106
2453351.5666	0.2735	0.4733	0.0189	2453351.5667	0.2735	0.2476	0.0098
2453354.5739	0.3404	0.4002	0.0064	2453354.5740	0.3404	0.2885	0.0042
2453355.5742	0.3626	0.3518	0.0200	2453355.5743	0.3626	0.2869	0.0200
2453357.5679	0.4069	0.3915	0.0200	2453357.5680	0.4069	0.2645	0.0200
2453462.9770	-0.2503	0.3009	0.0031	2453462.9772	-0.2503	0.3456	0.0022
2453464.9714	-0.2060	0.3091	0.0073	2453464.9715	-0.2060	0.3366	0.0042
2453466.9758	-0.1614	0.3921	0.0095	2453466.9763	-0.1614	0.2763	0.0042
2453476.9549	0.0604	0.8597	0.0141	2453476.9551	0.0604	0.1036	0.0059
2453480.9370	0.1489	0.6823	0.0122	2453480.9371	0.1489	0.1579	0.0096
2453481.9450	0.1713	0.6325	0.0101	2453481.9452	0.1713	0.1819	0.0103
2453483.9399	0.2156	0.5556	0.0112	2453483.9400	0.2156	0.2053	0.0106
2453487.9227	0.3042	0.4352	0.0060	2453487.9228	0.3042	0.2546	0.0062
2453488.9161	0.3262	0.4223	0.0042	2453488.9162	0.3262	0.2674	0.0050
2453490.9108	0.3706	0.3967	0.0124	2453490.9109	0.3706	0.2735	0.0067

2453494.8975	0.4592	0.3051	0.0085	2453494.8976	0.4592	0.3287	0.0085
2453496.9676	-0.4948	0.3137	0.0034	2453496.9677	-0.4948	0.3287	0.0037
2453500.8861	-0.4077	0.3160	0.0045	2453500.8862	-0.4077	0.3340	0.0049
2453501.8997	-0.3852	0.2833	0.0047	2453501.8998	-0.3852	0.3568	0.0019
2453502.9544	-0.3618	0.3086	0.0017	2453502.9545	-0.3618	0.3351	0.0019
2453503.8876	-0.3410	0.2843	0.0093	2453503.8877	-0.3410	0.3583	0.0061
2453504.9456	-0.3175	0.3013	0.0076	2453504.9457	-0.3175	0.3473	0.0054
2453506.9494	-0.2730	0.2567	0.0029	2453506.9491	-0.2730	0.3530	0.0029
2453507.8754	-0.2524	0.3035	0.0026	2453507.8751	-0.2524	0.3393	0.0036
2453509.8766	-0.2079	0.3075	0.0037	2453509.8771	-0.2079	0.3178	0.0027
2453510.8644	-0.1860	0.3094	0.0056	2453510.8641	-0.1860	0.3318	0.0035
2453511.8507	-0.1640	0.3353	0.0064	2453511.8508	-0.1640	0.3122	0.0049
2453512.8513	-0.1418	0.4029	0.0069	2453512.8514	-0.1418	0.2646	0.0046
2453513.8452	-0.1197	0.4869	0.0140	2453513.8454	-0.1197	0.2320	0.0097
2453520.8342	0.0356	0.9315	0.0317	2453520.8343	0.0356	0.0850	0.0285
2453524.8251	0.1243	0.7212	0.0151	2453524.8252	0.1243	0.1436	0.0142
2453525.8201	0.1464	0.7090	0.0151	2453525.8202	0.1465	0.1427	0.0118
2453526.8123	0.1685	0.6546	0.0118	2453526.8125	0.1685	0.1633	0.0076
2453527.8150	0.1908	0.6207	0.0216	2453527.8151	0.1908	0.1798	0.0062
2453528.8089	0.2129	0.5639	0.0203	2453528.8090	0.2129	0.2032	0.0070
2453529.8138	0.2352	0.5231	0.0161	2453529.8139	0.2352	0.2168	0.0063
2453530.8086	0.2573	0.5106	0.0080	2453530.8087	0.2573	0.2280	0.0061
2453531.8030	0.2794	0.4901	0.0130	2453531.8031	0.2794	0.2376	0.0063
2453532.8023	0.3016	0.4409	0.0075	2453532.8024	0.3016	0.2530	0.0054
2453533.7976	0.3238	0.4046	0.0091	2453533.7977	0.3238	0.2701	0.0050
2453535.7988	0.3682	0.3935	0.0044	2453535.7989	0.3682	0.2837	0.0058
2453536.7923	0.3903	0.3728	0.0054	2453536.7924	0.3903	0.2831	0.0060

2453537.7866	0.4124	0.3214	0.0105	2453537.7867	0.4124	0.3184	0.0079
2453538.7817	0.4345	0.3648	0.0036	2453538.7814	0.4345	0.3058	0.0038
2453539.7807	0.4567	0.3382	0.0037	2453539.7808	0.4567	0.3078	0.0049
2453543.7878	-0.4542	0.2143	0.0065	2453543.7880	-0.4542	0.3142	0.0060
2453547.7614	-0.3659	0.3082	0.0075	2453547.7616	-0.3659	0.3443	0.0042
2453548.7606	-0.3437	0.2690	0.0052	2453548.7607	-0.3437	0.3532	0.0071
2453549.7482	-0.3217	0.2958	0.0058	2453549.7484	-0.3217	0.3454	0.0054
2453550.7513	-0.2994	0.3588	0.0041	2453550.7514	-0.2994	0.3341	0.0061
2453551.7552	-0.2771	0.3109	0.0045	2453551.7553	-0.2771	0.3596	0.0036
2453552.7499	-0.2550	0.2540	0.0058	2453552.7500	-0.2550	0.3556	0.0026
2453554.7385	-0.2108	0.2872	0.0088	2453554.7387	-0.2108	0.3553	0.0103
2453555.7407	-0.1885	0.3331	0.0059	2453555.7408	-0.1885	0.3274	0.0076
2453556.7324	-0.1665	0.3666	0.0081	2453556.7321	-0.1665	0.2981	0.0040
2453557.7367	-0.1442	0.3761	0.0081	2453557.7369	-0.1442	0.2713	0.0032
2453558.7265	-0.1222	0.4859	0.0114	2453558.7267	-0.1222	0.2182	0.0054
2453560.7537	-0.0771	0.7752	0.0113	2453560.7538	-0.0771	0.1141	0.0093
2453561.7241	-0.0556	0.9075	0.0222	2453561.7238	-0.0556	0.0864	0.0130
2453563.7166	-0.0113	0.9649	0.0280	2453563.7167	-0.0113	0.0601	0.0165
2453565.7175	0.0332	0.9158	0.0206	2453565.7176	0.0332	0.0848	0.0145
2453567.7022	0.0773	0.8068	0.0263	2453567.7023	0.0773	0.1203	0.0241
2453627.6461	0.4096	0.3341	0.0073	2453627.6462	0.4096	0.2865	0.0057
2453628.7494	0.4341	0.3195	0.0092	2453628.7495	0.4341	0.2986	0.0044
2453629.6301	0.4537	0.3308	0.0067	2453629.6302	0.4537	0.3025	0.0059
2453631.6279	0.4981	0.2765	0.0075	2453631.6281	0.4981	0.3206	0.0056
2453632.7193	-0.4776	0.2540	0.0046	2453632.7194	-0.4776	0.3372	0.0051
2453634.7081	-0.4334	0.3045	0.0055	2453634.7083	-0.4334	0.3258	0.0082
2453636.7087	-0.3890	0.2782	0.0031	2453636.7088	-0.3890	0.3568	0.0036

2453637.6227	-0.3687	0.2320	0.0086	2453637.6229	-0.3687	0.3458	0.0083
2453638.7146	-0.3444	0.2482	0.0054	2453638.7147	-0.3444	0.3587	0.0031
2453639.7613	-0.3211	0.2332	0.0042	2453639.7615	-0.3211	0.3462	0.0093
2453641.6191	-0.2798	0.2550	0.0053	2453641.6192	-0.2798	0.3512	0.0051
2453642.7125	-0.2555	0.2323	0.0031	2453642.7126	-0.2555	0.3475	0.0043
2453643.6354	-0.2350	0.2524	0.0043	2453643.6356	-0.2350	0.3347	0.0039
2453644.7070	-0.2112	0.2439	0.0062	2453644.7071	-0.2112	0.3360	0.0048
2453648.6663	-0.1232	0.4884	0.0080	2453648.6664	-0.1232	0.2246	0.0060
2453652.6991	-0.0336	0.9467	0.0261	2453652.6992	-0.0336	0.0798	0.0110
2453653.6254	-0.0130	0.9542	0.0286	2453653.6255	-0.0130	0.0863	0.0199
2453655.6236	0.0314	0.9128	0.0181	2453655.6237	0.0314	0.0826	0.0148
2453657.6124	0.0756	0.8440	0.0141	2453657.6125	0.0756	0.1091	0.0048
2453667.6148	0.2979	0.4499	0.0092	2453667.6149	0.2979	0.2612	0.0075
2453668.6581	0.3211	0.4228	0.0119	2453668.6582	0.3211	0.2572	0.0078
2453669.6442	0.3430	0.4043	0.0090	2453669.6444	0.3430	0.2750	0.0045
2453671.6469	0.3875	0.3928	0.0067	2453671.6470	0.3875	0.2858	0.0062
2453672.5952	0.4086	0.3605	0.0039	2453672.5953	0.4086	0.3035	0.0041
2453673.5945	0.4308	0.3497	0.0054	2453673.5946	0.4308	0.3027	0.0041
2453674.5941	0.4531	0.3237	0.0075	2453674.5942	0.4531	0.3160	0.0046
2453679.5910	-0.4359	0.2913	0.0051	2453679.5912	-0.4359	0.3468	0.0050
2453680.5906	-0.4137	0.2794	0.0039	2453680.5907	-0.4137	0.3452	0.0037
2453688.5868	-0.2360	0.2882	0.0042	2453688.5869	-0.2360	0.3333	0.0042
2453690.5876	-0.1915	0.3032	0.0064	2453690.5871	-0.1915	0.3215	0.0026
2453691.6003	-0.1690	0.3140	0.0070	2453691.6004	-0.1690	0.3029	0.0070
2453694.5699	-0.1030	0.5867	0.0121	2453694.5690	-0.1030	0.1769	0.0063
2453695.5684	-0.0808	0.7691	0.0166	2453695.5685	-0.0808	0.1326	0.0113
2454257.8698	0.4167	0.3801	0.0129	2454257.8699	0.4168	0.3025	0.0159

2454258.8572	0.4387	0.3455	0.0092	2454258.8573	0.4387	0.3183	0.0082
2454259.8668	0.4611	0.3748	0.0124	2454259.8670	0.4611	0.3209	0.0078
2454260.8498	0.4830	0.3653	0.0106	2454260.8500	0.4830	0.3288	0.0084
2454261.8619	-0.4945	0.3581	0.0032	2454261.8620	-0.4945	0.3318	0.0071
2454264.8404	-0.4283	0.3215	0.0053	2454264.8405	-0.4283	0.3334	0.0059
2454265.8425	-0.4061	0.3152	0.0111	2454265.8426	-0.4061	0.3447	0.0089
2454266.8500	-0.3837	0.3071	0.0079	2454266.8501	-0.3837	0.3504	0.0071
2454268.8502	-0.3392	0.2944	0.0025	2454268.8503	-0.3392	0.3671	0.0069
2454269.8520	-0.3169	0.2977	0.0106	2454269.8521	-0.3169	0.3623	0.0106
2454270.8363	-0.2951	0.3041	0.0044	2454270.8358	-0.2951	0.3497	0.0047
2454272.8343	-0.2507	0.3001	0.0038	2454272.8344	-0.2507	0.3485	0.0089
2454273.8508	-0.2281	0.3142	0.0076	2454273.8509	-0.2281	0.3594	0.0059
2454275.8467	-0.1837	0.3374	0.0048	2454275.8468	-0.1837	0.3195	0.0100
2454276.8260	-0.1619	0.3483	0.0050	2454276.8255	-0.1619	0.3021	0.0081
2454277.8394	-0.1394	0.4252	0.0129	2454277.8395	-0.1394	0.2685	0.0166
2454278.8153	-0.1177	0.4545	0.0116	2454278.8154	-0.1177	0.2419	0.0102
2454279.8270	-0.0952	0.5954	0.0137	2454279.8271	-0.0952	0.1837	0.0065
2454280.8167	-0.0732	0.7082	0.0156	2454280.8168	-0.0732	0.1439	0.0209
2454281.8220	-0.0509	0.8568	0.0328	2454281.8221	-0.0509	0.1092	0.0367
2454282.8108	-0.0289	0.9316	0.0234	2454282.8109	-0.0289	0.0924	0.0090
2454284.8271	0.0159	0.9333	0.0520	2454284.8272	0.0159	0.1098	0.0365
2454285.8185	0.0379	0.9413	0.0322	2454285.8186	0.0379	0.0894	0.0220
2454370.7158	-0.0752	0.6839	0.0122	2454370.7159	-0.0752	0.1579	0.0052
2454373.6455	-0.0101	0.9664	0.0201	2454373.6456	-0.0101	0.0924	0.0132
2454380.6936	0.1466	0.8301	0.1829	2454380.6931	0.1466	0.1327	0.0333
2454381.6381	0.1676	0.8026	0.2436	2454381.6382	0.1676	0.0668	0.0742
2454388.6701	0.3239	0.4599	0.0060	2454382.6816	0.1908	0.1977	0.2139

2454390.6571	0.3680	0.4095	0.0111	2454388.6702	0.3239	0.2523	0.0043
2454391.6190	0.3894	0.4038	0.0066	2454390.6572	0.3680	0.2819	0.0050
2454392.6552	0.4124	0.3741	0.0073	2454391.6191	0.3894	0.2732	0.0050
2454393.6174	0.4338	0.3456	0.0037	2454392.6554	0.4124	0.2956	0.0067
2454394.6450	0.4567	0.3444	0.0092	2454393.6175	0.4338	0.3121	0.0031
2454737.6341	0.0798	0.8774	0.0249	2454394.6451	0.4567	0.3124	0.0038
2454747.6245	0.3019	0.4779	0.0113	2454737.6342	0.0798	0.0976	0.0176
2454749.6421	0.3467	0.3797	0.0095	2454747.6246	0.3019	0.2384	0.0065
2454753.6467	0.4357	0.3897	0.0085	2454749.6422	0.3467	0.2785	0.0056
2454755.6284	0.4798	0.3373	0.0032	2454753.6464	0.4357	0.2882	0.0040
2454757.6128	-0.4761	0.3482	0.0017	2454755.6286	0.4798	0.3241	0.0031
2454759.6097	-0.4317	0.3112	0.0069	2454757.6117	-0.4762	0.3235	0.0026
2454761.6225	-0.3870	0.3096	0.0066	2454759.6098	-0.4317	0.3379	0.0064
2454763.6212	-0.3426	0.2761	0.0017	2454761.6227	-0.3870	0.3268	0.0049
2454765.6309	-0.2979	0.3447	0.0020	2454763.6213	-0.3426	0.3354	0.0014
2454767.6278	-0.2535	0.3015	0.0068	2454765.6297	-0.2979	0.3474	0.0016
2454771.6390	-0.1644	0.3356	0.0052	2454767.6279	-0.2535	0.3464	0.0049
2454775.6237	-0.0758	0.6693	0.0122	2454771.6387	-0.1644	0.3237	0.0051
2454785.5943	0.1458	0.7205	0.0128	2454775.6234	-0.0758	0.1708	0.0159
2454985.8815	-0.4027	0.3048	0.0062	2454785.5944	0.1458	0.1432	0.0096
2454989.8708	-0.3140	0.3332	0.0081	2454985.8816	-0.4027	0.3443	0.0095
2454997.8476	-0.1367	0.3830	0.0070	2454989.8714	-0.3140	0.3668	0.0091
2454998.8416	-0.1147	0.4862	0.0073	2454997.8477	-0.1367	0.2746	0.0063
2454999.9180	-0.0907	0.5918	0.0181	2454998.8417	-0.1147	0.2220	0.0069
2455004.9123	0.0203	0.9457	0.0387	2454999.9181	-0.0907	0.1919	0.0166
2455006.8735	0.0639	0.8858	0.0304	2455004.9124	0.0203	0.0906	0.0396
2455098.7333	0.1055	0.8109	0.0420	2455006.8736	0.0639	0.1047	0.0257

2455099.7461	0.1280	0.7537	0.0153	2455098.7334	0.1055	0.1273	0.0414
2455100.7374	0.1500	0.7049	0.0169	2455099.7462	0.1280	0.1324	0.0183
2455101.7527	0.1726	0.6788	0.0097	2455100.7375	0.1501	0.1520	0.0160
2455102.7352	0.1945	0.6262	0.0180	2455101.7528	0.1726	0.1571	0.0097
2455106.7262	0.2832	0.5239	0.0108	2455102.7353	0.1945	0.1846	0.0190
2455109.6902	0.3490	0.4064	0.0321	2455106.7263	0.2832	0.2411	0.0138
2455133.5949	-0.1197	0.4444	0.0072	2455109.6903	0.3490	0.2589	0.0368
2455134.5942	-0.0975	0.5568	0.0156	2455133.5950	-0.1197	0.2568	0.0052
2455136.5930	-0.0530	0.8658	0.0187	2455134.5944	-0.0975	0.2041	0.0154
2455137.5922	-0.0308	0.9384	0.0125	2455136.5931	-0.0530	0.1131	0.0094
2455138.5918	-0.0086	0.9403	0.0228	2455137.5924	-0.0308	0.0872	0.0091
2455139.5915	0.0136	0.9422	0.0087	2455138.5919	-0.0086	0.0936	0.0150
2455143.5929	0.1025	0.8038	0.0178	2455139.5912	0.0136	0.0935	0.0098
2455144.5886	0.1247	0.7623	0.0144	2455143.5930	0.1025	0.1313	0.0170
2455146.5876	0.1691	0.6716	0.0103	2455144.5888	0.1247	0.1379	0.0122
2455151.5865	0.2802	0.5084	0.0064	2455146.5877	0.1691	0.1639	0.0098
2455295.9905	0.4897	0.3552	0.0036	2455151.5871	0.2802	0.2255	0.0053
2455296.9873	-0.4882	0.3235	0.0117	2455295.9907	0.4897	0.3158	0.0029
2455297.9847	-0.4660	0.3097	0.0087	2455296.9874	-0.4882	0.3346	0.0042
2455298.9820	-0.4438	0.3412	0.0061	2455297.9852	-0.4660	0.3395	0.0078
2455299.9802	-0.4216	0.3032	0.0065	2455298.9821	-0.4438	0.3286	0.0057
2455300.9776	-0.3995	0.3501	0.0107	2455299.9808	-0.4216	0.3420	0.0063
2455301.9747	-0.3773	0.3298	0.0074	2455300.9777	-0.3995	0.3307	0.0078
2455314.9773	-0.0883	0.6219	0.0552	2455301.9749	-0.3773	0.3435	0.0064
2455315.9658	-0.0664	0.7575	0.0251	2455314.9774	-0.0883	0.1947	0.0400
2455317.9492	-0.0223	0.9505	0.0164	2455315.9660	-0.0663	0.1390	0.0198
2455320.9492	0.0444	0.9244	0.0218	2455317.9493	-0.0223	0.0905	0.0115

2455321.9211	0.0660	0.8821	0.0125	2455320.9494	0.0444	0.0943	0.0174
2455323.9635	0.1114	0.7912	0.0178	2455321.9212	0.0660	0.0982	0.0123
2455326.9082	0.1768	0.6518	0.0153	2455323.9636	0.1114	0.1232	0.0117
2455328.9406	0.2220	0.5766	0.0104	2455326.9084	0.1769	0.1745	0.0140
2455335.9249	0.3773	0.3963	0.0090	2455328.9412	0.2220	0.2105	0.0076
2455337.9470	0.4222	0.3738	0.0033	2455335.9251	0.3773	0.2803	0.0064
2455463.7780	0.2189	0.5697	0.0225	2455337.9467	0.4222	0.2970	0.0048
2455464.7557	0.2406	0.5359	0.0213	2455463.7786	0.2189	0.2043	0.0092
2455465.7725	0.2632	0.5071	0.0200	2455464.7562	0.2406	0.2077	0.0148
2455495.6276	-0.0732	0.7492	0.0118	2455465.7726	0.2632	0.2335	0.0149
2455498.6706	-0.0056	0.9431	0.0277	2455495.6277	-0.0732	0.1371	0.0093
2455499.5940	0.0149	0.9705	0.0132	2455498.6707	-0.0056	0.0825	0.0258
2455501.5931	0.0593	0.8941	0.0116	2455499.5941	0.0149	0.0761	0.0128
2455502.5923	0.0815	0.8562	0.0100	2455501.5932	0.0593	0.0977	0.0094
2455503.5920	0.1038	0.7852	0.0129	2455502.5925	0.0816	0.1132	0.0086
2455504.5913	0.1260	0.7421	0.0099	2455503.5921	0.1038	0.1355	0.0087
2455508.6040	0.2152	0.5622	0.0073	2455504.5914	0.1260	0.1372	0.0083
2455509.6041	0.2374	0.5413	0.0099	2455508.6041	0.2152	0.1889	0.0113
2455510.6031	0.2596	0.5027	0.0077	2455509.6051	0.2374	0.2035	0.0069
2455511.6025	0.2818	0.5001	0.0153	2455510.6036	0.2596	0.2260	0.0050
2455513.6017	0.3262	0.4116	0.0110	2455511.6026	0.2818	0.2285	0.0057
2455516.6008	0.3929	0.3769	0.0120	2455513.6018	0.3262	0.2611	0.0074
2455517.6004	0.4151	0.3816	0.0109	2455516.6009	0.3929	0.2838	0.0078
2455518.6007	0.4373	0.3581	0.0111	2455517.6005	0.4151	0.2874	0.0106
2455519.5998	0.4596	0.3815	0.0165	2455518.6013	0.4374	0.3029	0.0061
2455523.5759	-0.4521	0.3272	0.0070	2455519.5999	0.4596	0.2927	0.0101
2455530.5745	-0.2965	0.3365	0.0037	2455523.5761	-0.4521	0.3262	0.0058

2455532.5745	-0.2521	0.3033	0.0048	2455530.5746	-0.2965	0.3566	0.0031
2455702.8364	-0.4679	0.2877	0.0046	2455532.5746	-0.2521	0.3483	0.0028
2455704.8436	-0.4233	0.2732	0.0055	2455702.8367	-0.4679	0.3540	0.0078
2455710.8254	-0.2903	0.2727	0.0119	2455704.8439	-0.4233	0.3379	0.0072
2455712.8101	-0.2462	0.2753	0.0142	2455706.8236	-0.3793	0.3364	0.0043
2455716.7975	-0.1576	0.3627	0.0102	2455710.8256	-0.2903	0.3522	0.0166
2455722.7974	-0.0242	0.9229	0.0193	2455712.8103	-0.2462	0.3288	0.0080
2455730.7621	0.1528	0.6016	0.0212	2455716.7978	-0.1576	0.2788	0.0085
2455732.7534	0.1970	0.5169	0.0204	2455722.7972	-0.0243	0.0824	0.0170
2455734.7646	0.2417	0.4792	0.0238	2455730.7635	0.1528	0.1431	0.0223
2455736.7470	0.2858	0.4046	0.0178	2455732.7537	0.1970	0.2098	0.0182
2455738.9235	0.3342	0.4032	0.0102	2455734.7649	0.2417	0.2311	0.0086
2455740.7558	0.3749	0.3428	0.0164	2455736.7467	0.2858	0.2692	0.0204
2455824.6469	0.2394	0.5320	0.0072	2455738.9249	0.3342	0.2597	0.0073
2455830.8015	0.3762	0.4123	0.0200	2455740.7560	0.3749	0.3081	0.0136
2455835.7877	0.4870	0.3268	0.0200	2455824.6472	0.2394	0.2218	0.0059
2455839.7761	-0.4243	0.3343	0.0200	2455830.8018	0.3762	0.2795	0.0200
2455840.7737	-0.4021	0.2856	0.0200	2455835.7880	0.4870	0.3492	0.0200
2455842.7681	-0.3578	0.3207	0.0200	2455839.7764	-0.4243	0.3280	0.0200
2455843.7644	-0.3357	0.3415	0.0200	2455840.7740	-0.4021	0.3451	0.0200
2455845.7599	-0.2913	0.3569	0.0200	2455842.7684	-0.3578	0.3446	0.0200
2455846.7568	-0.2692	0.2521	0.0200	2455843.7646	-0.3357	0.3659	0.0200
2455847.7532	-0.2470	0.4683	0.0200	2455845.7602	-0.2913	0.3205	0.0200
2455848.7505	-0.2249	0.3675	0.0200	2455846.7571	-0.2692	0.3474	0.0200
2455849.7483	-0.2027	0.4196	0.0200	2455847.7534	-0.2470	0.3401	0.0200
2455851.7425	-0.1584	0.4005	0.0200	2455848.7508	-0.2248	0.3197	0.0200
2455854.5872	-0.0951	0.7642	0.0157	2455849.7485	-0.2027	0.2985	0.0200

2455855.6013	-0.0726	0.9196	0.0113	2455851.7427	-0.1583	0.2807	0.0200
2455856.6016	-0.0504	0.9559	0.0065	2455854.5875	-0.0951	0.1333	0.0091
2455857.6290	-0.0275	0.9657	0.0242	2455855.6015	-0.0726	0.0912	0.0080
2455858.5989	-0.0060	0.9647	0.0122	2455856.6013	-0.0504	0.0907	0.0048
2455861.5966	0.0607	0.8515	0.0086	2455857.6293	-0.0275	0.0730	0.0218
2455862.6546	0.0842	0.7840	0.0092	2455858.5992	-0.0060	0.0779	0.0105
2455864.6680	0.1289	0.6843	0.0126	2455861.5969	0.0607	0.1118	0.0095
2455865.5939	0.1495	0.6700	0.0097	2455862.6548	0.0842	0.1272	0.0113
				2455864.6682	0.1289	0.1523	0.0059
				2455865.5941	0.1495	0.1536	0.0090

Photometry of SZ Cas

HJD	Phase	V-mag	V-err	HJD	Phase	U-B	U-B err	HJD	Phase	B-V	B-V err
2454075.7771	0.1252	9.6756	0.0060	2454075.7780	0.1253	0.9934	0.0178	2454075.7781	0.1253	1.4263	0.0141
2454076.5892	0.1848	9.7412	0.0057	2454076.5880	0.1847	1.1206	0.0194	2454076.5881	0.1847	1.4446	0.0095
2454077.7807	0.2722	9.8028	0.0039	2454077.7805	0.2721	1.1752	0.0144	2454077.7807	0.2721	1.5039	0.0067
2454080.5875	0.4780	9.9544	0.0022	2454080.5873	0.4779	1.2594	0.0162	2454080.5874	0.4779	1.5792	0.0064
2454081.7701	-0.4353	9.9837	0.0050	2454081.7699	-0.4354	1.2080	0.0145	2454081.7700	-0.4353	1.5445	0.0091
2454083.7645	-0.2891	9.9433	0.0035	2454083.7643	-0.2891	1.1389	0.0071	2454083.7645	-0.2891	1.4903	0.0050
2454085.7763	-0.1416	9.7580	0.0061	2454085.7761	-0.1416	1.0628	0.0289	2454085.7762	-0.1416	1.3948	0.0101
2454086.7809	-0.0679	9.6395	0.0040	2454086.7807	-0.0679	0.9726	0.0071	2454086.7809	-0.0679	1.3451	0.0076
2454088.7576	0.0770	9.6411	0.0037	2454088.7574	0.0770	1.0281	0.0168	2454088.7575	0.0770	1.3839	0.0038
2454090.7653	0.2243	9.7670	0.0034	2454090.7651	0.2242	1.1269	0.0183	2454090.7652	0.2242	1.4747	0.0092
2454094.7579	-0.4830	9.9725	0.0032	2454094.7577	-0.4830	1.2240	0.0143	2454094.7578	-0.4830	1.5628	0.0068
2454100.7467	-0.0438	9.6152	0.0019	2454100.7465	-0.0439	1.0161	0.0116	2454100.7466	-0.0439	1.3488	0.0064
2454101.6352	0.0213	9.6141	0.0021	2454101.6350	0.0213	1.0247	0.0170	2454101.6351	0.0213	1.3659	0.0124
2454102.7394	0.1023	9.6540	0.0089	2454102.7392	0.1022	1.0902	0.0233	2454102.7393	0.1022	1.3979	0.0113
2454103.7247	0.1745	9.7090	0.0026	2454103.7245	0.1745	1.1124	0.0317	2454103.7246	0.1745	1.4440	0.0096
2454104.7220	0.2476	9.7766	0.0025	2454104.7229	0.2477	1.3032	0.0169	2454104.7219	0.2476	1.4968	0.0068
2454105.7205	0.3209	9.8499	0.0053	2454105.7203	0.3208	1.2239	0.0269	2454105.7204	0.3208	1.5178	0.0090
2454107.7137	0.4670	9.9587	0.0025	2454107.7135	0.4670	1.2831	0.0232	2454107.7136	0.4670	1.5597	0.0052
2454108.6997	-0.4607	9.9825	0.0027	2454108.6996	-0.4607	1.2412	0.0140	2454108.6997	-0.4607	1.5498	0.0049
2454115.6975	0.0524	9.6356	0.0016	2454115.6974	0.0524	1.0262	0.0153	2454115.6975	0.0524	1.3665	0.0049
2454116.6998	0.1259	9.6876	0.0050	2454116.6996	0.1259	1.0830	0.0216	2454116.6998	0.1259	1.4055	0.0078
2454117.6902	0.1985	9.7413	0.0020	2454117.6879	0.1984	1.1289	0.0186	2454117.6891	0.1985	1.4548	0.0068

2454124.6677	-0.2898	9.9429	0.0073	2454124.6675	-0.2899	1.1173	0.0140	2454124.6677	-0.2898	1.4989	0.0100
2454125.6705	-0.2163	9.8793	0.0006	2454125.6668	-0.2166	1.1066	0.0326	2454125.6686	-0.2164	1.4475	0.0134
2454127.6588	-0.0705	9.6470	0.0042	2454127.6586	-0.0705	1.0109	0.0281	2454127.6588	-0.0705	1.3467	0.0081
2454128.6606	0.0030	9.6137	0.0034	2454128.6604	0.0029	0.9987	0.0140	2454128.6606	0.0029	1.3425	0.0071
2454134.6501	0.4421	9.9424	0.0032	2454134.6499	0.4421	1.3050	0.0316	2454134.6500	0.4421	1.5568	0.0059
2454135.6882	-0.4817	9.9745	0.0052	2454135.6880	-0.4818	1.2415	0.0255	2454135.6881	-0.4818	1.5530	0.0081
2454136.6511	-0.4111	9.9880	0.0047	2454136.6509	-0.4112	1.2291	0.0186	2454136.6510	-0.4112	1.5396	0.0058
2454137.7027	-0.3340	9.9690	0.0031	2454137.7025	-0.3341	1.1478	0.0150	2454137.7026	-0.3340	1.5052	0.0068
2454138.6521	-0.2644	9.9355	0.0039	2454138.6519	-0.2644	1.1499	0.0124	2454138.6520	-0.2644	1.4710	0.0106
2454140.6473	-0.1181	9.7168	0.0040	2454140.6472	-0.1181	0.9821	0.0167	2454140.6473	-0.1181	1.3721	0.0107
2454144.6743	0.1772	9.7181	0.0032	2454144.6720	0.1770	1.0893	0.0184	2454144.6732	0.1771	1.4405	0.0093
2454146.6737	0.3238	9.8536	0.0051	2454146.6735	0.3238	1.2135	0.0276	2454146.6737	0.3238	1.5144	0.0079
2454147.6709	0.3969	9.9117	0.0034	2454147.6718	0.3970	1.2936	0.0141	2454147.6709	0.3969	1.5338	0.0064
2454148.6590	0.4694	9.9627	0.0057	2454148.6588	0.4693	1.2511	0.0130	2454148.6590	0.4693	1.5350	0.0086
2454152.6565	-0.2375	9.9000	0.0033	2454152.6563	-0.2376	1.1102	0.0149	2454152.6564	-0.2375	1.4515	0.0080
2454153.6452	-0.1650	9.7957	0.0026	2454153.6450	-0.1651	1.0536	0.0231	2454153.6451	-0.1650	1.4140	0.0078
2454154.6505	-0.0913	9.6750	0.0044	2454154.6503	-0.0913	1.0362	0.0368	2454154.6504	-0.0913	1.3575	0.0059
2454160.6236	0.3467	9.8674	0.0041	2454160.6234	0.3466	1.2250	0.0128	2454160.6235	0.3466	1.5364	0.0051
2454166.6268	-0.2131	9.8654	0.0039	2454166.6267	-0.2132	1.1295	0.0295	2454166.6268	-0.2132	1.4469	0.0085
2454764.9770	-0.3387	9.9772	0.0035	2454764.9768	-0.3387	1.1832	0.0096	2454764.9769	-0.3387	1.5084	0.0076
2454765.9667	-0.2661	9.9349	0.0017	2454765.9665	-0.2661	1.0784	0.0119	2454765.9666	-0.2661	1.4761	0.0038
2454766.9550	-0.1936	9.8557	0.0053	2454766.9558	-0.1936	1.0930	0.0128	2454766.9549	-0.1936	1.4252	0.0128
2454767.9376	-0.1216	9.7304	0.0003	2454767.9384	-0.1215	1.0317	0.0103	2454767.9375	-0.1216	1.3777	0.0056
2454768.9672	-0.0461	9.6223	0.0023	2454768.9649	-0.0463	1.0014	0.0179	2454768.9661	-0.0462	1.3505	0.0054
2454769.9714	0.0276	9.6126	0.0053	2454769.9723	0.0276	1.0127	0.0094	2454769.9714	0.0275	1.3571	0.0059
2454770.9688	0.1007	9.6537	0.0034	2454770.9697	0.1007	1.0940	0.0082	2454770.9687	0.1007	1.3957	0.0068
2454771.9592	0.1733	9.7275	0.0022	2454771.9591	0.1733	1.1244	0.0163	2454771.9592	0.1733	1.4348	0.0140

2454773.9404	0.3186	9.8530	0.0016	2454773.9402	0.3186	1.1738	0.0150	2454773.9404	0.3186	1.5203	0.0057
2454774.9434	0.3921	9.9107	0.0014	2454774.9433	0.3921	1.2650	0.0114	2454774.9434	0.3921	1.5369	0.0030
2454775.9241	0.4640	9.9653	0.0009	2454775.9218	0.4639	1.2309	0.0099	2454775.9230	0.4640	1.5518	0.0031
2454778.9197	-0.3163	9.9651	0.0018	2454778.9174	-0.3165	1.1639	0.0064	2454778.9186	-0.3164	1.5042	0.0046
2454779.9204	-0.2429	9.9089	0.0027	2454779.9224	-0.2428	1.1406	0.0204	2454779.9214	-0.2429	1.4654	0.0058
2454782.8901	-0.0252	9.6163	0.0060	2454782.8910	-0.0251	0.9382	0.0450	2454782.8912	-0.0251	1.3562	0.0218
2454794.8954	-0.1449	9.7691	0.0013	2454794.8932	-0.1450	1.0286	0.0077	2454794.8943	-0.1450	1.3937	0.0049
2454801.8681	0.3664	9.8949	0.0027	2454801.8679	0.3664	1.2399	0.0113	2454801.8680	0.3664	1.5364	0.0036
2454802.8669	0.4397	9.9467	0.0022	2454802.8667	0.4396	1.2308	0.0223	2454802.8668	0.4396	1.5527	0.0043
2454803.8751	-0.4864	9.9783	0.0029	2454803.8750	-0.4864	1.2122	0.0164	2454803.8751	-0.4864	1.5545	0.0044
2454821.8219	-0.1705	9.8193	0.0024	2454821.8217	-0.1705	1.0485	0.0224	2454821.8218	-0.1705	1.4191	0.0050
2454829.8030	0.4148	9.9318	0.0024	2454829.8029	0.4147	1.2542	0.0125	2454829.8030	0.4147	1.5540	0.0038
2454830.7925	0.4873	9.9730	0.0019	2454830.7923	0.4873	1.2412	0.0203	2454830.7924	0.4873	1.5592	0.0058
2454831.7919	-0.4394	9.9885	0.0020	2454831.7917	-0.4394	1.2542	0.0130	2454831.7919	-0.4394	1.5435	0.0033
2454832.7855	-0.3665	9.9845	0.0023	2454832.7853	-0.3666	1.1996	0.0211	2454832.7854	-0.3666	1.5259	0.0053
2455097.8466	0.0693	9.6377	0.0118	2455097.8464	0.0692	1.0314	0.0323	2455097.8465	0.0692	1.3797	0.0119
2455098.8423	0.1423	9.6880	0.0053	2455098.8421	0.1422	1.0658	0.0193	2455098.8422	0.1422	1.4270	0.0148
2455099.8383	0.2153	9.7526	0.0082	2455099.8381	0.2153	1.1475	0.0132	2455099.8383	0.2153	1.4702	0.0105
2455100.8413	0.2888	9.8338	0.0078	2455100.8421	0.2889	1.2291	0.0230	2455100.8412	0.2888	1.5072	0.0132
2455102.0099	0.3745	9.9039	0.0024	2455102.0097	0.3745	1.2427	0.0168	2455102.0098	0.3745	1.5517	0.0067
2455102.8700	0.4376	9.9409	0.0038	2455102.8699	0.4376	1.2757	0.0112	2455102.8700	0.4376	1.5558	0.0060
2455106.8238	-0.2725	9.9291	0.0071	2455131.9464	-0.4304	1.2081	0.0119	2455106.8238	-0.2725	1.4655	0.0104
2455131.9466	-0.4303	9.9910	0.0045	2455134.9361	-0.2111	1.1307	0.0108	2455131.9466	-0.4303	1.5427	0.0049
2455134.9363	-0.2111	9.8733	0.0035	2455135.7449	-0.1518	1.1058	0.0252	2455134.9363	-0.2111	1.4452	0.0085
2455135.7441	-0.1519	9.7710	0.0057	2455136.7441	-0.0786	1.1015	0.0142	2455135.7440	-0.1519	1.4113	0.0113
2455136.7432	-0.0786	9.6443	0.0042	2455137.7351	-0.0059	0.9842	0.0171	2455136.7443	-0.0786	1.3567	0.0049
2455137.7353	-0.0059	9.6135	0.0036	2455151.6985	0.0180	1.0486	0.0173	2455137.7352	-0.0059	1.3475	0.0145

2455151.7009	0.0182	9.6039	0.0051	2455152.6959	0.0911	1.0402	0.0071	2455151.6997	0.0181	1.3573	0.0072
2455152.6950	0.0911	9.6406	0.0060	2455153.6980	0.1646	1.1001	0.0300	2455152.6961	0.0911	1.4044	0.0072
2455153.6971	0.1645	9.7100	0.0029	2455154.6951	0.2377	1.1485	0.0100	2455153.6970	0.1645	1.4439	0.0030
2455154.6963	0.2378	9.7770	0.0040	2455155.6959	0.3111	1.2011	0.0186	2455154.6963	0.2378	1.4796	0.0067
2455155.6983	0.3113	9.8393	0.0056	2455156.6853	0.3836	1.2384	0.0082	2455155.6972	0.3112	1.5282	0.0116
2455156.6855	0.3837	9.9127	0.0038	2455581.7189	-0.4505	1.1300	0.0117	2455156.6854	0.3836	1.5416	0.0061
2455581.7191	-0.4504	9.9912	0.0024	2455584.7110	-0.2311	1.1167	0.0203	2455581.7190	-0.4504	1.5528	0.0111
2455584.7112	-0.2310	9.9034	0.0034	2455598.6310	-0.2104	1.1232	0.0080	2455584.7111	-0.2310	1.4518	0.0076
2455598.6312	-0.2103	9.8796	0.0033	2455599.6179	-0.1380	1.0702	0.0090	2455598.6311	-0.2104	1.4501	0.0061
2455599.6159	-0.1381	9.7658	0.0038	2455603.6230	0.1557	1.1046	0.0106	2455599.6169	-0.1381	1.4010	0.0054
2455603.6232	0.1557	9.7270	0.0055	2455604.6315	0.2296	1.1884	0.0134	2455603.6231	0.1557	1.4399	0.0070
2455604.6306	0.2296	9.7911	0.0045	2455605.6153	0.3018	1.2555	0.0100	2455604.6306	0.2296	1.4737	0.0059
2455605.6155	0.3018	9.8566	0.0039	2455607.6130	0.4483	1.3417	0.0105	2455605.6154	0.3018	1.5145	0.0056
2455607.6121	0.4482	9.9614	0.0028	2455608.6179	-0.4781	1.3577	0.0101	2455607.6120	0.4482	1.5676	0.0050
2455608.6170	-0.4781	9.9849	0.0027	2455900.8705	-0.0484	0.9982	0.0161	2455608.6170	-0.4781	1.5556	0.0072
2455900.8707	-0.0484	9.6300	0.0066	2455911.8321	-0.2447	1.1428	0.0127	2455900.8706	-0.0484	1.3433	0.0131
2455911.8301	-0.2448	9.9067	0.0030	2455921.7965	0.4860	1.2880	0.0207	2455911.8311	-0.2447	1.4707	0.0039
2455921.7978	0.4861	9.9890	0.0033	2455922.7892	-0.4412	1.2577	0.0412	2455921.7977	0.4861	1.5645	0.0041
2455922.7894	-0.4412	9.9967	0.0021	2455924.8143	-0.2927	1.1575	0.0437	2455922.7893	-0.4412	1.5649	0.0052
2455924.8134	-0.2928	9.9506	0.0020	2455925.7848	-0.2216	1.0915	0.0188	2455924.8145	-0.2927	1.5068	0.0046
2455925.7839	-0.2216	9.8969	0.0032	2455926.7808	-0.1485	1.0995	0.0108	2455925.7849	-0.2216	1.4521	0.0059
2455926.7799	-0.1486	9.7802	0.0038	2455927.7764	-0.0755	0.9817	0.0397	2455926.7798	-0.1486	1.4022	0.0095
2455927.7765	-0.0755	9.6663	0.0022					2455927.7765	-0.0755	1.3540	0.0083

Photometry of SZ Cas, cont…

HJD	Phase	V-R	V-R err	HJD	Phase	R-I	R-I err
2454075.7802	0.1254	1.2295	0.0066	2454075.7803	0.1255	0.9102	0.0089
2454076.5893	0.1848	1.2552	0.0069	2454076.5884	0.1847	0.9276	0.0104
2454077.7808	0.2721	1.2724	0.0043	2454077.7809	0.2722	0.9385	0.0032
2454080.5876	0.4780	1.3124	0.0053	2454080.5877	0.4780	0.9619	0.0049
2454081.7702	-0.4353	1.3206	0.0053	2454081.7703	-0.4353	0.9542	0.0064
2454083.7646	-0.2891	1.2853	0.0037	2454083.7647	-0.2891	0.9346	0.0045
2454085.7763	-0.1416	1.2301	0.0086	2454085.7765	-0.1416	0.8997	0.0080
2454086.7810	-0.0679	1.1917	0.0042	2454086.7811	-0.0679	0.8850	0.0060
2454088.7587	0.0771	1.2110	0.0054	2454088.7599	0.0772	0.9006	0.0081
2454090.7653	0.2242	1.2666	0.0045	2454090.7654	0.2243	0.9293	0.0039
2454094.7579	-0.4830	1.3008	0.0033	2454094.7580	-0.4830	0.9729	0.0031
2454100.7468	-0.0439	1.2075	0.0036	2454100.7469	-0.0438	0.8778	0.0059
2454101.6363	0.0214	1.2077	0.0044	2454101.6364	0.0214	0.8905	0.0049
2454102.7394	0.1023	1.2280	0.0103	2454102.7396	0.1023	0.8988	0.0072
2454103.7248	0.1745	1.2512	0.0061	2454103.7249	0.1745	0.9154	0.0087
2454104.7220	0.2476	1.2705	0.0046	2454104.7221	0.2476	0.9368	0.0058
2454105.7225	0.3210	1.3135	0.0064	2454105.7226	0.3210	0.9309	0.0063
2454107.7137	0.4670	1.3221	0.0034	2454107.7139	0.4670	0.9480	0.0074
2454108.6998	-0.4607	1.3256	0.0032	2454108.6999	-0.4607	0.9487	0.0034
2454115.6976	0.0524	1.2173	0.0018	2454115.6977	0.0524	0.8897	0.0026
2454116.6999	0.1259	1.2381	0.0060	2454116.7000	0.1259	0.9097	0.0053
2454117.6903	0.1985	1.2545	0.0040	2454117.6893	0.1985	0.9237	0.0069
2454124.6696	-0.2897	1.2878	0.0078	2454124.6697	-0.2897	0.9282	0.0083
2454125.6688	-0.2164	1.2548	0.0030	2454125.6671	-0.2166	0.9239	0.0110
2454127.6589	-0.0705	1.2032	0.0042	2454127.6590	-0.0705	0.8860	0.0032
2454128.6607	0.0030	1.1998	0.0062	2454128.6608	0.0030	0.8918	0.0063

2454134.6501	0.4421	1.3212	0.0036	2454134.6502	0.4421	0.9579	0.0041
2454135.6882	-0.4818	1.3170	0.0060	2454135.6884	-0.4817	0.9583	0.0042
2454136.6511	-0.4111	1.3119	0.0051	2454136.6513	-0.4111	0.9544	0.0042
2454137.7028	-0.3340	1.3012	0.0032	2454137.7029	-0.3340	0.9460	0.0019
2454138.6521	-0.2644	1.2857	0.0042	2454138.6533	-0.2643	0.9413	0.0098
2454140.6474	-0.1181	1.2127	0.0050	2454140.6475	-0.1181	0.9005	0.0059
2454144.6733	0.1771	1.2508	0.0045	2454144.6724	0.1770	0.9150	0.0051
2454146.6756	0.3239	1.3024	0.0060	2454146.6757	0.3239	0.9387	0.0080
2454147.6710	0.3969	1.3196	0.0035	2454147.6711	0.3969	0.9433	0.0036
2454148.6591	0.4693	1.3279	0.0079	2454148.6592	0.4694	0.9603	0.0073
2454152.6566	-0.2375	1.2797	0.0037	2454152.6567	-0.2375	0.9237	0.0047
2454153.6453	-0.1650	1.2401	0.0037	2454153.6454	-0.1650	0.9100	0.0029
2454154.6506	-0.0913	1.2060	0.0073	2454154.6507	-0.0913	0.8882	0.0063
2454160.6237	0.3467	1.3028	0.0045	2454160.6238	0.3467	0.9404	0.0025
2454166.6269	-0.2131	1.2599	0.0052	2454166.6270	-0.2131	0.9190	0.0050
2454764.9771	-0.3387	1.2944	0.0040	2454764.9772	-0.3387	0.9556	0.0032
2454765.9678	-0.2660	1.2913	0.0026	2454765.9679	-0.2660	0.9305	0.0035
2454766.9561	-0.1936	1.2538	0.0058	2454766.9562	-0.1935	0.9262	0.0074
2454767.9376	-0.1216	1.2191	0.0030	2454767.9378	-0.1216	0.9032	0.0048
2454768.9662	-0.0462	1.1867	0.0068	2454768.9653	-0.0462	0.8879	0.0087
2454769.9715	0.0276	1.2044	0.0061	2454769.9716	0.0276	0.8921	0.0038
2454770.9689	0.1007	1.2156	0.0060	2454770.9690	0.1007	0.9053	0.0076
2454771.9593	0.1733	1.2484	0.0030	2454771.9594	0.1733	0.9272	0.0033
2454773.9405	0.3186	1.2963	0.0058	2454773.9406	0.3186	0.9480	0.0061
2454774.9435	0.3921	1.2993	0.0017	2454774.9436	0.3921	0.9615	0.0067
2454775.9231	0.4640	1.3179	0.0013	2454775.9222	0.4639	0.9710	0.0017
2454778.9198	-0.3163	1.2973	0.0020	2454778.9188	-0.3164	0.9413	0.0028

2454779.9205	-0.2429	1.2691	0.0027	2454779.9206	-0.2429	0.9293	0.0031
2454782.8913	-0.0251	1.1755	0.0092	2454782.8914	-0.0251	0.8967	0.0120
2454794.8955	-0.1449	1.2292	0.0030	2454794.8946	-0.1449	0.9073	0.0052
2454801.8682	0.3664	1.3036	0.0038	2454801.8683	0.3664	0.9588	0.0038
2454802.8670	0.4396	1.3177	0.0026	2454802.8671	0.4396	0.9618	0.0026
2454803.8752	-0.4864	1.3144	0.0034	2454803.8753	-0.4864	0.9634	0.0029
2454821.8219	-0.1705	1.2464	0.0026	2454821.8221	-0.1705	0.9165	0.0066
2454829.8031	0.4148	1.3196	0.0030	2454829.8032	0.4148	0.9497	0.0031
2454830.7925	0.4873	1.3163	0.0032	2454830.7926	0.4873	0.9629	0.0050
2454831.7920	-0.4394	1.3155	0.0021	2454831.7921	-0.4394	0.9608	0.0030
2454832.7855	-0.3666	1.3076	0.0035	2454832.7857	-0.3665	0.9550	0.0044
2455097.8467	0.0693	1.2225	0.0170	2455097.8468	0.0693	0.9087	0.0145
2455098.8423	0.1423	1.2363	0.0127	2455098.8425	0.1423	0.9190	0.0153
2455099.8384	0.2153	1.2707	0.0136	2455099.8385	0.2153	0.9272	0.0129
2455100.8413	0.2888	1.2924	0.0095	2455100.8414	0.2888	0.9504	0.0080
2455102.0089	0.3744	1.3079	0.0076	2455102.0079	0.3744	0.9646	0.0089
2455102.8701	0.4376	1.3216	0.0068	2455102.8702	0.4376	0.9689	0.0078
2455106.8239	-0.2725	1.2756	0.0103	2455106.8240	-0.2725	0.9467	0.0103
2455131.9467	-0.4303	1.3131	0.0072	2455131.9468	-0.4303	0.9606	0.0069
2455134.9364	-0.2111	1.2624	0.0038	2455134.9365	-0.2111	0.9257	0.0037
2455135.7441	-0.1519	1.2264	0.0090	2455135.7442	-0.1519	0.9181	0.0073
2455136.7433	-0.0786	1.1993	0.0093	2455136.7434	-0.0786	0.8989	0.0132
2455137.7353	-0.0059	1.2086	0.0062	2455137.7355	-0.0059	0.8952	0.0101
2455151.7009	0.0182	1.1888	0.0123	2455151.7000	0.0181	0.8915	0.0148
2455152.6951	0.0911	1.2114	0.0076	2455152.6952	0.0911	0.9130	0.0063
2455153.6961	0.1645	1.2548	0.0048	2455153.6952	0.1644	0.9203	0.0042
2455154.6953	0.2377	1.2809	0.0098	2455154.6944	0.2377	0.9398	0.0098

2455155.6984	0.3113	1.2997	0.0103	2455155.6985	0.3113	0.9540	0.0130
2455156.6855	0.3837	1.3095	0.0085	2455156.6857	0.3837	0.9571	0.0113
2455581.7191	-0.4504	1.3180	0.0035	2455581.7193	-0.4504	0.9738	0.0042
2455584.7112	-0.2310	1.2783	0.0065	2455584.7114	-0.2310	0.9378	0.0069
2455598.6312	-0.2103	1.2553	0.0038	2455598.6303	-0.2104	0.9422	0.0029
2455599.6171	-0.1381	1.2206	0.0070	2455599.6172	-0.1380	0.9260	0.0063
2455603.6232	0.1557	1.2496	0.0057	2455603.6234	0.1557	0.9314	0.0095
2455604.6307	0.2296	1.2672	0.0061	2455604.6308	0.2296	0.9452	0.0056
2455605.6156	0.3018	1.2947	0.0044	2455605.6157	0.3018	0.9631	0.0032
2455607.6132	0.4483	1.3254	0.0029	2455607.6133	0.4483	0.9719	0.0021
2455608.6171	-0.4781	1.3150	0.0045	2455608.6172	-0.4781	0.9755	0.0044
2455900.8707	-0.0484	1.2060	0.0066	2455900.8709	-0.0484	0.9042	0.0022
2455911.8301	-0.2448	1.2708	0.0039	2455911.8303	-0.2448	0.9459	0.0041
2455921.7978	0.4861	1.3245	0.0034	2455921.7969	0.4860	0.9839	0.0038
2455922.7895	-0.4412	1.3182	0.0025	2455922.7896	-0.4412	0.9779	0.0045
2455924.8146	-0.2927	1.2930	0.0031	2455924.8158	-0.2926	0.9509	0.0040
2455925.7839	-0.2216	1.2693	0.0041	2455925.7840	-0.2216	0.9455	0.0041
2455926.7799	-0.1486	1.2281	0.0044	2455926.7801	-0.1486	0.9286	0.0033
2455927.7766	-0.0755	1.2076	0.0092	2455927.7767	-0.0755	0.9095	0.0098

Photometry of SZ Tau

HJD	Phase	V-mag	V-err	HJD	Phase	b-y	b-y err
2453415.6326	0.4852	6.6865	0.0029	2453415.6325	0.4852	0.6462	0.0038
2453415.7360	-0.4820	6.7009	0.0038	2453415.7359	-0.4820	0.6357	0.0045
2453432.6914	-0.0973	6.3786	0.0043	2453432.6914	-0.0973	0.5278	0.0064
2453433.6865	0.2187	6.4925	0.0044	2453433.6865	0.2187	0.5845	0.0053
2453437.6724	0.4845	6.7001	0.0072	2453437.6723	0.4845	0.6477	0.0081
2453438.6689	-0.1990	6.4760	0.0061	2453438.6689	-0.1990	0.5629	0.0108
2453439.6657	0.1176	6.3922	0.0052	2453439.6656	0.1175	0.5586	0.0082
2453442.6592	0.0682	6.3661	0.0063	2453442.6591	0.0682	0.5399	0.0100
2453444.6523	-0.2988	6.5952	0.0047	2453444.6522	-0.2988	0.5882	0.0075
2453445.6511	0.0184	6.3479	0.0064	2453445.6510	0.0184	0.5330	0.0081
2453446.6432	0.3335	6.6051	0.0058	2453446.6432	0.3335	0.6194	0.0071
2453451.6333	-0.0818	6.3675	0.0073	2453451.6332	-0.0818	0.5377	0.0081
2453452.6335	0.2359	6.5085	0.0038	2453452.6335	0.2358	0.5896	0.0059
2453696.8202	-0.2160	6.4917	0.0008	2453696.8202	-0.2160	0.5529	0.0063
2453700.8185	0.0537	6.3541	0.0057	2453700.8184	0.0537	0.5338	0.0087
2453708.9033	-0.3787	6.6695	0.0040	2453708.9032	-0.3788	0.6032	0.0059
2453721.8860	-0.2557	6.5245	0.0037	2453721.8859	-0.2557	0.5669	0.0055
2453724.8611	-0.3109	6.5967	0.0028	2453724.8610	-0.3109	0.5934	0.0052
2453734.8014	-0.1541	6.4094	0.0085	2453734.8014	-0.1541	0.5353	0.0103
2453735.8035	0.1642	6.4366	0.0031	2453735.8034	0.1641	0.5621	0.0042
2453753.8014	-0.1201	6.3931	0.0044	2453753.8013	-0.1201	0.5311	0.0062

2453756.7866	-0.1721	6.4399	0.0042	2453756.7866	-0.1721	0.5460	0.0046
2453758.7836	0.4621	6.6947	0.0027	2453758.7835	0.4621	0.6311	0.0031
2453760.7618	0.0904	6.3696	0.0050	2453760.7618	0.0904	0.5411	0.0080
2453765.7714	-0.3187	6.6145	0.0236	2453765.7714	-0.3187	0.5974	0.0317
2453766.7650	-0.0032	6.3523	0.0195	2453766.7650	-0.0032	0.5269	0.0261
2453767.7605	0.3130	6.6030	0.0089	2453767.7604	0.3130	0.6127	0.0135
2453768.7543	-0.3714	6.6714	0.0088	2453768.7543	-0.3714	0.6061	0.0099
2453782.7068	0.0596	6.3797	0.0263	2453782.7046	0.0589	0.5156	0.0316
2453808.6491	0.2983	6.6020	0.0155	2453808.6490	0.2982	0.6027	0.0182
2453812.6387	-0.4347	6.7158	0.0133	2453812.6386	-0.4348	0.6209	0.0182
2454396.9625	0.1332	6.3987	0.0045	2454396.9625	0.1332	0.5616	0.0101
2454400.0371	0.1096	6.3923	0.0045	2454400.0370	0.1096	0.5479	0.0058
2454400.9371	0.3954	6.6462	0.0049	2454400.9370	0.3954	0.6328	0.0059
2454401.9561	-0.2810	6.5675	0.0038	2454401.9560	-0.2810	0.5764	0.0054
2454403.9495	0.3521	6.6217	0.0022	2454403.9494	0.3521	0.6216	0.0037
2454405.9981	0.0027	6.3409	0.0091	2454405.9980	0.0026	0.5224	0.0100
2454407.9825	-0.3671	6.6564	0.0057	2454407.9824	-0.3672	0.6068	0.0058
2454409.9745	0.2655	6.5359	0.0045	2454409.9745	0.2655	0.5960	0.0060
2454412.9409	0.2076	6.4737	0.0024	2454412.9408	0.2075	0.5816	0.0052
2454413.9908	-0.4590	6.6973	0.0032	2454413.9908	-0.4590	0.6323	0.0044
2454414.8294	-0.1927	6.4564	0.0034	2454414.8293	-0.1927	0.5499	0.0036
2454415.9433	0.1610	6.4346	0.0046	2454415.9433	0.1610	0.5549	0.0093
2454417.9842	-0.1908	6.4472	0.0059	2454417.9841	-0.1908	0.5414	0.0078
2454418.9805	0.1256	6.4017	0.0132	2454418.9805	0.1256	0.5437	0.0192
2454422.9781	0.3951	6.6656	0.0125	2454422.9781	0.3951	0.6193	0.0139
2454423.9740	-0.2886	6.5665	0.0089	2454423.9739	-0.2886	0.5850	0.0145
2454425.8896	0.3198	6.5932	0.0016	2454425.8895	0.3197	0.6044	0.0031

2454456.8777	0.1609	6.4465	0.0061	2454456.8777	0.1609	0.5558	0.0079
2454458.8531	-0.2118	6.4622	0.0114	2454458.8530	-0.2118	0.5522	0.0163
2454459.8457	0.1034	6.3785	0.0159	2454459.8456	0.1034	0.5426	0.0216
2454460.8369	0.4182	6.6883	0.0106	2454460.8368	0.4182	0.6236	0.0119
2454461.8643	-0.2555	6.5313	0.0082	2454461.8642	-0.2555	0.5554	0.0108
2454464.8621	-0.3035	6.6140	0.0171	2454464.8621	-0.3035	0.5810	0.0224
2454465.8611	0.0138	6.3469	0.0196	2454465.8610	0.0138	0.5192	0.0278
2454466.6580	0.2669	6.5498	0.0197	2454466.6580	0.2669	0.5894	0.0254
2454475.7866	0.1659	6.4314	0.0062	2454475.7865	0.1659	0.5640	0.0085
2454476.7773	0.4805	6.6977	0.0052	2454476.7772	0.4805	0.6301	0.0089
2454479.7751	0.4326	6.6778	0.0070	2454479.7750	0.4325	0.6252	0.0091
2454480.7635	-0.2535	6.5188	0.0065	2454480.7634	-0.2536	0.5655	0.0118
2454481.7662	0.0649	6.3614	0.0137	2454481.7661	0.0649	0.5282	0.0181
2454482.7604	0.3806	6.6490	0.0109	2454482.7603	0.3806	0.6215	0.0132
2454483.7644	-0.3005	6.5837	0.0091	2454483.7643	-0.3006	0.5810	0.0137
2454486.7468	-0.3534	6.6345	0.0091	2454484.7534	0.0136	0.5308	0.0111
2454494.7366	0.1840	6.4533	0.0146	2454486.7467	-0.3534	0.6019	0.0146
2454495.7622	-0.4903	6.7171	0.0087	2454494.7365	0.1840	0.5783	0.0175
2454496.7734	-0.1692	6.4372	0.0117	2454495.7622	-0.4903	0.6238	0.0124
2454498.7373	0.4545	6.7006	0.0096	2454496.7733	-0.1692	0.5321	0.0151
2454499.7294	-0.2304	6.5084	0.0133	2454498.7372	0.4545	0.6258	0.0115
2454503.7197	0.0368	6.3521	0.0182	2454499.7293	-0.2304	0.5547	0.0191
2454504.7031	0.3491	6.6205	0.0123	2454503.7217	0.0375	0.5253	0.0262
2454505.7264	-0.3259	6.6180	0.0088	2454504.7030	0.3491	0.6183	0.0166
2454508.7052	-0.3799	6.6852	0.0129	2454505.7264	-0.3259	0.5873	0.0098
2454509.6379	-0.0837	6.3810	0.0170	2454508.7052	-0.3799	0.5935	0.0135
2454821.7261	0.0284	6.3536	0.0054	2454509.6378	-0.0837	0.5287	0.0203

2454821.8608	0.0712	6.3585	0.0055	2454821.7260	0.0284	0.5274	0.0079
2454822.7074	0.3400	6.6191	0.0049	2454821.8607	0.0711	0.5391	0.0057
2454829.7078	-0.4368	6.7114	0.0031	2454822.7074	0.3400	0.6152	0.0063
2454829.8500	-0.3916	6.6925	0.0051	2454829.7078	-0.4368	0.6352	0.0034
2454830.6982	-0.1223	6.3912	0.0086	2454829.8499	-0.3917	0.6175	0.0053
2454831.7021	0.1966	6.4692	0.0066	2454830.6982	-0.1223	0.5287	0.0092
2454832.8252	-0.4468	6.7095	0.0021	2454831.7021	0.1965	0.5700	0.0103
2454838.6990	0.4186	6.6626	0.0146	2454832.8252	-0.4468	0.6397	0.0037
2454838.8025	0.4515	6.6907	0.0020	2454838.6989	0.4186	0.6410	0.0186
2454839.6749	-0.2715	6.5423	0.0036	2454838.8025	0.4515	0.6245	0.0049
2454839.8002	-0.2317	6.4983	0.0062	2454839.6748	-0.2715	0.5757	0.0049
2454840.6760	0.0465	6.3471	0.0089	2454839.7989	-0.2321	0.5619	0.0066
2454842.6770	-0.3181	6.5992	0.0080	2454840.6759	0.0464	0.5308	0.0090
2454844.6764	0.3169	6.6035	0.0037	2454842.6770	-0.3181	0.5956	0.0081
2454844.7861	0.3517	6.6249	0.0085	2454844.6763	0.3169	0.6131	0.0044
2454846.7920	-0.0112	6.3419	0.0080	2454844.7861	0.3517	0.6289	0.0091
2454847.7780	0.3019	6.5774	0.0072	2454846.7919	-0.0113	0.5252	0.0144
2454856.7780	0.1601	6.4342	0.0045	2454847.7779	0.3018	0.6113	0.0091
2454865.7522	0.0101	6.3546	0.0053	2454856.7780	0.1601	0.5618	0.0073
2454867.7471	-0.3564	6.6404	0.0034	2454865.7522	0.0101	0.5209	0.0085
2454873.7360	-0.4544	6.7113	0.0032	2454867.7471	-0.3564	0.6038	0.0038
2454875.7292	0.1786	6.4518	0.0043	2454873.7360	-0.4545	0.6383	0.0041
2455213.7664	-0.4686	6.7097	0.0023	2454875.7291	0.1785	0.5681	0.0053
2455221.6137	0.0236	6.3462	0.0074	2455213.7663	-0.4686	0.6304	0.0039
2455221.7454	0.0654	6.3577	0.0069	2455221.6136	0.0235	0.5185	0.0074
2455222.6172	0.3423	6.5949	0.0028	2455221.7441	0.0650	0.5450	0.0148
2455236.5997	-0.2172	6.4874	0.0028	2455222.6172	0.3423	0.6250	0.0056

2455236.7093	-0.1824	6.4513	0.0086	2455236.5996	-0.2173	0.5609	0.0050
2455240.7001	0.0850	6.3773	0.0093	2455236.7093	-0.1824	0.5446	0.0095
2455241.6910	0.3997	6.6651	0.0059	2455240.7001	0.0850	0.5382	0.0130
2455243.7210	0.0443	6.3504	0.0013	2455241.6909	0.3996	0.6232	0.0069
2455253.6765	0.2060	6.4893	0.0087	2455243.7209	0.0443	0.5291	0.0066
2455258.6939	-0.2006	6.4597	0.0067	2455253.6765	0.2060	0.5773	0.0121
2455259.6738	0.1106	6.3833	0.0065	2455258.6939	-0.2006	0.5520	0.0107
2455268.6784	-0.0298	6.3340	0.0063	2455259.6737	0.1105	0.5547	0.0100
2455270.6585	-0.4009	6.6783	0.0050	2455268.6771	-0.0302	0.5285	0.0134
2455271.6707	-0.0795	6.3546	0.0115	2455270.6584	-0.4010	0.6146	0.0074
2455273.6607	-0.4475	6.7071	0.0052	2455271.6694	-0.0799	0.5254	0.0148
2455274.6539	-0.1321	6.3898	0.0037	2455273.6607	-0.4475	0.6288	0.0068
2455275.6540	0.1855	6.4557	0.0094	2455274.6526	-0.1325	0.5294	0.0089
2455580.5975	0.0286	6.3546	0.0040	2455275.6527	0.1851	0.5732	0.0122
2455580.7695	0.0833	6.3726	0.0035	2455580.5974	0.0286	0.5277	0.0055
2455581.5900	0.3438	6.6172	0.0051	2455580.7682	0.0828	0.5395	0.0097
2455581.7675	0.4002	6.6626	0.0050	2455581.5912	0.3442	0.6232	0.0054
2455582.5902	-0.3385	6.6230	0.0039	2455581.7675	0.4002	0.6197	0.0065
2455582.7598	-0.2847	6.5691	0.0034	2455582.5901	-0.3386	0.6045	0.0058
2455583.5908	-0.0208	6.3461	0.0029	2455582.7597	-0.2847	0.5834	0.0063
2455583.7591	0.0327	6.3546	0.0067	2455583.5908	-0.0208	0.5316	0.0040
2455584.5914	0.2970	6.5779	0.0031	2455583.7590	0.0326	0.5356	0.0075
2455584.7597	0.3504	6.6231	0.0016	2455584.5914	0.2970	0.5993	0.0047
2455585.7536	-0.3339	6.6276	0.0054	2455584.7596	0.3504	0.6167	0.0038
2455588.5931	-0.4322	6.6976	0.0043	2455585.7535	-0.3340	0.6028	0.0060
2455588.7452	-0.3838	6.6790	0.0057	2455588.5931	-0.4322	0.6288	0.0070
2455589.7527	-0.0639	6.3592	0.0059	2455588.7451	-0.3839	0.6150	0.0066

2455591.7465	-0.4307	6.7012	0.0019	2455589.7526	-0.0639	0.5286	0.0086
2455592.5954	-0.1611	6.4307	0.0055	2455591.7464	-0.4307	0.6274	0.0055
2455595.7600	-0.1561	6.4257	0.0073	2455592.5953	-0.1612	0.5422	0.0079
2455596.7518	0.1589	6.4324	0.0052	2455595.7600	-0.1561	0.5400	0.0086
2455597.7477	0.4751	6.6969	0.0051	2455596.7517	0.1588	0.5583	0.0074
2455599.6913	0.0924	6.3791	0.0036	2455597.7489	0.4755	0.6339	0.0071
2455600.7450	0.4270	6.6791	0.0035	2455599.6913	0.0924	0.5493	0.0055
2455601.7416	-0.2565	6.5422	0.0060	2455600.7449	0.4270	0.6252	0.0043
2455602.7339	0.0586	6.3604	0.0059	2455601.7415	-0.2565	0.5757	0.0097
2455603.6898	0.3622	6.6342	0.0026	2455602.7338	0.0586	0.5403	0.0102
2455604.7298	-0.3075	6.6021	0.0036	2455603.6897	0.3622	0.6183	0.0047
2455605.7062	0.0026	6.3299	0.0004	2455604.7298	-0.3075	0.5871	0.0052
2455607.7047	-0.3627	6.6527	0.0054	2455605.7062	0.0026	0.5317	0.0051
2455608.7165	-0.0414	6.3567	0.0030	2455607.7046	-0.3628	0.6148	0.0068
2455614.7079	-0.1387	6.4068	0.0086	2455608.7164	-0.0415	0.5273	0.0034
2455615.6930	0.1742	6.4451	0.0048	2455614.7079	-0.1387	0.5326	0.0115
2455616.6944	0.4922	6.7051	0.0028	2455615.6929	0.1741	0.5665	0.0059
2455617.6769	-0.1958	6.4735	0.0038	2455616.6943	0.4921	0.6358	0.0034
2455621.6878	0.0780	6.3669	0.0080	2455617.6756	-0.1962	0.5582	0.0081
2455944.7763	-0.3165	6.6133	0.0053	2455621.6877	0.0779	0.5343	0.0101
				2455944.7762	-0.3165	0.5931	0.0064

Photometry of SZ Tau, cont…

HJD	Phase	c1	c1 err	HJD	Phase	m1	m1 err
2453415.6323	0.4851	0.5927	0.0078	2453415.6325	0.4852	0.2166	0.0063

2453415.7357	-0.4821	0.5923	0.0080	2453415.7359	-0.4820	0.2227	0.0065
2453432.6912	-0.0974	0.8143	0.0223	2453432.6913	-0.0973	0.1823	0.0148
2453433.6863	0.2186	0.7066	0.0165	2453433.6864	0.2187	0.1975	0.0104
2453437.6722	0.4845	0.5923	0.0219	2453437.6723	0.4845	0.2155	0.0165
2453438.6687	-0.1991	0.7374	0.0181	2453438.6688	-0.1990	0.1784	0.0151
2453439.6654	0.1175	0.7909	0.0130	2453439.6655	0.1175	0.1765	0.0121
2453442.6589	0.0681	0.8096	0.0225	2453442.6591	0.0682	0.1848	0.0175
2453444.6520	-0.2989	0.6712	0.0175	2453444.6522	-0.2988	0.2034	0.0143
2453445.6508	0.0183	0.8274	0.0202	2453445.6509	0.0183	0.1808	0.0141
2453446.6430	0.3334	0.6470	0.0143	2453446.6431	0.3334	0.2100	0.0106
2453451.6331	-0.0819	0.8235	0.0311	2453451.6332	-0.0818	0.1711	0.0163
2453452.6333	0.2358	0.6969	0.0121	2453452.6334	0.2358	0.2017	0.0098
2453696.8200	-0.2161	0.7104	0.0088	2453696.8201	-0.2161	0.2165	0.0091
2453700.8183	0.0537	0.8476	0.0123	2453700.8184	0.0537	0.1759	0.0130
2453708.9030	-0.3788	0.6413	0.0132	2453708.9032	-0.3788	0.2329	0.0097
2453721.8857	-0.2558	0.7222	0.0093	2453721.8858	-0.2558	0.1927	0.0083
2453724.8609	-0.3110	0.6877	0.0119	2453724.8610	-0.3109	0.1968	0.0099
2453734.8012	-0.1541	0.7891	0.0108	2453734.8013	-0.1541	0.1904	0.0124
2453735.8032	0.1641	0.7795	0.0093	2453735.8033	0.1641	0.1861	0.0064
2453753.8011	-0.1202	0.8186	0.0164	2453753.8012	-0.1202	0.1823	0.0103
2453756.7864	-0.1721	0.7718	0.0107	2453756.7865	-0.1721	0.1833	0.0072
2453758.7833	0.4620	0.6215	0.0068	2453758.7834	0.4621	0.2273	0.0055
2453760.7616	0.0903	0.8236	0.0231	2453760.7617	0.0903	0.1842	0.0174
2453765.7712	-0.3188	0.6524	0.0238	2453765.7713	-0.3187	0.2102	0.0384
2453766.7648	-0.0032	0.8317	0.0216	2453766.7649	-0.0032	0.1789	0.0322
2453767.7602	0.3129	0.6315	0.0167	2453767.7604	0.3130	0.2158	0.0181
2453768.7541	-0.3715	0.6410	0.0137	2453768.7542	-0.3714	0.2159	0.0138

2453782.7030	0.0584	0.8481	0.0250	2453782.7036	0.0586	0.1960	0.0382
2453808.6489	0.2982	0.6651	0.0145	2453808.6490	0.2982	0.2135	0.0216
2453812.6385	-0.4348	0.6066	0.0179	2453812.6386	-0.4348	0.2349	0.0232
2454396.9623	0.1331	0.7935	0.0152	2454396.9624	0.1331	0.1807	0.0156
2454400.0368	0.1095	0.8087	0.0090	2454400.0369	0.1095	0.1792	0.0082
2454400.9374	0.3955	0.6294	0.0089	2454400.9369	0.3954	0.2193	0.0087
2454401.9558	-0.2811	0.7007	0.0066	2454401.9560	-0.2810	0.1991	0.0076
2454403.9492	0.3520	0.6472	0.0089	2454403.9494	0.3521	0.2096	0.0060
2454405.9984	0.0028	0.8455	0.0139	2454405.9980	0.0026	0.1827	0.0129
2454407.9828	-0.3670	0.6604	0.0061	2454407.9823	-0.3672	0.2065	0.0073
2454409.9749	0.2656	0.6912	0.0079	2454409.9744	0.2655	0.2046	0.0081
2454412.9406	0.2075	0.7296	0.0124	2454412.9408	0.2075	0.1924	0.0092
2454413.9906	-0.4591	0.6173	0.0116	2454413.9907	-0.4591	0.2141	0.0082
2454414.8302	-0.1925	0.7508	0.0114	2454414.8293	-0.1927	0.1882	0.0078
2454415.9431	0.1610	0.7795	0.0139	2454415.9432	0.1610	0.1954	0.0142
2454417.9846	-0.1907	0.7672	0.0058	2454417.9841	-0.1908	0.1903	0.0095
2454418.9809	0.1257	0.8036	0.0208	2454418.9804	0.1256	0.1885	0.0260
2454422.9779	0.3951	0.6292	0.0120	2454422.9780	0.3951	0.2188	0.0164
2454423.9737	-0.2887	0.7120	0.0167	2454423.9738	-0.2887	0.1856	0.0203
2454425.8893	0.3197	0.6629	0.0135	2454425.8895	0.3197	0.2207	0.0097
2454456.8775	0.1608	0.7557	0.0133	2454456.8776	0.1608	0.1969	0.0127
2454458.8528	-0.2119	0.7337	0.0184	2454458.8530	-0.2118	0.2001	0.0212
2454459.8454	0.1033	0.8093	0.0286	2454459.8456	0.1034	0.1840	0.0302
2454460.8366	0.4181	0.6199	0.0087	2454460.8368	0.4182	0.2219	0.0137
2454461.8641	-0.2556	0.7050	0.0121	2454461.8642	-0.2555	0.2082	0.0147
2454464.8619	-0.3035	0.6781	0.0227	2454464.8620	-0.3035	0.2031	0.0285
2454465.8609	0.0137	0.8459	0.0264	2454465.8610	0.0138	0.1826	0.0361

2454466.6590	0.2672	0.6900	0.0180	2454466.6585	0.2670	0.2130	0.0306
2454475.7870	0.1660	0.7603	0.0140	2454475.7865	0.1659	0.1936	0.0129
2454476.7771	0.4805	0.6228	0.0129	2454476.7772	0.4805	0.2225	0.0133
2454479.7748	0.4325	0.6391	0.0123	2454479.7749	0.4325	0.2192	0.0130
2454480.7638	-0.2535	0.7282	0.0252	2454480.7633	-0.2536	0.1908	0.0217
2454481.7659	0.0648	0.8264	0.0377	2454481.7660	0.0648	0.1936	0.0322
2454482.7607	0.3807	0.6433	0.0110	2454482.7603	0.3806	0.2133	0.0160
2454483.7641	-0.3006	0.7143	0.0246	2454483.7643	-0.3006	0.1968	0.0233
2454484.7532	0.0135	0.8402	0.0196	2454484.7533	0.0135	0.1803	0.0180
2454486.7466	-0.3534	0.6688	0.0234	2454486.7467	-0.3534	0.2035	0.0235
2454494.7364	0.1839	0.7285	0.0217	2454494.7365	0.1840	0.1858	0.0238
2454495.7620	-0.4904	0.6368	0.0124	2454495.7621	-0.4903	0.2210	0.0163
2454496.7731	-0.1693	0.7771	0.0133	2454496.7732	-0.1692	0.1950	0.0186
2454498.7371	0.4545	0.6187	0.0104	2454498.7372	0.4545	0.2247	0.0136
2454499.7302	-0.2302	0.7152	0.0287	2454499.7293	-0.2304	0.1997	0.0295
2454503.7205	0.0371	0.8339	0.0347	2454503.7217	0.0375	0.1894	0.0379
2454504.7029	0.3491	0.6500	0.0190	2454504.7030	0.3491	0.2119	0.0225
2454505.7262	-0.3260	0.6809	0.0112	2454505.7263	-0.3259	0.2073	0.0129
2454508.7050	-0.3800	0.6329	0.0118	2454508.7051	-0.3799	0.2363	0.0158
2454509.6376	-0.0838	0.8295	0.0215	2454509.6378	-0.0837	0.1755	0.0262
2454821.7264	0.0285	0.8385	0.0102	2454821.7259	0.0283	0.1854	0.0114
2454821.8612	0.0713	0.8112	0.0246	2454821.8607	0.0711	0.1903	0.0181
2454822.7090	0.3405	0.6549	0.0043	2454822.7079	0.3402	0.2178	0.0075
2454829.7088	-0.4365	0.6028	0.0075	2454829.7077	-0.4368	0.2278	0.0062
2454829.8497	-0.3917	0.6569	0.0090	2454829.8498	-0.3917	0.2096	0.0082
2454830.6980	-0.1223	0.8107	0.0083	2454830.6981	-0.1223	0.1872	0.0110
2454831.7019	0.1965	0.7382	0.0158	2454831.7020	0.1965	0.2007	0.0162

2454832.8250	-0.4469	0.6132	0.0082	2454832.8251	-0.4468	0.2101	0.0058
2454838.6987	0.4185	0.6274	0.0120	2454838.6989	0.4186	0.2166	0.0219
2454838.8023	0.4514	0.6127	0.0104	2454838.8024	0.4514	0.2315	0.0088
2454839.6758	-0.2712	0.7130	0.0060	2454839.6747	-0.2715	0.1916	0.0062
2454839.7993	-0.2320	0.7195	0.0044	2454839.7988	-0.2321	0.1976	0.0073
2454840.6757	0.0464	0.8424	0.0096	2454840.6758	0.0464	0.1837	0.0105
2454842.6768	-0.3181	0.6823	0.0062	2454842.6769	-0.3181	0.1967	0.0088
2454844.6761	0.3168	0.6720	0.0129	2454844.6762	0.3168	0.2056	0.0102
2454844.7859	0.3517	0.6134	0.0165	2454844.7860	0.3517	0.2149	0.0142
2454846.7917	-0.0113	0.8436	0.0204	2454846.7919	-0.0113	0.1829	0.0215
2454847.7777	0.3018	0.6681	0.0129	2454847.7778	0.3018	0.2075	0.0125
2454856.7778	0.1600	0.7740	0.0128	2454856.7779	0.1600	0.1897	0.0122
2454865.7520	0.0100	0.8613	0.0144	2454865.7521	0.0100	0.1827	0.0140
2454867.7469	-0.3565	0.6619	0.0060	2454867.7470	-0.3564	0.2160	0.0045
2454873.7340	-0.4551	0.6220	0.0061	2454873.7353	-0.4547	0.2157	0.0053
2454875.7289	0.1784	0.7517	0.0163	2454875.7290	0.1785	0.1967	0.0128
2455213.7668	-0.4684	0.6248	0.0068	2455213.7662	-0.4686	0.2241	0.0061
2455221.6147	0.0239	0.8631	0.0079	2455221.6136	0.0235	0.1842	0.0087
2455221.7426	0.0645	0.8405	0.0159	2455221.7434	0.0648	0.1628	0.0200
2455222.6170	0.3422	0.6458	0.0069	2455222.6171	0.3422	0.2077	0.0081
2455236.5994	-0.2173	0.7349	0.0151	2455236.5995	-0.2173	0.1917	0.0067
2455236.7091	-0.1825	0.7592	0.0141	2455236.7092	-0.1825	0.1950	0.0110
2455240.7005	0.0851	0.8339	0.0161	2455240.7000	0.0849	0.1793	0.0183
2455241.6894	0.3991	0.6282	0.0051	2455241.6902	0.3994	0.2308	0.0080
2455243.7195	0.0439	0.8480	0.0147	2455243.7202	0.0441	0.1869	0.0116
2455253.6769	0.2061	0.7251	0.0177	2455253.6764	0.2059	0.1985	0.0183
2455258.6930	-0.2009	0.7461	0.0219	2455258.6932	-0.2008	0.1861	0.0198

2455259.6723	0.1101	0.8018	0.0136	2455259.6730	0.1103	0.1785	0.0145
2455268.6757	-0.0306	0.8641	0.0212	2455268.6764	-0.0304	0.1669	0.0191
2455270.6608	-0.4002	0.6392	0.0058	2455270.6590	-0.4008	0.2161	0.0093
2455271.6680	-0.0803	0.8386	0.0121	2455271.6687	-0.0801	0.1776	0.0179
2455273.6598	-0.4478	0.6156	0.0069	2455273.6606	-0.4475	0.2252	0.0084
2455274.6524	-0.1326	0.8118	0.0171	2455274.6519	-0.1327	0.1872	0.0138
2455275.6519	0.1849	0.7527	0.0189	2455275.6520	0.1849	0.1853	0.0188
2455580.5979	0.0287	0.8522	0.0082	2455580.5974	0.0286	0.1820	0.0075
2455580.7680	0.0828	0.8371	0.0133	2455580.7675	0.0826	0.1831	0.0149
2455581.5903	0.3439	0.6609	0.0074	2455581.5911	0.3442	0.2000	0.0065
2455581.7673	0.4001	0.6399	0.0082	2455581.7674	0.4002	0.2212	0.0088
2455582.5918	-0.3380	0.6715	0.0068	2455582.5907	-0.3384	0.2034	0.0077
2455582.7602	-0.2846	0.6991	0.0105	2455582.7597	-0.2847	0.1987	0.0094
2455583.5912	-0.0207	0.8579	0.0160	2455583.5907	-0.0208	0.1721	0.0117
2455583.7588	0.0326	0.8570	0.0105	2455583.7589	0.0326	0.1696	0.0107
2455584.5918	0.2971	0.6954	0.0165	2455584.5913	0.2970	0.2075	0.0112
2455584.7601	0.3506	0.6546	0.0085	2455584.7596	0.3504	0.2177	0.0061
2455585.7546	-0.3336	0.6857	0.0075	2455585.7534	-0.3340	0.1973	0.0068
2455588.5929	-0.4322	0.6103	0.0090	2455588.5930	-0.4322	0.2223	0.0096
2455588.7462	-0.3835	0.6568	0.0080	2455588.7451	-0.3839	0.2068	0.0084
2455589.7524	-0.0640	0.8405	0.0120	2455589.7526	-0.0639	0.1797	0.0128
2455591.7481	-0.4302	0.6427	0.0085	2455591.7470	-0.4306	0.2140	0.0078
2455592.5957	-0.1610	0.7910	0.0137	2455592.5952	-0.1612	0.1885	0.0116
2455595.7598	-0.1562	0.7906	0.0142	2455595.7599	-0.1561	0.1856	0.0132
2455596.7522	0.1590	0.7805	0.0079	2455596.7516	0.1588	0.1920	0.0100
2455597.7481	0.4753	0.6177	0.0107	2455597.7489	0.4755	0.2228	0.0089
2455599.6911	0.0923	0.8175	0.0114	2455599.6912	0.0923	0.1764	0.0101

2455600.7466	0.4275	0.6278	0.0050	2455600.7455	0.4272	0.2287	0.0057
2455601.7420	-0.2564	0.7168	0.0100	2455601.7415	-0.2565	0.1912	0.0130
2455602.7343	0.0588	0.8476	0.0114	2455602.7338	0.0586	0.1725	0.0139
2455603.6895	0.3621	0.6378	0.0080	2455603.6896	0.3621	0.2218	0.0064
2455604.7296	-0.3076	0.6861	0.0166	2455604.7297	-0.3075	0.2009	0.0130
2455605.7060	0.0025	0.8407	0.0163	2455605.7061	0.0025	0.1831	0.0123
2455607.7032	-0.3632	0.6490	0.0052	2455607.7039	-0.3630	0.2063	0.0082
2455608.7169	-0.0413	0.8576	0.0116	2455608.7164	-0.0415	0.1781	0.0060
2455614.7083	-0.1386	0.8108	0.0185	2455614.7078	-0.1387	0.1881	0.0182
2455616.6948	0.4923	0.6336	0.0066	2455615.6929	0.1741	0.1891	0.0086
2455617.6748	-0.1965	0.7509	0.0081	2455616.6943	0.4921	0.2148	0.0056
2455621.6876	0.0779	0.8219	0.0093	2455617.6749	-0.1964	0.1829	0.0111
2455944.7760	-0.3166	0.6831	0.0063	2455621.6877	0.0779	0.1897	0.0127
				2455944.7762	-0.3165	0.2031	0.0075

Photometry of VY Cyg

HJD	Phase	V-mag	V-err	HJD	Phase	U-B	U-B err	HJD	Phase	B-V	B-V err
2453665.7581	-0.3147	9.0349	0.0040	2453665.7579	-0.3147	1.2161	0.0067	2453665.7580	-0.3147	1.3171	0.0043
2453667.7527	-0.0608	8.3856	0.0053	2453667.7525	-0.0609	0.7865	0.0102	2453667.7526	-0.0608	0.9654	0.0073
2453669.6124	0.1759	8.4436	0.0043	2453669.6122	0.1758	0.8798	0.0046	2453669.6123	0.1758	1.0473	0.0047
2453670.6157	0.3036	8.4310	0.0028	2453670.6155	0.3035	0.9022	0.0071	2453670.6156	0.3035	1.0621	0.0039
2453671.6152	0.4308	8.7382	0.0057	2453671.6150	0.4307	1.0431	0.0051	2453671.6151	0.4307	1.2244	0.0064
2453672.6156	-0.4419	8.8815	0.0036	2453672.6153	-0.4420	1.1652	0.0063	2453672.6155	-0.4419	1.2832	0.0037
2453673.6149	-0.3147	9.0400	0.0041	2453673.6146	-0.3148	1.2366	0.0033	2453673.6148	-0.3147	1.3256	0.0046
2453674.6144	-0.1875	8.9191	0.0055	2453674.6142	-0.1875	1.0074	0.0068	2453674.6143	-0.1875	1.2011	0.0062
2453675.7322	-0.0453	8.3157	0.0055	2453675.7320	-0.0453	0.7541	0.0120	2453675.7321	-0.0453	0.9332	0.0086
2453677.7265	0.2086	8.4201	0.0064	2453677.7263	0.2085	0.8658	0.0090	2453677.7264	0.2086	1.0343	0.0074
2453678.7234	0.3354	8.5118	0.0042	2453678.7232	0.3354	0.9331	0.0117	2453678.7233	0.3354	1.1046	0.0054
2453679.6115	0.4485	8.7545	0.0031	2453679.6112	0.4484	1.0565	0.0080	2453679.6114	0.4485	1.2332	0.0033
2453680.6110	-0.4243	8.9037	0.0031	2453680.6107	-0.4244	1.1868	0.0043	2453680.6109	-0.4243	1.2931	0.0040
2453688.6074	-0.4066	8.9305	0.0069	2453688.6072	-0.4066	1.2188	0.0109	2453688.6073	-0.4066	1.3083	0.0081
2453689.6111	-0.2788	9.0504	0.0092	2453689.6108	-0.2789	1.1559	0.0129	2453689.6110	-0.2789	1.3055	0.0096
2453690.6150	-0.1511	8.8853	0.0090	2453690.6147	-0.1511	0.8947	0.0283	2453690.6149	-0.1511	1.1298	0.0117
2453691.6292	-0.0220	8.2454	0.0086	2453691.6289	-0.0220	0.7678	0.0185	2453691.6291	-0.0220	0.9039	0.0103
2453693.6061	0.2296	8.3976	0.0047	2453693.6059	0.2296	0.8786	0.0091	2453693.6060	0.2296	1.0355	0.0063
2453694.6051	0.3568	8.5927	0.0109	2453694.6049	0.3567	0.9711	0.0058	2453694.6050	0.3567	1.1543	0.0116
2453695.6048	0.4840	8.7878	0.0050	2453695.6046	0.4840	1.0968	0.0058	2453695.6047	0.4840	1.2524	0.0055

2453699.5750	-0.0107	8.2381	0.0059	2453699.5776	-0.0104	0.7810	0.0058	2453699.5763	-0.0105	0.9102	0.0068
2453701.5973	0.2467	8.3812	0.0038	2453701.5971	0.2466	0.8730	0.0108	2453701.5972	0.2467	1.0417	0.0051
2453702.6427	0.3797	8.6731	0.0026	2453702.6411	0.3795	0.9959	0.0036	2453702.6412	0.3795	1.1862	0.0033
2453703.6286	-0.4948	8.8128	0.0044	2453703.6284	-0.4948	1.1291	0.0065	2453703.6285	-0.4948	1.2503	0.0058
2453705.5970	-0.2443	9.0340	0.0027	2453705.5968	-0.2443	1.1247	0.0099	2453705.5969	-0.2443	1.2794	0.0030
2453706.5970	-0.1170	8.6684	0.0030	2453706.5968	-0.1170	0.8414	0.0106	2453706.5969	-0.1170	1.0825	0.0046
2453708.6057	0.1387	8.4403	0.0325	2453708.6055	0.1386	0.8588	0.0131	2453708.6056	0.1386	1.0213	0.0328
2453709.5968	0.2648	8.3920	0.0035	2453709.5966	0.2648	0.8673	0.0069	2453709.5967	0.2648	1.0335	0.0038
2453710.5969	0.3921	8.6998	0.0044	2453710.5967	0.3921	1.0183	0.0050	2453710.5968	0.3921	1.1931	0.0062
2453711.5970	-0.4806	8.8332	0.0040	2453711.5968	-0.4807	1.1382	0.0115	2453711.5969	-0.4806	1.2598	0.0048
2453712.5970	-0.3534	9.0077	0.0043	2453712.5968	-0.3534	1.2122	0.0097	2453712.5969	-0.3534	1.3196	0.0046
2453714.5973	-0.0988	8.5967	0.0036	2453714.5971	-0.0988	0.8380	0.0095	2453714.5972	-0.0988	1.0500	0.0048
2453724.5784	0.1715	8.4290	0.0280	2453724.5782	0.1715	0.8784	0.0309	2453724.5783	0.1715	1.0398	0.0317
2453725.5757	0.2985	8.4221	0.0119	2453725.5755	0.2985	0.8799	0.0123	2453725.5756	0.2985	1.0681	0.0128
2453726.5760	0.4258	8.7461	0.0005	2453726.5758	0.4258	1.0951	0.0234	2453726.5759	0.4258	1.2335	0.0048
2454001.8317	0.4584	8.7462	0.0042	2454001.8315	0.4584	1.0988	0.0118	2454001.8316	0.4584	1.2263	0.0046
2454003.7980	-0.2913	9.0344	0.0031	2454003.7978	-0.2914	1.1681	0.0023	2454003.7979	-0.2913	1.3158	0.0036
2454004.7433	-0.1710	8.8569	0.0066	2454004.7430	-0.1711	0.9872	0.0042	2454004.7432	-0.1710	1.1849	0.0069
2454005.7962	-0.0370	8.2667	0.0169	2454005.7960	-0.0370	0.7692	0.0170	2454005.7961	-0.0370	0.9311	0.0193
2454008.8188	0.3477	8.5368	0.0075	2454008.8186	0.3477	0.9415	0.0072	2454008.8187	0.3477	1.1393	0.0085
2454010.7937	-0.4010	8.9117	0.0102	2454010.7934	-0.4010	1.1941	0.0036	2454010.7936	-0.4010	1.3130	0.0106
2454012.7546	-0.1514	8.7879	0.0177	2454012.7543	-0.1514	0.9014	0.0118	2454012.7545	-0.1514	1.1662	0.0182
2454017.6820	0.4757	8.7531	0.0102	2454017.6801	0.4755	1.2150	0.0090	2454017.6803	0.4755	1.2479	0.0131
2454018.7569	-0.3875	8.9400	0.0052	2454018.7567	-0.3875	1.2318	0.0155	2454018.7568	-0.3875	1.3088	0.0080
2454023.7503	0.2481	8.3621	0.0078	2454023.7501	0.2480	0.8626	0.0080	2454023.7502	0.2480	1.0345	0.0079
2454025.7572	-0.4965	8.7889	0.0124	2454025.7570	-0.4965	1.1217	0.0109	2454025.7571	-0.4965	1.2672	0.0129
2454030.7496	0.1389	8.4078	0.0128	2454030.7494	0.1389	0.8645	0.0113	2454030.7495	0.1389	1.0397	0.0156

2454031.7488	0.2661	8.3693	0.0120	2454031.7486	0.2660	0.8405	0.0073	2454031.7487	0.2660	1.0401	0.0127
2454033.7530	-0.4789	8.8117	0.0173	2454033.7528	-0.4789	1.1195	0.0097	2454033.7529	-0.4789	1.2718	0.0178
2454037.7401	0.0286	8.2348	0.0040	2454037.7399	0.0286	0.7695	0.0050	2454037.7400	0.0286	0.9210	0.0061
2454039.7309	0.2820	8.3749	0.0118	2454039.7307	0.2819	0.8583	0.0158	2454039.7308	0.2819	1.0495	0.0147
2454040.7306	0.4092	8.7185	0.0008	2454040.7304	0.4092	1.0103	0.0371	2454040.7305	0.4092	1.2011	0.0012
2454047.7040	0.2967	8.3866	0.0226	2454047.7037	0.2967	0.9073	0.0179	2454047.7039	0.2967	1.0533	0.0228
2454049.7078	-0.4483	8.8400	0.0052	2454049.7076	-0.4483	1.1597	0.0098	2454049.7077	-0.4483	1.2806	0.0072
2454050.7003	-0.3219	9.0165	0.0109	2454050.7001	-0.3220	1.2085	0.0063	2454050.7002	-0.3219	1.3205	0.0123
2454057.6800	-0.4336	8.8615	0.0069	2454057.6797	-0.4336	1.1323	0.0076	2454057.6799	-0.4336	1.3097	0.0073
2454058.6732	-0.3072	9.0249	0.0054	2454058.6730	-0.3072	1.2150	0.0016	2454058.6731	-0.3072	1.3212	0.0055
2454059.6774	-0.1794	8.8830	0.0067	2454059.6772	-0.1794	0.9727	0.0081	2454059.6773	-0.1794	1.1926	0.0070
2454060.6633	-0.0539	8.3520	0.0039	2454060.6631	-0.0539	0.7850	0.0120	2454060.6632	-0.0539	0.9568	0.0049
2454061.6676	0.0739	8.2960	0.0137	2454061.6674	0.0739	0.7984	0.0086	2454061.6675	0.0739	0.9702	0.0139
2454062.6622	0.2005	8.4096	0.0038	2454062.6619	0.2005	0.8653	0.0085	2454062.6621	0.2005	1.0483	0.0056
2454064.6536	0.4539	8.7472	0.0044	2454064.6533	0.4539	1.0771	0.0080	2454064.6535	0.4539	1.2328	0.0080
2454067.6516	-0.1645	8.8400	0.0113	2454067.6514	-0.1645	0.9629	0.0146	2454067.6515	-0.1645	1.1755	0.0115
2454068.6509	-0.0373	8.2791	0.0097	2454068.6506	-0.0373	0.7712	0.0126	2454068.6508	-0.0373	0.9245	0.0098
2454069.6283	0.0871	8.3332	0.0060	2454069.6281	0.0871	0.8398	0.0030	2454069.6282	0.0871	0.9783	0.0066
2454070.6395	0.2158	8.4078	0.0069	2454070.6393	0.2158	0.8616	0.0190	2454070.6394	0.2158	1.0362	0.0071
2454071.6280	0.3416	8.5140	0.0109	2454071.6278	0.3416	0.9223	0.0256	2454071.6279	0.3416	1.1331	0.0134
2454072.6315	0.4693	8.7639	0.0055	2454072.6312	0.4693	1.1057	0.0150	2454072.6314	0.4693	1.2389	0.0074
2454075.6094	-0.1517	8.7850	0.0017	2454075.6092	-0.1517	0.9188	0.0052	2454075.6093	-0.1517	1.1613	0.0044
2454076.6077	-0.0246	8.2612	0.0002	2454076.6075	-0.0246	0.7524	0.0295	2454076.6076	-0.0246	0.9125	0.0051
2454077.6214	0.1044	8.3543	0.0078	2454077.6212	0.1044	0.8387	0.0092	2454077.6213	0.1044	1.0113	0.0099
2454078.6189	0.2314	8.3791	0.0066	2454078.6187	0.2313	0.8464	0.0187	2454078.6188	0.2313	1.0367	0.0076
2454079.6163	0.3583	8.5799	0.0070	2454079.6160	0.3583	0.9681	0.0125	2454079.6162	0.3583	1.1643	0.0074
2454080.6081	0.4845	8.7784	0.0137	2454080.6079	0.4845	1.1145	0.0060	2454080.6080	0.4845	1.2484	0.0141

2454081.6106	-0.3879	8.9314	0.0142	2454081.6104	-0.3879	1.1980	0.0059	2454081.6105	-0.3879	1.3189	0.0152
2454085.5991	0.1197	8.3835	0.0048	2454085.5988	0.1197	0.8641	0.0162	2454085.5990	0.1197	1.0237	0.0062
2454086.5972	0.2468	8.3673	0.0091	2454086.5969	0.2467	0.8598	0.0120	2454086.5971	0.2468	1.0439	0.0096
2454087.5849	0.3725	8.6297	0.0079	2454087.5847	0.3725	1.0108	0.0063	2454087.5848	0.3725	1.1851	0.0084
2454090.5807	-0.2462	9.0304	0.0017	2454090.5805	-0.2463	1.1613	0.0023	2454090.5806	-0.2462	1.2874	0.0020
2454733.7288	-0.3908	8.9564	0.0099	2454733.7286	-0.3909	1.1773	0.0065	2454733.7287	-0.3909	1.3155	0.0099
2454734.6776	-0.2701	9.0480	0.0051	2454734.6774	-0.2701	1.1487	0.0060	2454734.6775	-0.2701	1.3130	0.0058
2454737.7546	0.1215	8.4073	0.0060	2454737.7543	0.1215	0.8545	0.0139	2454737.7545	0.1215	1.0230	0.0085
2454738.6920	0.2408	8.3937	0.0002	2454738.6906	0.2407	0.8767	0.0055	2454738.6907	0.2407	1.0325	0.0020
2454741.7279	-0.3728	8.9800	0.0025	2454741.7276	-0.3728	1.2055	0.0054	2454741.7278	-0.3728	1.3184	0.0032
2454746.6942	0.2593	8.3781	0.0020	2454746.6914	0.2590	0.8518	0.0095	2454746.6928	0.2591	1.0509	0.0081
2454766.6114	-0.2058	8.9737	0.0051	2454766.6112	-0.2058	1.0533	0.0078	2454766.6113	-0.2058	1.2386	0.0055
2454767.6107	-0.0786	8.5047	0.0077	2454767.6105	-0.0786	0.8148	0.0099	2454767.6106	-0.0786	1.0111	0.0098
2454772.6076	-0.4426	8.8809	0.0038	2454772.6074	-0.4426	1.1818	0.0026	2454772.6075	-0.4426	1.2909	0.0045
2454776.6055	0.0662	8.3108	0.0046	2454776.6053	0.0662	0.8071	0.0052	2454776.6054	0.0662	0.9536	0.0048
2454777.6197	0.1953	8.4338	0.0022	2454777.6172	0.1950	0.8533	0.0097	2454777.6185	0.1951	1.0415	0.0026
2454785.6270	0.2144	8.4086	0.0023	2454785.6271	0.2144	0.8350	0.0161	2454785.6271	0.2144	1.0473	0.0044
2454786.6069	0.3391	8.5191	0.0038	2454786.6071	0.3391	0.9111	0.0093	2454786.6070	0.3391	1.1267	0.0044
2454788.6163	-0.4051	8.9357	0.0032	2454788.6165	-0.4051	1.1974	0.0027	2454788.6164	-0.4051	1.2986	0.0035
2454791.5992	-0.0255	8.2630	0.0069	2454791.5993	-0.0255	0.7514	0.0216	2454791.5993	-0.0255	0.9190	0.0145
2454801.5931	0.2465	8.3888	0.0038	2454801.5932	0.2465	0.8625	0.0050	2454801.5932	0.2465	1.0400	0.0051
2454803.5928	-0.4990	8.8079	0.0031	2454803.5930	-0.4990	1.1176	0.0038	2454803.5929	-0.4990	1.2571	0.0040
2454811.5898	-0.4812	8.8523	0.0041	2454811.5899	-0.4812	1.1297	0.0259	2454811.5899	-0.4812	1.2583	0.0050
2455097.7930	-0.0553	8.3704	0.0107	2455097.7932	-0.0553	0.7798	0.0125	2455097.7931	-0.0553	0.9406	0.0149
2455098.6114	0.0489	8.2856	0.0130	2455098.6116	0.0489	0.7868	0.0115	2455098.6115	0.0489	0.9360	0.0160
2455098.7894	0.0715	8.3120	0.0082	2455098.7895	0.0715	0.8033	0.0194	2455098.7895	0.0715	0.9579	0.0164
2455099.6251	0.1779	8.4382	0.0023	2455099.6253	0.1779	0.8508	0.0126	2455099.6252	0.1779	1.0438	0.0039

2455099.7845	0.1982	8.4219	0.0150	2455099.7858	0.1983	0.8726	0.0090	2455099.7857	0.1983	1.0384	0.0154
2455100.7620	0.3226	8.4626	0.0154	2455100.7579	0.3221	0.9224	0.0119	2455100.7600	0.3223	1.0811	0.0156
2455101.8296	0.4585	8.7618	0.0021	2455101.8298	0.4585	1.0934	0.0086	2455101.8297	0.4585	1.2185	0.0028
2455102.6223	-0.4406	8.8803	0.0008	2455102.6224	-0.4406	1.1680	0.0063	2455102.6224	-0.4406	1.2768	0.0027
2455102.7818	-0.4203	8.9069	0.0047	2455102.7831	-0.4202	1.1885	0.0041	2455102.7819	-0.4203	1.2886	0.0050
2455106.7693	0.0872	8.3519	0.0055	2455106.7694	0.0872	0.7841	0.0228	2455106.7694	0.0872	0.9742	0.0169
2455131.7009	0.2603	8.3918	0.0079	2455131.7011	0.2603	0.8607	0.0138	2455131.7010	0.2603	1.0416	0.0101
2455133.6933	-0.4861	8.8384	0.0062	2455133.6934	-0.4861	1.1202	0.0079	2455133.6934	-0.4861	1.2528	0.0079
2455134.6857	-0.3598	8.9968	0.0050	2455134.6859	-0.3598	1.2829	0.0096	2455134.6858	-0.3598	1.3284	0.0089
2455135.6865	-0.2325	9.0243	0.0038	2455135.6889	-0.2322	1.0857	0.0049	2455135.6866	-0.2325	1.2775	0.0053
2455136.6860	-0.1053	8.6280	0.0054	2455136.6862	-0.1052	0.8306	0.0099	2455136.6861	-0.1052	1.0632	0.0072
2455137.6782	0.0210	8.2365	0.0046	2455137.6783	0.0210	0.8070	0.0164	2455137.6783	0.0210	0.9047	0.0059
2455138.6779	0.1483	8.4347	0.0122	2455138.6781	0.1483	0.8636	0.0072	2455138.6780	0.1483	1.0343	0.0126
2455139.6769	0.2754	8.3883	0.0033	2455139.6771	0.2754	0.8763	0.0307	2455139.6770	0.2754	1.0295	0.0043
2455141.6675	-0.4712	8.8322	0.0051	2455141.6677	-0.4712	1.1669	0.0131	2455141.6676	-0.4712	1.2580	0.0060
2455143.6627	-0.2173	8.9838	0.0009	2455143.6628	-0.2173	1.0935	0.0039	2455143.6628	-0.2173	1.2517	0.0014
2455144.6583	-0.0906	8.5676	0.0047	2455144.6585	-0.0906	0.8538	0.0168	2455144.6584	-0.0906	1.0224	0.0051
2455145.6580	0.0366	8.2536	0.0076	2455145.6582	0.0367	0.7800	0.0067	2455145.6581	0.0366	0.9172	0.0085
2455146.6573	0.1638	8.4383	0.0028	2455146.6574	0.1638	0.8697	0.0091	2455146.6574	0.1638	1.0320	0.0068
2455151.6431	-0.2016	8.9625	0.0011	2455151.6433	-0.2016	1.0242	0.0083	2455151.6432	-0.2016	1.2270	0.0021
2455468.7871	0.1623	8.4399	0.0068	2455468.7884	0.1624	0.8492	0.0112	2455468.7883	0.1624	1.0371	0.0071
2455469.8041	0.2917	8.4152	0.0059	2455469.8042	0.2917	0.8779	0.0053	2455469.8042	0.2917	1.0392	0.0065
2455470.7818	0.4161	8.7331	0.0027	2455470.7820	0.4161	1.0137	0.0038	2455470.7819	0.4161	1.1982	0.0046
2455471.8069	-0.4534	8.8614	0.0052	2455471.8081	-0.4533	1.1797	0.0053	2455471.8070	-0.4534	1.2561	0.0055
2455476.7651	0.1776	8.4432	0.0104	2455476.7664	0.1778	0.8352	0.0051	2455476.7663	0.1778	1.0439	0.0115
2455477.7904	0.3081	8.4299	0.0064	2455477.7917	0.3083	0.8938	0.0096	2455477.7905	0.3081	1.0640	0.0079
2455478.7598	0.4315	8.7489	0.0050	2455478.7600	0.4315	1.0465	0.0037	2455478.7599	0.4315	1.2143	0.0056

2455479.7848	-0.4380	8.8840	0.0045	2455479.7849	-0.4380	1.1297	0.0038	2455479.7849	-0.4380	1.2771	0.0052
2455480.7544	-0.3146	9.0432	0.0081	2455480.7546	-0.3146	1.2402	0.0080	2455480.7545	-0.3146	1.3192	0.0084
2455481.7794	-0.1842	8.9229	0.0022	2455481.7806	-0.1840	1.0490	0.0109	2455481.7795	-0.1842	1.1988	0.0047
2455488.7530	-0.2966	9.0580	0.0029	2455488.7531	-0.2966	1.2033	0.0038	2455488.7531	-0.2966	1.2944	0.0032
2455490.7481	-0.0427	8.3241	0.0050	2455490.7482	-0.0427	0.8027	0.0077	2455490.7482	-0.0427	0.9246	0.0065
2455492.7596	0.2133	8.4137	0.0091	2455492.7598	0.2133	0.8787	0.0092	2455492.7597	0.2133	1.0338	0.0097
2455493.7463	0.3389	8.5277	0.0073	2455493.7464	0.3389	0.9689	0.0070	2455493.7464	0.3389	1.0915	0.0079
2455495.7363	-0.4078	8.9338	0.0037	2455495.7343	-0.4081	1.1349	0.0101	2455495.7353	-0.4080	1.2891	0.0042
2455498.7286	-0.0270	8.2673	0.0117	2455498.7287	-0.0270	0.7700	0.0185	2455498.7287	-0.0270	0.9034	0.0153
2455499.7234	0.0996	8.3669	0.0084	2455499.7236	0.0996	0.8157	0.0080	2455499.7235	0.0996	0.9900	0.0088
2455501.7168	0.3533	8.5835	0.0059	2455504.7085	-0.2659	1.1416	0.0074	2455501.7169	0.3533	1.1350	0.0059
2455502.7147	0.4803	8.7858	0.0056	2455508.6827	0.2399	0.8601	0.0039	2455502.7148	0.4803	1.2310	0.0064
2455503.7114	-0.3928	8.9643	0.0022	2455510.6783	0.4939	1.1412	0.0056	2455503.7115	-0.3928	1.2848	0.0030
2455504.7083	-0.2660	9.0627	0.0017	2455511.6751	-0.3793	1.2125	0.0053	2455504.7084	-0.2659	1.2889	0.0033
2455508.6825	0.2399	8.3988	0.0023	2455512.6942	-0.2496	1.1505	0.0028	2455508.6826	0.2399	1.0296	0.0030
2455510.6770	0.4937	8.8003	0.0037	2455513.6718	-0.1251	0.8612	0.0093	2455510.6771	0.4937	1.2529	0.0062
2455511.6749	-0.3793	8.9773	0.0023	2455515.6897	0.1317	0.8408	0.0119	2455511.6750	-0.3793	1.3124	0.0033
2455512.6930	-0.2497	9.0487	0.0038	2455516.6644	0.2557	0.8609	0.0194	2455512.6942	-0.2496	1.2878	0.0040
2455513.6717	-0.1252	8.7130	0.0036	2455517.6597	0.3824	1.0315	0.0098	2455513.6718	-0.1251	1.0986	0.0041
2455515.6896	0.1317	8.4250	0.0050	2455518.6570	-0.4907	1.1460	0.0080	2455515.6897	0.1317	1.0193	0.0104
2455516.6653	0.2559	8.3958	0.0041	2455519.6566	-0.3634	1.1221	0.0069	2455516.6654	0.2559	1.0293	0.0058
2455517.6596	0.3824	8.6805	0.0054	2455522.6657	0.0195	0.7352	0.0113	2455517.6597	0.3824	1.1782	0.0060
2455518.6569	-0.4907	8.8282	0.0044	2455523.6439	0.1440	0.8382	0.0119	2455518.6570	-0.4907	1.2487	0.0048
2455519.6565	-0.3634	9.0013	0.0040	2455525.6472	0.3990	0.9750	0.0084	2455519.6566	-0.3634	1.3134	0.0050
2455522.6655	0.0195	8.2489	0.0041	2455526.6469	-0.4738	1.1075	0.0045	2455522.6656	0.0195	0.9101	0.0050
2455523.6426	0.1439	8.4334	0.0051	2455527.6317	-0.3484	1.1878	0.0127	2455523.6438	0.1440	1.0367	0.0056
2455525.6470	0.3990	8.7180	0.0041	2455528.6316	-0.2212	1.0913	0.0027	2455525.6471	0.3990	1.1960	0.0049

2455526.6467	-0.4738	8.8438	0.0041	2455530.6313	0.0333	0.7527	0.0053	2455526.6468	-0.4738	1.2630	0.0046
2455527.6316	-0.3484	9.0189	0.0041	2455531.6317	0.1607	0.8429	0.0124	2455527.6317	-0.3484	1.3220	0.0042
2455528.6315	-0.2212	9.0097	0.0042	2455543.5920	-0.3171	1.1072	0.0108	2455528.6316	-0.2212	1.2578	0.0044
2455530.6311	0.0333	8.2654	0.0085	2455544.5849	-0.1907	0.9921	0.0049	2455530.6312	0.0333	0.9213	0.0089
2455531.6315	0.1606	8.4484	0.0058	2455545.5853	-0.0634	0.7878	0.0100	2455531.6316	0.1607	1.0400	0.0060
2455543.5918	-0.3171	9.0498	0.0054	2455546.6130	0.0674	0.7844	0.0178	2455543.5919	-0.3171	1.3280	0.0059
2455544.5847	-0.1908	8.9500	0.0041	2455554.5735	0.0805	0.7074	0.1245	2455544.5848	-0.1907	1.2096	0.0044
2455545.5852	-0.0634	8.4296	0.0045	2455823.8578	0.3532	0.9439	0.0044	2455545.5853	-0.0634	0.9698	0.0066
2455546.6128	0.0674	8.3148	0.0044	2455824.8462	0.4790	1.0926	0.0079	2455546.6129	0.0674	0.9598	0.0070
2455554.5734	0.0805	8.3451	0.0052	2455826.8492	-0.2661	1.1092	0.0092	2455554.5735	0.0805	0.9623	0.0055
2455823.8576	0.3531	8.5807	0.0039	2455827.8369	-0.1404	0.8966	0.0107	2455823.8577	0.3532	1.1346	0.0054
2455824.8461	0.4790	8.7817	0.0069	2455828.8316	-0.0138	0.7311	0.0045	2455824.8462	0.4790	1.2332	0.0079
2455826.8491	-0.2661	9.0552	0.0043	2455830.8252	0.2399	0.8368	0.0189	2455826.8492	-0.2661	1.2970	0.0055
2455827.8367	-0.1404	8.7832	0.0042	2455833.8183	-0.3791	1.1998	0.0013	2455827.8368	-0.1404	1.1336	0.0055
2455828.8315	-0.0138	8.2545	0.0025	2455834.8204	-0.2516	1.1387	0.0024	2455828.8316	-0.0138	0.9051	0.0045
2455830.8261	0.2400	8.3938	0.0019	2455839.8077	0.3832	0.9895	0.0122	2455830.8262	0.2401	1.0297	0.0045
2455833.8192	-0.3790	8.9732	0.0057	2455840.7978	-0.4908	1.1160	0.0116	2455833.8182	-0.3791	1.3049	0.0057
2455834.8203	-0.2516	9.0558	0.0048	2455841.7960	-0.3638	1.0096	0.0141	2455834.8204	-0.2516	1.2786	0.0052
2455839.8075	0.3831	8.6858	0.0030	2455842.7911	-0.2371	1.1590	0.0072	2455839.8076	0.3831	1.1848	0.0045
2455840.7965	-0.4910	8.8249	0.0040	2455843.7970	-0.1091	0.8191	0.0137	2455840.7977	-0.4908	1.2525	0.0052
2455841.7959	-0.3638	8.9727	0.0100	2455844.5869	-0.0086	0.7609	0.0183	2455841.7960	-0.3638	1.3286	0.0141
2455842.7909	-0.2372	9.0299	0.0028	2455844.6032	-0.0065	0.7716	0.0151	2455842.7910	-0.2371	1.2722	0.0028
2455843.7957	-0.1093	8.6523	0.0100	2455844.6196	-0.0044	0.7679	0.0279	2455843.7958	-0.1093	1.0784	0.0122
2455844.5849	-0.0088	8.2569	0.0008	2455844.6360	-0.0023	0.7405	0.0106	2455844.5860	-0.0087	0.9063	0.0040
2455844.6013	-0.0067	8.2503	0.0013	2455844.6523	-0.0003	0.7724	0.0116	2455844.6023	-0.0066	0.9152	0.0072
2455844.6176	-0.0047	8.2494	0.0016	2455844.6699	0.0020	0.7683	0.0056	2455844.6187	-0.0045	0.9128	0.0023
2455844.6340	-0.0026	8.2456	0.0017	2455844.6852	0.0039	0.7685	0.0386	2455844.6351	-0.0024	0.9170	0.0053

2455844.6504	-0.0005	8.2456	0.0019	2455844.7019	0.0061	0.7705	0.0116	2455844.6514	-0.0004	0.9081	0.0069
2455844.6668	0.0016	8.2458	0.0036	2455844.7183	0.0081	0.7457	0.0092	2455844.6679	0.0017	0.9092	0.0066
2455844.6833	0.0037	8.2481	0.0030	2455844.7835	0.0164	0.7502	0.0332	2455844.6843	0.0038	0.9073	0.0042
2455844.6999	0.0058	8.2475	0.0049	2455845.7831	0.1437	0.8402	0.0153	2455844.7010	0.0059	0.9104	0.0060
2455844.7164	0.0079	8.2423	0.0012	2455846.7802	0.2706	0.8920	0.0132	2455844.7174	0.0080	0.9154	0.0054
2455844.7816	0.0162	8.2539	0.0048	2455847.7849	0.3984	1.0290	0.0150	2455844.7826	0.0163	0.9053	0.0058
2455845.7829	0.1436	8.4380	0.0054	2455848.7822	-0.4746	1.0221	0.0140	2455845.7830	0.1437	1.0269	0.0092
2455846.7822	0.2708	8.3986	0.0057	2455849.7725	-0.3486	1.1215	0.0030	2455846.7812	0.2707	1.0270	0.0062
2455847.7847	0.3984	8.7109	0.0045	2455850.7694	-0.2217	1.0633	0.0134	2455847.7848	0.3984	1.2041	0.0062
2455848.7821	-0.4746	8.8393	0.0060	2455851.7743	-0.0938	0.8719	0.0140	2455848.7822	-0.4746	1.2553	0.0076
2455849.7712	-0.3488	9.0170	0.0035	2455852.7681	0.0327	0.7576	0.0202	2455849.7713	-0.3487	1.3172	0.0045
2455850.7692	-0.2217	9.0154	0.0049	2455853.7687	0.1600	0.8567	0.0173	2455850.7693	-0.2217	1.2561	0.0056
2455851.7741	-0.0938	8.5855	0.0011	2455854.7631	0.2866	0.8346	0.0047	2455851.7742	-0.0938	1.0387	0.0014
2455852.7679	0.0326	8.2567	0.0171	2455855.7512	0.4123	1.0387	0.0101	2455852.7680	0.0327	0.9177	0.0177
2455853.7685	0.1600	8.4402	0.0068	2455856.7463	-0.4610	1.1494	0.0087	2455853.7686	0.1600	1.0394	0.0073
2455854.7618	0.2864	8.4121	0.0045	2455857.7444	-0.3340	1.1728	0.0105	2455854.7619	0.2864	1.0435	0.0052
2455855.7499	0.4122	8.7234	0.0101	2455858.7411	-0.2071	1.0373	0.0100	2455855.7511	0.4123	1.2155	0.0106
2455856.7462	-0.4610	8.8573	0.0025	2455860.7411	0.0474	0.7716	0.0125	2455856.7463	-0.4610	1.2698	0.0029
2455857.7442	-0.3340	9.0276	0.0007	2455861.7384	0.1743	0.8758	0.0130	2455857.7443	-0.3340	1.3159	0.0017
2455858.7410	-0.2071	8.9794	0.0019	2455862.7490	0.3030	0.8907	0.0053	2455858.7411	-0.2071	1.2418	0.0035
2455860.7410	0.0474	8.2747	0.0082	2455864.7332	-0.4445	1.1640	0.0071	2455860.7411	0.0474	0.9321	0.0117
2455861.7382	0.1743	8.4448	0.0031	2455865.7387	-0.3165	1.2457	0.0159	2455861.7383	0.1743	1.0359	0.0049
2455862.7477	0.3028	8.4363	0.0040	2455866.7258	-0.1909	1.0404	0.0039	2455862.7478	0.3028	1.0513	0.0046
2455864.7331	-0.4445	8.8860	0.0039					2455864.7332	-0.4445	1.2844	0.0047
2455865.7386	-0.3165	9.0443	0.0043					2455865.7387	-0.3165	1.3088	0.0062
2455866.7257	-0.1909	8.9416	0.0060					2455866.7258	-0.1909	1.2105	0.0067

Photometry of VY Cyg, cont…

HJD	Phase	V-R	V-R err	HJD	Phase	R-I	R-I err
2453665.7581	-0.3147	0.9045	0.0044	2453665.7582	-0.3147	0.8174	0.0024
2453667.7527	-0.0608	0.7058	0.0068	2453667.7528	-0.0608	0.6857	0.0057
2453669.6125	0.1759	0.7582	0.0048	2453669.6126	0.1759	0.7179	0.0036
2453670.6158	0.3036	0.7621	0.0032	2453670.6159	0.3036	0.7278	0.0023
2453671.6153	0.4308	0.8523	0.0061	2453671.6154	0.4308	0.7838	0.0027
2453672.6156	-0.4419	0.8922	0.0037	2453672.6157	-0.4419	0.8015	0.0027
2453673.6149	-0.3147	0.9049	0.0043	2453673.6150	-0.3147	0.8139	0.0023
2453674.6145	-0.1875	0.8546	0.0057	2453674.6146	-0.1875	0.7749	0.0019
2453675.7322	-0.0453	0.6835	0.0064	2453675.7323	-0.0452	0.6741	0.0053
2453677.7266	0.2086	0.7668	0.0069	2453677.7267	0.2086	0.7159	0.0039
2453678.7234	0.3354	0.7960	0.0052	2453678.7236	0.3355	0.7401	0.0063
2453679.6115	0.4485	0.8615	0.0035	2453679.6116	0.4485	0.7861	0.0027
2453680.6110	-0.4243	0.8896	0.0032	2453680.6111	-0.4243	0.8063	0.0018
2453688.6074	-0.4066	0.8939	0.0071	2453688.6076	-0.4066	0.8075	0.0023
2453689.6111	-0.2788	0.8978	0.0099	2453689.6112	-0.2788	0.8161	0.0043
2453690.6150	-0.1511	0.7874	0.0109	2453690.6151	-0.1511	0.7297	0.0068
2453691.6292	-0.0220	0.6664	0.0089	2453691.6293	-0.0220	0.6664	0.0059
2453693.6061	0.2296	0.7472	0.0052	2453693.6063	0.2296	0.7176	0.0028
2453694.6051	0.3568	0.8169	0.0117	2453694.6053	0.3568	0.7552	0.0053
2453695.6048	0.4840	0.8687	0.0057	2453695.6050	0.4840	0.7879	0.0048
2453699.5750	-0.0107	0.6692	0.0060	2453699.5766	-0.0105	0.6547	0.0025
2453701.5974	0.2467	0.7377	0.0039	2453701.5975	0.2467	0.7271	0.0056
2453702.6413	0.3795	0.8397	0.0040	2453702.6400	0.3794	0.7704	0.0066

2453703.6286	-0.4948	0.8802	0.0059	2453703.6287	-0.4948	0.7877	0.0043
2453705.5970	-0.2443	0.8908	0.0032	2453705.5972	-0.2442	0.8047	0.0039
2453706.5970	-0.1170	0.7866	0.0037	2453706.5971	-0.1170	0.7337	0.0023
2453708.6057	0.1387	0.7628	0.0329	2453708.6059	0.1387	0.7127	0.0054
2453709.5968	0.2648	0.7525	0.0045	2453709.5969	0.2648	0.7157	0.0047
2453710.5969	0.3921	0.8509	0.0049	2453710.5971	0.3921	0.7695	0.0051
2453711.5971	-0.4806	0.8807	0.0041	2453711.5972	-0.4806	0.7924	0.0032
2453712.5970	-0.3534	0.9088	0.0052	2453712.5971	-0.3533	0.8146	0.0033
2453714.5973	-0.0988	0.7597	0.0046	2453714.5974	-0.0988	0.7186	0.0044
2453724.5785	0.1716	0.7615	0.0295	2453724.5786	0.1716	0.7181	0.0100
2453725.5757	0.2985	0.7694	0.0127	2453725.5758	0.2985	0.7233	0.0047
2453726.5761	0.4258	0.8621	0.0009	2453726.5762	0.4258	0.7810	0.0007
2454001.8317	0.4584	0.8774	0.0056	2454001.8318	0.4584	0.7908	0.0063
2454003.7980	-0.2913	0.9046	0.0037	2454003.7982	-0.2913	0.8223	0.0037
2454004.7433	-0.1710	0.8451	0.0067	2454004.7434	-0.1710	0.7787	0.0066
2454005.7962	-0.0370	0.6826	0.0177	2454005.7964	-0.0370	0.6733	0.0108
2454008.8205	0.3479	0.8116	0.0075	2454008.8206	0.3479	0.7669	0.0014
2454010.7937	-0.4010	0.8880	0.0105	2454010.7955	-0.4007	0.8350	0.0041
2454012.7563	-0.1512	0.8352	0.0178	2454012.7580	-0.1510	0.7716	0.0016
2454017.6804	0.4755	0.8749	0.0105	2454017.6789	0.4753	0.8058	0.0033
2454018.7570	-0.3875	0.9070	0.0062	2454018.7571	-0.3874	0.8142	0.0057
2454023.7503	0.2481	0.7453	0.0088	2454023.7504	0.2481	0.7372	0.0045
2454025.7572	-0.4965	0.8915	0.0126	2454025.7573	-0.4965	0.7929	0.0085
2454030.7496	0.1389	0.7558	0.0135	2454030.7498	0.1389	0.7209	0.0045
2454031.7488	0.2661	0.7577	0.0132	2454031.7489	0.2661	0.7282	0.0092
2454033.7531	-0.4789	0.8785	0.0207	2454033.7532	-0.4788	0.8135	0.0143
2454037.7401	0.0286	0.6775	0.0046	2454037.7402	0.0286	0.6797	0.0030

2454039.7309	0.2820	0.7639	0.0125	2454039.7311	0.2820	0.7298	0.0085
2454040.7306	0.4092	0.8714	0.0013	2454040.7307	0.4092	0.7876	0.0043
2454047.7040	0.2967	0.7751	0.0234	2454047.7041	0.2967	0.7339	0.0067
2454049.7079	-0.4482	0.8830	0.0071	2454049.7080	-0.4482	0.8030	0.0114
2454050.7003	-0.3219	0.9277	0.0122	2454050.7005	-0.3219	0.8157	0.0140
2454057.6800	-0.4336	0.8966	0.0086	2454057.6801	-0.4336	0.8154	0.0053
2454058.6732	-0.3072	0.9182	0.0056	2454058.6733	-0.3072	0.8264	0.0045
2454059.6774	-0.1794	0.8585	0.0069	2454059.6775	-0.1794	0.7856	0.0042
2454060.6634	-0.0539	0.7009	0.0053	2454060.6635	-0.0539	0.6900	0.0039
2454061.6676	0.0739	0.7122	0.0157	2454061.6678	0.0739	0.6976	0.0122
2454062.6622	0.2005	0.7697	0.0061	2454062.6623	0.2005	0.7345	0.0054
2454064.6536	0.4539	0.8769	0.0045	2454064.6537	0.4540	0.7922	0.0016
2454067.6517	-0.1645	0.8482	0.0115	2454067.6518	-0.1645	0.7786	0.0055
2454068.6509	-0.0373	0.6878	0.0116	2454068.6510	-0.0373	0.6813	0.0077
2454069.6283	0.0871	0.7147	0.0079	2454069.6285	0.0871	0.6982	0.0083
2454070.6396	0.2158	0.7579	0.0077	2454070.6397	0.2158	0.7207	0.0059
2454071.6281	0.3416	0.8069	0.0115	2454071.6282	0.3416	0.7613	0.0048
2454072.6315	0.4693	0.8748	0.0072	2454072.6316	0.4693	0.7931	0.0051
2454075.6094	-0.1517	0.8282	0.0038	2454075.6095	-0.1517	0.7701	0.0038
2454076.6077	-0.0246	0.6779	0.0033	2454076.6078	-0.0246	0.6744	0.0087
2454077.6215	0.1044	0.7369	0.0099	2454077.6216	0.1044	0.7087	0.0093
2454078.6189	0.2313	0.7671	0.0070	2454078.6190	0.2314	0.7332	0.0033
2454079.6163	0.3583	0.8270	0.0070	2454079.6164	0.3583	0.7691	0.0017
2454080.6098	0.4847	0.8806	0.0137	2454080.6099	0.4848	0.8016	0.0068
2454081.6106	-0.3879	0.9089	0.0144	2454081.6107	-0.3879	0.8195	0.0066
2454085.5991	0.1197	0.7480	0.0077	2454085.5992	0.1198	0.7206	0.0069
2454086.5972	0.2468	0.7553	0.0091	2454086.5973	0.2468	0.7269	0.0056

2454087.5850	0.3725	0.8448	0.0088	2454087.5851	0.3725	0.7700	0.0064
2454090.5807	-0.2462	0.9026	0.0029	2454090.5808	-0.2462	0.8140	0.0024
2454733.7289	-0.3908	0.8989	0.0103	2454733.7290	-0.3908	0.8188	0.0043
2454734.6777	-0.2701	0.9023	0.0065	2454734.6778	-0.2701	0.8220	0.0069
2454737.7546	0.1215	0.7374	0.0079	2454737.7547	0.1216	0.7202	0.0074
2454738.6908	0.2407	0.7714	0.0030	2454738.6897	0.2406	0.7153	0.0068
2454741.7279	-0.3728	0.9037	0.0026	2454741.7280	-0.3728	0.8202	0.0016
2454746.6930	0.2592	0.7384	0.0089	2454746.6918	0.2590	0.7227	0.0143
2454766.6114	-0.2058	0.8731	0.0051	2454766.6115	-0.2058	0.7900	0.0025
2454767.6107	-0.0786	0.7351	0.0082	2454767.6109	-0.0786	0.7051	0.0069
2454772.6076	-0.4426	0.8925	0.0040	2454772.6077	-0.4426	0.8106	0.0026
2454776.6056	0.0662	0.6964	0.0048	2454776.6057	0.0662	0.6893	0.0019
2454777.6199	0.1953	0.7583	0.0022	2454777.6202	0.1954	0.7210	0.0009
2454785.6282	0.2146	0.7503	0.0030	2454785.6285	0.2146	0.7303	0.0035
2454786.6071	0.3391	0.7832	0.0038	2454786.6073	0.3392	0.7462	0.0029
2454788.6165	-0.4051	0.9004	0.0039	2454788.6167	-0.4051	0.8171	0.0044
2454791.5993	-0.0255	0.6650	0.0070	2454791.5996	-0.0254	0.6767	0.0013
2454801.5933	0.2465	0.7491	0.0047	2454801.5935	0.2465	0.7198	0.0034
2454803.5930	-0.4990	0.8761	0.0034	2454803.5932	-0.4990	0.7974	0.0024
2454811.5900	-0.4812	0.8738	0.0041	2454811.5902	-0.4812	0.7913	0.0017
2455097.7932	-0.0553	0.7215	0.0134	2455097.7934	-0.0552	0.6906	0.0095
2455098.6116	0.0489	0.6913	0.0144	2455098.6129	0.0491	0.6934	0.0071
2455098.7895	0.0715	0.7294	0.0108	2455098.7898	0.0716	0.6917	0.0085
2455099.6263	0.1780	0.7656	0.0035	2455099.6266	0.1781	0.7289	0.0081
2455099.7847	0.1982	0.7695	0.0154	2455099.7850	0.1982	0.7373	0.0052
2455100.7622	0.3226	0.8012	0.0154	2455100.7613	0.3225	0.7417	0.0008
2455101.8298	0.4585	0.8982	0.0027	2455101.8311	0.4587	0.8069	0.0025

2455102.6224	-0.4406	0.9095	0.0039	2455102.6227	-0.4406	0.8268	0.0040
2455102.7830	-0.4202	0.9122	0.0053	2455102.7833	-0.4202	0.8241	0.0045
2455106.7695	0.0872	0.7161	0.0073	2455106.7697	0.0872	0.7090	0.0058
2455131.7011	0.2603	0.7531	0.0093	2455131.7013	0.2603	0.7300	0.0075
2455133.6935	-0.4861	0.8929	0.0063	2455133.6937	-0.4861	0.8085	0.0028
2455134.6859	-0.3598	0.9077	0.0062	2455134.6861	-0.3598	0.8238	0.0036
2455135.6867	-0.2324	0.8963	0.0057	2455135.6869	-0.2324	0.8187	0.0047
2455136.6862	-0.1052	0.7763	0.0058	2455136.6864	-0.1052	0.7499	0.0034
2455137.6795	0.0212	0.6956	0.0046	2455137.6797	0.0212	0.6776	0.0060
2455138.6781	0.1483	0.7752	0.0129	2455138.6783	0.1483	0.7326	0.0070
2455139.6771	0.2754	0.7700	0.0069	2455139.6773	0.2755	0.7403	0.0085
2455141.6677	-0.4712	0.9018	0.0052	2455141.6691	-0.4710	0.8174	0.0040
2455143.6628	-0.2173	0.8869	0.0014	2455143.6631	-0.2173	0.8132	0.0013
2455144.6585	-0.0906	0.7872	0.0060	2455144.6587	-0.0906	0.7276	0.0042
2455145.6582	0.0367	0.7013	0.0092	2455145.6585	0.0367	0.6884	0.0101
2455146.6574	0.1638	0.7879	0.0043	2455146.6577	0.1639	0.7355	0.0036
2455151.6433	-0.2016	0.8789	0.0029	2455151.6435	-0.2016	0.7936	0.0030
2455468.7873	0.1623	0.7747	0.0071	2455468.7876	0.1623	0.7365	0.0067
2455469.8043	0.2917	0.7893	0.0072	2455469.8045	0.2917	0.7510	0.0055
2455470.7820	0.4161	0.8717	0.0031	2455470.7822	0.4162	0.8069	0.0029
2455471.8071	-0.4534	0.9174	0.0081	2455471.8073	-0.4534	0.8251	0.0088
2455476.7664	0.1778	0.7748	0.0118	2455476.7666	0.1778	0.7345	0.0097
2455477.7906	0.3082	0.7896	0.0079	2455477.7908	0.3082	0.7446	0.0088
2455478.7600	0.4315	0.8857	0.0052	2455478.7602	0.4316	0.8025	0.0018
2455479.7850	-0.4380	0.9131	0.0062	2455479.7852	-0.4380	0.8230	0.0052
2455480.7546	-0.3146	0.9381	0.0082	2455480.7548	-0.3146	0.8360	0.0032
2455481.7796	-0.1842	0.8669	0.0030	2455481.7798	-0.1841	0.8007	0.0026

2455488.7531	-0.2966	0.9395	0.0038	2455488.7534	-0.2966	0.8435	0.0040
2455490.7494	-0.0425	0.7195	0.0065	2455490.7496	-0.0425	0.6908	0.0066
2455492.7598	0.2133	0.7735	0.0114	2455492.7600	0.2134	0.7307	0.0071
2455493.7475	0.3390	0.8236	0.0077	2455493.7478	0.3391	0.7600	0.0034
2455495.7354	-0.4080	0.9261	0.0041	2455495.7345	-0.4081	0.8291	0.0027
2455498.7287	-0.0270	0.7031	0.0149	2455498.7289	-0.0270	0.6885	0.0126
2455499.7236	0.0996	0.7411	0.0103	2455499.7238	0.0997	0.7263	0.0070
2455501.7170	0.3533	0.8372	0.0066	2455501.7173	0.3534	0.7744	0.0046
2455502.7148	0.4803	0.8915	0.0084	2455502.7151	0.4804	0.8169	0.0077
2455503.7116	-0.3928	0.9314	0.0042	2455503.7118	-0.3928	0.8388	0.0048
2455504.7085	-0.2659	0.9291	0.0023	2455504.7087	-0.2659	0.8340	0.0017
2455508.6838	0.2400	0.7732	0.0027	2455508.6840	0.2400	0.7349	0.0044
2455510.6772	0.4937	0.8791	0.0048	2455510.6775	0.4938	0.8111	0.0057
2455511.6751	-0.3793	0.9178	0.0040	2455511.6753	-0.3792	0.8334	0.0039
2455512.6931	-0.2497	0.8924	0.0039	2455512.6934	-0.2497	0.8402	0.0047
2455513.6719	-0.1251	0.8032	0.0040	2455513.6721	-0.1251	0.7613	0.0030
2455515.6898	0.1317	0.7439	0.0053	2455515.6900	0.1317	0.7304	0.0069
2455516.6644	0.2557	0.7725	0.0046	2455516.6635	0.2556	0.7344	0.0034
2455517.6598	0.3824	0.8531	0.0054	2455517.6600	0.3825	0.7942	0.0025
2455518.6570	-0.4907	0.8887	0.0044	2455518.6573	-0.4906	0.8190	0.0021
2455519.6566	-0.3634	0.9089	0.0044	2455519.6569	-0.3634	0.8403	0.0033
2455522.6657	0.0195	0.6872	0.0046	2455522.6659	0.0196	0.6846	0.0028
2455523.6428	0.1439	0.7618	0.0055	2455523.6442	0.1441	0.7306	0.0043
2455525.6472	0.3990	0.8626	0.0044	2455525.6474	0.3990	0.7954	0.0030
2455526.6480	-0.4736	0.8939	0.0043	2455526.6493	-0.4735	0.8183	0.0024
2455527.6317	-0.3484	0.9140	0.0044	2455527.6320	-0.3484	0.8304	0.0027
2455528.6317	-0.2211	0.8921	0.0043	2455528.6330	-0.2210	0.8144	0.0013

2455530.6313	0.0333	0.6816	0.0090	2455530.6315	0.0334	0.6890	0.0034
2455531.6328	0.1608	0.7645	0.0059	2455531.6330	0.1608	0.7317	0.0016
2455543.5920	-0.3171	0.9080	0.0057	2455543.5923	-0.3171	0.8304	0.0022
2455544.5860	-0.1906	0.8665	0.0046	2455544.5863	-0.1906	0.8010	0.0022
2455545.5853	-0.0634	0.7161	0.0056	2455545.5856	-0.0634	0.7011	0.0036
2455546.6130	0.0674	0.6992	0.0074	2455546.6132	0.0674	0.7153	0.0059
2455554.5735	0.0805	0.7233	0.0053	2455554.5738	0.0806	0.7067	0.0041
2455823.8578	0.3532	0.8276	0.0042	2455823.8580	0.3532	0.7800	0.0074
2455824.8462	0.4790	0.8873	0.0086	2455824.8465	0.4790	0.8120	0.0096
2455826.8504	-0.2660	0.9429	0.0046	2455826.8517	-0.2658	0.8309	0.0019
2455827.8369	-0.1404	0.8193	0.0048	2455827.8372	-0.1404	0.7710	0.0029
2455828.8317	-0.0138	0.6759	0.0037	2455828.8319	-0.0138	0.6838	0.0057
2455830.8252	0.2399	0.7636	0.0031	2455830.8243	0.2398	0.7438	0.0035
2455833.8194	-0.3790	0.9262	0.0062	2455833.8196	-0.3790	0.8326	0.0055
2455834.8205	-0.2516	0.9145	0.0049	2455834.8207	-0.2516	0.8387	0.0028
2455839.8077	0.3832	0.8684	0.0036	2455839.8079	0.3832	0.7809	0.0040
2455840.7967	-0.4910	0.8971	0.0044	2455840.7969	-0.4909	0.8223	0.0040
2455841.7960	-0.3638	0.9094	0.0141	2455841.7963	-0.3637	0.8544	0.0141
2455842.7911	-0.2371	0.8957	0.0035	2455842.7913	-0.2371	0.8254	0.0050
2455843.7959	-0.1092	0.7866	0.0101	2455843.7961	-0.1092	0.7397	0.0029
2455844.5860	-0.0087	0.6712	0.0014	2455844.5871	-0.0086	0.6754	0.0034
2455844.6024	-0.0066	0.6663	0.0022	2455844.6035	-0.0065	0.6804	0.0041
2455844.6187	-0.0045	0.6689	0.0028	2455844.6199	-0.0044	0.6722	0.0040
2455844.6351	-0.0024	0.6638	0.0029	2455844.6362	-0.0023	0.6684	0.0061
2455844.6515	-0.0004	0.6698	0.0038	2455844.6526	-0.0002	0.6744	0.0040
2455844.6679	0.0017	0.6657	0.0042	2455844.6690	0.0019	0.6783	0.0053
2455844.6844	0.0038	0.6707	0.0039	2455844.6855	0.0040	0.6783	0.0035

2455844.7010	0.0059	0.6697	0.0062	2455844.7022	0.0061	0.6780	0.0056
2455844.7175	0.0080	0.6646	0.0045	2455844.7186	0.0082	0.6795	0.0045
2455844.7827	0.0163	0.6877	0.0054	2455844.7838	0.0165	0.6727	0.0056
2455845.7831	0.1437	0.7562	0.0083	2455845.7833	0.1437	0.7264	0.0074
2455846.7813	0.2707	0.7739	0.0102	2455846.7815	0.2707	0.7428	0.0087
2455847.7849	0.3984	0.8582	0.0046	2455847.7851	0.3985	0.8006	0.0012
2455848.7822	-0.4746	0.8936	0.0066	2455848.7825	-0.4746	0.8086	0.0039
2455849.7714	-0.3487	0.9218	0.0036	2455849.7727	-0.3486	0.8395	0.0026
2455850.7694	-0.2217	0.9066	0.0050	2455850.7696	-0.2217	0.8188	0.0014
2455851.7743	-0.0938	0.7799	0.0062	2455851.7746	-0.0938	0.7348	0.0076
2455852.7681	0.0327	0.6894	0.0175	2455852.7683	0.0327	0.6900	0.0038
2455853.7687	0.1600	0.7628	0.0079	2455853.7689	0.1600	0.7380	0.0074
2455854.7620	0.2864	0.7712	0.0058	2455854.7622	0.2865	0.7442	0.0038
2455855.7501	0.4122	0.8713	0.0105	2455855.7503	0.4122	0.8066	0.0043
2455856.7464	-0.4610	0.9055	0.0052	2455856.7466	-0.4610	0.8205	0.0064
2455857.7444	-0.3340	0.9380	0.0034	2455857.7446	-0.3340	0.8416	0.0037
2455858.7411	-0.2071	0.8929	0.0053	2455858.7414	-0.2071	0.8084	0.0051
2455860.7412	0.0474	0.6978	0.0085	2455860.7414	0.0475	0.6977	0.0060
2455861.7384	0.1743	0.7680	0.0062	2455861.7387	0.1744	0.7387	0.0057
2455862.7479	0.3028	0.7770	0.0066	2455862.7481	0.3029	0.7463	0.0060
2455864.7333	-0.4445	0.9037	0.0044	2455864.7335	-0.4445	0.8269	0.0063
2455865.7399	-0.3164	0.9178	0.0046	2455865.7412	-0.3162	0.8319	0.0023
2455866.7259	-0.1909	0.8552	0.0061	2455866.7272	-0.1907	0.8052	0.0017